Institute of Physical Chemistry
Polish Academy of Sciences
Kasprzaka 44/52
01-224 Warsaw, Poland

Ph.D. Thesis

Spectroscopy, photophysics, tautomerism, and photodegradation of amino and nitro derivatives of porphycene

Idaresit Edet Mbakara

Supervisor: Prof. dr. hab. Jacek Waluk

This thesis was prepared within the International Doctoral Studies of the Institute of Physical Chemistry, Polish Academy of Sciences, Warsaw, Poland.

Warsaw, April 2024

Declaration of originality

I declare that the content of this thesis is the results of research carried out by myself or with support from others who are duly acknowledged.

To the best of my knowledge, the content of this thesis does not violate any copyright laws, as borrowed sentences or figures are appropriately referenced.

I certify that no part of my thesis has been or will be submitted for obtaining a degree or diploma by the Institute of Physical Chemistry, Polish Academy of Science, or elsewhere.

This thesis's copyright rests with the author; no information derived from it may be published without the author's consent.

WARSAW
16·04·2024

Place and date   **Signature**

Acknowledgment

Looking back in time, I acknowledge that this thesis would not have been possible without the immense direct or indirect support of many individuals.

First, I am grateful to my supervisor, Prof. dr. hab. Jacek Waluk, who gave me the opportunity to work in his research group - Photophysics and Spectroscopy of Photoactive Systems. I am deeply thankful for your tremendous support, scientific mentorship and discussions, interpretation of results, and walking me through the project while providing a healthy work environment.

I am thankful to Dr Agnieszka Gajewska and Dr Arkadiusz Listkowski for synthesizing my studied compounds. I am grateful to Dr Aleksander Gorski, specifically for spending time with me during the singlet oxygen and triplet lifetime experiments. Thankful to Dr Krzysztof Nawara for the help with isolating degradation products of amino porphycenes and Michał Kijak for the DFT calculations. I thank all the members of the team for the chats and discussions.

My heartiest thanks to my family, who helped me adjust to cultural differences till I could focus on my work. I express my immense gratitude to my parents, Mr Edet Mbakara and Mrs Nkoyo Mbakara, and all my siblings (Goodness, Ekomobong, Abasiemek, Unyimeabasi, Okokon, Grace, and Nya) because even though they were far away, they were always with me, seeing to my overall well-being. To my parents, who gave their all to sponsor my higher education training, I am thankful for everything. I would never be where I am today without my family. My sincere gratitude to my all-time favorite person and partner, Konrad Marzec, for all your support in making sure I am comfortable always. You were dedicated to cooking for me and making tea for me as many times as it would help me stay on my desk and write this thesis. Your kindness is not limited to the thesis writing. For this and many more, I am grateful.

Special thanks to my good friends Rukkie and Inibehe for all the long calls, for motivating me, and for keeping me company. To Sharat, Arun, Mounika, Karthika, thank you for all the support, chats, and fun times.

Lastly, my deepest and most sincere gratitude goes to myself for staying motivated and looking at the big picture through this research. I am so proud of the work I have done and achieved during this Ph.D. research.

Funding

List of publications

1. <u>Idaresit Mbakara,</u> Agnieszka Gajewska, Arkadiusz Listkowski, Michał Kijak, Krzysztof Nawara, Tatu Kumpulainen, Eric Vauthey, and Jacek Waluk. "Spectroscopic investigation of photophysics and tautomerism of amino-and nitroporphycenes." *Physical Chemistry Chemical Physics* 24, no. 48 (2022): 29655-29666. DOI: <u>10.1039/D2CP04555A</u>.

2. <u>Idaresit Mbakara</u>, Agnieszka Gajewska, Krzysztof Nawara, and Jacek Waluk. "Instability of 9-aminoporphycenes." *Journal of Porphyrins and Phthalocyanines* 27, no. 07n10 (2023): 1457-1464. DOI: <u>10.1142/S1088424623501122</u>.

3. Agnieszka Gajewska, <u>Idaresit Mbakara</u>, and Jacek Waluk. "2-nitro-7, 12, 17-tri-*tert*-butylporphycene: Spectroscopy, photophysics, and tautomerism." *Journal of Porphyrins and Phthalocyanines* 27, no. 01n04 (2023): 563-568. DOI: <u>10.1142/S1088424623500360</u>.

4. Photostability in 9-substituted porphycenes: Possible agents for photodynamic therapy? *In preparation.*

5. Photophysics of nitroporphycenes: substituent-position effects. *In preparation.*

Participation in national and international conferences

Oral presentations

1. <u>Idaresit Mbakara</u>, Agnieszka Gajewska, Arkadiusz Listkowski, and Jacek Waluk. "Photophysics and Photostability of Porphycenes Bearing Electron-Donating and Accepting Moieties." The 12th International Conference on Porphyrins and Phthalocyanines (ICPP-12), 10-15 July 2022, Madrid, Spain.

2. <u>Idaresit Mbakara</u>, Agnieszka Gajewska, Arkadiusz Listkowski, and Jacek Waluk. "Photophysical and photodegradation studies of porphycenes: influence of electron-donating and withdrawing moieties." European Meeting on Physical and Organic Chemistry, June 2023, Wrocław, Poland.

3. <u>Idaresit Mbakara</u>, Agnieszka Gajewska, Krzysztof Nawara, and Jacek Waluk. "Amino-Induced Instability of porphycenes." Molecules and Light Conference, fifth autumn meeting of the Polish Photochemistry Group, Krakow, 24-27 September 2023.

Poster presentation

1. <u>Idaresit Mbakara</u>, Agnieszka Gajewska, Arkadiusz Listkowski, and Jacek Waluk. "Photostability in Porphycenes: Influence of Electron donating and Electron-withdrawing Groups." The 11th International Conference on Porphyrins and Phthalocyanines (ICPP-11), 28 June - 3 July 2021, Virtual meeting.

Presentations outside of IPC PAS

1) <u>Idaresit Mbakara</u> "Spectroscopy, photophysics, and photostability of 9-substituted porphycenes" Webinar in Solar Energy Conversion group Faculty of Physics, Adam Mickiewicz University, Poznań, 24th February, 2023.

2) <u>Idaresit Mbakara</u> "Spectral characterization and tautomerization in Porphycenes" presentation at Prof. Eric Vauthey's group - Ultrafast Photochemistry Group of the University of Geneva, 28th November 2019.
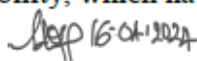
Short research visit

1) Ultrafast Photochemistry Group of the University of Geneva. 02.09.2019 – 02.12.2019
Photophysical characterization and femtosecond transient absorption measurements to investigate the excited state dynamics of porphycene derivatives.
Supervised by Prof. Eric Vauthey and Dr Tatu Kumpulainen
Funding**:** 666295-CREATE--H2020-WIDESPREAD-2014-2015/H2020-WIDESPREAD-2014-2

Abstract (Eng.)

Porphycenes are at the heart of 2nd generation photosensitization in Photodynamic Therapy (PDT) due to their intrinsic spectral, photophysical, and photobiological properties. Regarding fundamental studies of hydrogen transfer processes involving single or double proton transfer, porphycenes are known as models for such investigations. Here, a series of porphycene derivatives, substituted either with nitro, amino, or mixed nitro and amino groups, were studied. In order to ascertain their suitability in the above-mentioned applications, spectral, photophysical, and photostability characterization were performed using steady-state electronic absorption, emission, Magnetic Circular Dichroism (MCD) spectroscopy, and quantum chemical calculations. In addition, time-resolved studies were employed to characterize the excited state dynamics of these porphycenes. The specific influence of electron-donating and withdrawing groups and bulky *tert*-butyl groups, as well as the position of the substituent, were investigated.

In our studies, we found that substitution with the amino group results in red-shifted absorption bands in the spectra of aminoporphycenes. Nitroporphycenes (with the exception of the *meso*-tetraphenyl derivatives), on the other hand, showed marginal changes in absorption compared to parent unsubstituted porphycenes. Single emission is observed for both the amino and nitro series. The previous interpretation of dual emission in aminoporphycenes has to be abandoned. All nitro derivatives (except *tert*-butyl nitroporphycene) were better emitters than their amino counterparts. The introduction of bulky tertiary butyl groups results in a significant influence on the photophysics: loss of fluorescence and lack of population of the triplet state is evident in the *tert*-butyl derivatives, indicating the dominance of non-radiative processes. *Meso*-tetraphenyl substitution of porphycene, while varying the position of the nitro group to β or β' results in interesting chemistry. In the β' derivative, we observe a moderate yield of fluorescence, ~30% singlet oxygen (SO) generation, and a triplet state that lived up to 200 ns. The β counterpart is a weak emitter with ~1% yield of SO, and the triplet signal was too weak to be accurately determined, given the resolution of our instrument. Photodegradation studies revealed three orders of magnitude differences in photostability between the nitro and aminoporphycenes, with nitroporphycenes being more stable. All compounds showed a solvent effect in the obtained results. We conclude that several nitroporphycenes qualify as candidates for sensitization in PDT due to their photophysics and photostability, which have been established from this study.

(signature) 16·04·2024

Abstract (Pol.)

Dzięki swoim właściwościom spektralnym, fotofizycznym i fotobiologicznym, porficeny odgrywają ważną rolę jako fotouczulacze drugiej generacji w terapii fotodynamicznej (PDT). W obszarze badań podstawowych porficeny są używane jako modelowe cząsteczki do badania procesów przenoszenia wodoru obejmujących pojedynczy lub podwójny transfer. W niniejszej pracy zbadano szereg pochodnych porficenu podstawionych grupami nitrowymi, aminowymi lub jednocześnie grupami nitrowymi i aminowymi. W celu sprawdzenia przydatności tych związków w wyżej wymienionych zastosowaniach, zbadano ich widma, fotofizyke i fotostabilność, stosując techniki elektronowej absorpcji i emisji, spektroskopię magnetycznego dichroizmu kołowego (MCD) oraz obliczenia chemii kwantowej. Przeprowadzono ponadto badania czasowo-rozdzielcze, aby scharakteryzować dynamikę stanów wzbudzonego. Określono specyficzny wpływ podstawników elektrono-donorowych i akceptorowych, dużych grup *tert*-butylowych, a także położenia podstawnika na właściwości porficenów.

Ustalono, że podstawienie grupą aminową skutkuje w widmach aminoporficenów przesunięciem ku czerwieni pasm absorpcji. Natomiast nitroporficeny (z wyjątkiem pochodnych mezo-tetrafenylowych) wykazywały niewielkie zmiany absorpcji w porównaniu z macierzystym niepodstawionym porficenem. Zarówno dla serii aminowej, jak i nitrowej obserwuje się pojedynczą emisję, co oznacza, że należy skorygować uprzednie doniesienia o podwójnej fluorescencji aminoporficenów. Wszystkie pochodne nitrowe okazały się lepszymi emiterami niż ich odpowiedniki aminowe. Podstawienie dużymi grupami *tert*-butylowymi ma znaczący wpływ na fotofizykę: w pochodnych *tert*-butylowych widoczny jest spadek wydajności fluorescencji i brak obsadzenia stanu trypletowego, co wskazuje na dominację procesów bezpromienistych. Zaobserwowano wyraźne różnice przy podstawieniu mezo-tetrafenyloporficenu grupą nitrową w pozycji β lub β'. Pochodna β' wykazuje umiarkowaną wydajność fluorescencji, wytwarzanie tlenu singletowego z wydajnością około 30% i żyjący 200 ns stan trypletowy. Odpowiednik β jest słabym emiterem, wydajność tworzenia tlenu singletowego wynosi 1%, a sygnał od trypletu był zbyt słaby, aby można go było dokładnie scharakteryzować, biorąc pod uwagę rozdzielczość naszego instrumentu. Badania fotodegradacji wykazały różnice w fotostabilności pomiędzy nitro i aminoporficenami sięgające trzech rzędów wielkości. Nitroporficeny są bardziej stabilne. We wszystkich badanych związkach zaobserwowano efekty rozpuszczalnikowe. Wnioskujemy, że

pewne nitroporficeny kwalifikują się jako potencjalne fotouczulacze w PDT ze względu na swoje parametry fotofizyczne i fotostabilność.

Table of Contents

Section I

Chapter 1

1.1 Introduction

For well over a century, porphyrins (**Pr**s - see Scheme 1) and their derivatives have been a subject of interdisciplinary scientific interest due to their unique physicochemical, biological, and spectral properties. These properties make them suitable for various fundamental and applied scientific research. Porphyrins (scheme 1), fluorescing dyes identified to be naturally present in leaves and biological matter, are unique players in light-mediated processes in nature and several biological functions, and as such, got dubbed the *pigments of life*.[1,2] The name *'pigment of life'* is entirely justified because porphyrins form the base structure for most macromolecules useful for several biological functions and light-dependent processes in nature. The haem protein, for instance - an oxygen carrier - is an iron porphyrin, and cytochrome c - the substance responsible for electron transport - is also an iron porphyrin. The chlorophylls responsible for photosynthesis are magnesium porphyrinoids, phycocyanin - the light-harvesting agent in algae, and phytochrome - a bile pigment useful in light-mediated processes in plants; all possess porphyrins as their base structure. Moreover, vitamin B12, an essential element in metabolism, contains a cobalt-porphyrin structure. The apparent significance of porphyrins in naturally occurring light-mediated processes singled out porphyrin and its derivatives as molecules of interest to researchers. Worthy of mention is that **Pr** gets its name from porphyrion (πορφυριων) - a Greek word for purple, and the free base structure of **Pr** is named porphine – according to the Fischer nomenclature.[3] There is extensive literature detailing the properties, spectroscopy, photophysics, photochemistry, and applications of porphyrins.[4–7] A search of the word porphyrin in the Web of Science returns above seventy thousand research reports at the time of writing this thesis. This large number of appearances of porphyrin in literature points to the amount of work done studying porphyrins and a direct correlation to their importance and applications. The use of porphyrins in various applications is well documented.
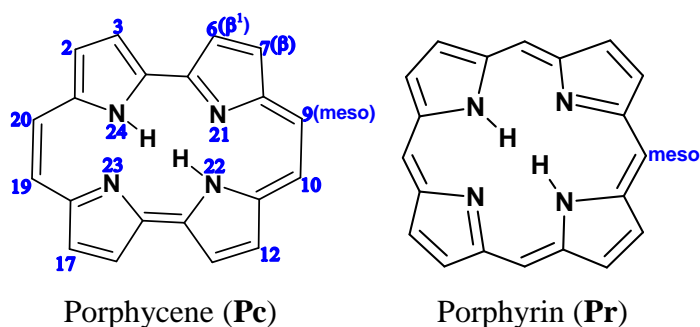
Porphycene (**Pc**)   Porphyrin (**Pr**)

Scheme 1

Duong La recently reviewed photocatalytic applications of self-assembled porphyrin-based nanostructures in environmental treatment,[8] other applications include optical

energy or information storage devices,[9] solar energy conversion, nano-catalysts, photo-electronics, sensing,[10] and photodynamic therapy (**PDT**).[11–14] Photodynamic therapy has been one of the significant areas of application of porphyrins, with porphyrins taking up a central position as first-generation photosensitizers in cancer and tumor phototherapy.[15–17]

Photodynamic therapy (**PDT**) is a tumor treatment modality that applies visible light and molecular oxygen in the presence of a photosensitizer to photo-destroy tumor cells via cytotoxic reactions instigated by reactive oxygen species (**ROS**). Since the birth of photosensitizer (**PS**) via the discovery of hematoporphyrin in 1841 by Scherer, a series of research have been conducted, and discoveries made on photosensitizers. Remarkable evolution has been witnessed in the field of porphyrin-derived photosensitizers - from the first[18] generation: hematoporphyrin (hematoporphyrin-derivative and Photofrin-11), to the second[19–22] generation: Texafrins, Benzoporphyrins (Verteporfin), 5-Aminolevulinic acid (ALA), Protoporphyrin IX, Purpurins, 5,10,15,20-Tetrakis(3-hydroxyphenyl), Chlorins (Meta-tetrahydro-phenylchlorin, mTHPC, Temoporfin), phthalocyanines, naphthalocyanines, porphycenes, and even third[23–25] generation photosensitizers. Subsequent to the successful use of first-generation photosensitizing agents, their limitations were quickly identified to include dark toxicity,[18,26] low tissue selectivity, inefficient light penetration through the skin (due to shorter wavelength of light), higher doses of light requirement, and complexity of the photosensitizer.[27] With these limitations, the development of the so-called second-generation photosensitizing agent was pertinent, and this motivated research into new, efficient **PDT**-sensitizing agents.

Porphycene (**Pc**), a reshuffled porphyrin first synthesized by Vogel[28] in 1986, has gained prominence as a second-generation **PS** in **PDT**. Unique spectral and photophysical properties distinguish porphycenes as efficient 2nd generation sensitizers in **PDT**. These properties,[29] ranging from high molar absorptivity in the red region of the spectrum, low cytotoxicity, high yield of triplet state formation, and high quantum yield of singlet oxygen generation, make an efficient photosensitizer. Sequel to the synthesis of **Pc**, other isomers of porphyrin have been synthesized (Figure 1.1): corrphycene,[30] hemiporphycene,[31–33] and isoporphycene.[34,35] Most of these compounds were synthesized in their substituted forms. Free-base unsubstituted corrphycene has only been recently synthesized by the group of Professor Waluk (Arkadiusz Listkowski & Jacek Waluk, private information).

Porphyrin   Porphycene

Corrphycene   Hemiporphycene   Isoporphycene

[18]porphyrin-(2.2.0.0)   [18]porphyrin-(3.1.0.0)   [18]porphyrin-(4.0.0.0)

N-confused porphyrin   Doubly N-confused porphyrin   Neo-confused porphyrin
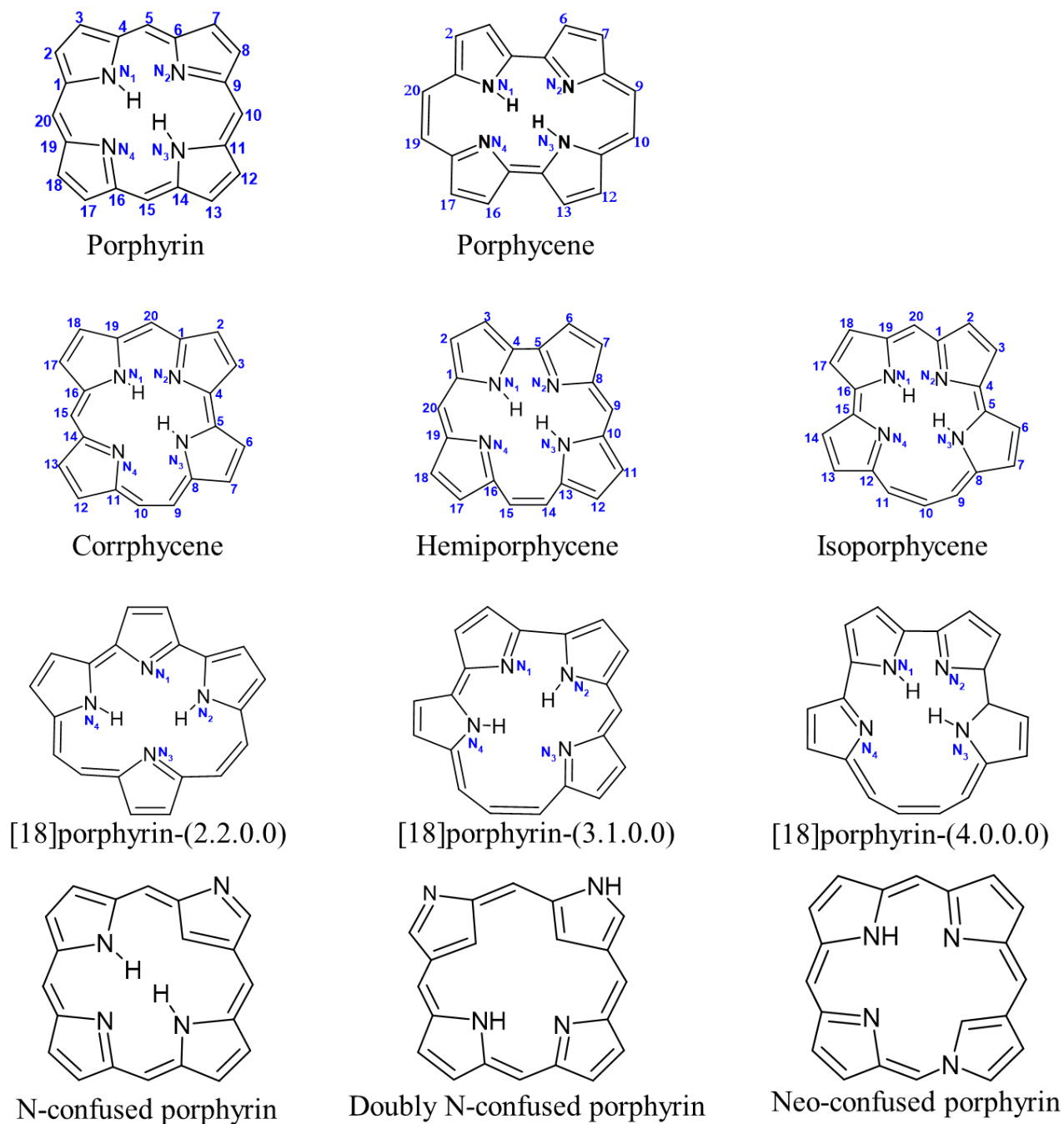
Figure 1.1 Isomers of porphycene

On the basis of spectral properties, **Pc** exhibits similarities to parent porphyrin, however, with variations in their relative intensity of the Soret bands to the Q bands. Quantitative evaluation of these properties shows distinctive photophysical and tautomeric properties in both macrocycles.[36] Porphycenes' unique spectral and photophysical properties set them aside for interesting chemistry in both fundamental and applied studies. The advantages of porphycenes in **PDT** are highlighted

to include a lower concentration of the **PS** and low light doses required. This is a direct consequence of higher absorptivity (by porphycene) in the physiological window (> 620 nm) of the spectrum, where light penetrates deeper into skin tissues.[37] The high quantum yield of triplet state formation, increased generation of singlet oxygen, and, of course, low dark toxicity are unique properties distinguishing **Pc** as better **PS** over **Pr**. Extensive reported use of porphycene in **PDT** is contained in literature.[18,37–44] Efficient antimicrobial activity has been observed for porphycene and its 2,7,12,17-tetrakis(β-methoxyethyl) derivative.[45] Temocene,[29] for instance, a porphycene analog of Temoporfin, has been reported to possess higher photostability and lower dark toxicity compared to temoporphin.[29] The outcome of **PDT** using 2nd generation **PS** has mainly been satisfying. However, the need to further engineer more target-specific **PS**s to reduce or eliminate phototoxicity to normal tissues has motivated scientists to develop the so-called third-generation **PS**. Third-generation[25] sensitizers are basically the incorporation of 2nd generation sensitizers with drug delivery or targeting agents such as liposomes, protein, carbohydrates, antibodies, and nanoparticles. Lee reported enhanced uptake of chlorin E6 by tumor cells when the **PS** was embedded in nanoparticles,[24] also increased levels of generated **ROS** were observed in their experiment. Enhanced cancer imaging and treatment were observed as a response to incorporating chlorin E6 into gold vesicles.[46] Stronger affinity for a DNA target strand was obtained for a porphycene-DNA hybrid than in an unmodified oligonucleotide.[47] Other than the use of **Pc** in **PDT**, extensive research has been performed on the spectroscopy and photophysics of porphycenes.[36,48–53] This chapter takes a deep dive into the porphycene molecule, its structure, properties, reactions, applications, and photostability.

1.2 Porphycenes: structure, properties, and reactions

1.2.1 Structure and chemical properties of porphycene

Porphycene (**Pc**), a structural isomer of porphyrin, first synthesized by Vogel and his co-workers, demonstrated significant similarities in spectroscopic and photophysical data to the parent porphyrin. Among the porphyrin isomers, **Pc** is the most stable one according to calculations and has received tremendous attention in terms of research, spectroscopic,[36,50,53] and electrochemical[54,55] characterization. Following the laboratory synthesis of **Pc**, other stable porphyrin isomers have been synthesized: hemiporphycene,[31–33] corrphycene,[30,56] and isoporphycene.[34,35] While the higher energy isomers are yet to be synthesized, a specific class of

Pr – the "inverted" or "confused" porphyrins and "neo-confused" porphyrins have also been reported.[57–59] The porphycene structure is an 18 π electron system comprising bipyrrole units linked by ethylene bridges while maintaining the general $C_{20}N_4H_{14}$ formula of porphyrinoids. The **Pc** structure can be rearranged in eight unique ways which ensure the preservation of the "Nitrogen-in" characteristic of the cavity (Figure 1.1). Systematic nomenclature of porphyrinoids follows the [18] porphyrin-($n_1.n_2.n_3.n_4$) pattern, where the content of the square bracket signifies the participating π electrons in the conjugation path and n_i ($0 \leq n_i \leq 4$) denotes the number of the methine groups in each bridging unit, beginning with the highest number and moving toward the next highest one. The parent **Pr** is, therefore, called [18]porphyrin-(1.1.1.1), while porphycene is [18]porphyrin-(2.0.2.0).

Compared to other isomers of **Pr**, free-base unsubstituted **Pc** is the most stable and most studied isomer. The stability has been linked to stronger intramolecular hydrogen bonds in **Pc**, which correlates with shorter distances between nitrogen atoms. When porphycene is complexed with metals, the stability order is reversed; in this case, metal complexes with **Pr** become more stabilized because its square-shaped inner cavity favors the lodging of metal ions.[36] The inner core of the porphycene macrocycle is isolated from the environment with distinctively defined geometry; this sets **Pc** as an ideal model for evaluating the mechanism of intramolecular double hydrogen bond and tautomerization. Worthy of mention is the susceptibility of this well-defined cavity to perturbation resulting from peripheral substitution. Susceptibility of the ring structure to external perturbations offers porphyrin-based systems a 'pre-design' advantage to fit research needs, allowing for systematic modulation of spectral, electronic, and structural properties of the system for desired research purposes. Moreover, the nature and electronic structure of the substituents result in either the strengthening or weakening of the hydrogen bond strength.[52] **Pc** has been useful in both fundamental and applied research.

On the one hand, unique photophysical and spectral properties distinguish **Pcs** as compounds of interest in various applications such as dye-sensitized solar cells,[60] optical sensing,[10] photovoltaics,[61–63] biomimetic models, photocatalysis,[64–68] information storage,[69] photoelectronics, conductors,[70,71] switches,[72] and molecular transistors,[73] liquid crystalline materials,[74] and artificial heme.[75–81] On the other hand, hydrogen bonding properties make them

the subject of fundamental research in intramolecular double hydrogen transfer and cooperativity effect in hydrogen bonds.[52]

1.2.2 Absorption properties of porphycene

The spectroscopic properties of **Pc** are well known, most importantly the electronic absorption and fluorescence properties. The absorption spectrum of **Pc** at a glance is similar to that of parent porphyrin (Figure 1.2); however, differences exist in the intensity and wavelength of absorbed light. Similarly, as in porphyrins, the absorption spectrum of **Pc** is characterized by three bands in the region 500 – 700 nm, which make up the Q (L) bands, and higher energy Soret (B) bands in the region ca. 300 - 400 nm. Electronic transitions in porphyrins have previously been assigned and labeled using the perimeter model.[82–85] The lowest energy transition is L_1, followed by L_2 and higher energy transitions correspond to B_1 and B_2, see Figure 1.2. For porphyrins, the intensity of the Q bands is ~15 times lower than that of the Soret region. However, **Pc** presents a 3:1 intensity ratio for the Soret and Q bands. Relative to **Pr**, red-shifted Q bands are observed for **Pc**, with the shift being larger for L_2. The red-shifted absorption bands of **Pc**, higher absorption coefficient in the red region (relative to **Pr**) of the electromagnetic spectrum (which penetrates deeper into body tissues), high yield of triplet state, and quantum yield of singlet oxygen make porphycenes interesting as photosensitizers in **PDT**.[37,43,86]

Similar to **Pr**, bands L_1 and L_2 constitute the lower energy transitions in **Pc** and are assigned respectively to S_1 and S_2 transitions. The S_1 and S_2 transitions in **Pc** have comparable oscillator strengths and lie closer to each other than in **Pr**.[87,88] Figure 1.3 depicts the difference in the energy gap of HOMO and LUMO orbitals in **Pc** & **Pr**. The energy gap between the two lowest energy HOMO orbitals is smaller than the ΔLUMO in **Pc**. On the other hand, the gap between HOMOs and LUMOs is comparable in **Pr**. While the absorption spectrum of **Pc** exhibits a bathochromic shift in the Q-region, a hypsochromic shift is observed in the Soret, all relative to **Pr**. The absorptivity in **Pc** – specifically in the low energy region records higher intensity contrasting **Pr**. The reverse is the case in the Soret region, where **Pr** has a higher intensity. However, this is partially compensated as a broader Soret band in **Pc**.
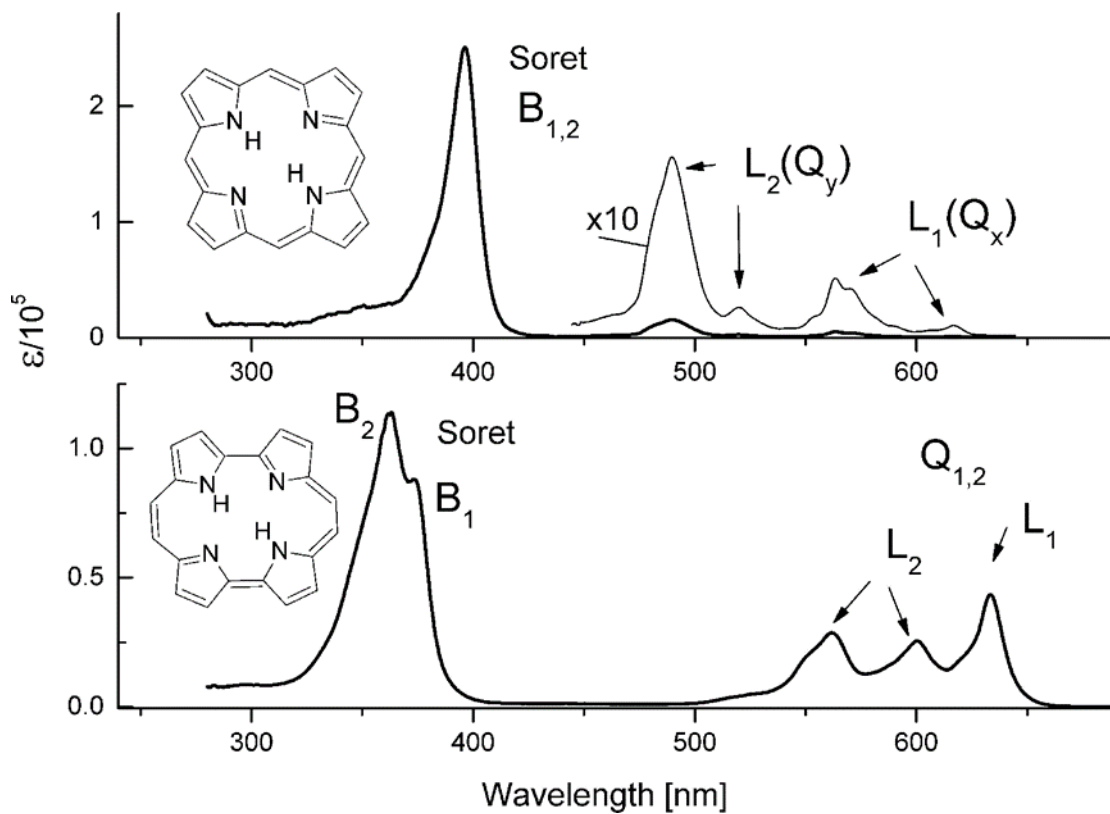
Figure 1.2 Absorption spectra in toluene of porphyrin (top) and porphycene (bottom), measured at 273 K. Reprinted from ref.[36]
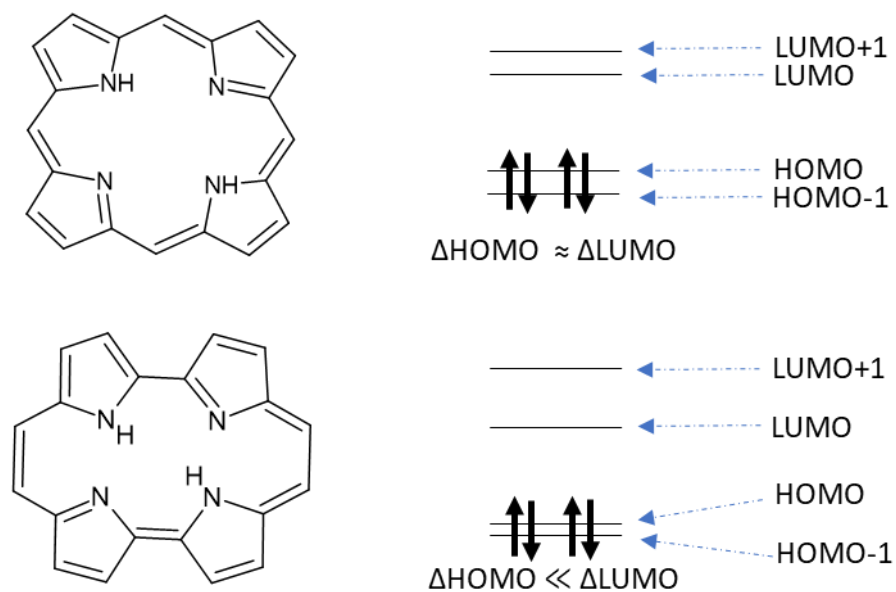
Figure 1.3 Orbital energy level diagram for the two HOMOs and LUMOs in porphyrin (top) and porphycene (bottom).

1.2.3 Photophysics, fluorescence characteristics, and excited state deactivation pathways

Extensive reports on the photophysical properties of **Pc** and their derivatives are contained in the literature.[36,48,50,53] In terms of emissive properties, the fluorescence spectrum of **Pc** takes the same pattern as in **Pr**, characterized by a strong emission at ca. 633 nm with a vibronic component at ~690 nm. **Pc** is a strong emitter with 36 – 49% quantum yield of fluorescence (ϕ_f) depending on the solvent used.[49,89–92] These ϕ_f values are ten times larger than those obtained under the same conditions for **Pr**. However, both compounds have similar fluorescence decay times (about 10 ns). The dissimilarity in absorption spectra of **Pc** and **Pr**, along with higher ϕ_f in **Pc** have their roots in a larger radiative constant for **Pc** ($3.5 \times 10^7 \text{ s}^{-1}$), an order of magnitude higher than that of **Pr** ($4.3 \times 10^6 \text{ s}^{-1}$). This radiative property is also directly linked to **Pc** being classified as a hard chromophore (ΔHOMO << LUMO) in contrast to **Pr**, a soft chromophore (ΔHOMO $\approx$ LUMO), see Figure 1.3. Details on the HOMO-LUMO pairs in **Pc** and **Pr** are discussed in section 1.4 of this thesis.

The first excited singlet state deactivation in **Pc** follows a competitive channel between fluorescence, intersystem crossing (**ISC**), and internal conversion (**IC**) since all three processes have a comparable probability of occurrence.[48,52] Deactivation of a higher S_2 excited state follows three pathways according to Waluk and coworkers:[93,94] (i) ultrafast intramolecular vibrational redistribution, (ii) $S_1 \leftarrow S_2$ internal conversion, and (iii) energy exchange with surrounding solvent resulting in thermal equilibration of the molecule. Relaxation from S_3/S_4 states into S_2/S_1 states followed an ultrafast (50 fs) channel in 9,10,19,20-tetraalkyl substituted porphycenes. Solvent effects play a pivotal role in the deactivation of excited states. For instance, the influence of solvent on the deactivation channels has been reported for 9,10,19,20-tetramethyl and 9,10,19,20-tetrapropyl porphycenes.[95] The fluorescence quantum yields of these compounds which were extremely low in non-viscous solvents, increased with increasing solvent viscosity. In the study, Waluk and co-workers identified the primary deactivation channel as internal conversion. They proposed a model for understanding the excited state deactivation dynamics based on this study and theoretical calculations.[96]

1.2.4 Triplet state and singlet oxygen generation

Intersystem crossing to the triplet state is a viable deactivation channel in porphycenes. The energy of the triplet state in **Pc** has been determined as 10370 cm^{-1} for **Pc**[97,98] and 12870 cm^{-1} in **Pr**.[99,100] Triplet state for **Pc** in non-deaerated solutions lives for 150 ns,[97] in contrast to ~200 µs reported for deaerated solutions. Efficient singlet oxygen generation has, over the years, been a crucial parameter in qualifying photosensitizing agents. The triplet yield for **Pc** in various solvents is estimated to lie between 0.30 and 0.42,[36,101] which is one-half the value observed for **Pr**. However, despite the lower yield in singlet oxygen generation for **Pc** compared to **Pr**, **Pcs** are better sensitizers due to their high absorption coefficient in the red region of the spectrum.

1.2.5 Influence of substitution on porphycenes

The influence of substitution is an essential factor in the studies of these macrocycles. Spectral, photophysical, and photobiological properties of **Pc** are known to be significantly perturbed by peripheral and inner core substitution. Reports of uniquely substituted **Pcs** are documented in detail.[36,52] Nonell and co-workers performed a detailed study on unsymmetrical **Pcs** focusing on 9-substitution.[102–106] The nature, position, and chemical properties of the substituent present a varying degree of perturbation. Relative to the parent **Pc**, a 2,7,12,17-fourfold-symmetric alkyl substitution presents minimal influence on the absorption spectra: a few nanometers (4 - 5 nm) red shift in the low energy bands and about 12 nm in the high energy Soret bands. Waluk's team has demonstrated the changes in absorption for a stepwise addition of *tert*-butyl groups to **Pc** at β (2,7, 12, and 17) positions to obtain mono, di, tri, and tetra *tert*-butyl substituted porphycenes.[107] In Waluk's study, the absorption pattern of the four compounds was nearly identical, except for a few nm red-shift with an increasing number of *tert*-butyl groups. Absorption spectra stayed similar to **Pc** for β-substitution leading to tetramethyl,[108] ethyl,[108] propyl,[48,108] and tetra-*n*-hexylporphycene.[109] Significant changes were, however, observed upon further addition of four substituents at the β' position, resulting in 2,3,6,7,12,14,16,17-octa-alkyl substituted derivatives.

	R$_1$	R$_2$	R$_3$	R$_4$
1:	tBu	H	H	H
2:	tBu	tBu	H	H
3:	tBu	tBu	tBu	H
4:	R$_1$ = R$_2$ = R$_3$ = R$_4$ = tBu
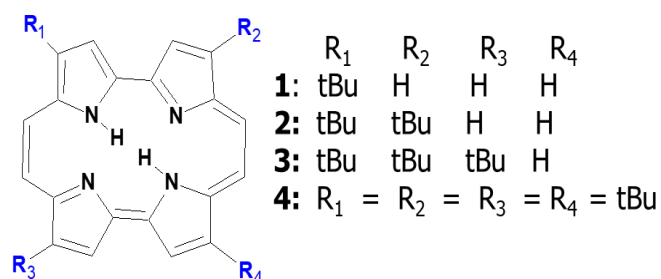
Such changes highlight the significance of the β' position and suggest contributions from both steric and electronic effects. For these derivatives, up to about 30 nm red shift is observed for the Q and Soret bands.[110–112]

Meso (position 9, 10, 19, 20) tetra-substitution with alkyl groups exerts similar red-shifted absorption spectra as the *β, β′*-octa-alkylated **Pc**. However, with a different shape and intensity of the Q bands.[95,113,114] A comparison of the absorption spectra of 9,20-dimethylporphycene and 10,19-dimethyl-2,7-di-*tert*-butylporphycene further spotlights the insensitivity of the *β* position. Both spectra show remarkable similarities in terms of pattern and intensity.[115] The *meso* position presents an attractive opportunity for engineering compounds of interest due to its sensitivity to substitution; researchers have looked into the influence of somewhat neutral, electron donating and accepting moieties located at the *meso* position[50,102,116,117] Aryl-substituted porphycenes have also been extensively studied.[116,118–121] The first synthesis of aryl-functionalized **Pc** was by Nonell's group.[118] From the above reports, the absorption spectra are influenced to a greater extent by *β*-phenyl substitution than *β*-alkyl substitution. A red shift of about 30 nm in the Q region is obtained for *β*-phenyl substitution versus 5 nm in the alkyl counterpart.

Metalloporphycenes: This involves the substitution of two inner hydrogen atoms in free-base porphycene by a metal. Metallation of planar **Pc**s changes their symmetry from C_{2h} to D_{2h}. On the other hand, in **Pr**, metallation results in a symmetry increase from D_{2h} to D_{4h} and a degenerate excited state for the Soret and Q regions. This change in symmetry following metallation is evident as the 'thinning' of the absorption band in metal-base **Pc** compared to its free-base counterparts. Complexes of **Pc** containing nickel,[49,108,122–125] iron (III),[54,75,76,78,81,122,126] zinc,[54,65,74,110,122,124,126,127] cobalt,[54,65,122,128] and copper[122,129–131] have been investigated using UV/vis spectroscopy. Electronic spectroscopy has also been a helpful technique in evaluating the redox processes of **Pc** complexes.[122,123,128,132]

1.3 Studies of isolated porphycene molecules

1.3.1 Porphycenes isolated in gas, glass, and polymer matrices

Nitrogen and argon matrix isolation techniques have been employed to obtain the absorption spectra of **Pc**[88,133–135] and its tetrapropyl,[88] tetra-*tert*-butyl,[135,136] 9-acetoxy-2,7,12,17-tetrapropyl,[51] and dibenzo[137] derivatives. In the study by Waluk and co-workers, the origins and locations of S_1 and S_2 transitions in **Pc** were accurately determined using quantum chemical calculations combined with fluorescence anisotropy, Raman, IR, and neutron scattering experiments.[88,138] The closeness of the two transitions (in contrast to **Pr**) and the exact transition energies of S_0-S_1 and S_0-S_2 could be evaluated from high-resolution spectra obtained in matrices. An analysis of the site structure properties in rare gas matrices of **Pr**,[139,140] **Pc**[141] and its derivative[135] has been performed using molecular dynamics and density functional theory simulations.

1.3.2 Porphycenes isolated in supersonic jets

Studies of porphycene **Pc** isolated in a supersonic jet presented splitting of lines (Figure 1.4) in the fluorescence excitation spectra into doublet features. This splitting was absent when inner hydrogen atoms were substituted with deuterium, confirming coherence of the double hydrogen tunneling process.[142–145] Using laser spectroscopy, jet studies have been reported for 2,7,12,17-tetra-*tert*-butylporphycene[146] and *meso*-substituted (9,10,19,20-tetramethyl and 9,10,19,20-tetrapropyl derivatives) porphycenes.[147]

1.3.3 Porphycenes isolated in helium nanodroplets

Porphycenes studied in helium nanodroplets were characterized by the absence of doublets in fluorescence excitation spectra.[143,144,148] Splitting was, however, observed in the fluorescence spectra, designating the origin of tunneling to be S_0, while the doublet energy in S_1 was nearly degenerate.
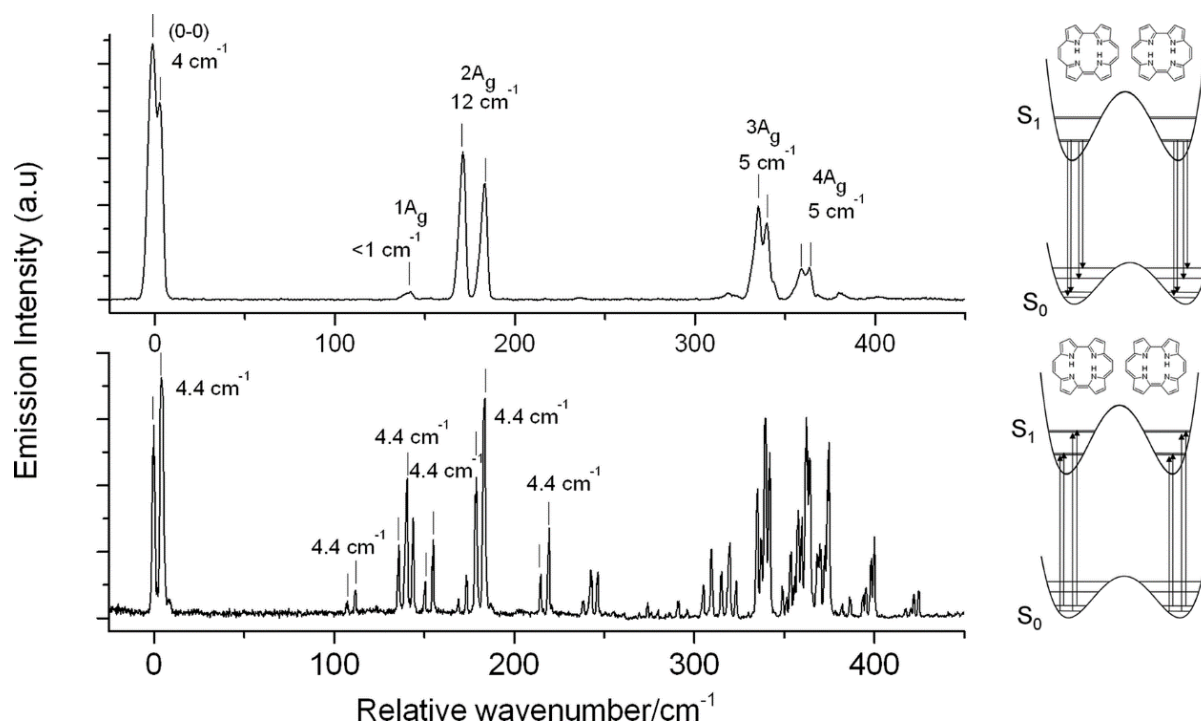
Figure 1.4 Spectra of porphycene isolated in a supersonic jet. Bottom, fluorescence excitation (LIF) and top, fluorescence recorded for excitation into the 0–0 origin band (16 163 cm^{-1}). Tunneling splitting values are presented for selected vibronic levels. Frequencies are given relative to the 0–0 excitation energy. Reprinted from ref.[145]

1.4 Magnetic Circular Dichroism and its interpretation using the Perimeter Model

Magnetic circular dichroism (MCD) spectra of porphycenes are interpreted in terms of the perimeter model of aromatic systems.[82,84,85] The MCD spectrum, intensities, and signs are characterized using the Faraday parameters A, B, and C. In the perimeter model, a system of interest is assumed to be a derivative of an ideal $(CH)_n$ perimeter consisting of $4N+2$ π electrons. This system is subject to perturbations, such as the substitution with heteroatom or bridging effects. These disruptions directly affect the energy splitting of the HOMOs and LUMOs of studied systems. Moreover, when a specific form of perturbation is applied to different positions of the same perimeter, varying degrees of the energy splitting patterns in the HOMOs and LUMOs are observed (Figure 1.5). MCD spectra have been reported for parent **Pc** and its derivatives.[49,95]
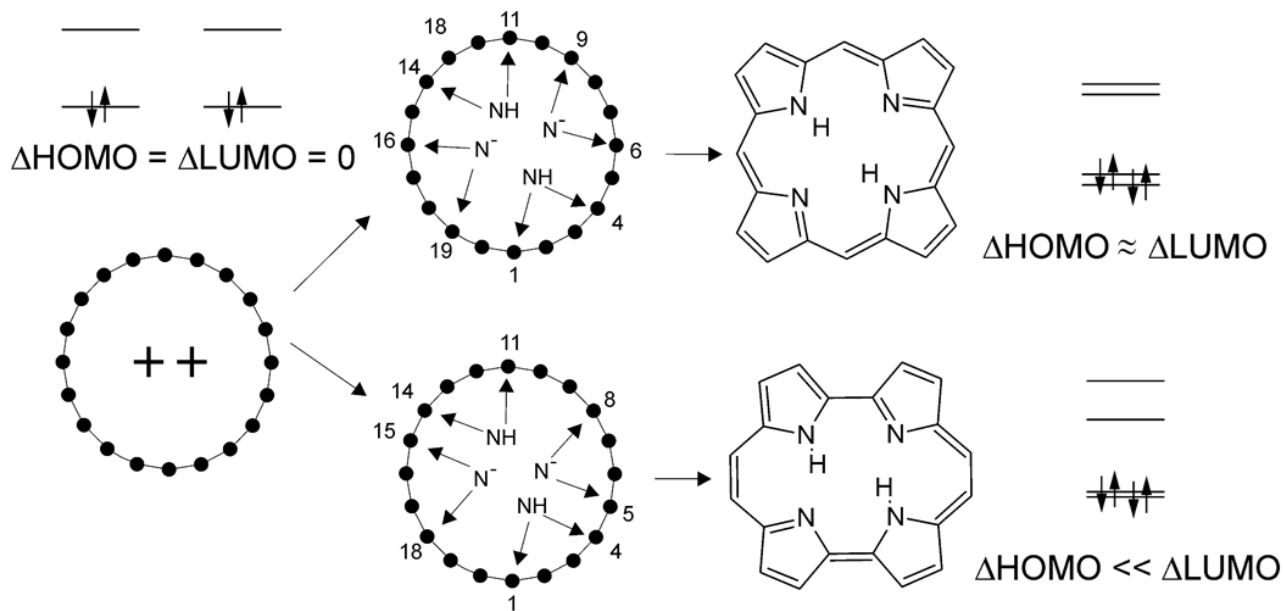
Figure 1.5 Derivations of porphyrin and porphycene from an ideal $C_{20}H_{20}^{2+}$ perimeter and the resulting energy splitting of the HOMO and LUMO. Reprinted from ref.[49]

Consider an ideal perimeter where there is a degeneracy between each pair of HUMO and LUMO such that $\Delta HOMO = \Delta LUMO$. In analyzing the Soret and Q electronic transitions in porphyrinoids, the energy splitting of the HOMO and LUMO pairs is of utmost relevance. This energy splitting (Figure 1.5) between the two pairs of orbitals can either result in the so-called "soft" or "hard" chromophore, depending on the magnitude of the splitting. Chromophores in the "hard" category can either be positive-hard ($\Delta HOMO \gg \Delta LUMO$) or negative-hard ($\Delta HOMO \ll \Delta LUMO$). Therefore, porphyrin with energy difference $\Delta HOMO \approx \Delta LUMO$ is classified as a "soft"[52,89] chromophore, whereas porphycene, a negative "hard"[49,89] chromophore, has $\Delta HOMO \ll \Delta LUMO$. The presence of even very 'weak' perturbations exerts a significant influence on the signs and magnitude of the MCD spectra and the relative absorption intensities of the Q and Soret bands in "soft" chromophores, hence their classification as "soft." In contrast, the hard chromophores, where there is a significant difference in energy splitting between the HOMO and LUMO pairs, and thus, perturbations have to be strong enough to lift this difference for the changes in the MCD spectra to be observed. Therefore, this 'hard' property in porphycenes is observed as similarities in the recorded absorption and MCD spectra of different porphycene derivatives because substitution in porphycenes (being hard chromophores) results in small effects in their absorption patterns and MCD.[49,89]

1.5 Tautomerization in Porphycenes

Free base unsubstituted porphycene can exist in three unique tautomeric forms: *trans*, *cis-1*, and *cis-2*, with each form being doubly degenerate (Figure 1.6). The *trans* form is predicted to be the most stable specie, while the *cis-2* form lies 30 kcal/mol higher and the least stable. The well-isolated core of the **Pc** structure allows proton transfers around and between the four nitrogen atoms, giving rise to tautomerization, the so-called double hydrogen transfer in **Pc**s. Studies of tautomerization in porphycenes have been performed in the condensed phase[149,150] and at a single molecule level.[145,151–153] Symmetric double minimum property (Figure 1.7) distinguishes **Pc**s as models for studying tunneling effects in hydrogen. While it is well known that substitution influences tautomeric properties, the *meso*-substituted porphycenes have been proposed as attractive models for studies of hydrogen bonding properties due to the sensitivity of this position to perturbation.[95] The *meso* position, in particular, offers the possibility of studying cooperativity between hydrogen bonds in the same molecule, mode selectivity, and coupling between modes.

Double hydrogen transfer in symmetric porphycenes is described in terms of the symmetric double minimum (Figure 1.7), with tunneling being the primary route for the transfer process.[154] A minimum activation energy of 32 kJ/mol is required to overcome the energy barrier.[155] Quantum tunneling of the two protons can be concerted or stepwise, depending on the study media.[154] Stronger hydrogen bonds and shorter N-N distances (2.63 Å) in **Pc** lead to faster rates of tautomerization at RT relative to **Pr** (N-N distance: 2.90 Å). The shape, dimensions, and substitution patterns of these molecules have been demonstrated to impact significantly the tautomerization rates. Thus, the rectangular shape of the **Pc** inner cavity (which places the NH⋯ N atoms in a nearly linear fashion) and shorter N-N distances favor faster translation of hydrogen atoms within the internal nitrogen atoms.

Studies on the tautomeric properties of **Pc** revealed fast tautomerization rates even at lower temperatures, contrasting the "freezing" of hydrogen atoms observed for **Pr** in the ground state.[156] Exceptionally fast tautomeric rates were also observed for *β*-tetrasubstituted and *meso*-tetra substituted **Pc** using ^{15}N CPMAS and ^{13}C mass spectroscopies.[157]

trans (0.0 kcal/mol)   *cis1* (~2 kcal/mol)   *cis2* (~30 kcal/mol)
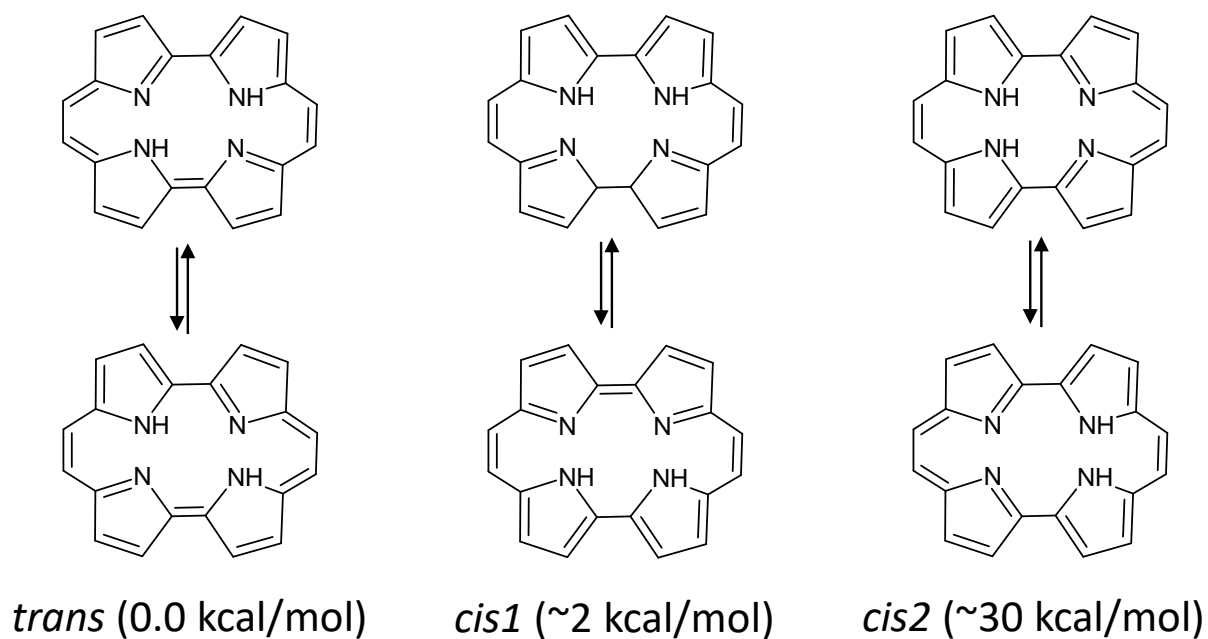
Figure 1.6 Pair-wise equivalent tautomeric forms of porphycene and their relative energies.
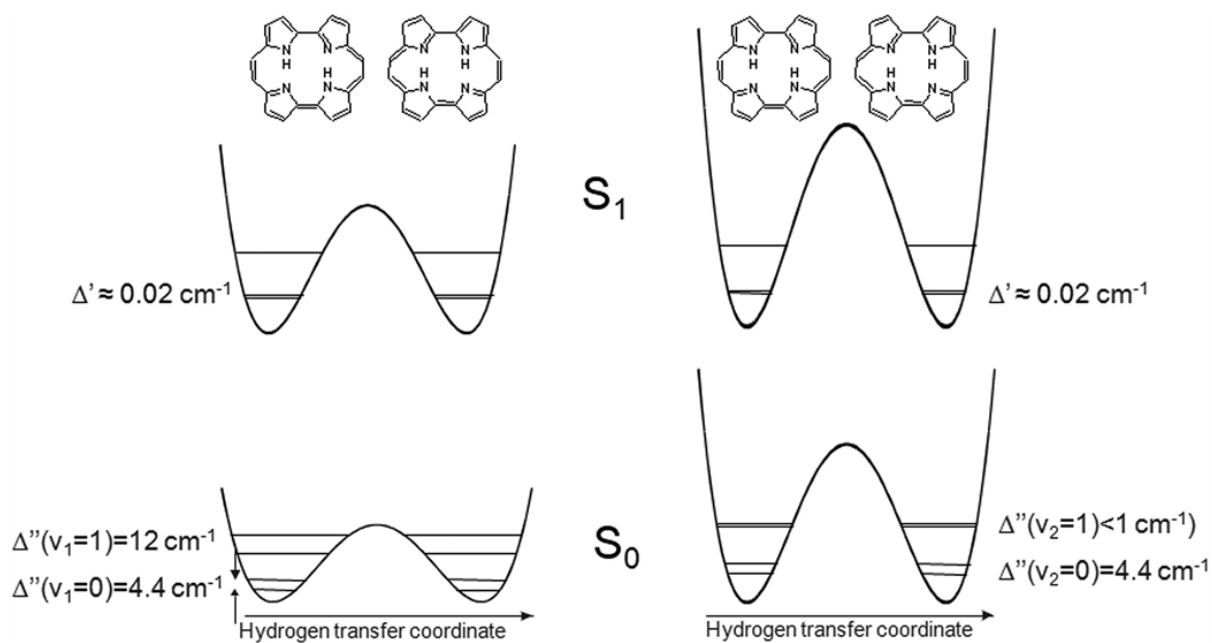
Figure 1.7 Left and right: crossings of the potential energy surface along two different vibrational coordinates. Reprinted from ref.[36]

The mechanism of double proton transfer in **Pc** has been determined to be concerted,[155,158,159] while **Pr,** on the other hand, follows a stepwise thermally activated proton transfer pattern. Further studies by Waluk and co-workers revealed a multidimensional tautomerization pathway that is vibrational mode dependent. Excitation of specific vibrational modes was either inhibitory or acceleratory to the tunneling process.[104,145]

The symmetric double minimum character is either maintained or destroyed during peripheral substitution in porphycene.[104,160] Since **Pc** exists in different tautomeric forms, the assignment of transitions to specific tautomeric forms and energy levels can be tricky, especially in the unsymmetrically substituted **Pc**. Assignment of these bands in symmetric free-base, unsubstituted **Pc** is not trivial either. However, with the help of MCD and anisotropy, these transitions have been accurately assigned.[49,88] The perimeter model employed in the analysis of the HOMO-LUMO splitting patterns in **Pc** is exceptionally useful in describing signs and patterns obtained from magnetic circular dichroism spectra. Relative intensities in absorption are also accurately predicted with the help of the perimeter model and subsequently confirmed by experiments in porphycene, hemiporphycene, and corrphycene.[49,161,162] Therefore, the following section describes the methods so far employed in the determination of rates of tautomerization.

1.5.1 Methods of studying tautomerization: NMR

NMR experiments have been employed in tautomeric studies of porphyrins in an ensemble of molecules in solution[163–165] and the solid phase.[166–168] For porphyrins, studies using deuterated and tritium forms while varying the temperature reveal the tautomeric pathway is stepwise in the ground electronic state. Analysis of the double hydrogen transfer process was described (Figure 1.8) as follows: thermal activation is required for the tunneling of the first hydrogen atom, which leads to the *cis* form. A minimum energy (E_m) equivalent to 24.0 kJ mol^{-1} is sufficient for the tunneling process. This minimum tunneling energy consists of the summation of energy required for the rearrangement of the molecular structure and the energy gap between the *trans* and *cis* forms. Moving from the *cis* structure, two routes are possible. (i) a transfer of the second hydrogen leading to the other *trans* form or (ii) a return of the system to the initial *trans* form. Langer et al.[155] determined the rate constants of hydrogen transfer in crystalline porphycene using ^{15}N CPMAS NMR. The values were determined to fall between 4.24×10^6 s^{-1} and 3.66×10^8 s^{-1} when

monitored at 228 K and 355 K, respectively. Tautomerization in **Pc** is established to follow a concerted process indicated by the strong coupling of both hydrogen atoms. Both **Pc** and **Pr** exhibit a single NMR ^{1}H peak at elevated temperatures; however, a gradual lowering of the temperature results in broadening the peak and subsequent splitting into two for **Pr**, indicating "locking" of the tautomerization process. In **Pc**, however, four narrow peaks were observed when the temperature was lowered below 213 K.
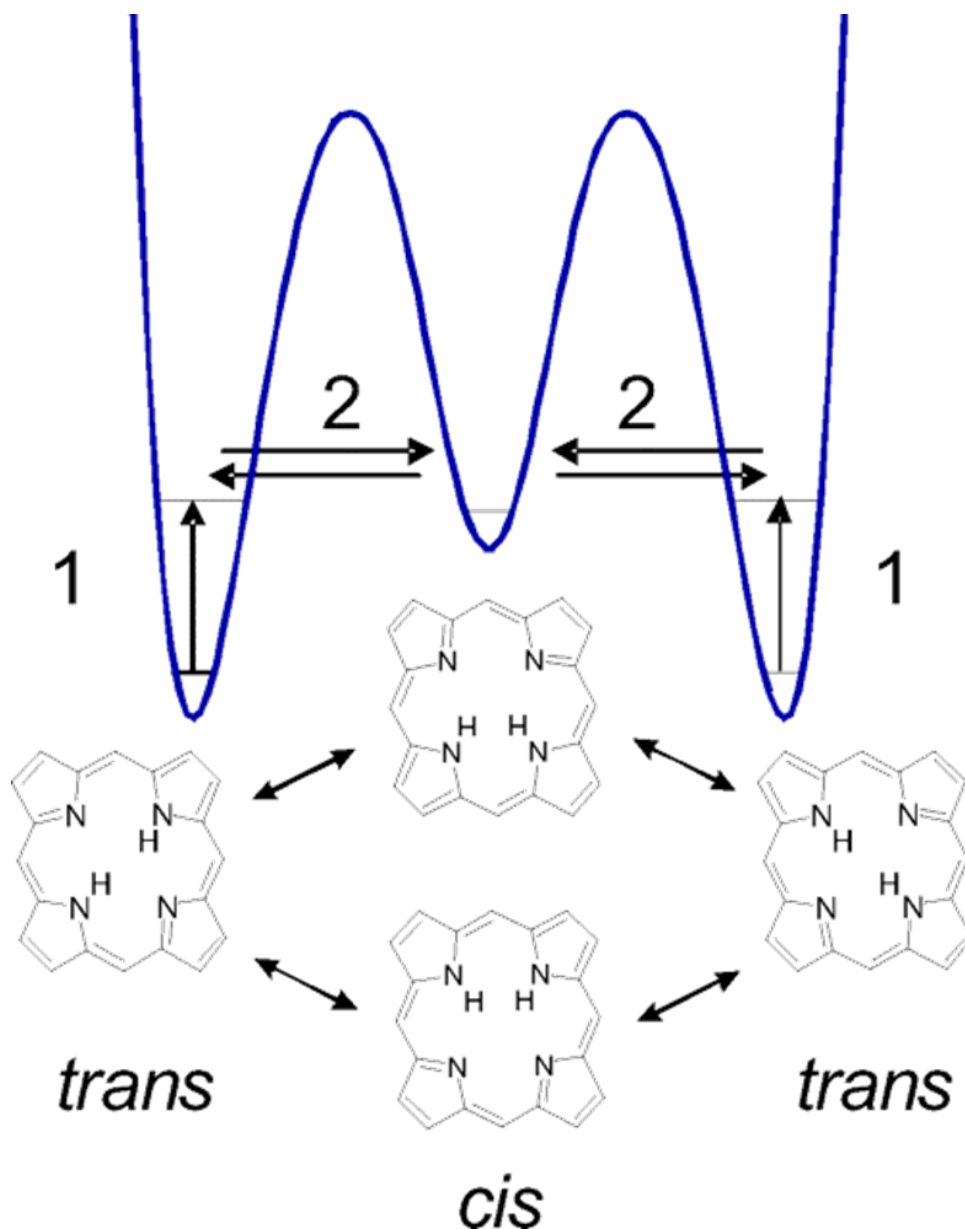
Figure 1.8 Ground-state tautomerization in porphyrin indicating a stepwise process. Step 1 corresponds to thermal activation, while step 2 corresponds to a single hydrogen transfer via tunneling. Reprinted from ref.[169]

1.5.2 Tautomerization in the condensed phase

Tautomerization studies of porphycenes in the condensed phase are well documented following studies by Waluk and co-workers.[93,95,104,115,149,154,160,170–173] In the early nineties,[49] Waluk and coworkers observed fluorescence depolarization in **Pc**; it was surmised that a fast-intramolecular double proton transfer existed in the lowest excited singlet state. The rate of double proton transfer in **Pc** was extremely rapid in the ground and excited state.[49] It was further determined by Waluk's group that the direction of the transition moment changes upon tautomerization due to reflection in the plane perpendicular to the molecular plane. They suggested a procedure for evaluating rates of *trans-trans* tautomerization in the excited state and, thus, the absolute direction of the transition moment.[171] This procedure was further confirmed after obtaining similar values for α (Figure 1.9) regardless of the technique used: steady state or time-resolved fluorescence anisotropy, single molecule spectroscopy using polarized light,[151] and ultrafast pump-probe absorption studies.[172] On the basis of the change in the direction of the transition moment during tautomerization, an even more general procedure that allows for the determination of tautomerization rates in both ground and excited states was also proposed. This procedure has its basis in an ultrafast polarized femtosecond pulse, which excites the sample, accompanied by a delayed-polarized probe pulse, and has been employed to ascertain rates of double hydrogen transfer in **Pc** and several derivatives, with tautomerization rates ranging from tens of fs to hundreds of ps.[104,149,160,172,174,175] Femtosecond transient absorption studies performed at varying temperatures yielded the tautomerization rates for **Pc** and its tetra-*tert*-butyl derivative.[154] Femtosecond techniques revealed that tautomerization followed three unique processes: (i) "deep" tunneling, (ii) tunneling via activation of specific vibrational modes, and (iii) high-energy activated route.
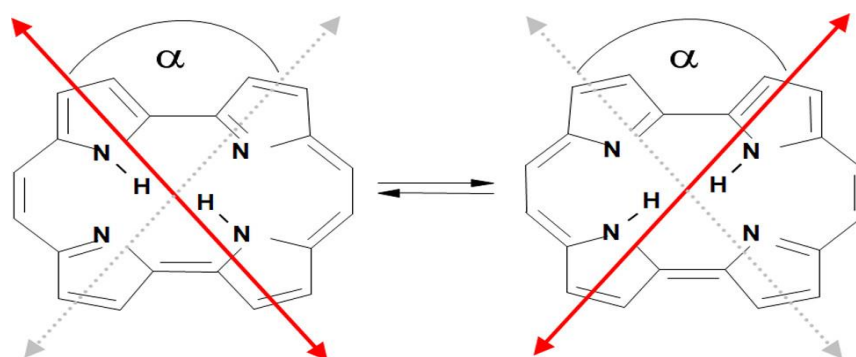
Figure 1.9 Effect of double hydrogen transfer on the direction of the S_0–S_1 transition moment in porphycene. Reprinted from ref.[36]
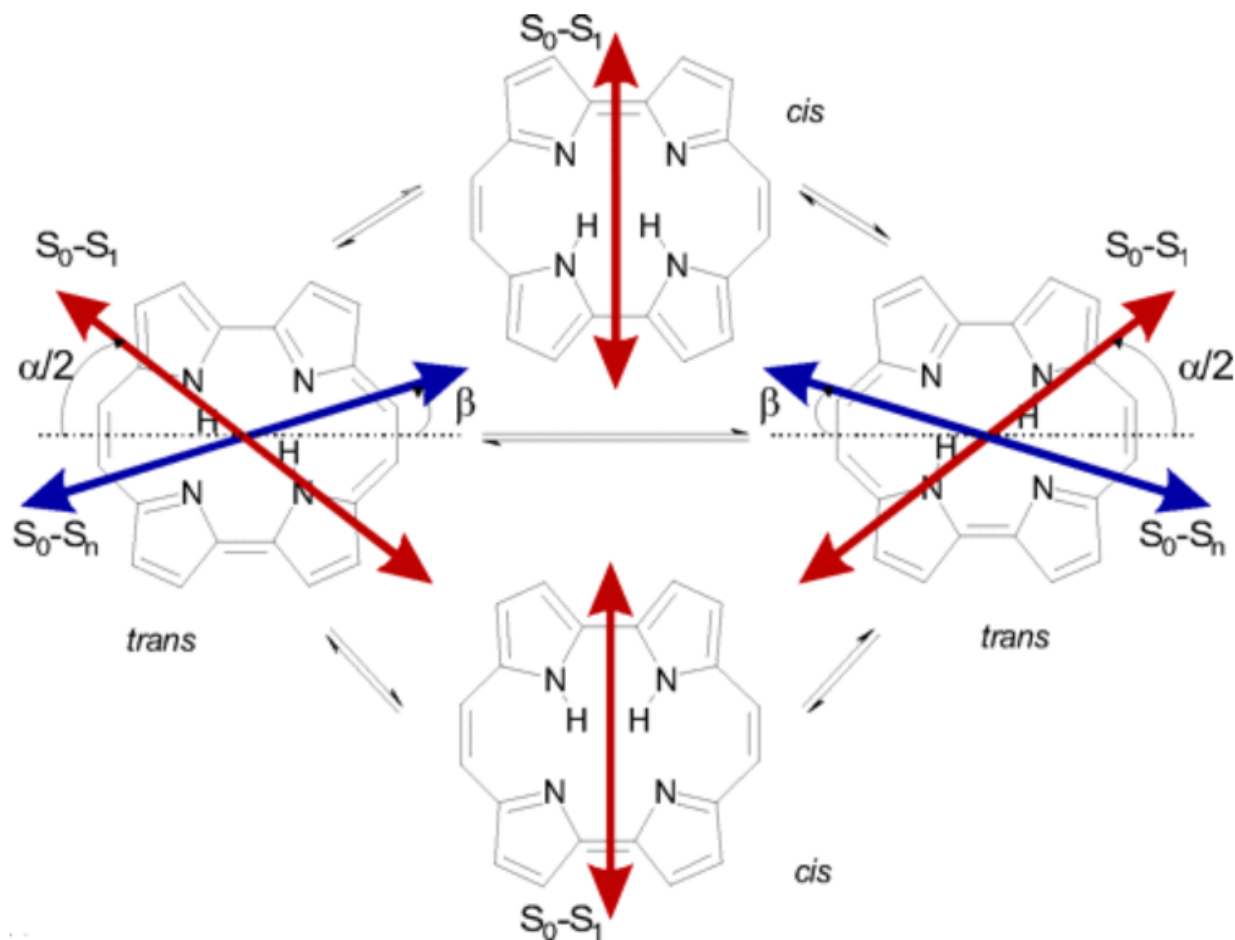
Figure 1.10 Trans and cis tautomeric forms of porphycene and changes of transition moment directions accompanying trans−trans conversion. See the text for details. Reprinted from ref.[169]

1.5.3 Tautomerization in isolated single molecules probed by fluorescence, Raman, and scanning probe microscopy studies

The first investigation of tautomerization in an isolated single molecule of porphycene was performed using confocal fluorescence microscopy.[151] The study exploits the transition moment change in **Pc** upon S_0-S_1 transition as the two *trans* tautomeric forms of **Pc** are known to exhibit an angle of 70-80 degrees (Figure 1.9 -Figure 1.10). Analysis of spatial fluorescence patterns excited by azimuthally polarized light revealed a double-lobe and a ring-shaped fluorescence pattern (Figure 1.11). The ring-shaped fluorescence pattern is explained on the basis of an angle of ~72° existing between two equivalent transition dipole moments. The two transition moments simulate equally populated *trans* tautomeric forms in a single **Pc** molecule.
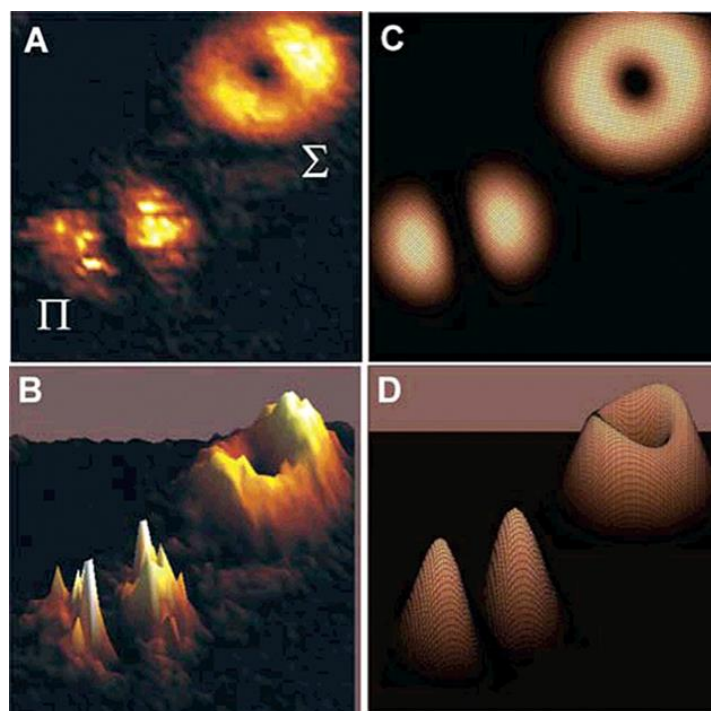
Figure 1.11 (A) Confocal fluorescence images of single porphycene molecules embedded in a PMMA polymer film showing two typical fluorescence patterns: a ring pattern for molecule Σ and a double-lobe pattern for molecule Π. (B) 3D plot of (A). (C) Simulation assuming two differently oriented transition dipole moments for the trans-species forming an angle of 72° (D) 3D plot of (C). Reprinted from ref.[151]
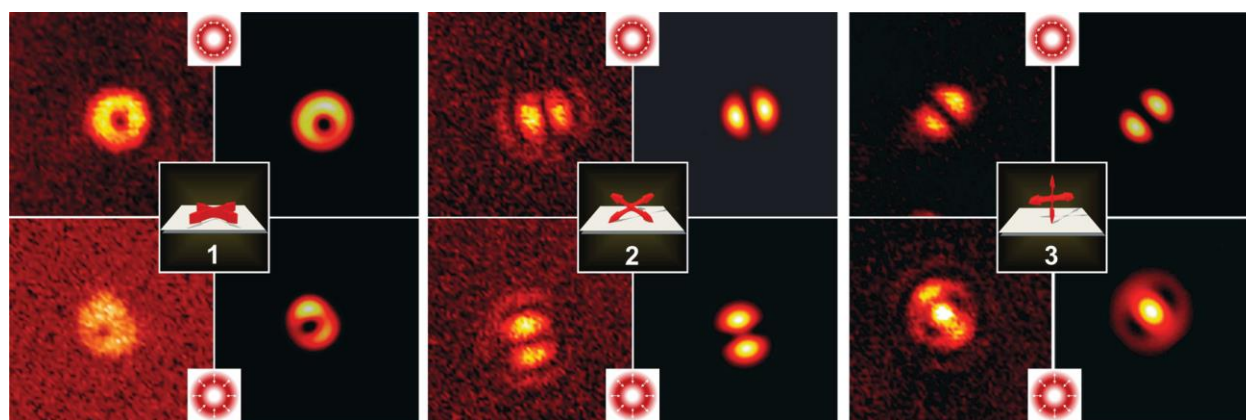
*Figure 1.12 Confocal fluorescence images of 2,7,12,17-tetra-tert-butylporphycene (**ttPc**). Three single molecules of differently oriented **ttPc** embedded in PMMA film. Experiment (left) and simulation (right): (1) Molecule lying flat on the surface, (2,3) molecules oriented perpendicular to the molecular plane. Reprinted from ref.[152]*

On the other hand, the difference in the spatial orientation of a molecule results in different fluorescence patterns. This idea has been employed in the determination of orientation patterns of single porphycene molecules (Figure 1.12).[152] Therefore, the double-lobe fluorescence pattern in Figure 1.11 is explained based on the mode of the excitation beam and the 3D spatial placement of the molecule.

Surface-enhanced Resonance Raman Spectroscopy (SERRS) is also a technique that has found profound use in single-molecule studies of **Pc**: SERRS spectra were recorded for **Pc** layered on silver and gold nanostructures.[176,177] A recent study revealed inhibitory effects on the observation of SERRS spectra with the increasing number of bulky substituents.[178] The study further confirms the role substituting species play on not just the properties of porphycenes but also the ability of these compounds to be observed in certain studies, such as SERRS, especially at the single-molecule level.

Scanning probe microscopy for single molecule studies of **Pc** is another useful technique for probing tautomerization in **Pc**s. Kumagai and others discussed the controlled hydrogen transfer process at a single-molecule level.[72] Rates of tautomerization of porphycene were established via STM scan. The fascinating aspect of this study was the possibility of modulating the rate of proton exchange between the *cis1-cis1* tautomers, opening up interesting research into single molecular switches functioning on the basis of tautomerization. It is important to note that the surrounding environment, such as an interacting surface, significantly affects which tautomeric form is energetically favored and thus stabilized. For **Pc** adsorbed on a Cu (110) surface, the *cis-1* form is the stable specie. However, on a Cu (111) surface, the *trans* form is the most stable.[145,179]

1.6 Applications of Porphycenes

Relative to other isomers of porphyrins, porphycenes have received tremendous attention. Since the first synthesis, detailed studies are available in the literature on the photophysics[48,50,53] of porphycenes. Porphycene was observed to possess a higher extinction coefficient than porphyrin in regions above 620 nm, where living tissues are relatively translucent. Upon illumination, efficient generation of singlet oxygen, useful in photodynamic therapy, was observed for porphycenes, which led to the proposition and subsequent use of porphycenes as sensitizers in phototherapy.[37] Successful use of porphycene derivatives in photodynamic therapy has been reported.[29,37,38,40,43,44,86,180,181]

In addition, the application of porphycenes in understanding tautomeric equilibria, intramolecular hydrogen transfer, cooperativity in intramolecular hydrogen bonds, and design of molecular switches,[72] photosynthetic and light harvesting materials, photovoltaics and other applications is a pointer to the fact that detailed understanding of their photophysics, tautomerization mechanism, and photostability cannot be overemphasized.

1.6.1 Photodynamic therapy (PDT)

Cancer is the leading cause of death worldwide and a primary global public health concern. The International Agency for Research on Cancer reports data on global cancer burden as contained in GLOBOCAN 2020.[182,183] Their research gives insight into the incidence and mortality for thirty-six different cancers (excluding nonmelanoma skin cancer) in 185 countries of the world. Estimated new cancer cases worldwide are placed at 18.1 million, and a whopping 9.9 million deaths occurred in 2020 due to cancer.[182,183] It is important to note that this data excludes children. It is projected that in 2040, global cancer will increase to 28.4 million, according to GLOBOCAN. Given the reported number of current and projected cancer occurrences and deaths, it is imperative that the implementation of cancer prevention strategies and curative measures be prioritized. Methods of treating cancer can depend on the type, location, and stage of the cancer. These factors determine which method is eventually employed. Cancer treatment methods range from biomarker testing, chemotherapy, hormone therapy, hyperthermia, immunotherapy, and photodynamic therapy, among others. Photodynamic therapy is a renowned treatment model for cancer.

Photodynamic therapy (**PDT**) is a clinically approved cancer treatment modality that involves using visible light and molecular oxygen in the presence of a photosensitizer to photo-destruct tumor cells via cytotoxic reactions instigated by reactive oxygen species (**ROS**). The **ROS** are made up of hydroxyl radicals, superoxide radicals, singlet oxygen, and hydrogen peroxide, which incite a series of reactions with photoexcited photosensitizer and ultimately result in cell death.[184] The 'photodynamic effect' was first reported by Raab[185] in 1900 and Von[186] four years later. In their report, Raab and Von demonstrated the possibility of cell death via photosensitization of specific fluorophores. Then, in 1948, the affinity of porphyrins and metalloporphyrins to growing tissues was first reported by Figge and co-workers.[187,188] Their data suggested the preferential accumulation of porphyrins in embryonic and neoplastic tissues. In addition, red fluorescence was

observed in mice that were injected with porphyrins and activated with UV light. This finding birthed the era of tumor detection with porphyrinoids. Following these reports, the successful use of crude hematoporphyrin derivative for cancer detection in cancer patients has been documented.[189] Moreover, experiments by Lipson and co-workers indicated more significant sensitizing effects with increased amounts of the hematoporphyrin derivative (**HPD**) injections at the expense of tissue selectivity.[190,191] Schwartz, in his experiments, discovered that the crude hematoporphyrin comprising a mixture of monomers, dimers, and oligomers was more effective in tumor localization than pure hematoporphyrin (**HP**). Gregorie reported further use of **HPD** for tumor detection in patients.[192,193] After confirming the selective uptake and retention of **HP**, photodynamic destruction effects of **HP** were observed on glioma cells in rats following administration of **HP** and activation by light.[194] Dougherty and his group at the Roswell Park Cancer Institute dedicated a series of studies on **HPD** and its lethal effect on tumors; they identified singlet oxygen as the toxic substance responsible for cell death during **PDT**, their research findings led to the approval of **PDT** as a cancer treatment procedure by the U.S. Food and Drug Administration.[195–198] So far, **PDT** has been employed in treating lung cancer,[199] skin and esophageal cancer,[21] arthritis,[184] as well as cancer of the larynx.[200] **PDT** and its results depend primarily on selectivity, specificity, and proper photosensitizer localization.[25] This speaks to the importance of the choice of specific photosensitizer. Moreover, the influence of the nature of cells and conditions of illumination cannot be overlooked when considering the potential outcome of **PDT**.

Specific characteristics make an efficient photosensitizer in **PDT**, and these properties include:[201]

1. high absorptivity in the region between 650 and 850 nm;
2. high quantum yields of the triplet state and singlet oxygen generation;
3. the desired compound has to be stable and of known composition;
4. low dark toxicity;
5. specificity (preferential retention or localization by target cells);
6. must be readily soluble in body fluids;
7. availability.

Porphyrinoids exhibit these properties, with porphycenes also demonstrating tremendous potential as sensitizers. The evidenced use of porphycenes in **PDT** is abundant in the literature.[37,38,202] Moreover, photodynamic inactivation of microorganisms has been reported for *meso*-tetrasubstituted porphycenes.[55,203] Specifically, enhanced interaction with studied cells was observed with amino substitution - an advantage due to the amino group's sensitivity to biological applications. This sensitivity offers the possibility of easily protonating the amino substituent, resulting in better interactions with biological tissues. In another study, the antimicrobial property is reported for *β*-tetra-methoxyporphycene.[45]

1.6.1.1 The process of photodynamic therapy

The processes leading to cell death via photodynamic action can follow either of the two routes expressed in Figure 1.13. When a photosensitizer (**PS**) is excited with visible light of suitable wavelength, the **PS** can either fluoresce (useful for localization or diagnosis of tumor cells), or it can participate in chemical reactions leading to cell death. These reactions can occur via two pathways:[204,205]
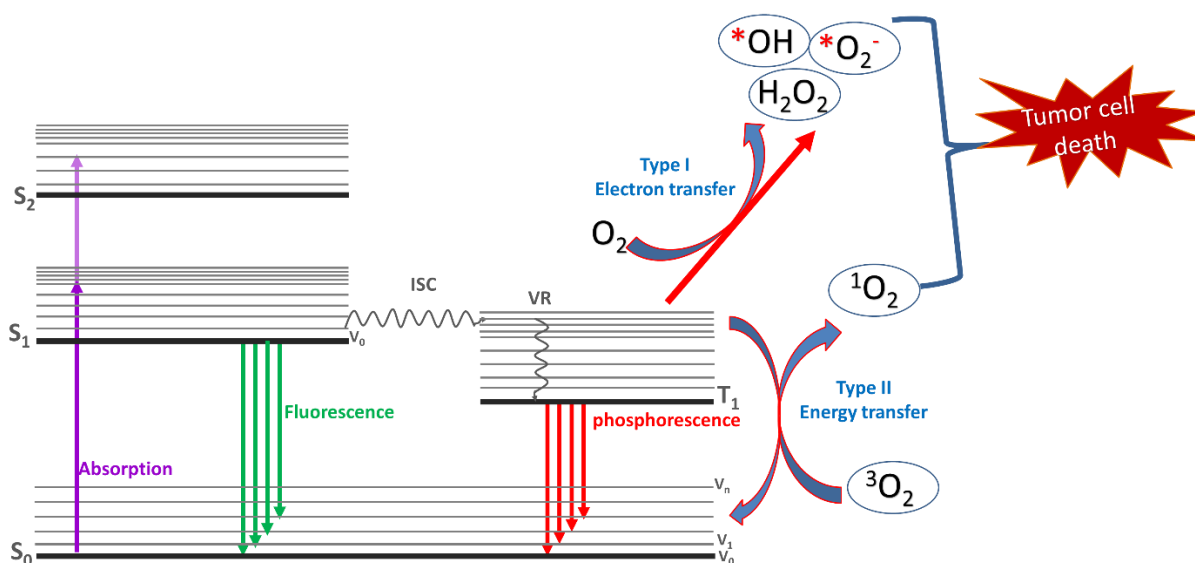
Figure 1.13 Diagram showing the PDT Process and the two types of photodynamic cell death

Type I: In this process, the ground state electron is excited to the first excited state, which then undergoes **ISC** to the first excited triplet state, during which it interacts with oxygen in the environment to generate reactive oxygen species (**ROS**) - radical anion oxygen, hydroxy radical, superoxide anions, and hydrogen peroxide. The **ROS** readily penetrate biological membranes while reacting with a photosensitizer, resulting in the annihilation of tumor cells.

Type II: This process involves an energy transfer from the sensitizer to molecular oxygen. Here, an excited sensitizer in the excited triplet state undergoes an energy-transfer-type reaction to molecular oxygen ($^3O_2$), thereby generating reactive singlet oxygen ($^1O_2$), which results in damage to cancerous cells. Since singlet oxygen plays a vital role in cell death, efficient generation of singlet oxygen is a determinant property of a **PS**.

1.6.2 Fundamental research

The application of porphycenes in the fundamental study of intramolecular hydrogen bonding, single or double hydrogen transfer processes, and tautomerization has been discussed in detail in section 1.5

1.7 Photostability

Photochemical stability, alternatively known as photostability, is one of the most important properties that establish the unique application of dyes. The photostability of a dye is its ability to withstand a series of excitations and relaxation back to the electronic ground state without undergoing irreversible damage. The loss of initial optical properties following cycles of excitation-relaxation process is termed photobleaching or photodegradation.[206] There is a clear distinction between photobleaching, blinking (alternation between radiative and dark states), and quenching (the non-radiative relaxation of a dye molecule to the ground state during the excited state lifetime).[207] The dye structure, study media, and illumination power are essential parameters that determine the photochemical stability of investigated dyes. Depending on the excited state lifetime of the studied dye, photobleaching could occur after a few excitation events or after many of them. The desired degree of photostability is a factor in the application of interest. For instance, high photostability of dyes is required in applications such as dye-sensitized photovoltaic cells,[208] whereas efficient photobleaching or low photostability is desired in applications involving

treatment of pollutants, fluorescence loss in photobleaching (FLIP) and fluorescence recovery after photobleaching (FRAP).[209] On the other hand, modulated stability is required in the case of PDT.[210]

When studying photochemical stability, understanding the behavior of the fluorophore, surrounding media, and illuminating power is critical to quantitatively determining photobleaching. Different methods of characterizing photobleaching have been described to include:

- Determination of 'death number' as the mean number of photons emitted by a fluorophore till it is photobleached;
- Photobleaching half-life: the time period between peak fluorescence event and the time to half of the maximum intensity;
- The amount of pump energy absorbed by a fluorophore before its fluorescence intensity is half the initial value.

These methods of characterizing photobleaching are somewhat unreliable, given a significant concern that the photobleaching process and kinetics are not unimolecular, nor is it a one-step process. Most importantly, it does not always follow a mono-exponential kinetics. Therefore, following the IUPAC recommended definition for photochemical processes, photostability/photobleaching can be expressed in terms of the photodegradation quantum yield of the studied dye upon exposure to UV/Vis light, equation (1.1):

$$\text{photodegradation quantum yield } (\phi_b) = \frac{\text{number of photobleached molecules}}{\text{total number of photons absorbed}} \quad (1.1)$$

While performing photodegradation quantum yield experiments, it is essential to ensure the uniform illumination of the whole sample volume, achieved mainly by constant stirring during the illumination process. To accurately determine the yield of photobleaching, the power of the light used must be known. Then, by monitoring the absorbance as a function of time combined with some mathematical manipulation, accurate yields of photobleaching can be determined. Details of this determination are described in section 4.2.6

1.7.1 Mechanisms of photodegradation

Processes leading to photobleaching consist of multi-step, complex reactions which depend on specific dyes and excitation conditions. These processes could follow either the oxygen-dependent pathway or the oxygen-independent pathway.

1.7.1.1 Oxygen-dependent pathway

The oxygen-dependent pathway involves a reaction between an excited fluorophore, molecular oxygen, or reactive oxygen species (**ROS**). The reactive oxygen species consisting of peroxides, superoxides, hydroxyl radicals, and singlet oxygen react with excited dye systems, resulting in photobleaching of the fluorophore. The process involves an excited fluorophore in the first excited singlet state undergoing intersystem crossing to an excited triplet state, where it sensitizes ground state molecular oxygen, $^3O_2$ ($^3\Sigma_g$), via energy transfer resulting in ROS. The sensitization process results in a highly reactive oxygen species – the singlet oxygen, $^1O_2$ ($^1\Delta_g$). The generated singlet oxygen participates in photochemical processes, resulting in an irreversible loss of fluorescence in a previously fluorescing dye.[211] The role of oxygen in photobleaching is a multi-dimensional process: (i) quenching of the triplet state, which directly enhances photostability, (ii) direct oxidation of the dye or generation of radical oxygen species, which accelerates photobleaching. It is, therefore, intuitive to assume that the removal of oxygen in the reaction system could enhance photostability, but this is not always the case. For instance, oxygen-filled solutions of zinc porphyrins exhibited ten times higher photostability compared to degassed ones.[212] In a separate report, the removal of oxygen from the reacting medium enhanced photostability in cyanine dyes,[213] and for fluorine compounds.[214] Therefore, the absence or presence of oxygen in the system does not absolutely speak to the photostability or the lack of it in specific dyes. Other ways of improving photostability are via the introduction of self-healing[215] or protective agents such as cyclooctatetraene (COT)[216] during the design of the fluorophore.

1.7.1.2 Oxygen-independent pathway

Evidence of deoxygenation resulting in not improved photostability suggests another pathway toward photobleaching other than the oxygen-mediated route.[217] It is well known that the triplet state plays an acceleratory role in the photobleaching process. Eliminating the triplet, however,

does not always enhance photostability.[217] The oxygen-independent photobleaching pathway involves the photoionization of excited fluorophores to give reactive intermediates, such as free radicals, a process more efficient in polar media.

1.7.1.3 Photostability in porphyrins and porphycenes

While there exist extensive studies on the photochemical stability of porphyrins, porphycenes, on the other hand, have not received quite as much attention. Studies on the photostability of porphyrins reveal that the photobleaching process occurs via oxidation with singlet oxygen species.[210,218] The mechanisms of photobleaching characteristic of porphyrinoids can be classified as:

- Photo-modification: here, illumination results in a change of fluorescence intensity or absorbance while retaining the main structure of the chromophore
- Photodestruction or total photobleaching: illuminating the chromophore results in the breakage of the dye structure into smaller fragments.

Sequel to the known use of porphycenes as efficient sensitizers in **PDT**, the need to investigate the photostability of **Pc** cannot be overemphasized, particularly for the new series of porphycenes presented in this study. At a single molecular level, enhanced photostability is reported for porphycenes substituted with bulky *tert*-butyl groups.[153] The higher stability is explained as a screening effect from the bulky *t*-butyl groups, and it speaks to the influence of substitution on photostability. Therefore, one could wonder what the degree of photostability will be in the case of porphycenes substituted with strong electron donating and withdrawing groups like the ones presented in this study. Similarly, decreased efficiency of photobleaching was observed for single molecule **Pc** immobilized on metal nanoparticles.[177] Temocene, a porphycene match of temoporfin, exhibited higher photostability and efficiency in tumor cell localization compared to temoporfin.[29] Photooxidative properties of *meso*-sulfonatoporphycenes have been studied.[219] The study revealed high photocatalytic response and photostability in disulfonated porphycene relative to tetrakis(sulfonatophenyl)porphyrin (TPPS). While photobleaching in porphyrins has been a subject of interest for many researchers, not much has focused on porphycenes. In particular, no comparison has been made on the photostability between derivatives containing electron acceptors and donor substituents, such as nitro and aminoporphycenes. The next section gives some

background on the available studies of 9-substituted porphycene, with focus on nitro and aminoporphycene derivatives.

1.8 Porphycenes: substitution with nitro and amino groups

Braslavsky and co-workers have investigated a series of 9-substituted porphycenes.[50] While there are more frequent studies on aminoporphycenes, nitroporphycene, on the other hand, is less studied. Nonell's group did extensive work on 9-amino-substituted porphycenes: 9-amino-2,7,12,17-tetrakis(2-methoxyethylporphycene, 9-amino-2,7,12,17-tetra-phenylporphycene,[102] 9-amino-2,7,12,17-tetra-*n*-propylporphycene and methoxyethyl derivative.[105] For nitroporphycenes, a report is available on 9-nitro-2,7,12,17-tetraphenylporphycene,[102] 9-acetoxy-19-nitro,2,7,12,17-tetra-*n*-propylporphycene,[220] and 9-nitro-2,7,12,17-tetra-*n*-propylporphycene.[220] While the substitution of tetraphenylporphycene with a mild acetoxy group resulted in marginal changes in the absorption spectra, the strong electron-withdrawing effect of the nitro group led to more significant perturbations.[102] The greatest influence was observed with amino substitution, as the lowest energy band exhibited a red shift of ~110 nm. Short-lived biexponential excited singlet lifetime and fluorescence quenching were reported for 9-amino-2,7,12,17-tetraphenylporphycene.[102] Aminoporphycenes are interesting compounds due to their sensitive active site, which offers ease of protonation and enhances interaction with biological cells; their photochemical stability is of utmost importance in applications such as the photoinactivation of microorganisms. More studies on porphycenes asymmetrically substituted at 9-position are documented in other publications[102–105,220] and the book chapter by Nonell.[106]

Free-base porphycenes substituted with electron-donating (NH_2) and withdrawing (NO_2) moieties will be the focus of this research work. The influence of these substituents, whose positions are varied on the macrocycle, is discussed in terms of substituent and/or position dependence. This dissertation also contains studies on the *meso*-tetraphenylporphycenes substituted with the nitro group at positions two or three, corresponding to *β* and *β′,* respectively. Results obtained will be compared with the available data on 9,10,19,20-tetramethylporphycene (mTPPo), 9,10,19,20-tetraphenylporphycene (TPPo), 9,10,19,20-tetra-*n*-propylporphycene,[106] tetraphenyl-*meso*-dinitro derivatives,[116] *meso*-tetraphenylporphycene[221] with methyl[221] acetoxy[222] and nitro, bromo and fluoro groups.[222]

Tetra-*meso* substitution of porphycene with alkyl groups was reported to significantly lower the quantum yield of fluorescence relative to parent unsubstituted porphycene.[95] In the results section, I present two compounds with phenyl groups at *meso*, one with a nitro group at the *β* and the second with the nitro group at the *β′* position. The experimental findings demonstrate the influence of substitution, and the obtained results are compared to what is reported in the literature for aryl groups at the *meso* position.

Compounds investigated in this study were carefully selected for the sake of novelty, in order to focus the investigation on the varying substituent and position dependencies of the photophysical properties. Given the prominence of amino groups in terms of their sensitivity in biological applications, this research establishes the photostability of aminoporphycenes for such applications. Regarding the less-studied nitro porphycenes, this study reveals the photophysical properties of a series of nitroporphycenes. In combination with photodegradation studies, suggestions are made with respect to the potential use of nitroporphycenes in PDT.

Chapter 2

2.1 Goals

The question now is: "Why is it important to know more about porphycenes?"

Given the detailed background on applications of porphycenes, as detailed in section 1.6, it is safe to say that investigating the photophysical properties of a new series of porphycenes cannot be overemphasized. For any successful application of a chromophore in light-mediated processes, the photophysical and spectral properties as well as photochemical stability, serve as a guide for these applications. Although there exist some documented reports on the photophysical properties of some porphycenes and their derivatives, there is, however, a dearth of information on the photostability of porphycenes, with that of nitro and amino-substituted porphycenes being non-existent. Photostability is one of the critical properties that directly influence the application of organic dyes where either high stability or low stability is required. Bearing in mind, the nature, structure, and position of peripheral substituents are known to either result in moderate or dramatic changes in the spectral and photophysical properties of this system. It is, therefore, essential to address how this influence of peripheral substituents extends to the photostability of porphycenes, especially in the case of electron-donating and withdrawing species. Therefore, this Ph.D. research work aims to study the spectroscopy, photophysics, and photostability of a new series of porphycenes substituted with electron-donating (NH_2) and electron-withdrawing (NO_2) moieties. The combined influence of alkyl substitution alongside the electron donating/withdrawing elements is also examined. Worthy of note is that there is no previously reported information regarding the photochemical stability of the studied compounds. Position-dependencies of the photophysical properties are illustrated in *meso*-tetraphenyl porphycenes substituted with a nitro group variedly placed at *β* and *β'* positions. In a separate series of the porphycenes tagged the '*pull,*' '*push,*' and '*push-pull*' derivatives, we illustrate the combined effect of tetra *tert*-butyl groups at *β* and two other substituents at *meso* positions 9 and 19. The *pull* derivative corresponds to tetra *tert*-butyl groups at *β* and two nitro groups at *meso*. The *push* and *push-pull* maintain a similar configuration as the *pull* derivative but with two amino groups and amino and nitro groups at the *meso* position, respectively. The investigated compounds are listed in Table 2.1, and their structures are illustrated in Figure 2.1.

Summarily, this research work will answer the following questions:

- What are the specific spectroscopic properties of the systems?

- What are the photophysical properties exhibited by the macrocycles?

- What are the tautomeric properties and timescale?

- Are these compounds suitable for application in PDT?

- What is the degree of photostability of these systems if employed as photosensitizers in phototherapy?

- Are they rather useful as dyes in applications requiring low stability?

- What role do electron donating or electron withdrawing groups play in the photophysics, photochemistry, and phototautomerization of these systems?

- What role does alkyl substitution (such as bulky *tert*-butyl, and *n*-propyl groups) play in the photophysics, photochemistry, and phototautomerization of these systems?

- How does the nature (viscosity, polarity, and ability to form hydrogen bonds) of the environment/solvent influence the photophysics and photochemistry of the studied systems?

- What pathway does our systems take during degradation upon illumination with UV/visible light?

- What is the mechanism of phototautomerization of the studied systems?

- What is the position dependence of a substituent on the photochemical properties of these systems?

Table 2.1: Compounds investigated in this dissertation

S/N	Abbreviation	Compound
1	**Pc**	Porphycene – *reference compound*
2	**Pr**	Porphyrin – *reference compound*
3	**APc**	9-aminoporphycene
4	**NPc**	9-nitroporphycene
5	**ttPc**	2,7,12,17-tetra-*tert*-butylporphycene – *reference compound*
6	**tprAPc**	9-amino-2,7,12,17-tetrapropylporphycene
7	**tprNPc**	9-nitro-2,7,12,17-tetrapropylporphycene
8	**ttAPc**	9-amino-2,7,12,17-tetra-*tert*-butylporphycene
8	**ttNPc**	9-nitro-2,7,12,17-tetra-*tert*-butylporphycene
9	**ttdAPc**	9,19-di-amino-2,7,12,17-tetra-*tert*-butylporphycene
10	**ttdNPc**	9,19-di-nitro-2,7,12,17-tetra-*tert*-butylporphycene
11	**ttANPc**	9-amino-19-nitro-2,7,12,17-tetra-*tert*-butylporphycene
12	**2NttPc**	2-nitro-7,12,17-tri-*tert*-butylporphycene
13	**tphPc**	9,10,19,20-tetraphenylporphycene – *reference compound*
14	**2tphNPc**	2-nitro-9,10,19,20-tetraphenylporphycene
15	**3tphNPc**	3-nitro-9,10,19,20-tetraphenylporphycene

Parent compounds

Porphycene (**Pc**)

2,7,12,17-tetra-*tert*-butylporphycene (**ttPc**)

9-substituted porphycenes

9-aminoporphycene **(APc)**

9-nitroporphycene (**NPc**)

9-substituted-*β*-tetrapropylporphycenes

9-amino-2,7,12,17-tetrapropylporphycene **(tprAPc)**

9-nitro-2,7,12,17-tetrapropylporphycene **(tprNPc)**

9-substituted-*β*-tetra-*ter*t-butylporphycenes

9-amino-2,7,12,17-tetra-*tert*-butylporphycene **(ttAPc)**

9-nitro-2,7,12,17-tetra-*tert*-butylporphycene **(ttNPc)**

Figure 2.1 Structure of compounds investigated in this research work

9-substituted-*β*-tetra-*tert*-butylporphycenes
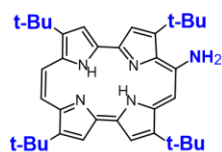
9-amino-2,7,12,17-tetra-*tert*-butylporphycene **(ttAPc)**
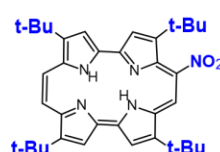
9-nitro-2,7,12,17-tetra-*tert*-butylporphycene **(ttNPc)**
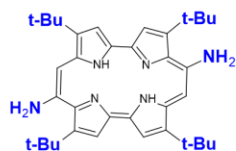
9,19-disubstituted-*β*-tetra-t*ert*-butylporphycenes
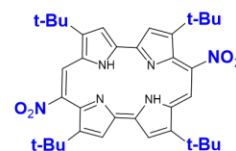
9,19-di-amino-2,7,12,17-tetra-*tert*-butylporphycene **(ttdAPc)**

9,19-di-nitro-2,7,12,17-tetra-*tert*-butylporphycene **ttdNPc**
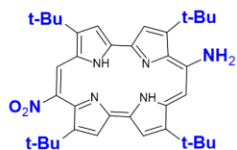
9-amino-19-nitro-2,7,12,17-tetra-*tert*-butylporphycene **(ttANPc)**

Meso-tetraphenyl substituted porphycenes
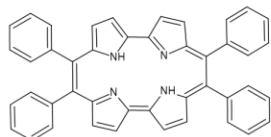
9,10,19,20-tetraphenylporphycene **(tphPc)**
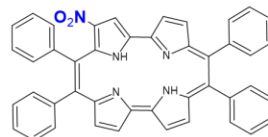
2-nitro-9,10,19,20-tetraphenylporphycene **(2tphNPc)**
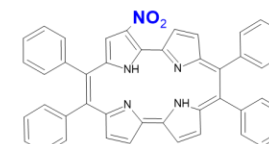
3-nitro-9,10,19,20-tetraphenylporphycene **(3tphNPc)**

2-nitro-*β*-tri-*tert*-butylporphycene
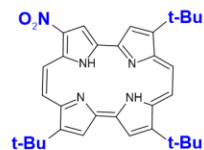
2-nitro-7,12,17-tri-*tert*-butylporphycene **(2NttPc)**

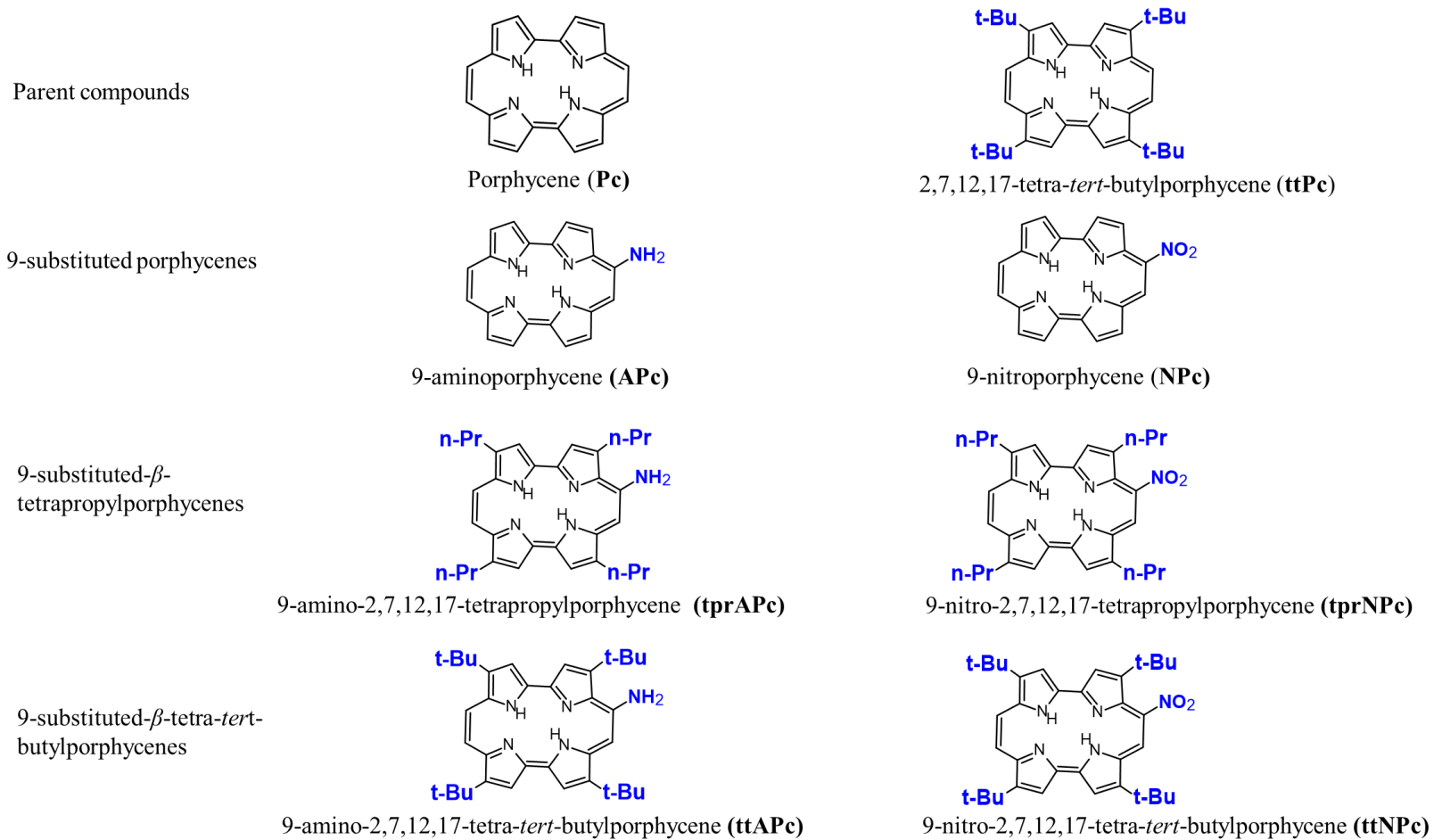*Figure 2.1 (continued): Structure of compounds investigated in this research work*

2.2 Methodology

Here, the methods of achieving the above-listed goals are highlighted; further details on the methodology are described in section 4.2. The methods through which the goals of the research work have been achieved are steady-state electronic absorption and fluorescence measurements, time-resolved fluorescence studies, fluorescence anisotropy, MCD, transient absorption studies, and quantum chemical calculations.

2.3 Potential impact

The outcome of this research will particularly be useful to researchers and pharmaceutical industries in phototherapy, as this research provides information as to whether these series of porphycenes are suitable candidates for phototherapy. This work, being a fundamental research, will also be useful to scientists generally interested in understanding aromatic macrocyclic systems such as those in this research. This research work highlights expectations in terms of tautomerization and double hydrogen transfer in the case of aminoporphycenes and nitroporphycenes presented in this study. Relevant data on the degree of photostability of the studied systems is provided herein. Accurate photophysical data is also provided for our systems of interest, which will form the basis for further research on potentially new derivatives.

2.4 Scope of Thesis

This research work is centered around compounds shown in Figure 2.1 and will focus on the characterization of their spectroscopy, photophysics, and photochemical stability when exposed to UV/Vis light. Contrast will be made between these properties as they pertain to electronic donating and withdrawing groups. It can be asked whether the influence of a certain substituent on the **Pc** macrocycle is position-dependent; therefore, two porphycene derivatives substituted with a nitro group in positions 2 and 3 are reported, and position-dependent effects are highlighted.

Chapter 1 gives an overview of porphyrinoids, generally and specifically, porphycenes. The properties, structure, reactivity, and applications of porphycenes are highlighted, laying a solid foundation for readers regarding the literature data on porphycenes.

Chapter 2 concisely describes the justification for the research, the questions to be answered by this study are succinctly listed, and the potential scientific impact thereof.

Chapter 3 is a superficial description of basic photophysics, photochemistry, and solvation dynamics as it applies to this study.

Chapter 4 describes in detail the methodology of the research.

Chapter 5 details the photophysical and spectroscopic properties of three series of aminoporphycenes (9-aminoporphycene (**APc**), 9-amino-2,7,12,17-tetra-*n*-propylporphycene (**tprAPc**), and 9-amino-2,7,12,17-tetra-*tert*-butylporphycene (**ttAPc**)) and three series of nitroporphycenes (9-nitroporphycene (**NPc**), 9-nitro-2,7,12,17-tetra-*n*-propylporphycene (**tprNPc**), and 9-nitro-2,7,12,17-tetra-*tert*-butylporphycene (**ttNPc**)). Here, with the help of MCD and quantum chemical calculations, we assign transitions in the absorption spectra to specific tautomers.

In Chapter 6, the unique case where nitration of 2,7,12,17-tetra-*tert*-butylporphycene (**ttNPc**) results in 2-nitro-7,12,17-tri-*tert*-butylporphycene (**2NttPc**) is explored. In this chapter, the **2NttPc** is contrasted with other nitro derivatives of porphycenes – singly substituted nitroporphycene (**NPc**), nitroporphycene with tertiary butyl groups (**ttNPc**) and double nitro with *tert*-butyl groups (**ttdNPc**).

Chapter 7 takes a deep dive into a unique property of aminoporphycenes, which is instability. The report in this chapter establishes that all studied aminoporphycenes degrade as a function of time and solvent. The degradation, although occurring in the dark and as a photoinduced process, is more efficient in the latter. Based on experimental observation, it is certain that aminoporphycenes emit single fluorescence.

Chapter 8 discusses the photostability of amino and nitroporphycenes. A three-order-of-magnitude difference is obtained from the calculation of the photobleaching quantum yield of

the electron-donating and electron-withdrawing derivatives of porphycene. The obtained values further confirm the instability in aminoporphycenes.

Chapter 9 describes the '*pull',*' '*push,*' and '*push-pull*' porphycene derivatives, that is, the 9,19-dinitro-2,7,12,17-tetra-*tert*-butylporphycene (**ttdNPc**), 9,19-di-amino-2,7,12,17-tetra-*tert*-butylporphycene (**ttdAPc**), and 9-amino-19-nitro-2,7,12,17-tetra-*tert*-butylporphycene (**ttANPc**).

Chapter 10 discusses the position effect in 9,10,19,20-tetraphenylporphycenes when a nitro group is placed at β position in one derivative and placed at β' in the second compound. Results from this study are compared with literature and with other studied nitroporphycenes.

Chapter 11 can be referred to as an executive summary and future recommendations.

Chapter 3

3.1 Concepts of photochemistry and photophysics

Since this thesis is centered around the interaction of porphycenes with light, it is essential to look into the basics of light-matter interaction. Therefore, this chapter describes the physical and chemical effects of light-matter interactions known as photophysics and photochemistry, respectively. Photochemistry details the chemical changes (constituting the rearrangement of electrons and nuclei in chemical structures) occurring in atoms or molecules as a result of the absorption of electromagnetic radiation. Photophysics, on the other hand, encompasses the various deactivation processes following the absorption of electromagnetic radiation. The concept of photochemistry and photophysics is important while describing the various phenomena that occur from the moment a material interacts with light and is excited, to its relaxation to the ground state. This relaxation could occur via radiative or non-radiative routes. When light interacts with matter, there are various possible outcomes. Light could either be absorbed, transmitted, refracted, diffracted, or scattered. Absorption and luminescence, specifically fluorescence, as they pertain to the studied systems in this dissertation, will be the focus of this chapter. Otherwise, more details on the topic are available[223–226] for interested readers.

3.1.1 Light and matter interaction

Light is an electromagnetic (**EM**) wave comprising the electric field component, **E**, and the magnetic field component, **H**. The term light, in this case, constitutes the near ultra-violet ($\lambda = 200 – 380$ nm) and the visible ($\lambda = 380 – 800$ nm) region of the electromagnetic spectrum (Figure 3.1). The electric and magnetic field components are described by the Maxwell wave equations. The electric field which characterizes the optical wave is defined as:

$$E(\mathbf{r}, t) = \hat{e}A(\mathbf{r}, t) \exp\left[i(\mathbf{kr} - \omega t)\right] \tag{3.1}$$

where $\hat{e}$ is the unit vector designating the direction of polarization or propagation of the electric field, $A(\mathbf{r}, t)$ and ($\mathbf{kr}$ - ωt), respectively, are the amplitude and the phase of the wave, r is the position vector, and ω the angular frequency ($\omega = 2\pi/T$, with T being the period). The element k,

is the wave vector, signifying the direction of propagation of the wave. It can be expressed in terms of wavelength, λ, and angular frequency.

$$|\mathbf{k}| = k = \frac{2\pi}{\lambda} = \frac{n\omega}{c} \tag{3.2}$$

where k is the angular wavenumber, c is the speed of light, and n = 1 in vacuum.

Also, the relationship between frequency and wavelength is as expressed in equation (3.3)

$$\nu = c/\lambda \tag{3.3}$$

where ν is the frequency.
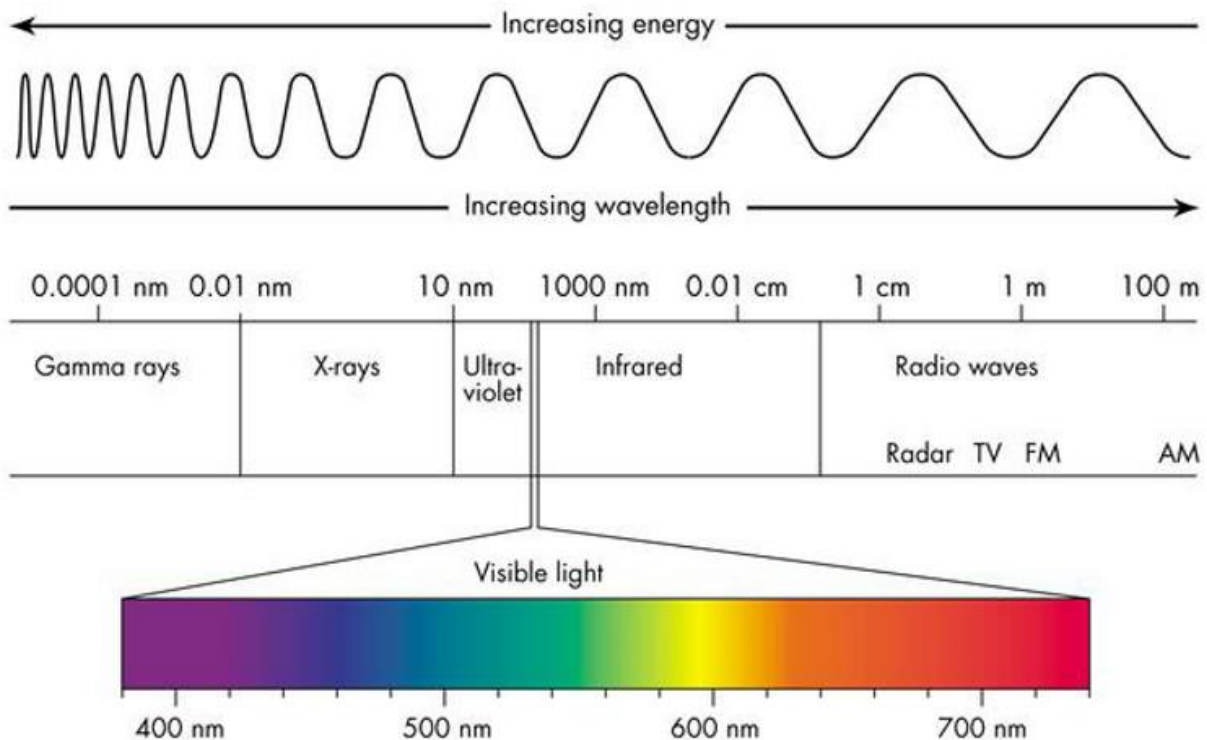
Figure 3.1 The electromagnetic spectrum. Adapted from ref.[227]

3.1.2 Absorption of light

When light interacts with matter, the resulting phenomenon varies depending on the wavelength of the light and the composition of the material. Light, upon striking a material, could either be absorbed, transmitted, scattered, refracted, reflected, polarized, or diffracted. Absorption of light is said to occur when light of a specific frequency impinges on a material (containing electrons that oscillate at the same frequency with incident light), resulting in an electronic transition from the ground, lowest energy state to an excited, higher energy state.

According to the first law of photochemistry (Grotthuss, 1817 and Draper, 1843), only absorbed light is useful in any photochemical reaction. In 1905, Albert Einstein postulated the quantum theory of light. Einstein's explanation of the Planck's equation was revolutionary. He explained that light is made of *quanta*, which was later named *photons* by Gilbert Lewis. Therefore, a photon is a packet of electromagnetic radiation corresponding to energy, hν. It is the smallest bundle of energy at a certain frequency. Quantum theory postulates the quantized nature of energy levels of matter. In this theory, organic compounds possess characteristic discrete energy levels comprising vibrational and electronic levels. The implication of discrete energy levels in a molecule is that only a specific frequency of light can be absorbed for an absorption process to take place. The absorbed frequency of light must coincide with the energy difference between the initial (i) and final (f) states. Absorption of light results in electronic transitions from one level to another, a process known as excitation. The various possible electronic orbitals during an excitation process are shown in Figure 3.2.

Molecular orbitals (MOs) consist of bonding (σ and π), non-bonding (n), and anti-bonding (σ* and π*) orbitals. These are necessary for electronic transitions from one level to another. A π orbital is formed from a sideways overlap of atomic p-orbitals, resulting in a π bond. A sigma orbital, on the other hand, is either formed from two atomic s orbitals or two p atomic orbitals or from one s and p orbitals. A sigma σ bond is the bond formed when σ orbitals are formed. Two orbitals play a vital role in absorption and emission studies – the HOMO (Highest Occupied Molecular Orbital) and LUMO (Lowest Unoccupied Molecular Orbital).
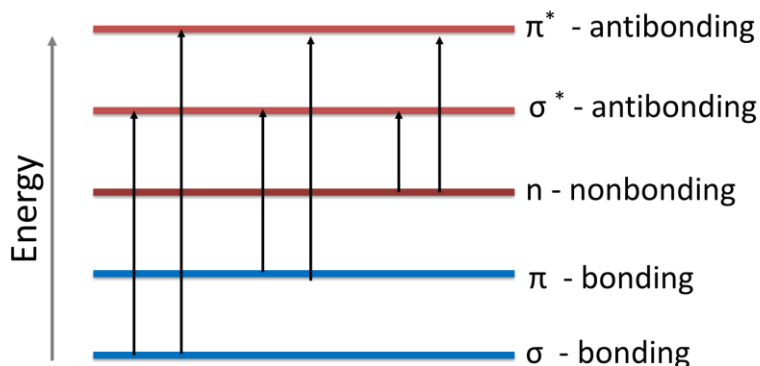
Figure 3.2 Possible electronic transitions

Summarily, light, according to quantum theory, has a wave-particle dual nature. While the wave nature of light characterizes light with wavelength, the particle nature characterizes light with a photonic component, whose energy relies on the frequency of the light, ν, expressed by the Planck-Einstein equation:

$$E = h\nu = hc\tilde{\upsilon} = \frac{hc}{\lambda} \qquad (3.4)$$

where h is the Planck's constant, $\tilde{\upsilon} = 1/\lambda$ the wavenumber of light.

Since each wavelength of light corresponds to a specific frequency (energy), absorption, therefore, occurs when the energy of the incident light is just enough - matches the energy gap between the initial (i) and final (f) state – the Bohr condition as expressed in equation (3.5).

$$\Delta E = h\nu = E_f - E_i \qquad (3.5)$$

Electronic transitions are governed by two major rules: allowing or forbidding specific transitions (see section 3.1.5). For an electronic transition to be allowed, the transition dipole moment must be non-zero. From the frontier molecular orbital point of view in organic compounds, electronic transition entails a π-π^* (and in some cases n-π^*) transition. The lowest energy transition is often well described as that from the HOMO (ground state, lower energy) to the LUMO (excited state, higher energy) of a molecule. The smaller the energy gap between HOMO and LUMO, the lower the energy required for electronic transition, and vice versa. In addition, the color of light eventually absorbed is determined by the magnitude of the light energy. The quantum mechanical condition for absorption to occur is the interaction between the transition dipole moment of the molecule and the electric field of the light.

3.1.3 Electronic states

The stationary states of molecules possess discrete energy levels described by the Schrödinger equation (**SE**):

$$H\Psi = E\Psi \qquad (3.6)$$

Where Ψ is the wavefunction, and H is the Hamiltonian operator which acts on the wavefunction. While Ψ is known as the eigenfunction, E is called the eigenvalue, and it corresponds to an allowed energy state. The eigenvalues and their corresponding eigenfunctions for hydrogen atoms are known as the atomic orbitals (**AO**s). Whereas the Schrödinger equation can be solved exactly for

a hydrogen atom, solving the exact eigenfunctions for molecules is not possible. Therefore, for systems of chemical interest, approximation methods are employed to determine the energy level with high accuracy. The *Born-Oppenheimer* (BO) approximation is often used for this purpose. Since the nuclei are much heavier and move relatively slower than the electrons, the **BO** approximation assumes the nuclei to be stationary at arbitrary positions, and then the Schrödinger equation is solved only for the wavefunction of the electrons.[223] The **BO** approximation allows us to solve the **SE** for specific nuclear separation, and from this, the evaluation of the energy of the molecule as a function of bond length is obtained from the potential energy curve Figure 3.3. From the curve, the bond dissociation energy, D_0, and the equilibrium bond length, R_e, can be determined.
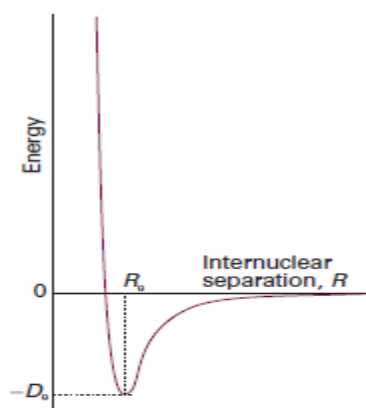
Figure 3.3 A potential energy curve. Reprinted from ref.[223]

Allowed transitions are governed by the Einstein coefficient, B_{fi} which tells the probability of a transition to occur, equation(3.7):

$$\kappa' = \frac{h\nu_{fi}}{c} B_{fi}(N_f - N_i) \tag{3.7}$$

where κ' is the absorption coefficient, h is the Planck constant, ν is the frequency, c is the speed of light, B, is the Einstein coefficient, N_i and N_f are the population of atoms in the lower and final state, respectively. The Einstein coefficient, in turn, depends on the transition dipole moment (μ_e), which must be non-zero for absorption to occur, as expressed in equation (3.8). The transition dipole moment (μ_e) is a quantum chemical parameter that involves the integral of the molecular wavefunction of the initial Ψ_i and final Ψ_f states of a molecule.

$$B_{if} = B_{fi} = \frac{|\mu_{if}|^2}{6\mathcal{E}_0 \hbar^2} \quad \mu_{fie} = \int \Psi_f(\mu_e)\Psi_i \, d\tau_e = \langle \Psi_f | \mu_e | \Psi_i \rangle \neq 0$$

(3.8)

3.1.4 The Beer-Lambert law

In absorption spectroscopy, the absorbance (A) of a sample is defined as the log to base 10 of the incident light vs. that of the transmitted light, equation (3.9). When an absorption measurement is performed, an absorption spectrum is obtained. The absorption spectrum provides information on the optical properties of a solution, such as the wavelengths of light absorbed by the molecule.

$$A = \log_{10} \frac{I_0}{I}$$ (3.9)

where I_0 and I are the intensities of the incident and transmitted light, respectively.

The Beer-Lambert law states that there is a direct proportional relationship between the absorbance and the concentration of a sample in solution. This proportionality holds at lower concentrations where there is the absence of aggregation in absorbing molecules.

$$A = \varepsilon cl$$ (3.10)

where A is the absorbance, l is the optical path length in cm, c is the molar concentration of the solution, and ε is the molar extinction coefficient ($M^{-1} cm^{-1}$). If Beer-Lambert's law is obeyed, a plot of the absorbance as a function of concentration should be linear.

The absorption spectrum is recorded using a spectrophotometer. Here, the wavelength of incident light on the sample is varied using a monochromator, and the intensity of transmitted light for every wavelength is recorded on the detector.

3.1.5 Selection rules

Transitions observable in the electronic spectrum of a molecule are governed by selection rules.

Spin rule

This rule holds that ideally, only transition between states of the same multiplicity is allowed; that is, while singlet-triplet and triplet-singlet transitions are forbidden, singlet-singlet and triplet-triplet transitions are allowed. However, in reality, weak interaction between wavefunctions of different multiplicities via spin-orbit coupling results in observable transitions between singlet and triplet states (Figure 3.4). These transitions, although of very low absorptivity, are still detectable and observed and are most tenable in the presence of heavy atoms such as iodine or bromine. The forbidden transitions are those of which the transition dipole moment is zero.
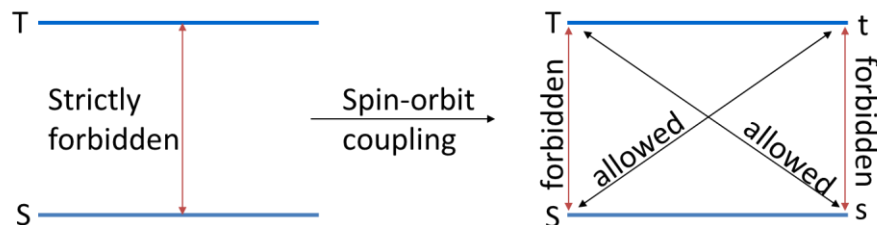
Figure 3.4 Illustration of allowed and forbidden transitions

For spin-forbidden transitions (such as phosphorescence) in a singlet-triplet transition, the absorptivity and, of course, the decay rate constant are usually some orders of magnitude lower than that of fluorescence (a singlet-singlet transition).

Symmetry rule

This is the orbital or Laporte's selection rule, which states that for a molecule with a center of symmetry, forbidden transitions are those of the same sub-shell. In this context, d-d or p-p transitions are forbidden. Allowed transitions are those in which the change in total angular momentum (ΔL) between the final (L_f) and initial (L_i) orbital angular momentum equals ± 1. Allowed transitions are those accompanied by a change of parity. That is, u→g and g→u transitions are allowed, but g → g and u → u transitions are not allowed. Forbidden transitions can be weakly allowed if the center of symmetry is lost, for instance, due to vibration. Such weakly allowed transition is due to vibronic coupling.

3.1.6 Franck-Condon Principle

The Franck-Condon principle explains the vibrational structure in the electronic spectra of molecules (Figure 3.5). This principle supposes that the rapid nature of an electronic transition does not allow a vibrating molecule to change its internuclear distance appreciably during the transition. This is due to the large difference in mass between electrons and their nuclei. According to the principle, the most intense vibronic transitions occur from the ground vibrational state to the vibrational state lying vertically above it (left of Figure 3.5). Transitions occurring between other vibrational levels are of lower intensity. In the quantum mechanical model (right of Figure 3.5) of the Franck-Condon principle, transitions occur from a vibrational ground state whose wavefunction overlaps the excited state wavefunction. Therefore, during an electronic transition,

two vibrational wavefunctions must overlap significantly for the occurrence of a transition from one vibrational level to another.
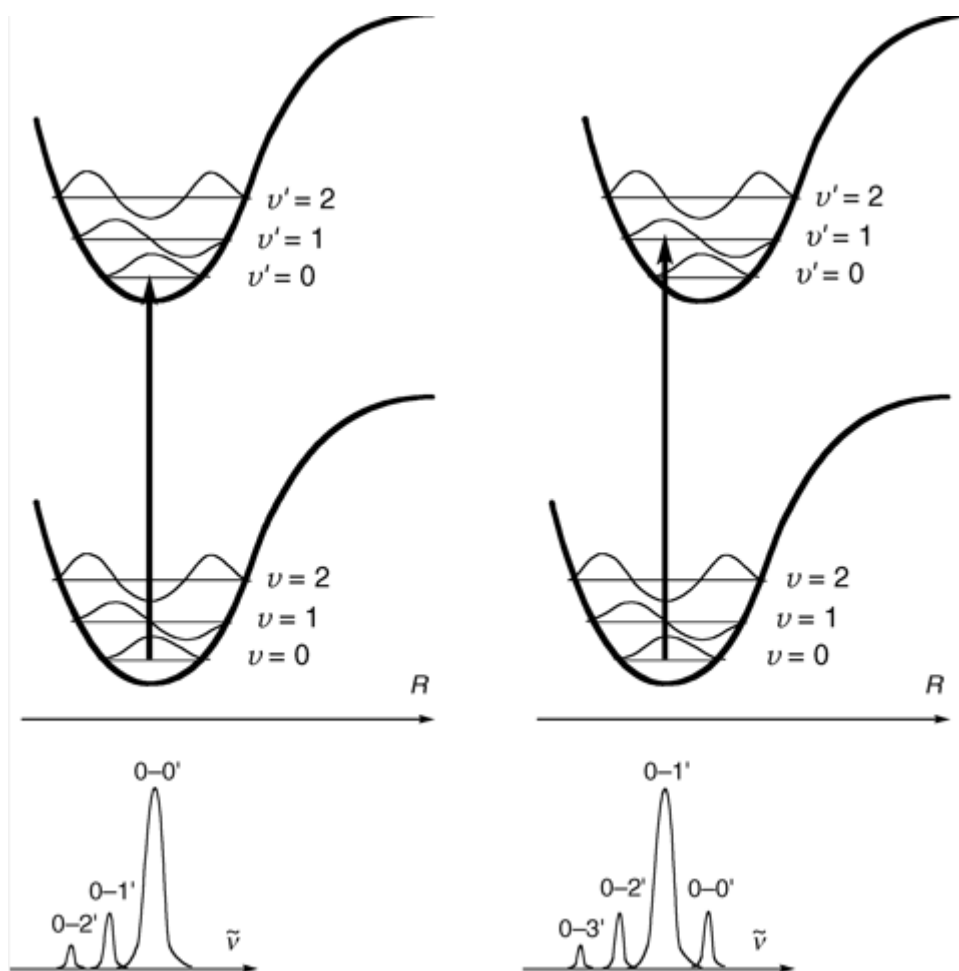
Figure 3.5 The Franck-Condon principle. Reprinted from ref.[225]

3.1.6.1 The Franck-Condon factors

Since the transition dipole moment μ_{fi} must be non-zero for an allowed transition, equation (3.11), the Franck-Condon factor, therefore, describes the intensity of a transition, and it is directly proportional to the square modulus of the magnitude of the transition dipole moment, $|\mu_{fi}|^2$

$$\mu_{fi} = \langle f|\mu|i \rangle \tag{3.11}$$

The dipole moment operator operates over the sum of all the nuclei and electrons in the molecule.

3.2 Relaxation of the excited state

Consider a molecule that undergoes electronic transition (from the ground state to an excited state) following the absorption of light of a specific frequency. The molecule can exist in the excited state for time periods ranging from picoseconds to nanoseconds and even microseconds. The longevity of the excited state is characterized by fluorescence lifetimes. Various photophysical processes can lead to the relaxation of an excited molecule to the ground state. These processes describe the deactivation pathways for the excited state and are demonstrated in the Jabłoński diagram (Figure 3.6). Excited state deactivation can follow a radiative (involving photon emission) or non-radiative (energy dissipation without photon emission) route. In Figure 3.6, the straight arrows represent the radiative pathways, while the wavy arrows represent the non-radiative pathways. The Jabłoński diagram shows the different electronic levels (bold black lines), vibrational levels (thin black lines) in each electronic state, absorption process, and pathways by which the excited state is deactivated. The vibrational states can be assigned a number $v = 0$ to n. Typically, molecules at room temperature occupy the lowest vibrational level in the ground electronic singlet state S_0. Upon excitation, transition occurs from a singlet ground state to a singlet state of higher energy S_n, with $n > 0$. The greater the photon absorbed, the higher the state to which the molecule is excited. When a molecule is transitioned from the $v = 0$ of the ground states to that of the excited state, the 0-0 transition is said to be observed.
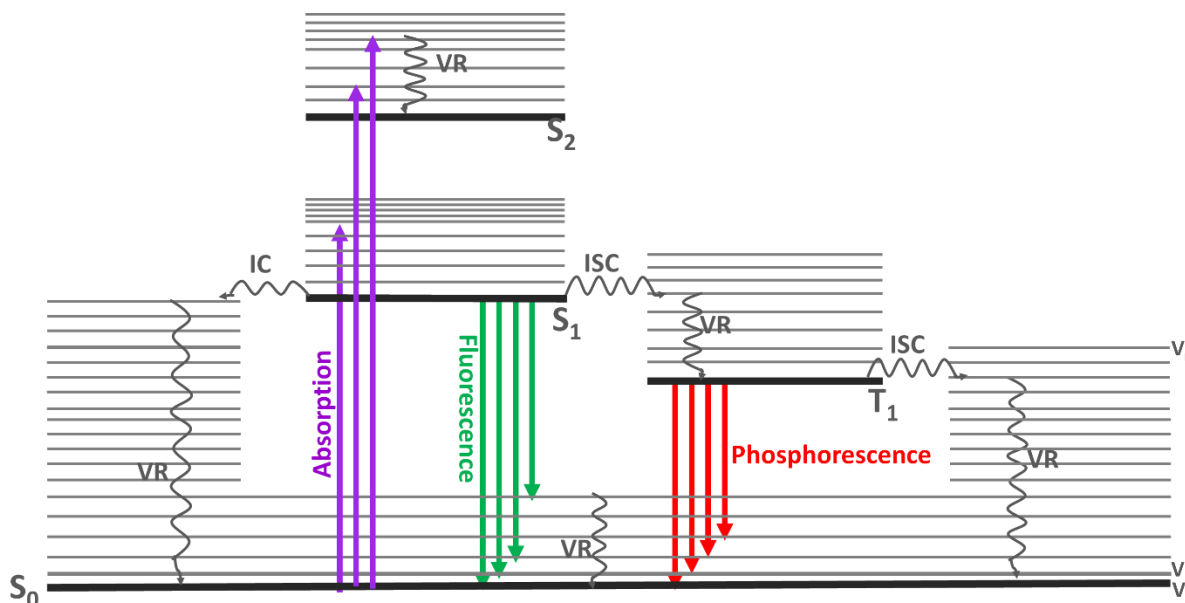
Figure 3.6 The Jabłoński diagram of a molecule photoexcited from the ground state (S_0) to the first excited singlet (S_1), second excited singlet (S_2), and first excited triplet (T_1) state. Electronic energy levels are represented by thick black lines, while thin gray lines indicate vibrational states. VR: vibrational relaxation, IC: internal conversion, ISC: intersystem crossing.

3.2.1 Radiative deactivation pathway

Fluorescence and phosphorescence are the radiative pathways through which an excited molecule can be relaxed to the ground state. In this section, our focus will be on fluorescence only. Fluorescence (like absorption) exhibited by many molecules is rather broad, with structureless bands in contrast to structured bands expected of transitions from specific vibrational levels (of an electronic state) in the ground state to specific vibrational levels in the excited electronic state. Molecules occupy the lowest energy level at equilibrium. The relative population of molecules in the vibrational energy levels is described by the Boltzmann law. The Boltzmann law evaluates the ratio of the numbers of molecules N_1 and N_0 in the 1 and 0 vibrational levels of the energy E_1 and E_0, respectively, equation (3.12).

$$\frac{N_1}{N_0} = e^{[-\frac{E_1 - E_0}{kT}]} \qquad (3.12)$$

where T is the absolute temperature and k is the Boltzmann constant (k = 1.3807×10^{-23} J K^{-1})

3.2.1.1 Fluorescence

Excited electrons can lose energy via fluorescence and relax to lower energy levels. During this process, photons are emitted which have somewhat lower energy than the frequency of light initially absorbed. The energy of the given-off photon during fluorescence is less than the absorbed energy because some of it is lost as thermal energy to the surrounding media during collision of the solute with solvent molecules. This explains why emission spectra typically lie at lower energy relative to the absorption.

Fluorescence occurs when the emission of photons accompanies $S_0 \leftarrow S_1$ relaxation. Fluorescence is observed between states of the same multiplicity. According to Kasha's rule,[228] fluorescence occurs only from the lowest excited electronic state. This implies that if there is excitation to higher energy singlet states, IC must occur, bringing excited molecules to v_0 of S_1 for fluorescence to occur. Kasha's rule is a consequence of the energy gap law: the energy gap between higher states of a given multiplicity is much less than that between the lowest S_1 or T_1 state and the ground state. Worthy of mention is that there are exceptions to Kasha's rule. For example, compounds with atypically large S_2-S_1 energy difference, such as zinc tetraphenylporphyrin, fluorescence can be observed from both S_1 and S_2. Kasha also suggested that a similar fluorescence emission spectrum is observed regardless of the wavelength of excitation. Molecules in $S_1(v=0)$ can relax either via radiative or non-radiative paths. However, the significant energy difference between S_1 and S_0 makes non-radiative relaxation (IC) a less favorable pathway, and thus, fluorescence has a higher probability of occurrence in this case. The efficiency of emitted photons during a fluorescent event is quantified by the fluorescent quantum yield, ϕ_{fl}. According to Vavilov, the fluorescent quantum yield is independent of the wavelength of excitation.[225] The fluorescent quantum yield is expressed as the ratio of the radiative rate constant and the sum of the rate constants of all possible deactivation pathways, equation (3.13), and it is independent of the excitation wavelength.

$$\phi_f = \frac{k_r}{k_r + k_{nr}} = k_r \tau \qquad (3.13)$$

where $k_r = \phi/\tau$ is the radiative rate constant, and k_{nr} is the non-radiative rate constant, which equates to the sum of $k_{IC} + k_{ISC}$. The period of time in which an excited molecule dwells in the

excited state is characterized by the emission decay profile known as the excited state lifetime, τ_f and expressed as:

$$\tau_f = \frac{1}{k_r + k_{nr}} \tag{3.14}$$

Worthy of note is the difference between τ_f and the natural lifetime τ_0, also known as the radiative lifetime. This is the lifetime when all non-radiative channels are prevented from occurring. Figure 3.7 summarizes the rate constants of radiative and non-radiative processes occurring during and after the excitation of an electron.

$$\tau_0 = \frac{1}{k_r} \tag{3.15}$$
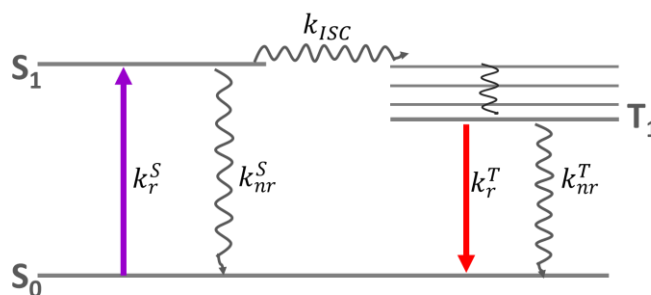
Figure 3.7 Modified Jabłoński diagram, illustrating radiative and non-radiative rate constants, k_r and k_{nr}, respectively. The superscripts S and T denote the singlet and triplet states, respectively.

During an emission event, the emission usually (but not always) exhibits a mirror image of the absorption band. The mirror image is explained as the vibrational levels spacing is similar for the ground and excited state, which results in a fluorescence spectrum that strongly resembles the mirror image of the absorption spectrum. The difference between the maximum fluorescence and lowest energy absorption band is known as the Stokes shift. Stokes first observed that fluorescence will always lie at lower energies relative to the absorption. In most cases, however, the fluorescence band overlaps the absorption band and poses as a deviation from Stokes law. Cases of such deviation have been clearly explained by Einstein: at RT, some molecules exist at vibrational levels higher than v_0 (in the ground and higher electronic state), when such a molecule is excited, they will emit at a frequency higher than the lowest energy absorption band. This gives

rise to the overlap between absorption and emission bands. The deviation from Stokes law is eliminated at low temperatures.

3.2.1.2 Phosphorescence

A molecule in an excited triplet state can relax to the S_0 state via phosphorescence. Although the triplet-singlet transition is forbidden, phosphorescence can be observed via spin-orbit coupling. Due to the forbidden nature of the transition, non-radiative is the primary de-excitation pathway from the triplet to the singlet ground state.

3.2.2 Non-radiative deactivation

As discussed in section 3.2, there are various deactivation pathways for an excited system. In addition to the radiative pathway discussed above, an excited molecule can lose energy without emitting photons via the so-called non-radiative route. These pathways include internal conversion (IC), intersystem crossing (ISC), and vibrational relaxation (VR), as discussed in the next sections.

3.2.2.1 Vibrational relaxation (**VR**)

An excited system in the S_1 or S_2 state quickly dissipates energy via vibrational relaxation from a higher energy vibrational state (of S_1 and S_2) to $v = 0$ of S_1, then follows fluorescence as the system goes back to the ground state (see Figure 3.6). **VR** occurs very rapidly after absorption on a time scale between 10^{-14} and 10^{-11}s. During **VR**, energy is dissipated to other vibrational modes as kinetic energy. The kinetic energy is distributed to different quantum states of the molecule via a process known as intramolecular vibrational energy redistribution (**IVR**). In addition, there is a redistribution of energy to the environment, a process known as vibrational cooling (**VC**).

3.2.2.2 Internal conversion

A different form of non-radiative relaxation is also obtainable between S_1 and S_0, and this is known as internal conversion. When there exists a strong overlap between vibrational and electronic energy levels, an excited system can return from a vibrational level of a higher electronic state to a vibrational level in a lower electronic state. This process is the internal conversion, and it occurs within electronic states of the same multiplicity. When the eigenstates of vibrational and electronic levels become closely distributed, such that the vibrational levels of a higher electronic state are

low enough energy so that they overlap with some of the higher vibrational levels of the ground state. This overlap makes it more likely for an electronic transition between higher electronic vibrational levels to the ground state. While IC follows a time scale between $10^{-11} – 10^{-9}$s, VR occurs between 10^{-12} and 10^{-10}s. The IC process has a lower likelihood of occurrence in $S_0 \leftarrow S_1$ because the higher energy difference between S_0 and S_1 makes IC energetically unfavorable. This is in accordance with the energy gap law.

3.2.2.3 Intersystem crossing

Another possible de-excitation pathway from S_1 is intersystem crossing (**ISC**) to the triplet T_1 state. **ISC** is a spin-forbidden process; however, it occurs via a spin-orbit coupling process. For **ISC** to occur, there must be a spin rotation resulting from the magnetic coupling of the spin with other motion. The rates (probability) of **ISC** may be quite small or comparable to radiative processes depending on the states and the studied systems. The efficiency of **ISC** increases in the presence of heavy atoms or paramagnetic systems.

3.3 Solvation dynamics

In this section, we will describe the influence of the environment, specifically solvent effects, on the behavior of an excited fluorophore. Solvent, by simple definition, is a continuum distinguished by its static dielectric constant, ε_s, and refractive index, n. In the condensed phase, the interaction between the solvent and the solute presents a significant influence on the absorption and emission spectra. The degree of influence is usually lower in the absorption than in the emission spectra. During electronic transitions, there is a change in the electronic distribution of the molecule. As a result, the permanent electric dipole moment, $\overrightarrow{\mu_P}$ and the polarizability $\hat{\alpha}$ vary upon electronic transition. A molecule, not in vacuum, experiences influence from the electric field generated by its environment. The electric field interacts with the $\overrightarrow{\mu_P}$ and $\hat{\alpha}$ resulting in changes in the energies of the electronic states. This is known as solvation energy in the liquid phase. Solvent molecules oscillate around the solute particles, resulting in the broadening of the absorption and emission bands. In addition, changes in the nature or composition of solvent can result in shifts in the spectra, the so-called solvatochromic shifts. These shifts are a direct consequence of the changes occurring in the solvent energy. The changes in the absorption and emission spectra as a result of changes in

the solvation energy are referred to as solvatochromism. The interactions between a solute and its environment (solvent, in this case) can be classified into:

    I.   Non-specific interactions – These interactions are independent of the chemical nature of the solute.

    II.   Specific interactions: This includes interactions arising due to specific properties of the solute and the chromophore. Such interactions include but are not limited to the formation of hydrogen bonds between the solute and the solvent and charge-transfer interactions.

Consider a fluorophore with a ground state dipole moment, μ_G and an excited state dipole moment, μ_E. When the fluorophore is excited, the solvent molecules reorient themselves around μ_E (Figure 3.8). This reorientation process by the solvent molecules stabilizes the excited state, and the magnitude of stabilization has a direct proportionality with solvent polarity. Therefore, greater solvent polarity results in emission to lower frequencies or longer wavelengths. It is important to note that the more polar the fluorophore, the greater its sensitivity to solvent polarity, and the reverse is the case for less polar fluorophores.

The theory of solvent effects on a given fluorophore is given by the Lippert-Mataga equation. In this theory, the fluorophore is considered a dipole in a continuum of characteristic dielectric constant (Figure 3.8), excluding other interactions (such as charge transfer states and hydrogen bonding) that may influence emission. The Lippert-Mataga equation expresses the influence of solvent-fluorophore interactions on the energy difference (cm^{-1}) between the ground and excited states. This difference is a function of the refractive index, n, and dielectric constant of the solvent, ε_s. The Lippert-Mataga equation also expresses that the Stokes shift (solvatochromic shift) is dependent on the magnitude of change in the dipole moment of the ground and excited state ($\Delta\mu = \mu_E - \mu_G$).

$$\Delta\tilde{v} = \tilde{v}_A - \tilde{v}_F = \frac{2}{hc}\left(\frac{\varepsilon - 1}{2\varepsilon + 1} - \frac{n^2 - 1}{2n^2 + 1}\right)\frac{(\mu_E - \mu_G)^2}{a^3} + \text{constant} \qquad (3.16)$$

where h is the Planck constant, c is the velocity of light, a denotes the radius of the cavity in which the solute resides, and $\Delta\tilde{v}$ is the orientation polarizability, which describes the interaction of solvent molecules with the solute.
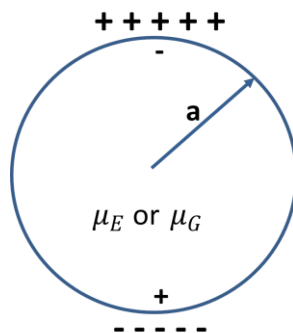
Figure 3.8 The solvent-fluorophore interaction

$\tilde{v}_A$ and $\tilde{v}_F$ are the wavenumbers of the absorption and emission, respectively. For most organic molecules, the magnitude of excited state dipole moment μ_E is greater than μ_G. This implies a larger stabilization in the excited state relative to the ground state.

$$\left(\frac{\varepsilon - 1}{2\varepsilon + 1} - \frac{n^2 - 1}{2n^2 + 1}\right) = f(\varepsilon) - f(n^2) = \Delta f \tag{3.17}$$

A bathochromic shift of the absorption spectrum due to solvatochromism is classified as a positive solvatochromism, and the negative counterpart corresponds to a hypsochromic shift.
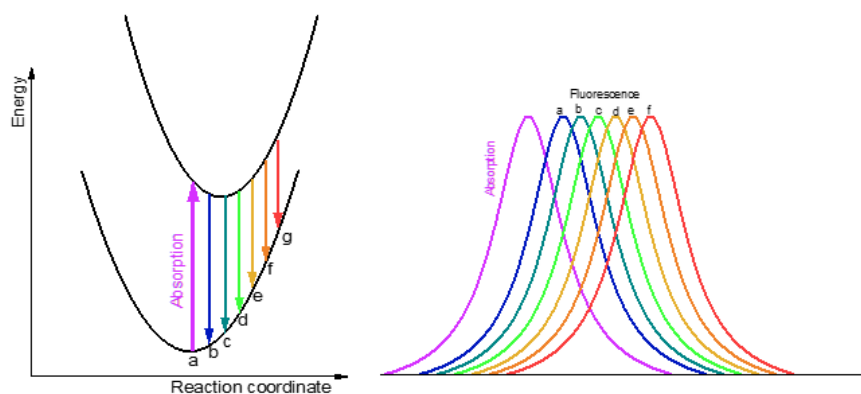
Figure 3.9 Illustration of solvent effects on the fluorescence spectra, a consequence of the dynamic Stokes shift.

The *dynamic Stokes shift,* (Figure 3.9), gives information on the rate at which solvent relaxation takes place. The dynamic Stokes shift illustrates the change in the maxima of the emission

spectrum as a function of solvent relaxation and time. Here, the emission spectrum recorded immediately after excitation maintains a maximum close to the absorption band maxima, but this maximum shifts to longer wavelengths with solvent relaxation. Upon completion of solvent relaxation, the maxima remain unchanged. Since the time scale for the solvent relaxation is very short, fluorescence is usually observed from the relaxed excited state.

3.4 The excitation spectra

The excitation spectrum is an indication of which wavelength of light a fluorophore would absorb to emit at specific wavelengths. It helps with the determination of which specific specie is responsible for any specified fluorescence emission. The difference between an absorption and an excitation spectrum is that, while the former gives information on all wavelengths of light absorbed by a sample, the latter gives insight into the change in the fluorescent intensity as a function of the excitation wavelength. The excitation spectrum is measured using a spectrofluorometer, here, an emission monochromator is set to a known wavelength of emission by the sample, while the excitation monochromator scans across the excitation range of interest. The intensity of emission as a function of excitation wavelength is then recorded on the detector. The excitation spectrum is expected to coincide with the absorption spectra if Kasha and Vavilov's rules are obeyed.

Chapter 4

4.1 Materials and methods

This section describes the materials, solvents, and techniques used in this research.

4.1.1 Solvents

Solvents used in this thesis were of spectroscopic grade and were used as received and are listed in Table 4.1.

Table 4.1: solvents used during this research work

Abbreviation	Solvent	Chemical formula	Source
ACN	acetonitrile	C_2H_3N	Merck
Tol	toluene	$C_6H_5\text{-}CH_3$	Merck
n-Hex	*n*-hexane	C_6H_{14}	Merck
EtOH	ethanol	CH_3CH_2OH	Merck
DMSO	dimethyl sulfoxide	$(CH_3)_2SO$	Merck
THF	tetrahydrofuran	C_4H_8O	Merck
2-MeTHF	2-methyltetrahydrofuran	$C_5H_{10}O$	Merck
Lp	liquid paraffin		Merck
CH_3COOH	acetic acid		Chempur
1-Oct	1-octanol	$C_8H_{18}O$	Sigma-Aldrich

4.1.2 Materials - samples

Compounds investigated in this dissertation were synthesized by Dr. Agnieszka Gajewska and Dr. Arkadiusz Listkowski of the Department of Photochemistry and Spectroscopy, Institute of Physical Chemistry, Polish Academy of Sciences. Synthetic methods are described elsewhere for **APc**,[229] **tprAPc**,[230] **ttAPc**,[231] **NPc**,[229] **tprNPc**,[229,230] **ttNPc**,[231] **2NttPc**.[232] The investigated molecules, and their abbreviations are contained in Table 2.1, and their structure is presented in Figure 2.1.

4.2 Methods

4.2.1 Steady-state electronic absorption and emission

Electronic absorption spectra were measured using a Shimadzu 2700 UV/Vis spectrophotometer. Electronic emission and excitation spectra were measured using three different spectrofluorimeters: Cary Eclipse (Varian) or Edinburgh FS 090 CDT equipment or Fluorolog-3 from Horiba. The obtained fluorescence spectra were corrected for instrument sensitivity. The samples were contained in 1.0 cm quartz cuvettes.

Fluorescence quantum yield measurements were performed using the relative[233] method for solutions (reference and sample) with matching optical densities (OD) at the wavelength of excitation. OD at the excitation wavelength was kept below 0.1 to avoid inner filter effects resulting from reabsorption. Calculations for fluorescence quantum yield have been performed using the equation(4.1):

$$\Phi_f = \frac{\int F(\lambda)}{\int F_{ref}(\lambda)} \frac{n^2}{n_{ref}^2} \frac{1 - 10^{-A^{ref}}}{1 - 10^{-A}} \Phi_f^{ref} \tag{4.1}$$

Where Φ_f and Φ_f^{ref} are the fluorescence QY of the sample and reference, respectively, $\int F(\lambda)$ is the integrated fluorescence intensity (area), n is the refractive index of the solvent, and the fraction of light hitting the sample and getting absorbed is represented by $1 - 10^{-A}$ where A is the absorbance and subscript 'ref' refers to the reference.

4.2.2 Steady-state fluorescence anisotropy

The technique involves the excitation of an ensemble with vertically polarized light, during which molecules whose absorption transition dipole aligns parallel to the direction of the polarized excitation beam have a higher probability of getting excited. The preferential photoexcitation occurs via a process known as photoselection, the basis of fluorescence anisotropy. In the photoselection process, an ensemble of randomly oriented molecules is excited with a linearly polarized light. As a result, the molecules are excited (*photoselected*) if their transition moment orientation lies parallel to that of the exciting light. Polarized excitation results in largely polarized

emission. The degree of polarization of fluorescence is determined by the so-called fluorescence anisotropy, r, expressed as:

$$r = \frac{I_{\parallel} - I_{\perp}}{I_{\parallel} + 2I_{\perp}}, \quad -0.2 \leq r \leq 0.4 \tag{4.2}$$

where $I_{\parallel}$ and $I_{\perp}$ are the intensities of the parallel and perpendicular components of the emission relative to the electric vector of the linearly polarized incident beam. The isotropic or total fluorescence intensity is proportional to the denominator of equation (4.2). That is:

$$I_{iso} = I_{\parallel} + 2I_{\perp} \tag{4.3}$$

Fluorescence anisotropy, r, depends on ϕ such that r = 0.4 if $\phi = 0°$ and r= -0.2 if $\phi = 90°$.

$$r = \frac{3\cos^2\phi - 1}{5} \tag{4.4}$$

Generally, the value of r is influenced by a range of factors:

- Rotational diffusion of the fluorophore during its lifetime;
- Transfer of energy between emitting fluorophores;
- Overlap of differentially polarized transitions within the range of excitation or emission wavelengths observed;
- A process that changes the transition moment direction, e.g., hydrogen transfer.

4.2.3 Triplet lifetimes and singlet oxygen determination

Since bare, unsubstituted porphycene generates singlet oxygen with high yields, it is curious to know the yields of singlet oxygen generation and triplet lifetimes of our studied porphycenes. The quantum yields of singlet oxygen formation of studied molecules were determined via equation (4.5).

$$\phi_{\Delta} = \frac{\int F(\lambda)}{\int F_{ref}(\lambda)} \frac{n^2}{n_{ref}^2} \frac{1 - 10^{-A^{ref}}}{1 - 10^{-A}} \phi_{\Delta}^{ref} \tag{4.5}$$

where ϕ_Δ and ϕ_Δ^{ref} are the singlet oxygen (SO) formation quantum yield of the sample and reference, respectively, $\int F(\lambda)$ is the integrated intensity (area) of SO phosphorescence, n is the refractive index of the solvent, and the fraction of light hitting the sample and getting absorbed is represented by $1 - 10^{-A}$ where A is the absorbance and subscript 'ref' refers to the reference. The setup for determination of singlet oxygen yields and triplet lifetimes was based on a home-built transient absorption set-up with time-resolution down to nanoseconds timescale. The excitation source was an Opotek Radiant 355 laser, tunable between 210 – 2500 nm, pulse width of 5 ns and repetition rate of 10 Hz, with the pulse energy ranging between 230 μJ and 500 μJ. The probe was a continuous Xe lamp (Energetiq EQ-99-Plus-EU). The photomultiplier was a Hamamatsu R955 photomultiplier and a Yokogawa (Tokyo, Japan) DL9140 fast oscilloscope. Similar setup was used to determine the lifetime of triplet state. Concentrations in the order of 10^{-6} M were used for the triplet state experiments.

4.2.4 Time-resolved fluorescence measurement

Time-resolved fluorescence (TRF) measurement is a powerful tool in the analysis and investigation of dynamics in the excited state. It offers resolution up to femtosecond time scales. One major advantage of the TRF method is providing molecular information from fluorescence, which is otherwise lost during the averaging process in steady-state methods. Time- correlated single photon counting (TCSPC) is one of the most frequently used techniques in TRF measurements. It is considered the most sensitive method for determining fluorescence decay times. The principle of TCSPC is based on the excitation of a sample using a pulsed laser or LED and the detection of the individual arrival times of the emitted photons from the sample. The excitation light pulse triggers the start signal, and a stop signal is triggered once a fluorescence photon from the sample reaches the detector. The difference between the start and stop time gives information about the arrival time of each photon. Repetition of the individual photon detection process as a function of time can be stored in a histogram, which gives information on the fluorescence lifetime of the sample. The above-described mode of obtaining fluorescence lifetimes is the forward mode, which, however, is limited by the pulse pile-up. To overcome this pile-up, the *reverse* mode can be employed, where an emitted photon from a sample serves as the *start* signal, and the excitation pulse is the *stop* signal. The reverse mode has profound applications in Fluorescence Lifetime Imaging Microscopy (FLIM).

4.2.4.1 Setup

Fluorescence decay times were recorded using two different home-built TCSPC setups. Both of these gave similar results of lifetime for samples measured. Set-up one is made up of a Picoquant LDH pulsed laser centered at 375 nm, with a 100 ps pulse at a variable repetition rate, a long-pass filter employed to remove the residual excitation beam just before collection of the emission, a Digikröm CM110 monochromator, Becker&Hickl PMC 100-4 photomultiplier and a PicoQuantTimeHarp 100 PC card. Here, the fluorescence lifetimes were determined using Picoquant Fluofit 3.3 software. The sample holder was a 1.0 cm quartz cuvette.
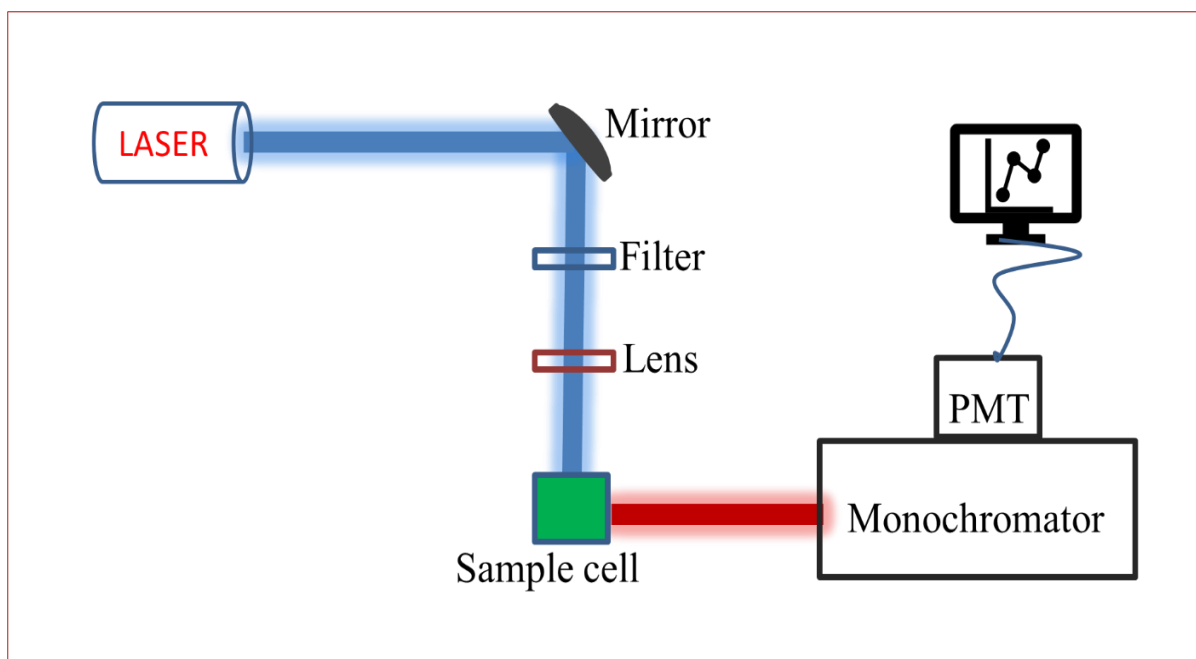
Figure 4.1 Simplified scheme of the Time-Correlated Single Photon Counting (TCSPC) set-up one

For the second home-built setup, a tunable wavelength Fianium FemtoPower1060 laser is the excitation source. The source is characterized by a 6 ps pulse width, pulse energy of 1.6 nJ, and repetition rate of 10/20/40/60 MHz. The emission was collected by a Digikröm CM112 double grating monochromator working in a subtractive mode. An HPM-100-40 hybrid detector (Becker & Hickl) coupled to a Becker & Hickl SPC-830 TR-SPC module serves as the detection system. The decay profiles were analyzed using commercially available packages: SPC Image software, version 5.7 (Becker & Hickl), and FAST version 3.5.0 (Edinburgh Instruments). To ensure reliable

values are obtained in non-singly exponential decays, two different procedures were used: (i) iterative reconvolution (ii) distribution analysis.
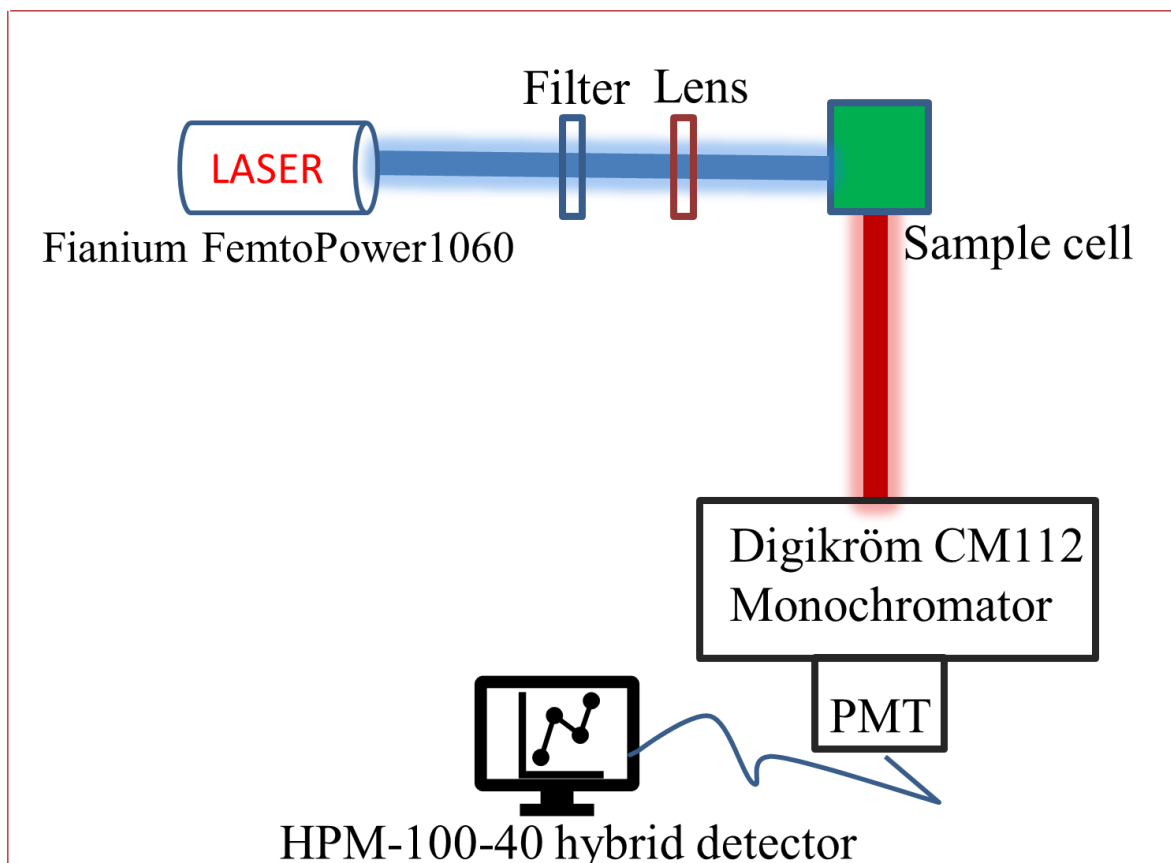
Figure 4.2 schematics of the Time-Correlated Single Photon Counting (TCSPC) set-up two

4.2.5 Magnetic Circular Dichroism

Circular dichroism is a form of absorption spectroscopy that specializes in the study of chiral molecules. The idea of CD is based on the differential absorption of right and left circularly polarized light by chiral molecules. A typical CD experiment results in a CD spectrum. Magnetic circular dichroism (MCD) spectroscopy is a very sensitive technique in the study of the difference in absorption of right and left circularly polarized light in samples exposed to strong magnetic fields, H_o. This magnetic field is oriented parallel to the direction of light propagation. MCD is a type of absorption spectroscopy, however, in this case, differential absorption of left or right circularly polarized light is being measured.[223,234]

Michael Faraday, in 1845, discovered the magneto-optical effect, which states that when light passes through a medium in the presence of a magnetic field, the plane of polarization of the light rotates. MCD offers advantages such as the detection of transitions that would otherwise not be visible in electronic absorption spectra. It is useful in decoupling overlapping transitions and offers the possibility of studying both solid and liquid samples. MCD is particularly useful in assigning transitions in electronic UV-visible absorption spectra, it provides information about the structure, coordination number in complexxes, and spin states and, therefore, is unique in structural analysis.

4.2.5.1 Theory of MCD

The underlying principle of MCD is the Beer-Lambert law, equation (4.6), which implies that MCD depends on the concentration and absorptivity of the sample. The theory of MCD is generally expressed by the equation:

$$\Delta A = A_L - A_R \rightarrow \Delta\varepsilon = \varepsilon_L - \varepsilon_R = \frac{\Delta A}{lc} \ [M^{-1}cm^{-1}] \tag{4.6}$$

Where ΔA is the change in absorbance, ε is the absorptivity (M^{-1} cm^{-1}), l is the path length of the cell, c is the molar concentration (mol L^{-1}; M) subscript L and R represent left and right circularly polarized light, respectively,
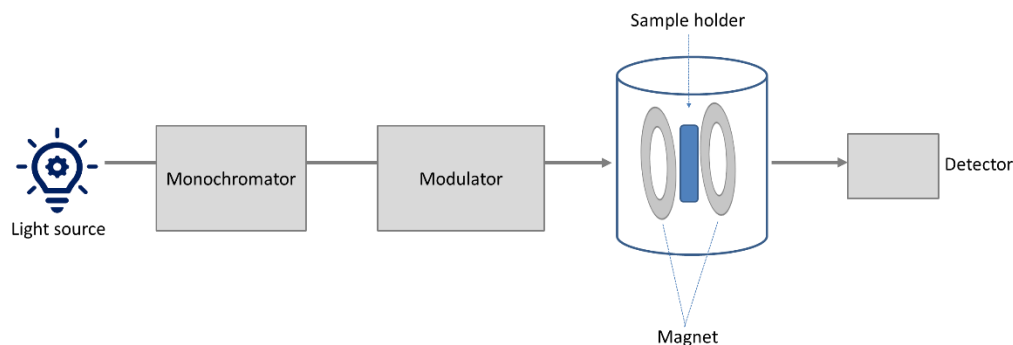
Figure 4.3 Schematic representation of the magnetic circular dichroism setup

Experimentally, three contributing factors (A, B, C) are used in describing ellipticity when temperature conditions are maintained such that the Zeeman energies $<< \kappa T$ and the absorption line width is large compared to the Zeeman splitting. The observed MCD spectrum can be expressed mathematically as:

$$\Delta A = \gamma\beta H_0 cb[A_1\left(-\frac{\delta f}{\delta E}\right) + \left(B_0 + \frac{C_0}{\kappa T}\right)f(E)] \tag{4.7}$$

where ΔA is the change in absorbance, γ = a spectroscopic constant $(N\pi^2\alpha^2\log e)/(250\ hcn)$, N is Avogadro's constant, α is the constant of proportionality between the electric field of the absorbing material and the electric field of the light, h is the Planck's constant, c = speed of light, n is the refractive index, β is the Bohr magneton H_0 is the magnetic field strength, κ is the Boltzmann constant and T is the absolute temperature, f(E) is a Gaussian line shape function. A_1, B_0, and C_0 represent the MCD parameters – A, B, and C, respectively where A_1 is multiplied by the derivative of the absorption profile, while B_0 and C_0 are the absorptive signals in the MCD spectrum.

A different version of equation (4.6), which describes the magnitude of the MCD spectra, is shown in Equation (4.8):

$$\text{MCD }\alpha\ \Delta A_\pm \equiv A_- - A_+ \tag{4.8}$$

Where the (+) and (-) terms denote the right and left circularly polarized light respectively. This implies that the MCD signal can either be positive or negative for a given absorption.

Magnetic circular dichroism (MCD) spectra reported in this dissertation were recorded using a Jasco J-1500 CD spectrometer equipped with an electromagnet (1.36 T field strength). A simplified scheme of the MCD setup used is shown in Figure 4.3. MCD spectra were recorded for both sample and reference, and the MCD signal from the reference was subtracted from that of the sample to yield the raw MCD data. **Important note**: the reference here is the sample whose MCD spectra is obtained without the presence of a magnet.

4.2.6 Set-up for irradiation

An important determinant property for the usability of dyes in various light-required applications is photostability. The study of photostability of dyes for varying applications cannot be overemphasized. A detailed description of the concept of photostability is contained in section 1.7. The set up used for the illumination of samples for the purpose of studying their resistance to degradation when exposed to light (photobleaching) is described as follows: a LED from Thorlabs, with a power of 56 mW, centered at 565 nm was used as the illumination source, the emitted light was focused on the cuvette using a lens. To ensure proper illumination of the whole sample

volume, the sample cell was placed on a magnetic stirrer for continuous stirring throughout the illumination period. Samples were irradiated at specified time intervals while observing the decrease in concentration via recorded changes in absorbance. Investigated samples were contained in quartz cells of 1 cm pathlength. The spectral profile of each diode $p(\lambda)$ was recorded and multiplied by a factor c to obtain the intensity profile, $I_0(\lambda)$ whose integral results in the number of photons emitted per second. Calculation of the quantum yield of photodegradation was done only within 10% of degradation to eradicate (or reduce to the barest minimum) the possibility of considering photoproducts in the calculation.

QY of photodegradation is generally expressed as equation (4.9):

$$\phi_b = \frac{N}{Q_{total}} = \frac{\text{number of photobleached molecules}}{\text{total number of absorbed photons}} \tag{4.9}$$

Equation (4.9) can also be expressed as equation (4.10) where $N_b(t)$ is the number of photobleached molecules over time t, $Q_{total}(t)$ is the total number of photons absorbed by the sample from the initial irradiation time (t = 0) to time t. The number of photons absorbed per time unit by the irradiated sample at time t is given as $Q_{abs}(t)$.

$$\phi_b = \frac{N_b(t)}{Q_{total}(t)} \tag{4.10}$$

where

$$N_b(t) = \frac{(A_0 - A_t) \times N_{av} \times V}{1000 \times \varepsilon \times l} \tag{4.11}$$

$$Q_{total}(t) = \int_0^t Q_{abs}(t)dt \tag{4.12}$$

$$Q_{abs}(t) = \int_{\lambda_1}^{\lambda_2} I_0(\lambda) \times \left(1 - 10^{A(\lambda,t)}\right)d\lambda \tag{4.13}$$

where A_0 and A_t are the absorbances observed before irradiation (t = 0) and after irradiation over t, respectively. N_{AV} is the Avogadro number, V is the sample volume in Liters, ε is the molar absorptivity and l is the optical path length. ϕ_b was determined from a plot of A_0/A_t against F(t).

$$\frac{A_0}{A_t} = 1 + bF(t) \tag{4.14}$$

$$F(t) = \frac{Q_{total}(t)}{A_t} \tag{4.15}$$

According to equation (4.14), a plot of A_0/A_t against $F(t)$ should give a perfect straight line assuming zero interference from photoproducts. However, for all the studied compounds, deviation from linearity was observed after the first several observed points, indicating absorption by the photoproducts.
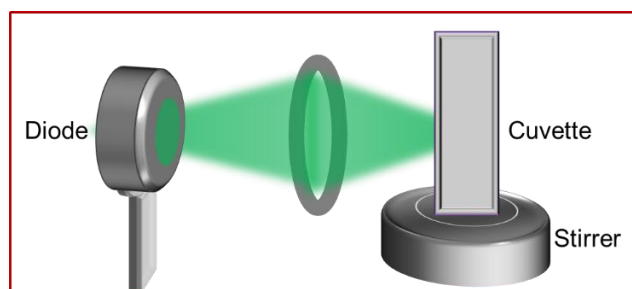
Figure 4.4 Setup for photoirradiation

4.2.7 Femtosecond (fs) transient absorption (TA)

Transient absorption has it basis in flash photolysis. It is a pump-probe experiment procedure where a sample is excited using a high energy light pulse (pump), thereby populating the excited state. Then, a lower energy pulse is used as the probe pulse to measure the changes in the absorption as a function of wavelength and time. During a TA experiment, the obtained spectra is the difference between the absorbance of the sample (ΔA) in the presence and absence of pumping. TA spectroscopy is successful in probing the excited state dynamics of the singlet, triplet, electron and energy transfer mechanisms, among others.

The setup for transient absorption has been described previously.[235,236] The light source was an amplified Ti:Sapphire system (Spitfire, Spectra-Physics), centred at 800, generating 100 fs pulses nm at a 1 kHz repetition rate. A fraction of the output of the amplifier was split into two for use as pump and probe. Components of both the pump and probe beams are described in detail in literature.[236]

4.2.8 Quantum chemical calculations

Theoretical chemistry calculations for ground state studies of molecules was performed using the Gaussian 16 suite of programs.[237] The density functional theory (DFT) method with a hybrid B3LYP and its long-range corrected modification CAM-B3LYP functionals were chosen. The excited state energies were obtained in the framework of the time-dependent DFT (TD-DFT) approach. The Pople's split-valence 6-31+G** basis set was applied. The frequency analysis was performed for all stationary points. A vibrational frequency scaling factor of 0.964 was used to obtain zero-point vibrational energy (ZPVE) corrections. Quantum chemical calculations were performed mostly by Michał Kijak and Prof. Jacek Waluk.

Section II

Chapter 5

5.1 Spectroscopy, photophysics, and tautomerism in amino and nitroporphycenes

Porphycenes, specifically 9-substituted porphycenes, have received attention due to the reactivity of the *meso* position. As carefully detailed in Chapter 1, while there are minimal studies on nitroporphycenes, aminoporphycenes have received a little more attention due to the possibility of the amino group interacting with biological matter. For suitable application of these dyes, especially as photosensitizers in PDT and studies of hydrogen bonding and proton transfers, we present the results of spectroscopic characterization, photophysical and tautomeric parameters for the series of compounds shown in Figure 5.1

This chapter discusses our research work already published in the literature.[231] Results herein are presented (Figure 5.1) for 9-aminoporphycene (**APc**), 9-nitroporphycene (**NPc**), 9-amino-2,7,12,17-tetra-*n*-propylporphycene (**tprAPc**), 9-nitro-2,7,12,17-tetra-*n*-propylporphycene (**tprNPc**), 9-amino-2,7,12,17-tetra-*tert*-butylporphycene (**ttAPc**) and 9-nitro-2,7,12,17-tetra-*tert*-butylporphycene (**ttNPc**). Porphycene (**Pc**) and 2,7,12,17-tetra-*tert*-butylporphycene (**ttPc**) were used as reference compounds. The results presented answer the question of how nitro and amino substituents (electron withdrawing and donating moieties, respectively) influence porphycenes' spectroscopic, photophysical, and tautomeric properties. The influence of alkyl substituents, such as propyl and bulky *tert*-butyl moieties, is also revealed.

5.2 Experimental procedure

Stationary absorption studies were performed at room temperature (25ºC) on a Shimadzu UV2700 spectrophotometer. Stationary fluorescence and excitation spectra were recorded on Cary Eclipse (Varian) spectrophotometer, Edinburgh FS 900 CDT spectrofluorimeter, and Horiba Jobin Yvon instruments - Fluorolog and FluoroMax-4. The sample was held in a 1 cm pathlength quartz cuvette. Syntheses of the studied compounds were carried out by Dr. Agnieszka Gajewska and Dr. Arkadiusz Listkowski. Quantum chemical calculations were done by Michał Kijak using the Gaussian 16 suite of programs.[237]
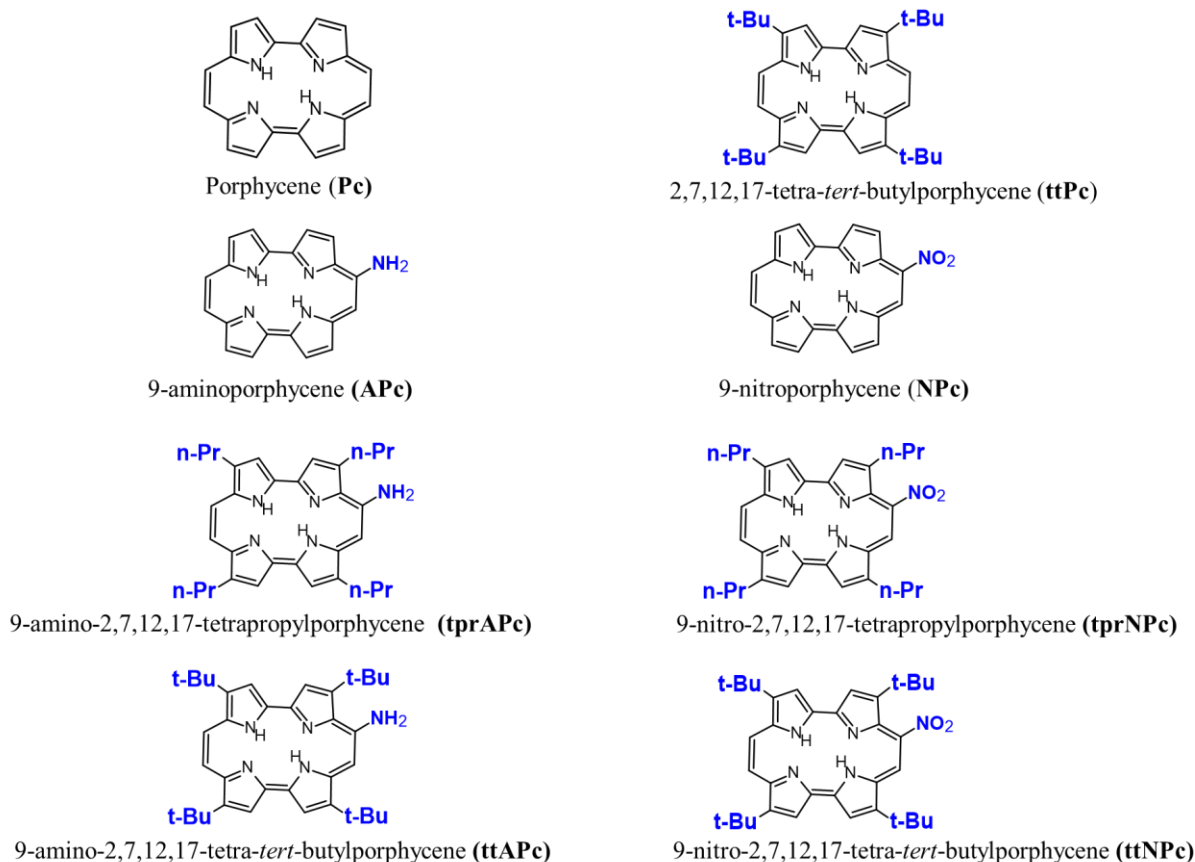
Figure 5.1 Structural formula of compounds reported in Chapter 5

5.3 Results and discussion

5.3.1 Quantum chemical predictions for the different tautomeric forms

It is known that **Pc** and its symmetrically substituted derivatives can exist in six pairwise degenerate tautomeric forms (Figure 5.2), where R_2 = H), resulting in three unique tautomeric forms. This degeneracy is lifted in asymmetrically substituted derivatives such as the 9-amino and 9-nitro derivatives (Figure 5.1). According to predicted energies, the two lowest energy *trans* forms co-exist in the ground electronic state of both amino and nitro porphycene. These forms are nearly equivalent in energy (Table 5.1). While *trans-1* is the lowest energy form in **APc**, *trans-2* is calculated as the most stable form in **NPc**. The ground state energy gap between the two *trans-*species in **APc** and **NPc** is below 0.5 kcal/mol. However, upon excitation to the lowest excited S_1 state, the gap increases by more than five times in **NPc** and by one order of magnitude in **APc**. In addition, in the S_1 state, the *cis-1* form of **NPc** and the *cis-2* form of **APc** are predicted to be more

stabilized than the higher energy *trans* form. The stabilization of the *cis* form (relative to the *trans*) in the S_1 state suggests the possibility of the *cis* specie being present in the S_1 state.
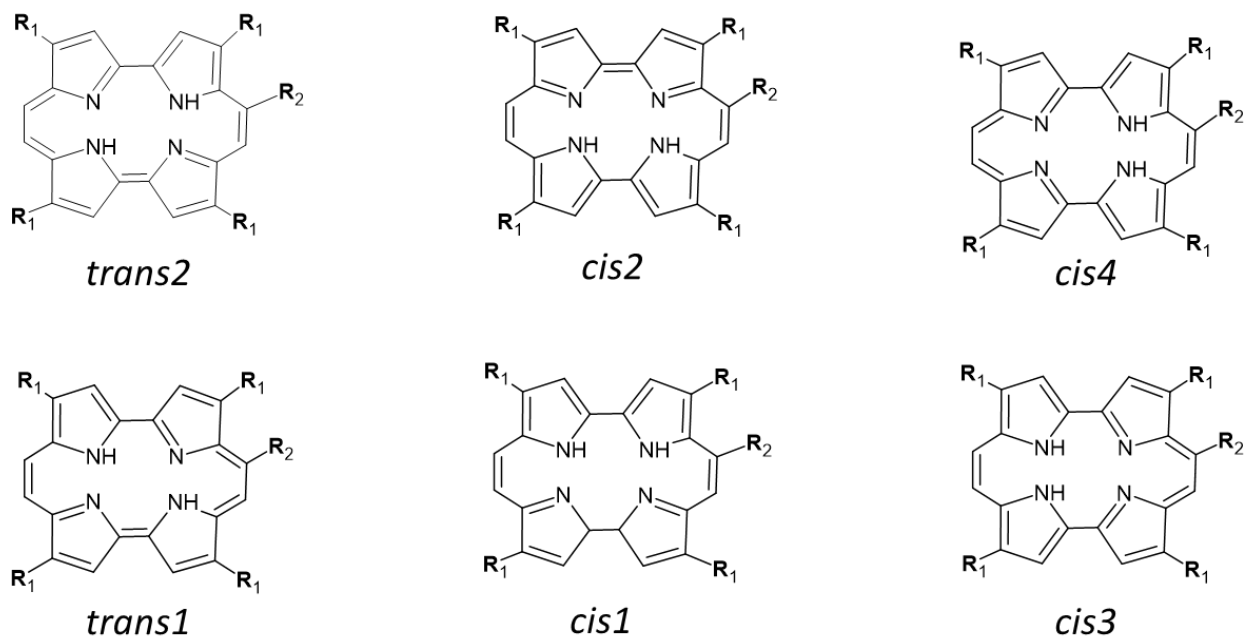
Figure 5.2 Possible tautomeric forms of meso-substituted porphycenes

The four-fold introduction of propyl groups to porphycene (**tprAPc**) at the β position does not result in significant changes in the relative energies (Table 5.1) of the tautomers and their dipole moments (Table 5.2). Similar result as in **APc** and **tprAPc** is obtained for **ttAPc**; the ground state energy gap between the two *trans* forms in **APc** and **tprAPc** is about 0.3 kcal/mol. This gap is further reduced in **ttAPc**, with the energy difference between *trans-1* and *trans-2* being 0.06 kcal/mol. In the S_1 state, all three amino derivatives have relatively significant energy differences (~3 kcal/mol) between the *trans* tautomeric forms.

Table 5.1 Calculated relative energies (kcal mol^{-1}) of the tautomeric forms of porphycene (**Pc**), 9-aminoporphycene (**APc**), and 9-nitroporphycene (**NPc**), 9-amino-2,7,12,17-tetra-*n*-propylporphycene (**tprAPc**), 9-nitro-2,7,12,17-tetra-*n*-propylporphycene (**tprNPc**), 9-amino-2,7,12,17-tetra-*tert*-butylporphycene (**ttAPc**), and 9-nitro-2,7,12,17-tetra-*tert*-butylporphycene (**ttNPc**)

		trans		*cis*	
S$_0$[a]	**Pc**	0.00 (0.00)		2.30 (1.74)	
	tprPc	0.00 (0.00)		2.27 (1.76)	
	ttPc	0.00 (0.00)		2.07 (1.53)	
		trans-1	*trans-2*	*cis-1*	*cis-2*
	APc	0.00 (0.00)	0.28 (0.24)	2.03 (1.51)	2.55 (1.91)
	NPc	0.42 (0.37)	0.00 (0.00)	2.60 (1.98)	2.16 (1.64)
	tprAPc	0.00 (0.00)	0.22 (0.15)	2.02 (1.48)	2.33 (1.70)
	tprNPc	0.06 (0.10)	0.00 (0.00)	2.44 (1.93)	1.83 (1.33)
	ttAPc	0.00 (0.00)	0.06 (0.00)	1.63 (1.14)	2.10 (1.53)
	ttNPc	-0.01 (0.04)	0.00 (0.00)	2.20 (1.72)	1.51 (1.15)
		trans		*cis*	
S$_1$[a]	**Pc**	0.00 (0.00)		1.99 (1.67)	
	tprPc	0.00 (0.00)		1.85 (1.37)	
	ttPc	0.00 (0.00)		1.68 (1.28)	
		trans-1	*trans-2*	*cis-1*	*cis-2*
	APc	0.00 (0.00)	3.20 (2.69)	5.54 (4.36)	2.10 (1.67)
	NPc	2.35 (2.08)	0.00 (0.00)	2.29 (1.85)	3.76 (3.10)
	tprAPc	0.00 (0.00)	2.92 (2.20)	5.24 (4.02)	1.77 (1.39)
	tprNPc	0.29 (0.11)	0.00 (0.00)	1.98 (1.54)	2.13 (1.42)
	ttAPc	0.00 (0.00)	3.22 (2.82)	5.26 (4.21)	1.69 (1.50)
	ttNPc	-0.55 (-0.69)	0.00 (0.00)	1.84 (1.34)	1.40 (0.88)

[a] in parentheses, zero-point corrected values

Table 5.2 Calculated permanent dipole moment for the tautomeric forms of porphycene (**Pc**), 9-aminoporphycene (**APc**), and 9-nitroporphycene (**NPc**), 9-amino-2,7,12,17-tetra-*n*-propylporphycene (**tprAPc**), 9-nitro-2,7,12,17-tetra-*n*-propylporphycene (**tprNPc**), 9-amino-2,7,12,17-tetra-*tert*-butylporphycene (**ttAPc**), and 9-nitro-2,7,12,17-tetra-*tert*-butylporphycene *(***ttNPc***)*

		trans		*cis*	
$\mu(S_0)$ [D]	**Pc**	0.00		1.31	
	tprPc	0.06		1.40	
	ttPc	0.00		1.44	
		trans-1	*trans-2*	*cis-1*	*cis-2*
	APc	2.30	2.47	2.99	2.40
	NPc	6.54	6.85	6.66	7.05
	tprAPc	2.22	2.43	3.10	2.29
	tprNPc	6.11	6.27	6.09	6.66
	ttAPc	2.09	2.40	2.98	2.39
	ttNPc	6.91	6.89	6.66	7.32
$\mu(S_1)^a$ [D]		*trans*		*cis*	
	Pc	0.00		1.20	
	tprPc	0.04		1.07	
	ttPc	0.00		1.19	
		trans-1	*trans-2*	*cis-1*	*cis-2*
	APc	3.63	3.79	3.95	3.72
	NPc	6.77	8.68	8.23	7.72
	tprAPc	3.50	3.77	3.87	3.49
	tprNPc	7.57	8.16	7.84	7.82
	ttAPc	3.04	3.41	3.39	3.14
	ttNPc	7.96	8.43	8.12	8.49

[a]calculated for the optimized S_1 geometeries

5.3.2 Electronic absorption spectroscopy

Spectroscopic study is a valuable tool in the characterization of porphycenes and its derivatives. The electronic absorption and emission study of porphycenes elucidates the absorbed wavelengths of light, the absorptivity, and the relative intensities of the bands. Porphycenes, like porphyrin, exhibit characteristic absorption bands categorized into the lower energy Q (L) bands and the higher energy Soret (B) bands. The Q bands in porphycene are about ten times the intensity of similar bands in porphyrin. This feature, among others, makes **Pc** advantageous as a sensitizer in PDT compared to porphyrin. The Soret bands in both **Pc** and **Pr** (Figure 1.2) consist of the B_1 and B_2 bands, with that of **Pc** being broader and blue-shifted relative to **Pr**.

5.3.2.1 Porphycene and substitution with tertiary butyl groups.

As seen in Figure 5.3, four-fold substitution of **Pc** with *tert*-butyl (**ttPc**) groups results in absorption patterns similar to that of parent unsubstituted **Pc**. Characteristic "three fingers" make up the Q bands, and in the Soret region, two bands are observed. With the help of quantum chemical calculations, alongside experiments in cold matrices, the absorption bands have been accurately assigned to specific tautomeric forms and transition states.[49,88] The lowest energy band correlates with the origin of S_1 transition. The middle band contains contributions from both the vibronic transition of S_1 and the origin of S_2, while the highest energy band pertains to a vibronic transition of S_2. Both **ttPc** and **Pc** are employed as references in this study.

5.3.2.2 9-Aminoporphycenes

Absorption spectra of amino porphycenes (Figure 5.4) show a red-shifted band ($\sim$2000 cm^{-1}), in contrast to what is observed typically for parent porphycene. The peak at $\sim$17,650 cm^{-1} is present in all aminoporphycenes and the unsubstituted **Pc**. Given the theoretical prediction of degeneracy in the two *trans* tautomers of aminoporphycenes, the absorption spectra represent a summation of both contributions. The Q-bands in aminoporphycenes consist of five transitions (Figure 5.4), each originating from any of the *trans* forms (or both) and being a transition to S_1 or S_2 or a complex combination of both. Calculated transition energies[231] for S_1 and S_2 states suggest that the lowest energy transition (Q_1) correlates with *trans-1* absorption (see Figure 5.4).
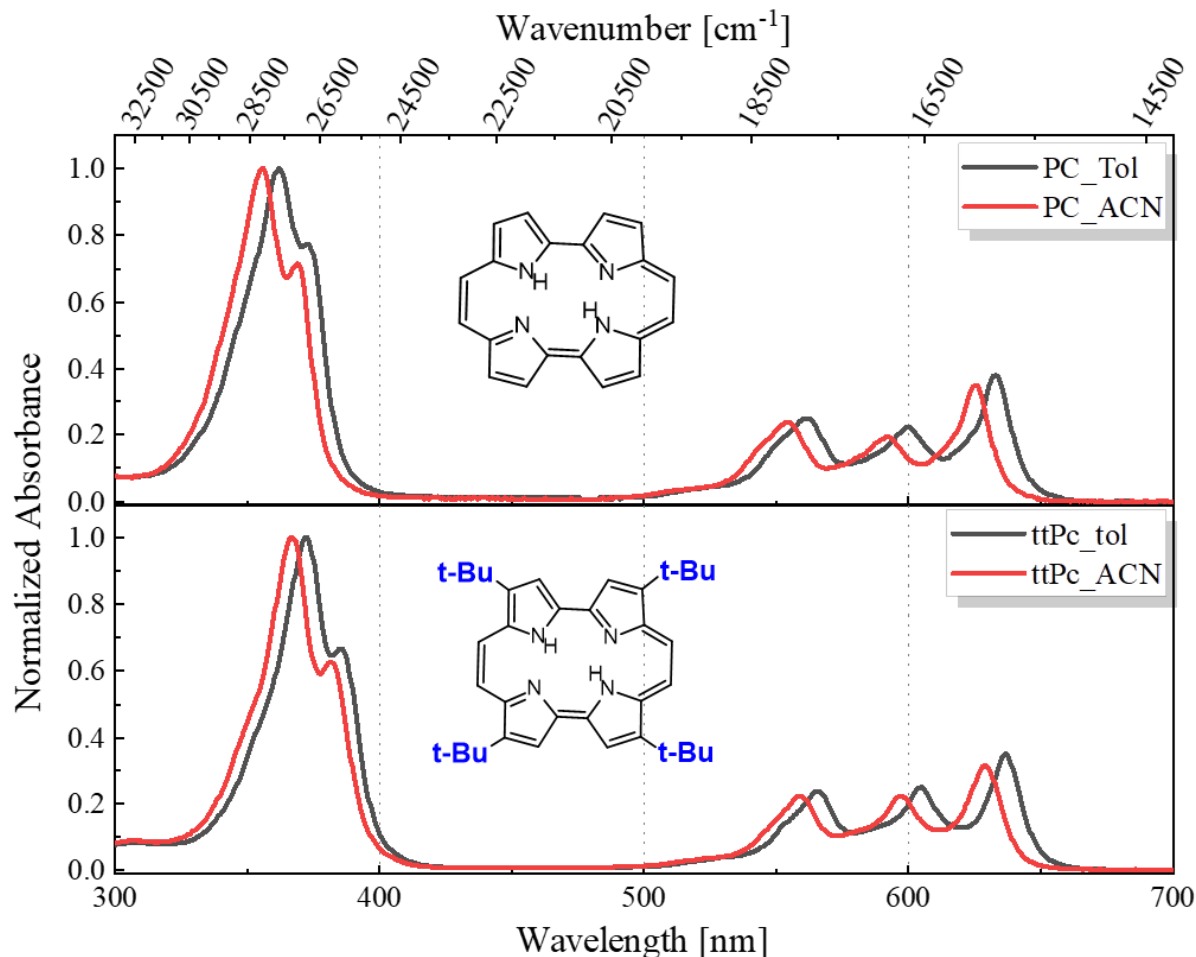
*Figure 5.3 Room temperature absorption spectra of top: porphycene (**Pc**) and bottom: 2,7,12,17-tetra-tert-butylporphycene (**ttPc**). The red line is acetonitrile, and the black line is toluene.*

Next to the lowest energy transition is a higher intensity absorption (Q_2) from *trans-2* lying ca. 900 cm^{-1} to the blue region. Two weak bands are observed at 15 800 cm^{-1} and 16 860 cm^{-1}, respectively, corresponding to Q_3 and Q_4. The last member of the Q-bands, Q_5, is observed at 17 650 cm^{-1}. Given the chemical inequivalence of the tautomeric form of asymmetrical porphycenes coupled with the calculated degeneracy in energy, it is expected therefore, that the absorption pattern in amino porphycenes is a complex overlaying of the unique tautomeric forms and transitions to different states. Thus, the assignment of the bands is not trivial. Fluorescence anisotropy and MCD, combined with theoretical calculations, have been employed to assign the bands accurately. Porphycene being a hard chromophore (described in section 1.4) implies that substitution or tautomerization does not change the MCD sign because of the significant energy difference between its LUMO orbitals. For this reason, a positive/negative MCD sign corresponds

to S_1/S_2 absorption regardless of the absorbing tautomer. In addition, it is possible to separate vibronic transitions from the origins of transitions since similar MCD sign is usually observed for the vibronic features and the electron origin.[227]
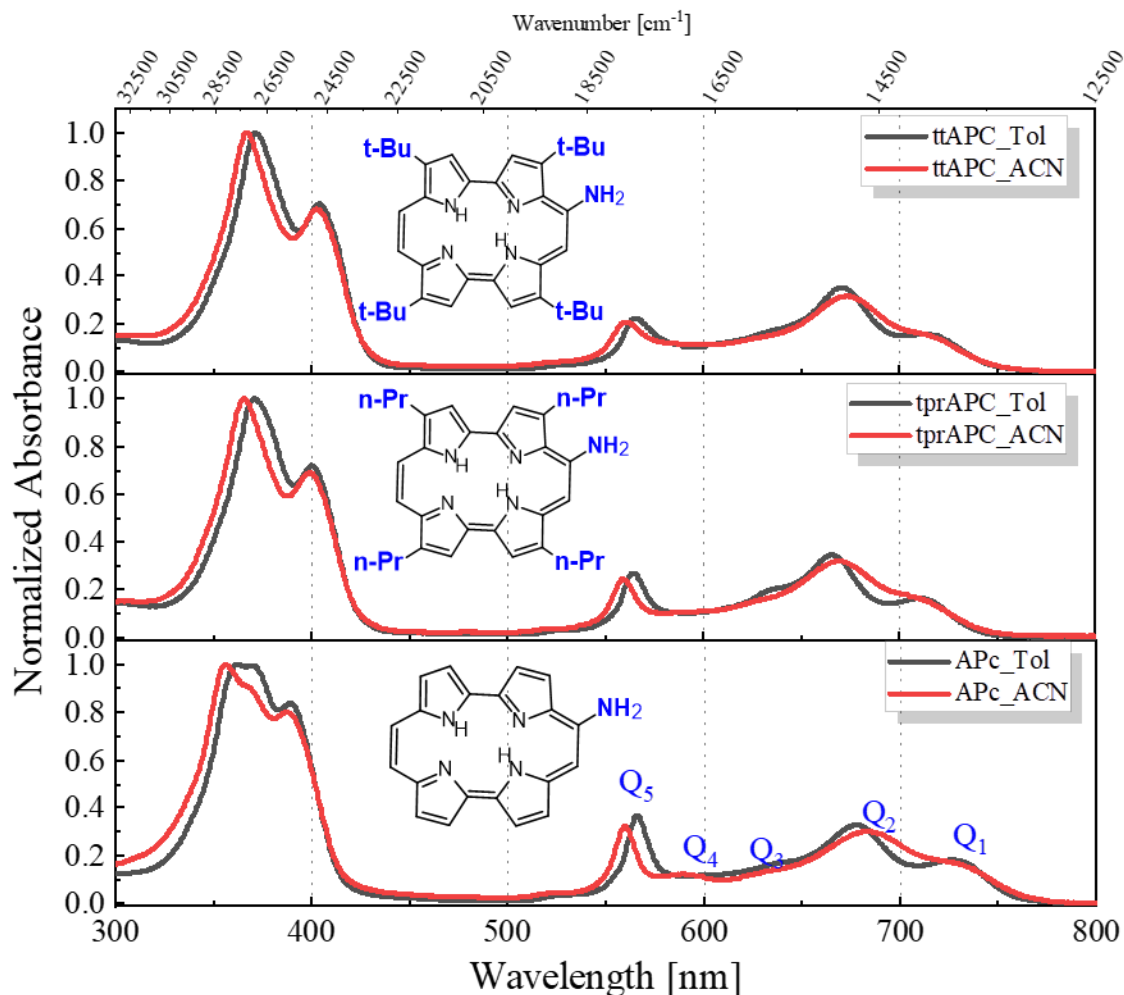
*Figure 5.4 Absorption spectra of **APc** (bottom), **tprAPc** (middle), and **ttAPc** (top) in toluene (**black**) and acetonitrile (**red**).*

In emission anisotropy, a known principle guiding the transition moments in symmetric porphycenes is followed: transition moments for each *trans* tautomer lie nearly perpendicular to each other in S_0-S_1 and S_0-S_2 transitions. Furthermore, the transition moments in *trans-1* and *trans-2* form a substantial angle, both for S_1 and S_2.[151,172] Considering this theory, positive anisotropy values for the emission occurring from *trans-1* signifies that the form initially excited coincides with either S_1(*trans-1*) or S_2(*trans-2*). On the other hand, a negative anisotropy value corresponds to S_1(*trans-2*) or S_2(*trans-1*). It is important to note that this theory holds for symmetrically

substituted or unsubstituted porphycenes. For some unsymmetrically substituted porphycene, a complex picture is reported where the transition moments in *trans-1* and *trans-2* tautomers exceptionally do not form a substantial angle, both for S_1 and S_2. Such a case was first observed for 9-amino-2,7,12,17-tetraphenylporphycene.[104] Similar observation is confirmed in the amino porphycenes reported in this dissertation (Figure 5.5). The not-so-large angle in transition[231] moments between the *trans-1* and *trans-2* tautomeric forms makes the distinction between two *trans*-tautomeric forms based on emission anisotropy rather tricky. Quantum chemical calculations, on the other hand, point to the retainment of nearly orthogonal directions of transition moments for S_0–S_1 and S_0–S_2 upon substitution with the amino group. Based on quantum theory, MCD, and emission anisotropy, absorption bands in aminoporphycenes have been accurately assigned; see Figure 5.6 and Table 5.3.
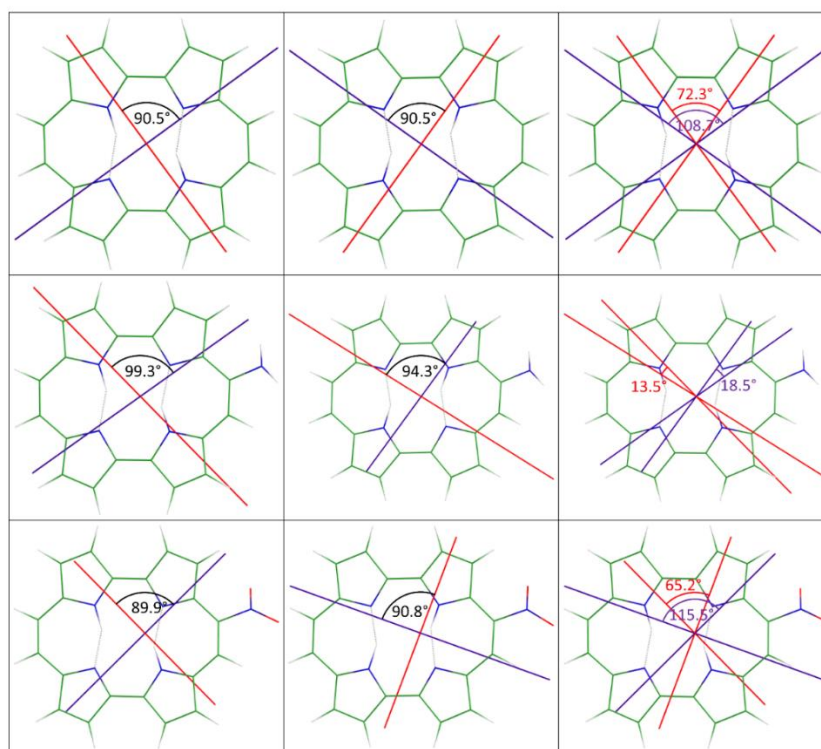
*Figure 5.5 Calculated directions of S_1←S_0 (red) and S_2←S_0 (violet) transitions in **Pc** (top), **APc** (middle), and **NPc** (bottom) in the trans-1 (left column) and trans-2 (middle column) forms. The right column shows transition moment directions for both forms. The respective angles are marked in the drawings. Reprinted from ref.[231]*

*Figure 5.6 Bottom, absorption of **APc** in toluene (a) and of **ttAPc** in paraffin (b). Middle, MCD of **APc** in toluene. Top, anisotropy of fluorescence excitation of **ttAPc** in paraffin, monitored at 735 nm. Reprinted from ref.[231]*

*Table 5.3 Assignment of absorption bands in **APc***

λ (cm^{-1})	Transitions (tautomeric form)	Comment
13 755	S$_1$(*trans-1*)	S$_1$(0-0)
14 760	S$_1$(*trans-2*)	S$_1$(0-0)
15 800	S$_2$(*trans-2*)	S$_2$(0-0)
16 750	S$_2$(*trans-1*)	S$_2$(0-0)
16 860	S$_2$(*trans-2*)	vibronic feature
17 650	S$_2$(*trans-1*)	vibronic feature

The absorption spectra (Figure 5.6) show solvatochromic effects with bathochromic shifts observed in less polar solvent - toluene. Therefore, the lowest transition is observed in toluene at 13 755 cm^{-1} (which coincides with the calculated value), with the subsequent transition lying 1005 cm^{-1} higher at 14 760 cm^{-1}. Two weak bands are observed at 15 800 cm^{-1} and 16 860 cm^{-1} just before the most intense transition in the Q region located at 17 650 cm^{-1}. Based on the negative signal of the MCD and emission anisotropy, these weak bands are assigned to the S$_2 \leftarrow$S$_0$ transition, while the band at 17 650 cm^{-1} corresponds to the vibronic structure of S$_2$. Details on the assignments of specific transitions to unique tautomeric forms have been described[231] and summarized in Table 5.3. Experimental data were a good match with calculations (Figure 5.7), and when combined with MCD and anisotropy, the assignment of bands was possible.

*9-Aminoporphycene-2,7,12,17-tetra-tert-butylporphycene (**ttAPc**) and 9-Aminoporphycene-2,7,12,17-tetra-n-propylporphycene (***tprAPc**)*

Absorption spectra of **ttAPc** and **tprAPc** follow the same pattern of 9-aminoporphycene (**APc**) with a more profound splitting of the Soret band in **ttAPc** and **tprAPc** relative to **APc**. Solvent effects result in a red-shift for non-polar solvents, similar to what is obtained in **APc**. Calculations and experiments suggest the absorption bands' assignment closely follows the pattern of **APc**. The S$_1$ transition energies of two *trans* forms of **ttAPc** lie at slightly higher energies than that of **APc**. In S$_2$, a different picture is observed, *trans-2* is red-shifted, whereas, for *trans-1,* the transition energy remains the same within experimental error. Each predicted and experimentally observed transition energy is discussed in detail in our paper.[231]
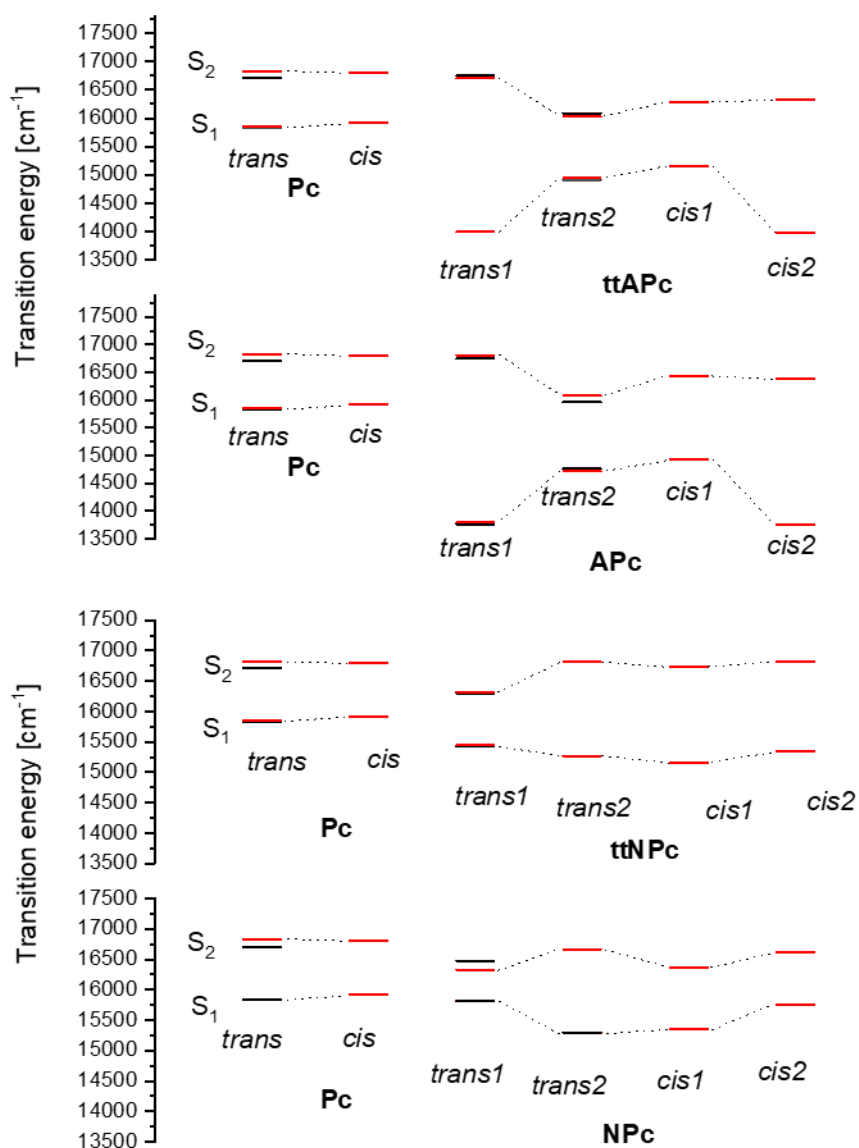
*Figure 5.7 Comparison of calculated (red bars) and experimentally observed (black bars) S_1 and S_2 transition energies in different tautomeric forms of **Pc** and its amino and nitro derivatives. Reprinted from ref.[231]*

5.3.2.3 9-nitroporphycenes

Quantum chemical calculations for nitroporphycenes predict the two *trans* tautomers to be almost degenerate and most stable forms. In **NPc**, the *trans-2* form is stabilized in contrast to **APc,** where the *trans-1* form is the most stabilized. Very broad bands characterize the Soret region in the absorption spectra of the three nitro-derivatives, as presented in Figure 5.8. These bands have been carefully assigned to specific tautomers and transitions as shown in Figure 5.9.[231]
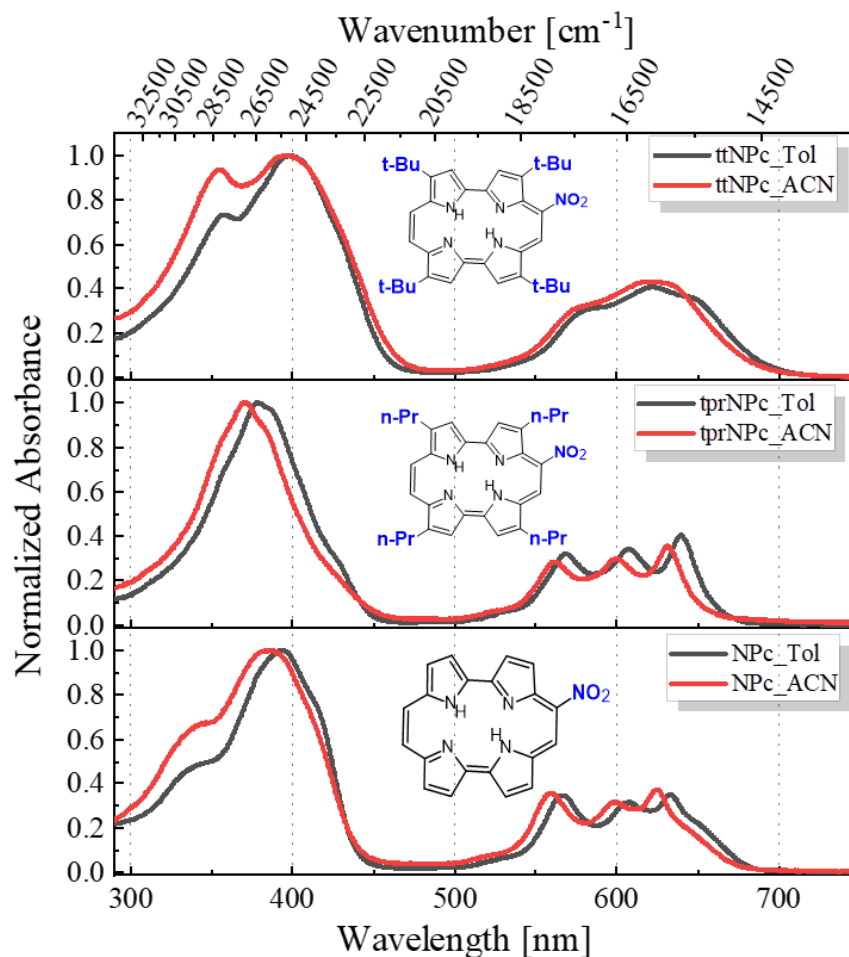
*Figure 5.8 Absorption spectra of **NPc** (bottom), **tprNPc** (middle), and **ttNPc** (top) in toluene (**black**) and acetonitrile (**red**).*

As evident in Figure 5.8, all nitro derivatives retain the "three-finger" absorption pattern in the low-energy region. This pattern is characteristic of most porphycenes, excluding the amino derivatives where at least five bands were observed. The most notable difference is observed for the **ttNPc** where the fingers in the low energy region are not well-structured like in the **tprNPc**

and **NPc** counterparts. This uniqueness in **ttNPc** is due to steric interactions between the periphery's nitro group and the surrounding bulky tertiary butyl substituents.
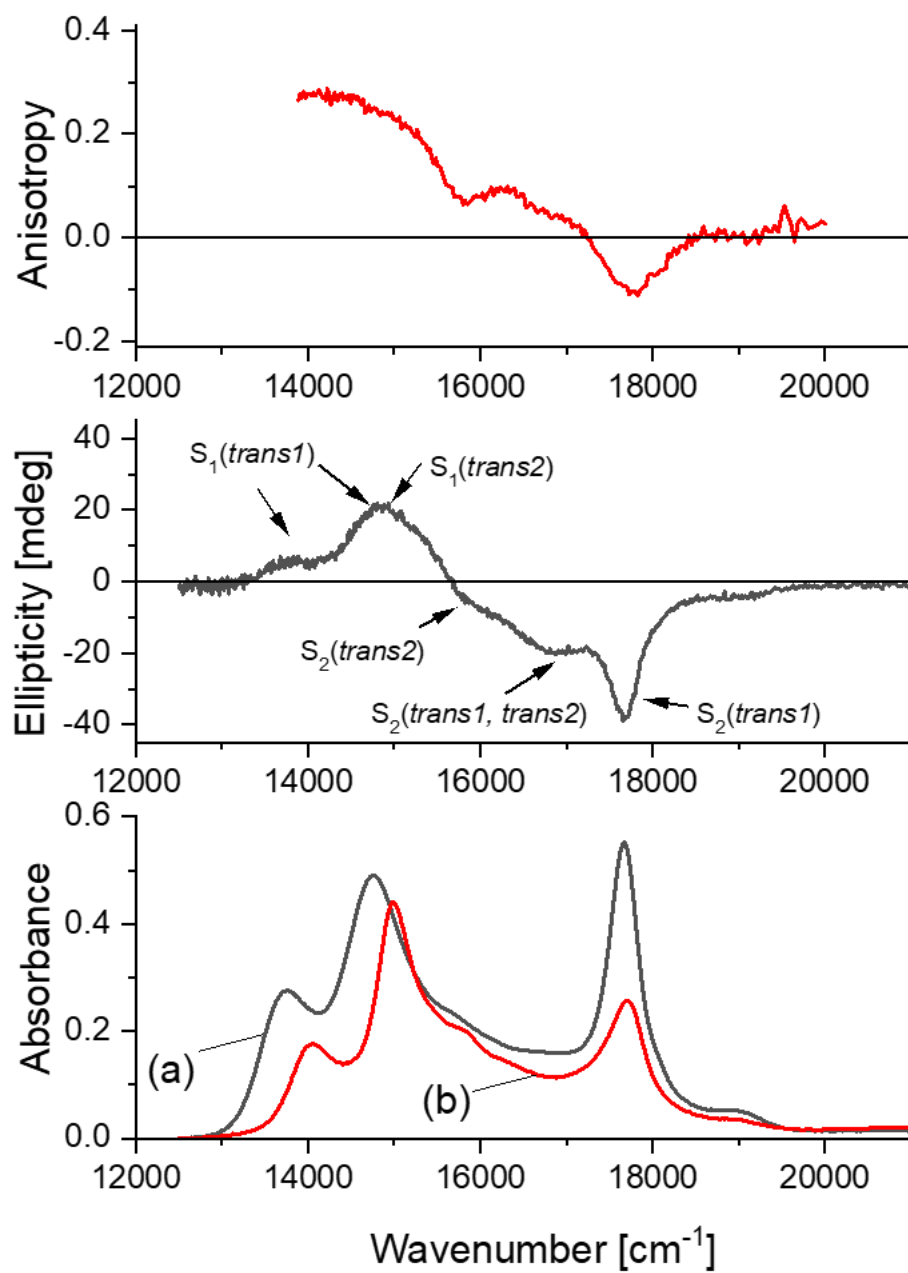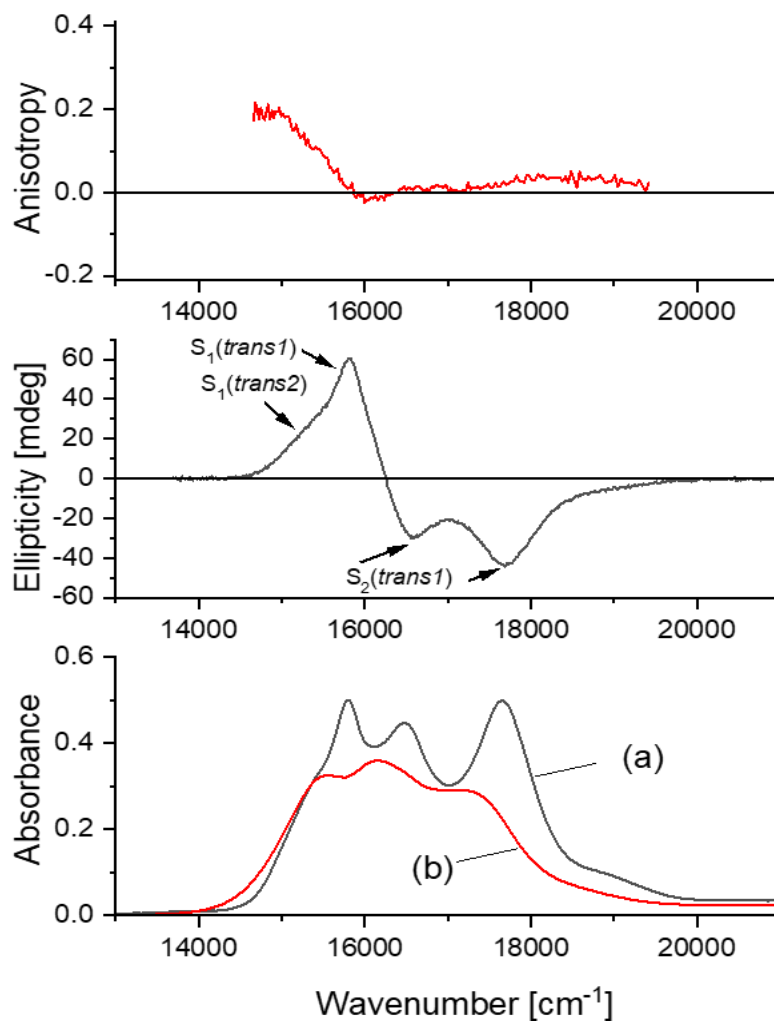

*Figure 5.9 Bottom, absorption of **NPc** in toluene (a) and **ttNPc** in paraffin (b). Middle, MCD of **NPc** in toluene. Top, anisotropy of fluorescence excitation of **ttNPc** in paraffin, monitored at 710 nm. Reprinted from ref.*[231]

Similar to **APc**, the calculated transition energies match the experimental results in **NPc**. Figure 5.7 visualizes the energy ordering and the transition patterns observed for both nitro and amino derivatives.

5.4 Fluorescence measurements and photophysical data

5.4.1 Aminoporphycenes

Fluorescence spectra of the three amino derivatives **APc**, **tprAPc,** and **ttAPc** follow the same pattern, with the most intense band coinciding with the lowest energy band – F_1. In **APc**, two unique bands (F_2 and F_3) of weaker intensity are observed in the high-energy region with peaks at 668 nm (F_2) and 635 nm (F_3). An interesting observation was that intensity ratios of the F_1/F_2 and F_2/F_3 bands were largely dependent on the excitation wavelength, the solvent used, and the age of the sample solution. This points to the fact the emissions F_2 and F_3 originate from species different from aminoporphycene.
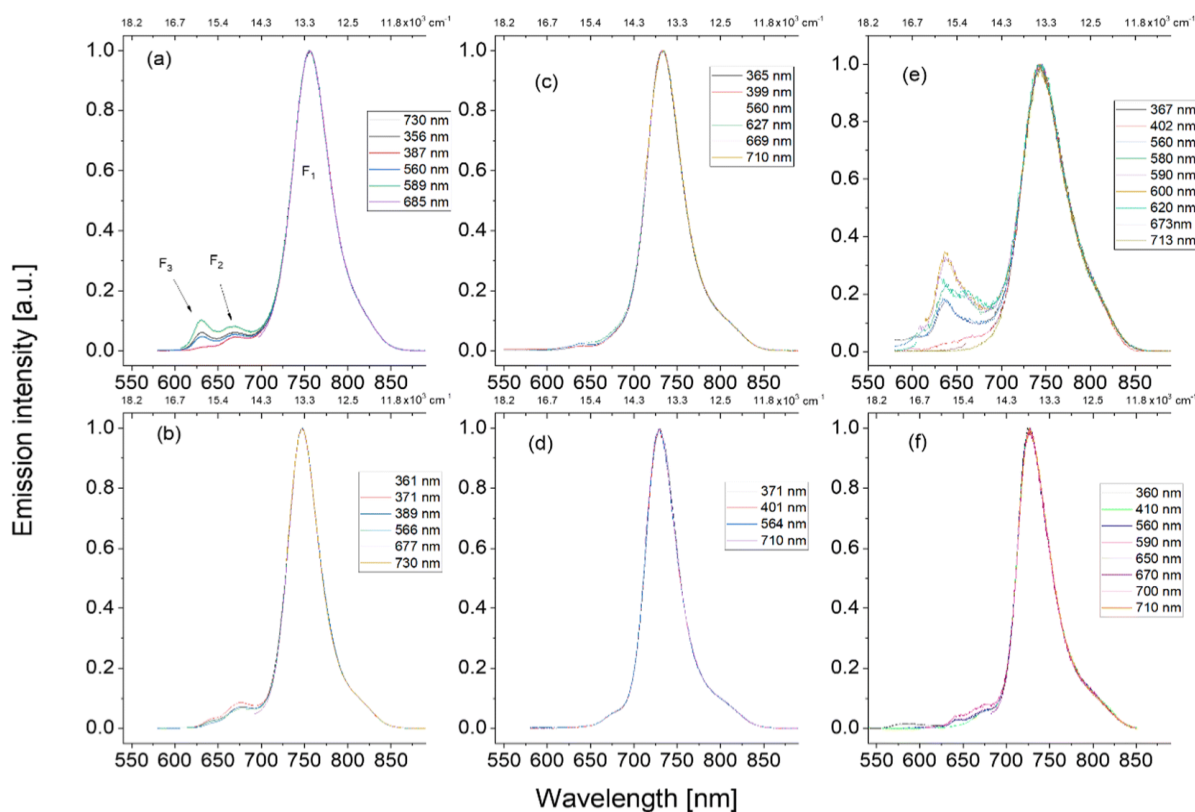
Figure 5.10 Room temperature fluorescence spectra: **APc** *(a),* **tprAPc** *(c), and* **ttAPc** *(e) in acetonitrile,* **APc** *(b) and* **tprAPc** *(d) in toluene, and* **ttAPc** *(f) in paraffin. The spectra were normalized to the F_1 maximum. Excitation wavelengths have been color-coded. Reprinted from ref.[231]*

The observation of a total of three bands (F_1, F_2, and F_3) in the emission spectra of **APc** is a recent finding versus what was earlier reported for *β*-tetrapropyl, tetramethoxyethyl, and tetraphenyl aminoporphycenes.[105] In the earlier report, '*dual fluorescence*'- F_1 and F_2 were observed and assigned to *trans-1* and *trans-2* tautomers, respectively.[103,105] The authors explained this on the basis that tautomerization occurred in higher S_n states but not in the S_1 state. In S_1, the high-energy tautomer (*trans-2*) was supposed not to tautomerize to the low-energy *trans-1* form, implying a non-equilibration between the two forms in the lowest excited state, and both *trans* forms had different energies; therefore, emission with different lifetimes was observed from each of the tautomers.

In the series of fluorescence experiments performed for **tprAPc** during the present research work, it was observed that fluorescence spectra obtained for freshly synthesized and purified samples, F_3 and F_2 bands, were almost non-existent; at the same time, F_1 was the main emission band. However, the F_3 and F_2 bands gradually increased with an increasing number of days as the sample solution aged (Figure 5.11).[238] These extra two bands have now been assigned to the degradation products of aminoporphycene – a process established to occur in the dark and in the presence of light. The growth of the bands was observed to be more pronounced in acetonitrile than in non-polar solvents. For **APc** and **ttAPc**, traces of F_2 and F_3 are seen even in freshly synthesized-purified samples. However, these bands steadily grow similarly as in **tprAPc**. More details on this specific observation and the instability of aminoporphycenes are described in Chapter 7 of this thesis.

In fluorescence excitation experiments of aminoporphycenes (Figure 5.12), when monitored at F_1, the spectrum matches that of the absorption. In contrast, the excitation spectra of F_2 and F_3 look similar but are different from the absorption spectra. This is true for the three amino derivatives of porphycene. The difference in the excitation spectra of F_2 and F_3 bands to the absorption spectra indicates that F_2 and F_3 emissions do not originate from aminoporphycene. Instead, this is emission from the products of degradation of aminoporphycene.

Regarding fluorescence quantum yields, all three aminoporphycenes are weak emitters (see Table 5.4), with the yield being lower in acetonitrile than in toluene. This trend is followed not just by aminoporphycene but by all investigated compounds (Figure 5.14). The weakest emitter in the amino series is **ttAPc**, an effect due to the steric interaction between the bulky *tert*-butyl groups and the amino substituent. A similar situation is observed for the **ttNPc**, confirming the bulky

groups' interference with the substituent at position nine. The decay lifetimes are summarized in Table 5.5; the excited state lifetimes are between 1 ± 0.05 ns and 3 ± 0.10 ns for all three amino derivatives when monitored at the low energy region, except in the case of **ttAPc,** where the decay is subnanosecond in toluene/acetonitrile, but 10 times longer lifetimes is observed just from changing the solvent to paraffin. These decay times in amino porphycenes are quite rapid compared to parent porphycene, which exhibits a lifetime of 9-11 ns, depending on the solvent.
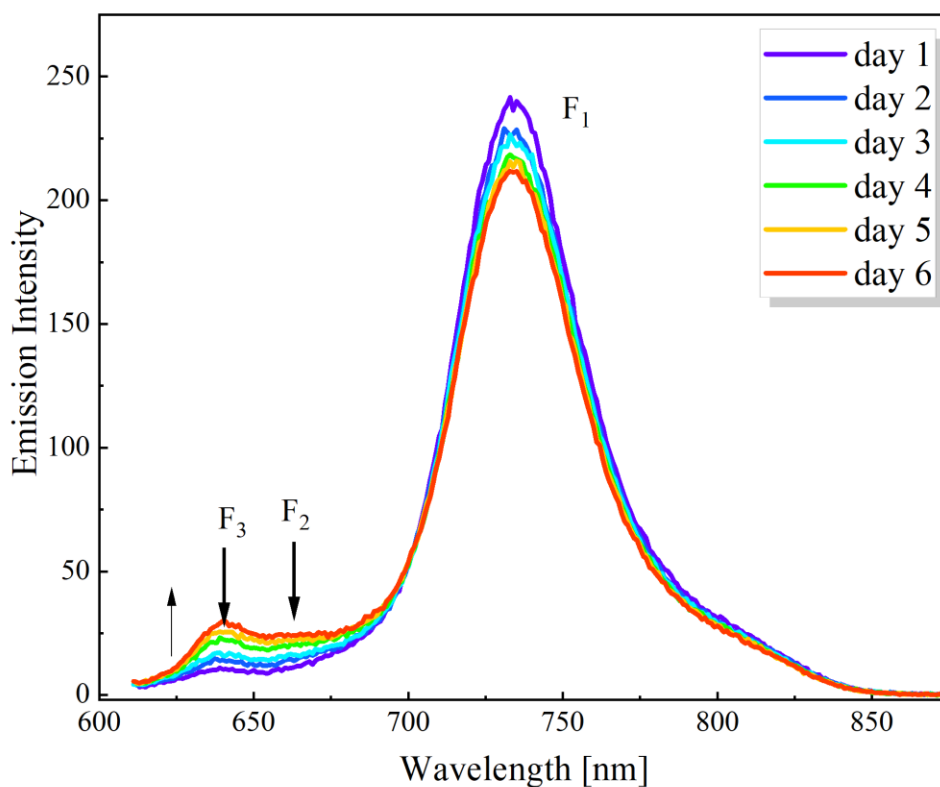
Figure 5.11 Fluorescence of a sample of **tprAPc** *in acetonitrile recorded at one-day intervals from the moment of synthesis. The arrow shows the increase of the band peaking at 640 nm. The excitation wavelength was 600 nm.*

When the lifetimes of aminoporphycenes were monitored at F_2 (670 nm), a fast decay component was observed, which indicates an extremely rapid transformation of *trans-2* to *trans-1*.This rapid transformation is understood on the basis that the *trans-1* is stabilized relative to the *trans-2* in S_1 (see Table 5.1), which favors a quick transformation of *trans-2* to *trans-1*; as such, the latter

tautomer is responsible for the main emission band. Moreover, this explanation holds for the reason the excitation spectra (monitored at F_1) match the absorption spectra (which consist of the *trans-1*, *trans-2*, and possibly the *cis-1*). The decay lifetime was extremely rapid (sub ns) for **ttAPc** in toluene and an order of magnitude higher in liquid paraffin (1.01 ± 0.05), pointing to solvent viscosity effects in the photophysical properties of these porphycenes.
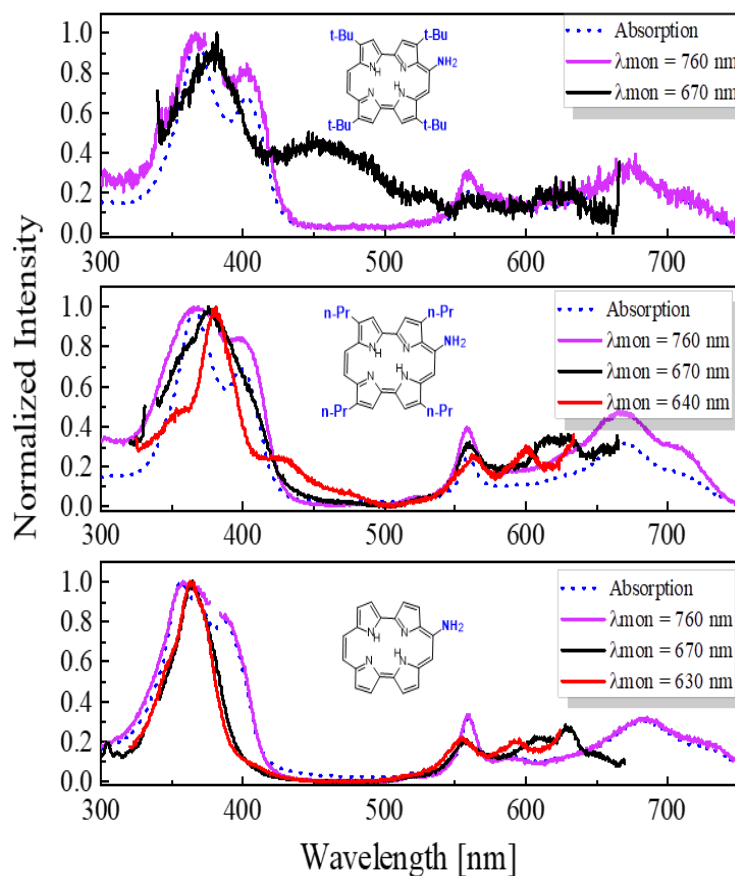
*Figure 5.12 Fluorescence excitation spectra of **APc** (bottom), **tprAPc**(middle), and **ttAPc** (top) in acetonitrile*

5.4.2 Nitroporphycenes

The three nitro derivatives emit a single fluorescence pattern (Figure 5.13), similar to parent porphycene, independent of the excitation wavelength. The spectra of the three compounds exhibit a few nm red shift in toluene relative to acetonitrile. The highest emitter among the nitro-series is 9-nitroporphycene, with a 10% fluorescence quantum yield (Figure 5.14). The decay lifetimes (Table 5.5) are monoexponential and range between 2 ± 0.1 ns and 5 ± 0.2 ns, depending on the solvent.[231] The quantum yield of emission follows a trend **NPc** > **tprNPc** > **ttNPc** for the nitro

derivatives (Table 5.4). The worst emitter in the list, **ttNPc**, yielded fluorescence in the order of 10^{-4}. This very low emission is due to the interference of the *tert*-butyl moieties with the nitro substituent. The other member of the group, **tprNPc**, exhibited a 3 times higher quantum of yield of emission when studied in non-polar solvents versus polar solvents.

Table 5.4 Fluorescence quantum yields (293 K). For aminoporphycenes, the values are calculated from F_1 emission only.

	Solvent	ϕ_{fl} [a]
APc	toluene	0.03
	acetonitrile	0.01
tprAPc	toluene	0.04
	acetonitrile	0.02
ttAPc	*n*-hexane	3.6×10^{-3}
	acetonitrile	6×10^{-4}
NPc	toluene	0.10
	acetonitrile	0.06
tprNPc	toluene	0.03
	acetonitrile	0.009
ttNPc	*n*-hexane	4×10^{-4}
	toluene	3×10^{-4}
	acetonitrile	6×10^{-4}
	ethanol	3×10^{-4}
	DMSO	5×10^{-4}

[a] Estimated maximum error: ±20% for $\phi_{fl} > 10^{-2}$, ±30% for lower values
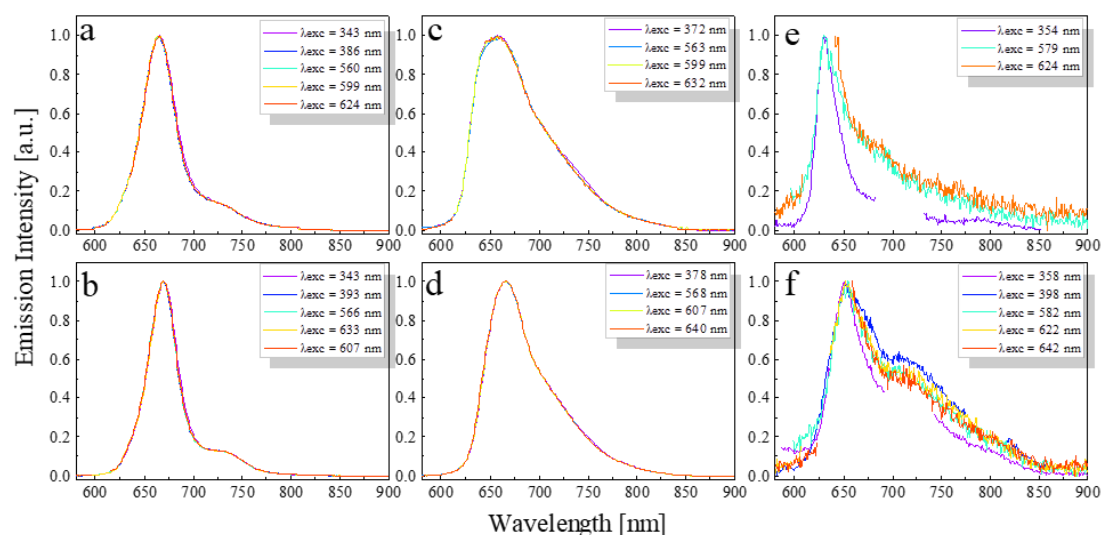
*Figure 5.13 Room temperature fluorescence spectra: **NPc**, **tprNPc**, and **ttNPc** in acetonitrile (a, c, and e) and toluene (b, d, and f). Excitation wavelengths have been color-coded.*
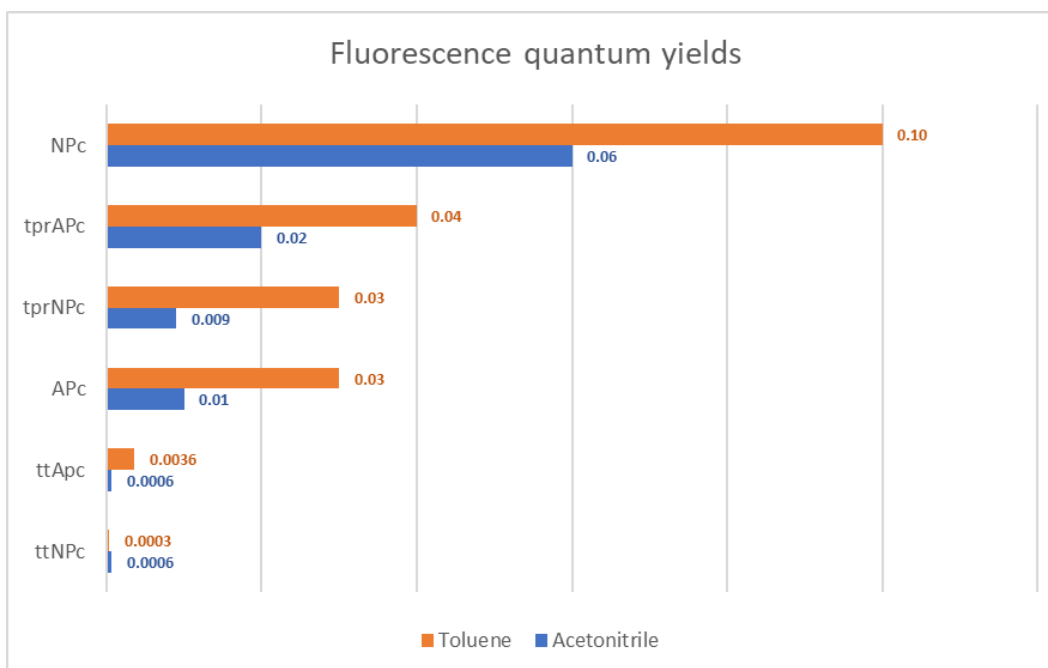
Figure 5.14 Trends in fluorescence quantum yields

While **tprNPc** yields a 3% emission quantum yield in toluene, 0.9% is observed in acetonitrile. The trend in emission for both amino and nitro-porphycenes is presented in Figure 5.14. As a collective, better quantum yields of emission are observed in toluene vs acetonitrile. The tertiary butyl derivatives in both amino and nitro-porphycenes were the weakest emitters, and this unique behavior points to the influence the tertiary butyl groups have on the properties of these macrocycles.

The aminoporphycenes (**APc** and **tprAPc**) exhibited moderate yields in the quantum yields of singlet oxygen (SO) formation (Table 5.6), with the exception of **ttAPc**. On the other hand, **NPc** and **tprNPc** generated excellent yields of singlet oxygen, 50% and 61%, respectively. When nitro or amino porphycene was substituted with tetrapropyl groups at the β position, the yields of SO were better than without the propyl groups. When bulky *t*-butyl groups were introduced at β, however, no yield in SO was observed, as in the case of **ttAPc** and **ttNPc**. Again, this is a pointer to how varying substitution affects the photophysics of porphycenes. In addition, there is a trend in the observed yields as a function of solvent, with higher SO generation being observed in toluene, which is a less polar solvent.

Table 5.5 Decay times of excited singlet state

	Solvent	τ_{fl}(ns)
APc	toluene	2.00 ± 0.05[a]
	n-hexane	2.60 ± 0.10 [a]
	acetonitrile	1.40 ± 0.05 [a]
	methanol	1.00 ± 0.05 [a]
tprAPc	toluene	2.40 ± 0.05 [a]
	acetonitrile	1.90 ± 0.05 [a]
ttAPc	toluene	0.15 ± 0.03 [a]
	paraffin	1.01 ± 0.05 [a]
NPc	toluene	$3.40 \pm 0.$
	n-hexane	4.40 ± 0.2
	acetonitrile	2.70 ± 0.2
	acetonitrile:water 80:20 v/v	2.20 ± 0.1
tprNPc	toluene	1.10 ± 0.10
	acetonitrile	0.50 ± 0.00
ttNPc	*n*-hexane	[b]
	toluene	[b]
	acetonitrile	[b]

[a] Observed decay for the low energy band. [b]decay too short (<50 ps) to be reliably determined

Table 5.6 Quantum yield of singlet oxygen generation and triplet lifetimes

	Solvent	τ_T(ns)	ϕ_Δ
APc	toluene	118	0.21
	acetonitrile	-	0.12
tprAPc	toluene	165	0.26
	acetonitrile	-	0.28
ttAPc	toluene	[a]	0.05
	acetonitrile	-	0.02
NPc	toluene	164	0.49
	acetonitrile	-	0.49
tprNPc	toluene	192	0.61
	acetonitrile	-	[a]
ttNPc	toluene	[a]	0.03
	acetonitrile	-	0.01

[a]decay too short (<50 ps) to be reliably determined. - decay was not determined in acetonitrile

5.4.3 Summary

Spectroscopy:

- Substitution of porphycene with nitro and amino group at the *meso* position leads to changes in the absorption spectra. New red-shifted bands are explicitly observed for the aminoporphycenes.

- The specific influence of alkylation is not observable in the spectra of **tprAPc**, **ttAPc**, **tprNPc**, and **ttNPc**, as such influence is overshadowed by that of nitro and amino groups.

- Only the *trans-1* is responsible for the emission in the amino series since the *trans-2* form quickly transforms to the *trans-1* in the lowest excited state.

- Previous misconception of dual emission in amino derivatives is demonstrated; fluorescence is confirmed to be single emission, with two other bands being a consequence of the degradation of aminoporphycenes.

- Single emission is also observed for nitro derivatives.

Photophysics:

- Both nitro and amino porphycenes presented in this chapter are moderate or weak emitters with substantial rates of non-radiative processes.

- Both derivatives are attractive models for more detailed studies on ground and excited state tautomerization mechanisms.

- 9-nitroporphycene is the highest emitter among the studied compounds, with a 10% yield of emission.

- The *tert*-butyl derivatives are the weakest emitters in both the nitro and amino categories. This weak emission is associated with the steric interactions between the 9-substituent and the bulky *tert*-butyl groups. This interaction varies substantially in S_0 and S_1 states, as suggested by calculations.

- Nitroporphycenes are moderate emitters with a 50% yield of singlet oxygen generation and, therefore, qualify as photosensitizers in PDT, with the exception of the *tert*-butyl nitro derivative.

Tautomerism

- Two *trans* forms are present in the electronic ground state, but one in the S_1 state, and tautomerism favors the most stable form.

- While studying the lifetimes of amino porphycenes, a very fast decay component is observed when monitored at the high-energy region. This suggests that the double hydrogen transfer in S_1 occurs in a few picoseconds.

- A complex mechanism for the proton transfer is expected for **APc** and **NPc,** given the asymmetry in 9-substituted derivatives. According to our findings, we have suggested three routes for the proton transfer in the ground state,[231] two of which are a step-by-step process involving the *cis-1* and *cis-2* tautomers as intermediates. The third route is a nonsynchronous-concerted double transfer of hydrogen.

Chapter 6

6.1 Spectroscopy, photophysics, and tautomerism of 2-nitro-7,12,17-tri-*tert*-butylporphycene.

This chapter discusses the research work described in a published manuscript.[232] *Agnieszka Gajewska, **<u>Idaresit Mbakara,</u>** and Jacek Waluk (**2023**). 2-nitro-7,12,17-tri-tert-butylporphycene: Spectroscopy, photophysics, and tautomerism. Journal of Porphyrins and Phthalocyanines. https://doi.org/10.1142/S1088424623500360. The compounds discussed in this chapter were synthesized by Dr. Agnieszka Gajewska, a synthetic chemist in Prof. Waluk's team at the Institute of Physical Chemistry Polish Academy Sciences, Warsaw, Poland.*

Many significant scientific discoveries and advancements have resulted from accidental discoveries or unintended outcomes. One such discovery occurred while Dr. Gajewska synthesized 9-nitroporphycene (**NPc**), a process which also 'unintentionally' yielded 2-nitro-7,12,17-tri-*tert*-butylporphycene (**2NttPc**). As already mentioned in section 1.6, porphycenes have found prominence in various applications due to their characteristic photophysical and tautomeric properties, making them suitable for applications such as photocatalysis, PDT, and molecular switches.[18,72] It has also been confirmed that the nature, number, and position of substituents influence the spectral properties of porphycenes.[239–242] Substituents such as alkyl, aryl groups, and hetero atoms have been reported to significantly influence the photophysical characteristics of porphycenes.[36] Moreover, the dimensions of the porphycenes' inner cavity are either extended or reduced depending on the substituent and the position.[52] One could, therefore, wonder how nitro groups can modify porphycene's photophysical and spectral properties when placed at different positions on the compound, especially in the case of single or double substitutions, and also when the nitro moiety is introduced together with *tert*-butyl groups.

9-nitroporphycene (**NPc**)   9-nitro-2,7,12,17-tetra-*tert*-butylporphycene (**ttNPc**)   9,20-dinitro-2,7,12,17-tetra-*tert*-butylporphycene (**ttdNPc**)   2-nitro-7,12,17-tri-*tert*-butylporphycene (**2NttPc**)
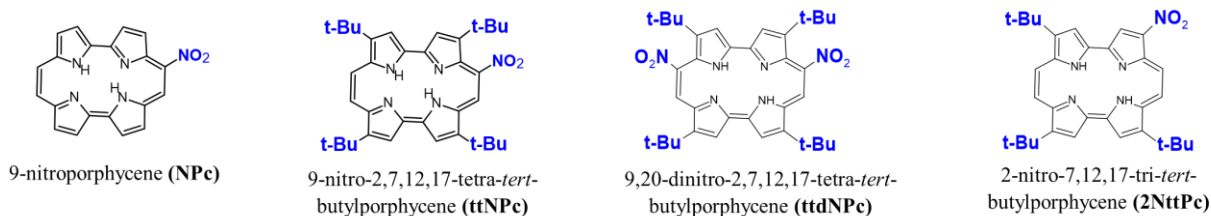
Figure 6.1 Studied compounds

This chapter shows the relationship between substituent position and the spectral, photophysical, and tautomeric properties of four porphycene derivatives (Figure 6.1). The synthetic processes for the presented compounds have been described in detail for **NPc**,[243] **ttNPc**,[231] and **2NttPc**.[232] The nitration of 2,7,12,17-tetra-*tert*-butylporphycene (**ttNPc**), a process that involves dissolution of the compound in dichloromethane and acetic acid, followed by the addition of silver nitrate, resulted in expected products – **ttNPc and ttdNPc,** as well as **2NttPc,** a by-product. The by-product of that synthetic process, **2NttPc**, is the subject of investigation in this chapter.

As seen in Figure 6.2, the absorption spectra of **NPc**, **ttNPc**, **2NttPc,** and **ttdNPc** retain the general pattern of porphycene regardless of the substituent, however, with unique bands or structures pertaining to the number and position of the nitro group(s). The insensitivity of porphycenes to substitution stems from porphycenes being classified as hard chromophore (ΔHOMO $\ll$ LUMO) in contrast to porphyrin, a soft chromophore (ΔHOMO $\approx$ LUMO). This classification implies that significant perturbation is required for major changes to be observed in the absorption spectra of porphycenes. Thus, the characteristic features of the Soret and Q-bands are retained for the four porphycene derivatives presented. More structured bands are observed in the Q-region for the **NPc** and **2NttPc**; **ttNPc and ttdNPc,** on the other hand, show a broad Q-band. This 'structureless' feature is explained on the basis of steric interaction between the nitro group in position 9 (*meso*) and the *t*-butyl group in position 2 (*β*) of the macrocycle. Another consequence of the steric interaction is the deviation from planarity (Figure 6.3) in the case of **ttNPc** compared to **NPc** and **2NttPc.**

The MCD spectra of the four porphycene derivatives (Figure 6.2) suggest the Soret band is made up of at least four electronic transitions. This observation is counterintuitive by merely looking at the absorption spectra. In the Q region, at least two transitions are observed. Worthy of note is the presence of a shoulder at ~650 nm in NPc (Figure 6.2 (d-bottom)), and this absorption band has been predicted by calculations to belong to the *trans-2* form of **NPc,** also calculated to be energetically the most stable.[231]
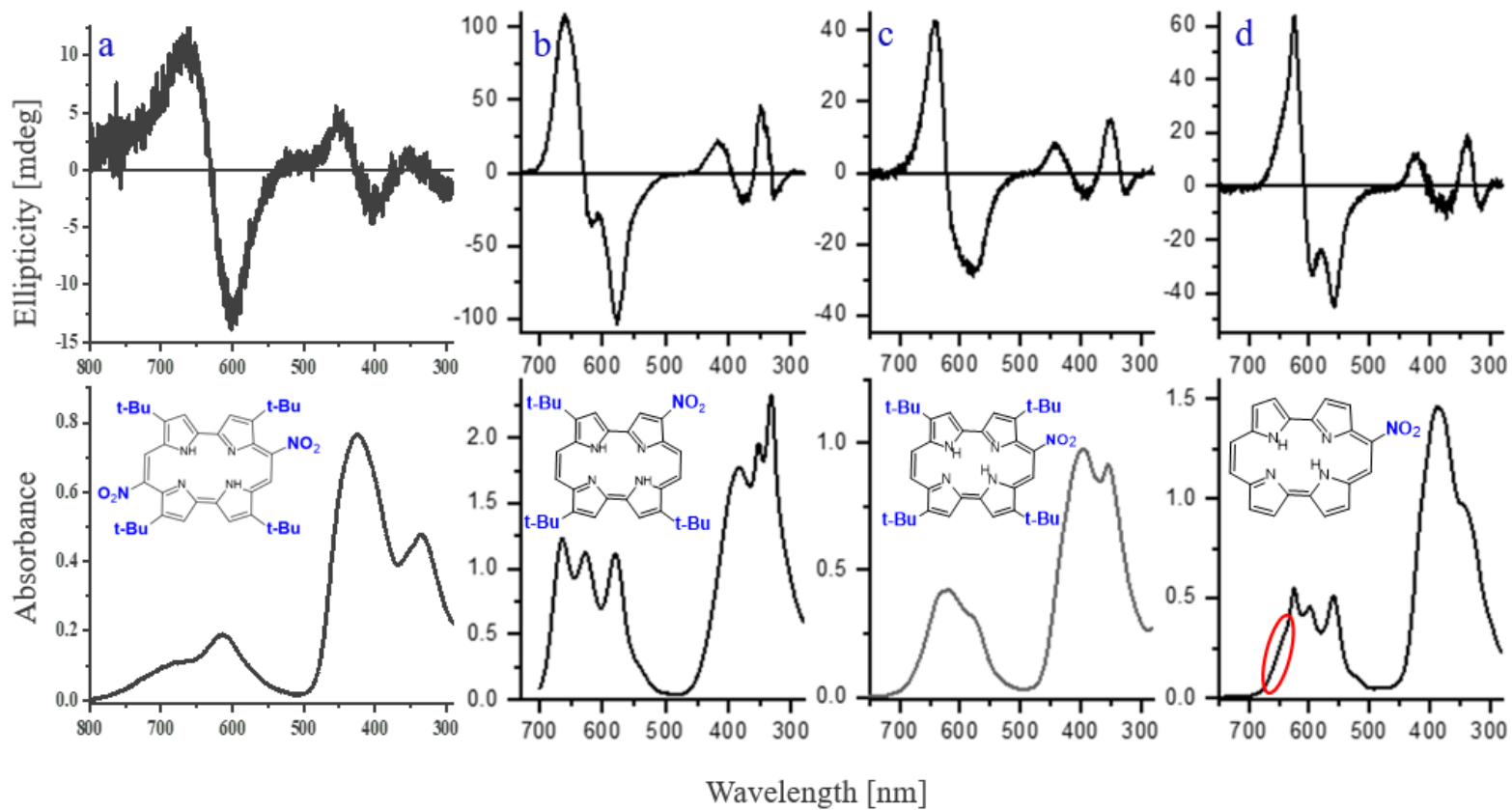
*Figure 6.2 Room temperature MCD (top) and absorption (bottom) spectra of nitroporphycenes in acetonitrile. From left to right: **ttdNPc** (a), **2NttPc** (b), **ttNPc** (c), and **NPc** (d). The red circle indicates the shoulder in **NPc**. Adapted from ref.[232]*

Regarding planarity (Figure 6.3), while **2NttPc** is planar, **ttNPc** has a non-planar structure with the NO_2 moiety being twisted by a 40° angle from the molecular plane. The N-N distances in the two compounds show a deviation from rectangularity in **ttNPc** as the picometer dimensions of the N-N distances portray a trapezoidal shape. On the other hand, a rectangular shape is maintained in **2NttPc**. The degree of twisting along the molecular plane for **ttNPc** varies in S_0 and S_1, according to calculations.[232]
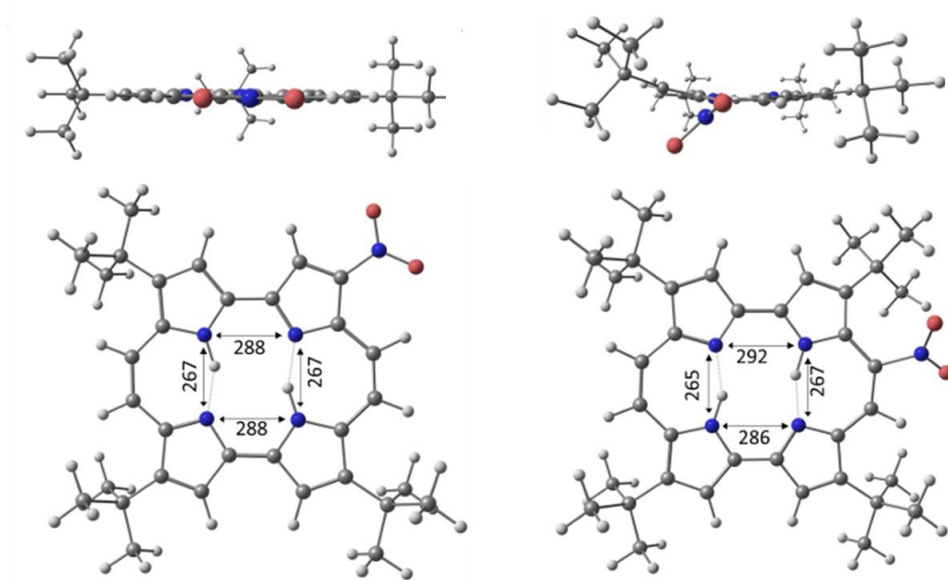
*Figure 6.3 Calculated geometries of **2NttPc** (left) and **ttNPc** (right). The top images demonstrate the planarity of **2NttPc** and nonplanarity of **ttNPc**. Adapted from ref.[232]*

*Table 6.1 Quantum yields of fluorescence and lifetimes of fluorescence of **2NttPc**, **NPc**, and **ttNPc***

		ϕ_{fl}	$\tau(ns)$
2NttPc	toluene	0.17	
	acetonitrile	0.08	4.7
	n-hexane		6.1
NPc	toluene	0.10	
	acetonitrile	0.06	2.7
	n-hexane		4.4
ttNPc	toluene	3×10^{-4}	a
	acetonitrile	6×10^{-4}	a
	n-hexane		a

[a] decay too short to be reliably determined

The three nitro derivatives exhibit single emission independent of excitation wavelength, typical of parent unsubstituted porphycene (Figure 6.4). For **2NttPc,** the emission consists of a primary fluorescence 0-0 band peaking at 684 nm in both toluene and acetonitrile, indicating similar dipole moment values in S_0 and S_1. The 0-0 emission band is followed by a low-intensity vibrational band. Recorded fluorescence bands are broader in polar solvents than in non-polar toluene. At room temperature, **2NttPc** is a moderate emitter, with a quantum yield of fluorescence comparable to **NPc** in both polar and non-polar solvents (Table 6.1). On the other hand, **ttNPc** is an extremely weak emitter since the butyl groups interact strongly with the nitro group. The excited state of **2NttPc** lives for ~6 ns in *n*-hexane and ~4 ns in acetonitrile (Table 6.1); the fit was mono-exponential, confirming that the emission originates from one tautomer (Figure 6.6). The other possibility is the S_1 equilibration between the *trans-1* and *trans-2* forms, but the spectral data do not indicate this.
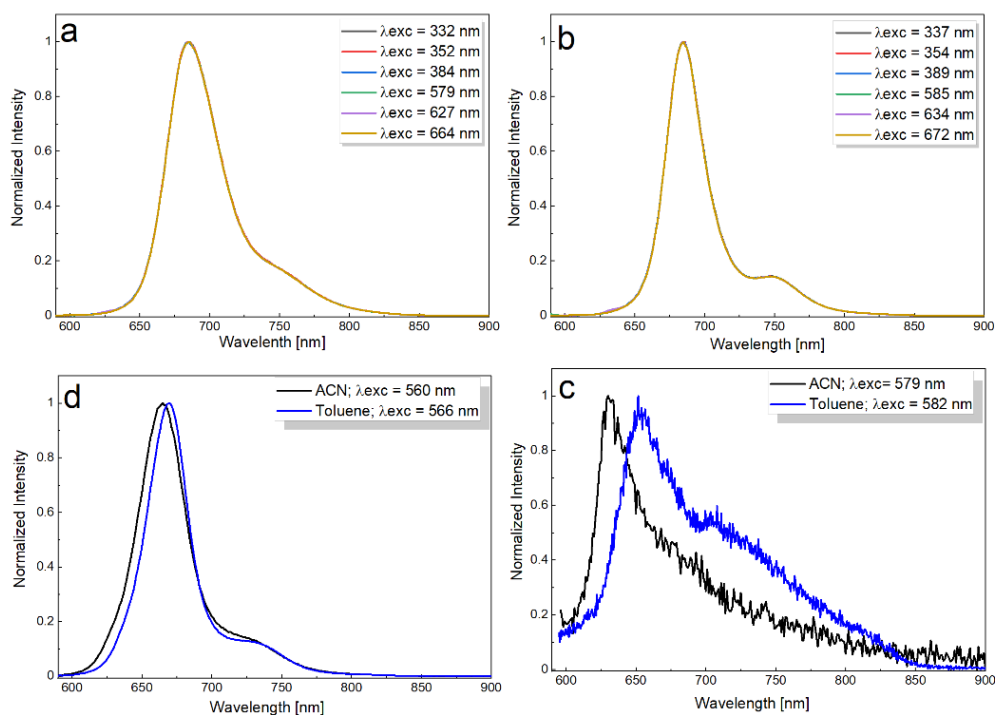
*Figure 6.4 Top: Room temperature emission spectra of 2-nitro-7,12,17-tri-tert-butylporphycene (**2NttPc**) in acetonitrile (a) and toluene (b). Bottom: RT emission spectra of 9-nitroporphycene (**NPc**) (c) and 2,7,12,17-tetra-tert-butylporphycene (**ttNPc**) (d). Black line: acetonitrile, blue line: toluene.*

6.2 Tautomerism

Calculations suggest that one tautomeric form is responsible for the emission in **2NttPc**. This suggestion is corroborated by the monoexponential kinetics of the decay profile in conjunction with the absorption, emission, and excitation spectra (Figure 6.5). Fluorescence excitation spectra coincide with the absorption spectra. Quantum chemical calculations for **2NttPc** predict the *trans-1* tautomer to be the lowest energy tautomer species, and this form is responsible for the emission. This contrasts with what is calculated for **ttNPc** and **NPc.** In NPc, the *trans-2* form lies at lower energy relative to the *trans-1*, while in **ttNPc**, both *trans* tautomers are nearly degenerate.[231] Table 6.2 shows the calculation energies of the different forms of **2NttPc.** The *trans-2* is destabilized, and given the monoexponential fluorescence decay, the *trans-1* form is the only emitting species.

*Table 6.2 Calculated relative energies (kcal mol^{-1}) and permanent dipole moments in the ground electronic state of the tautomeric forms of 2-nitro-6,12,17-tri-tert-butylporphycene (**2NttPc**)*

	E^a (kcal mol^{-1})	μ [D]	N$_1$-N$_4$ (pm)	N$_2$-N$_3$ (pm)
trans-1	0.00 (0.0)	8.48	267	267
trans-2	1.58 (1.41)	8.65	265	266
cis-1	2.11 (1.57)	9.56	263	263
cis-2	3.55 (2.79)	7.63	261	262

^{a} in parentheses, zero-point corrected values
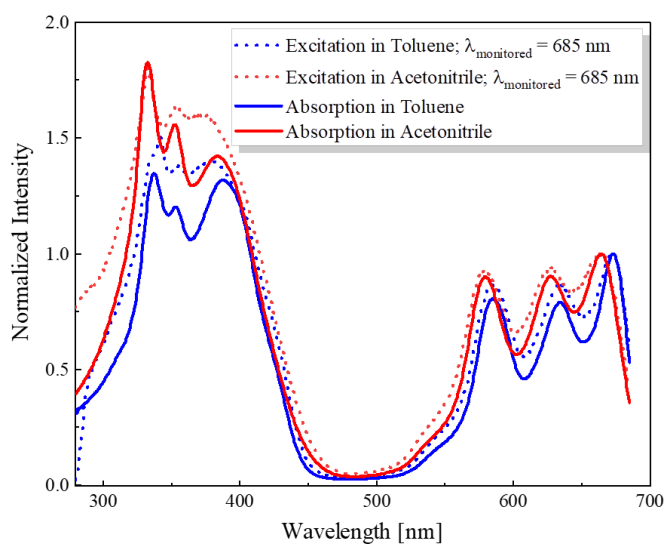
*Figure 6.5 Fluorescence excitation and absorption spectra of **2NttPc** in acetonitrile and toluene.*
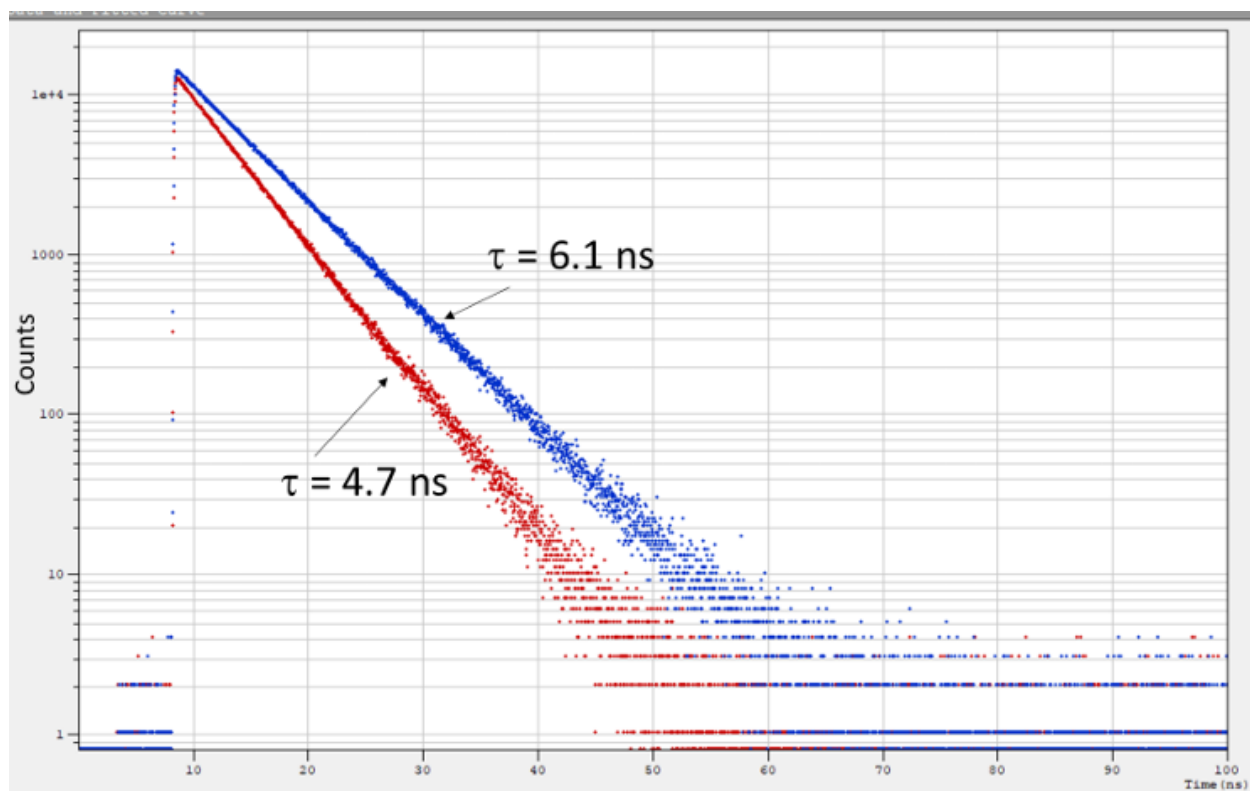
Figure 6.6 Fluorescence decay profiles obtained for 2NttPc in n-hexane (blue) and acetonitrile (red) solutions at 293 K. Reprinted from ref.[232]

6.3 Summary

The photophysical and tautomeric properties of nitro-substituted porphycenes are influenced not only by the substituent but also by its position. Placing the nitro group at the *meso* (9) position results in the near degeneracy of the two *trans* tautomers in S_0, as in the case of **NPc**. However, when the nitro group is introduced at the *β* position (e.g., **2NttPc**), the degeneracy is lifted, resulting in a 1.5 kcal energy gap between *trans-1* and *trans-2*. This points to the non-trivial influence of substituent position on the resulting properties of porphycenes. The four studied compounds differ in their absorption pattern and emissive properties. **2NttPc** emits a single emission with monoexponential decay kinetics. Higher yield of fluorescence and longer excited state lifetimes are observed compared to **NPc**.

Further studies are recommended for the introduction of a new substituent at the *β′* position.

Chapter 7

7.1 Instability of 9-aminoporphycenes.

This chapter discusses our findings of the actual emission pattern for aminoporphycenes (Figure 7.1). Something unusual was observed during my preliminary experiments to determine the fluorescence quantum yield of amino-porphycenes described in Chapter 5. Following the measurement of absorption spectra (Figure 7.2), fluorescence experiments were performed on the studied aminoporphycenes. While obtaining the emission data, I observed two new bands - F_2 and F_3 in the high-energy region of **tprAPc** (Figure 7.3 - right). The presence of F_2 and F_3 bands, in addition to the F_1 band, was rather a new observation versus what I had in previous experiments (Figure 7.3 - left). My first intuition was that I had somehow introduced some impurities into the sample solution. Therefore, I prepared a new solution (a sample of **tprAPc** in acetonitrile) for my experiments and immediately recorded fluorescence the same day. With the new solution, the F_2 and F_3 bands were almost non-existent, consistent with the left side of Figure 7.3. A few days later, I used the same solution to perform the emission experiments to test for the reproducibility of my initial results. Then, I observed an increase in the emission intensity of the F_2 and F_3 bands versus day 1. I left the solution for a few more days, repeated similar experiments, and got an even higher intensity of F_2 and F_3. Notably, the F_2 and F_3 appearance is observed only in acetonitrile in contrast to non-polar solvents such as toluene. In addition, a more puzzling observation was that the F_2 and F_3 intensities were significantly higher when excited between wavelengths of 560 nm and 620 nm – see Figure 7.3. This observation strongly suggests that aminoporphycenes are unstable and degrade over time. The high-energy bands (F_2 and F_3) appear with the degradation of aminoporphycenes, which is a function of time, solvent, and excitation wavelength.

9-aminoporphycene **(APc)**   9-amino-2,7,12,17-tetrapropylporphycene **(tprAPc)**   9-amino-2,7,12,17-tetra-*tert*-butylporphycene **(ttAPc)**
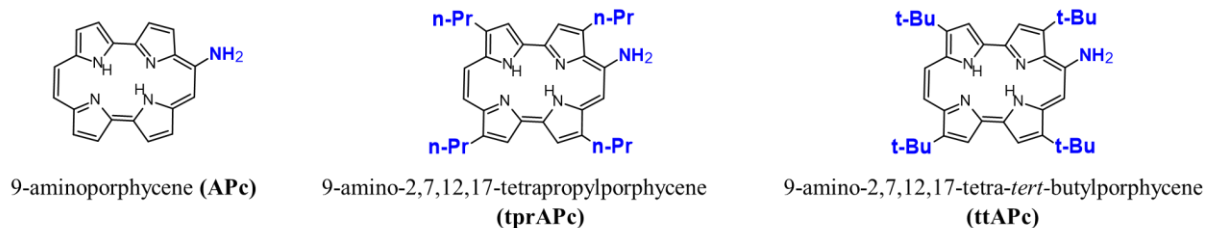
Figure 7.1 Structure of aminoporphycene derivatives reported in Chapter 7

In order to confirm the origin of F_2 and F_3 bands, a more systematic series of experiments were performed on the three aminoporphycene derivatives reported in this study (Figure 7.1). These experiments aimed to ascertain the main emission band of aminoporphycene and to characterize the possible structure(s) of the degradation products responsible for F_2 and F_3 emissions.
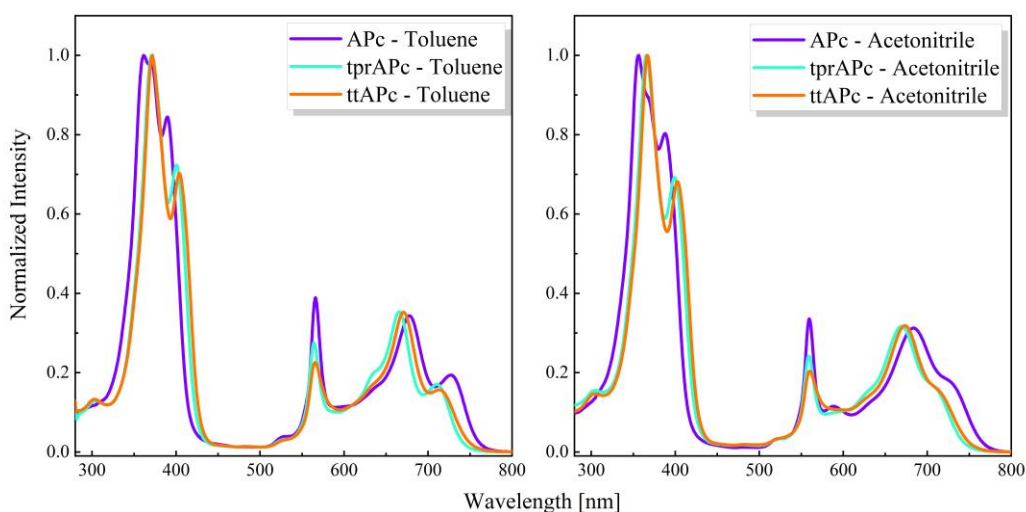
*Figure 7.2 Room temperature absorption spectra of **APc** (purple), **tprAPc** (green), and **ttAPc** (red)*
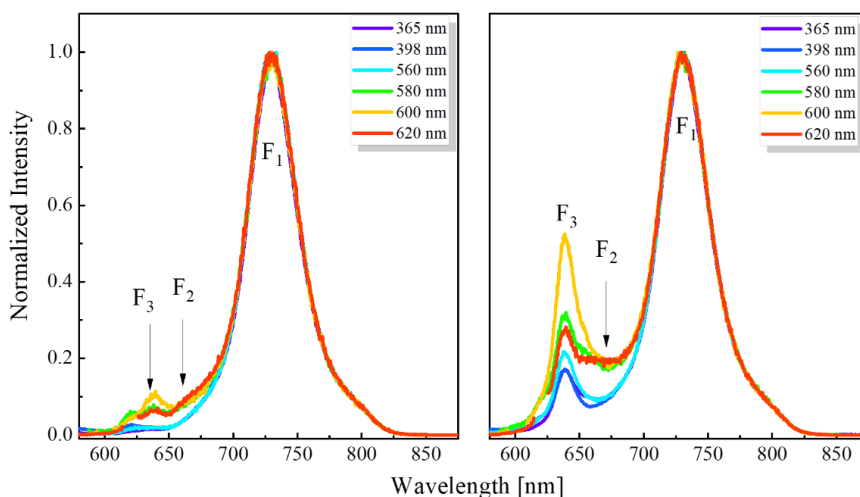
*Figure 7.3 Emission spectra of **tprAPc** in acetonitrile obtained from Fluorolog. Left: freshly prepared sample and right: an old sample solution*

A little more background: previous reports on aminoporphycenes proposed this set of porphycenes to be unique due to their *'dual-fluorescence'* property.[102,105] Our initial experiments, which suggest the time-dependence appearance of a second (and even third) emission band, only raised questions about whether truly aminoporphycenes exhibit dual fluorescence. This chapter will focus on evidence for or against the dual fluorescence property of aminoporphycene.

Porphycene, usually exhibit a single fluorescence band. Such pattern of fluorescence has been documented for porphycene derivatives with the exception of aminoporphycenes, where dual fluorescence was reported for 9-amino-2,7,12,17-tetrapropylporphycene, 9-amino-2,7,12,17-tetramethoxyethylporphycene, and 9-amino-2,7,12,17-tetraphenylporphycene.[106] Nonell and coworkers, in their study of aminoporphycenes, suggested dual emission, with F_1 and F_2 corresponding to emission from *trans-1* and *trans-2,* respectively. Their report explained this unusual behavior with a model that assumes a non-equilibration of the two lowest energy *trans* tautomers in the lowest excited state. This non-interconversion results in a single emission from each of the tautomers that make up the two emission bands.[103,106]

Discussion

A solution of 9-amino-2,7,12,17-tetrapropylporphycene (**tprAPc**) was prepared using acetonitrile as the solvent, and emission was recorded as a function of time (24 h intervals) to observe the appearance of the F_2 and F_3 bands. Increasing intensity of both bands was observed with time (Figure 7.4), indicating that these bands do not originate from the aminoporphycenes themselves. When similar experiments (using fresh sample solutions and aged solutions) were performed for **APc** and **ttAPc**, a considerable contribution from F_2 and F_3 is observed even for a freshly prepared solution made from old samples of aminoporphycene (Figure 7.5), and their intensities were comparable to F_1 intensity, specifically for the old samples. It is important to note that solutions of the studied compounds showed no changes in absorption regardless of whether the solutions were prepared from fresh, pure, or aged samples.
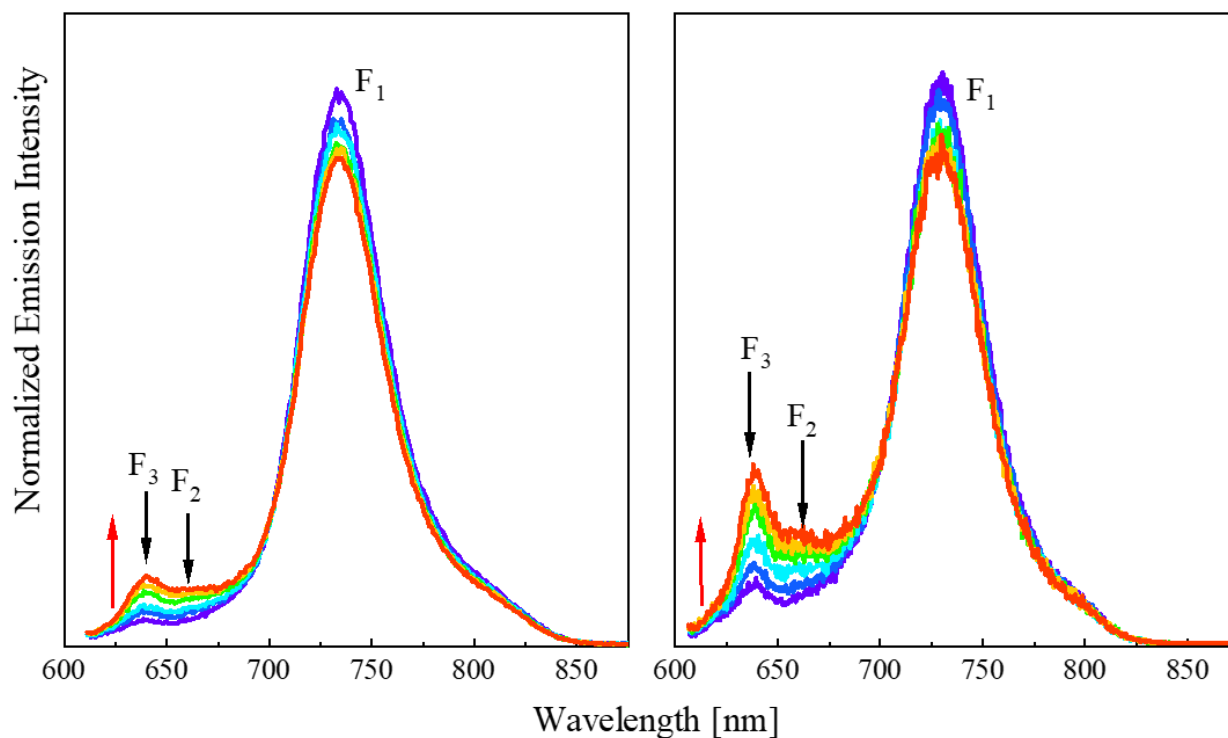
Figure 7.4 RT emission spectra of **tprAPc** *in acetonitrile recorded over 6 consecutive days, excitation wavelength 600 nm. The red arrow signifies the daily growth of F₂ and F₃ band with time. Left; spectra obtained for Cary Eclipse and right: obtained from Fluorolog*
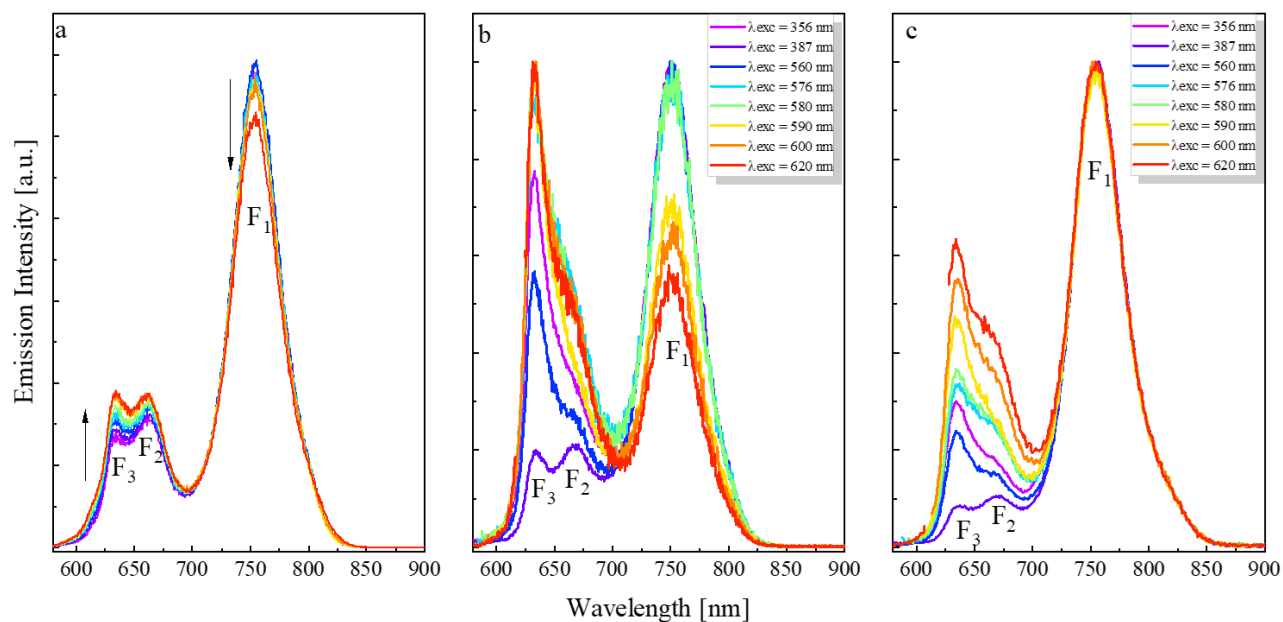
Figure 7.5 Emission spectra of freshly synthesized and purified solution of **APc** *(a). Emission spectra of an old sample of* **APc** *showing comparable intensities of F₂/F₁ and F₃/F₁, recorded across different instruments - Fluorolog (b) and Cary Eclipse - Varian (c). Experiments were performed in acetonitrile.*
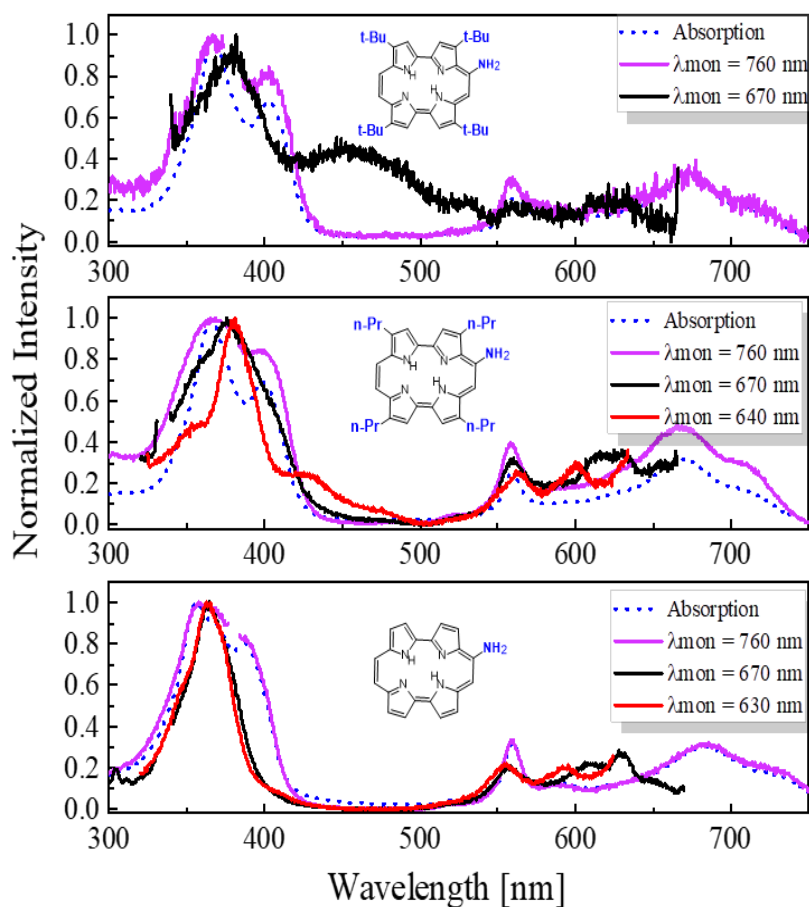
*Figure 7.6 Fluorescence excitation spectra of **APc** (bottom), **tprAPc**(middle), and **ttAPc** (top) in acetonitrile*

In our experiments, we take into account possible instrument artifacts that may influence the shape and pattern of the emission, and we recorded the time-dependence growth of **tprAPc** on two instruments (Fluorolog from Horiba and Varian-Cary Eclipse). This check across instruments is necessary to eliminate the possibility of either F_2 or F_3 bands being an artifact specific to a particular instrument. The same pattern of emission was observed regardless of the instrument (Figure 7.4), which confirms the presence of three bands in the emission spectra of aminoporphycenes. Excitation wavelengths between 560 nm – 620 nm were identified to significantly increase the intensity of F_2 and F_3 bands such that both bands became comparable to F_1. The excitation spectra of F_1 match the absorption spectra precisely. On the other hand, the excitation spectra of F_2 and F_3 are both similar but definitely different from that of F_1 (Figure 7.6).

7.2 Separation of degradation products of aminoporphycenes

Attempts have been made to separate the photoproducts (F_2 and F_3) from the main emission (F_1) of aminoporphycene.[238] First, using thin-layer chromatography to separate 9-amino-2,7,12,17-tetrapropylporphycene (**tprAPc**), we identified two additional spots (pdt1 and pdt2) on the plate.
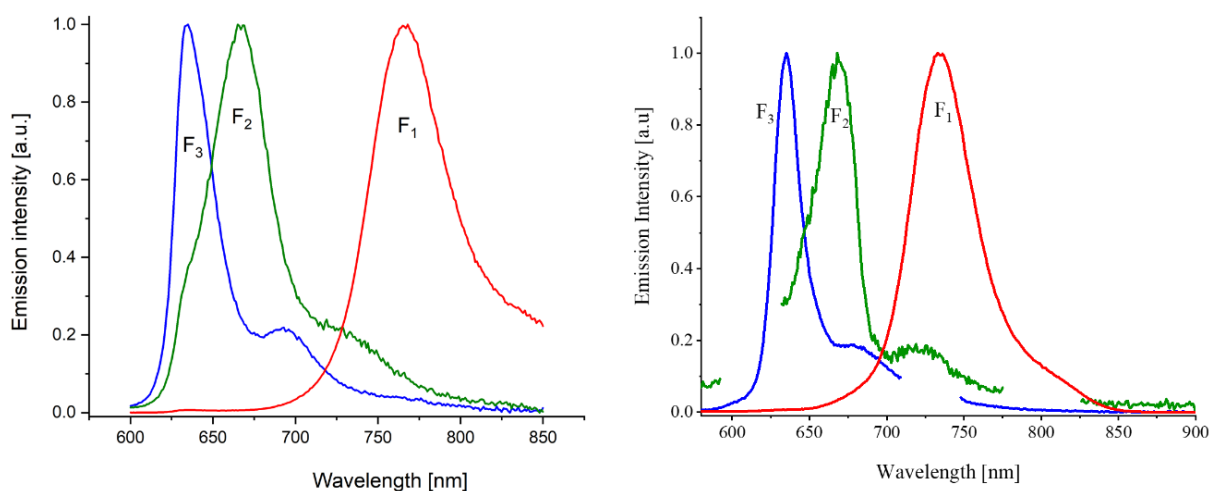
*Figure 7.7 Fluorescence spectra of pure 9-aminoporphycene (F_1) and its degradation products (F_2 and F_3) obtained after LC separation for fractions containing water and acetonitrile 20:80 v/v mixture (**left**). Emission spectra of pure 9-amino-2,7,12,17-tetrapropylporphycene (F_1) and its degradation products (F_2 and F_3) obtained after TLC separation using CH_3Cl_2 (**right**).*

When emission spectra were recorded for the photoproducts, a single emission was observed for both species, pdt1 and pdt2, which matched precisely the F_3 and F_2 emission, respectively, in **tprAPc** (

Figure 7.7 - right). A similar observation is seen for **APc** (left side of Figure 7.7)**,** which is separated from the degradation products using liquid chromatography-mass spectrometry. These products are then characterized using steady-state fluorescence measurements. This further points to the fact that aminoporphycenes are unstable and that F_2, as well as F_3 emissions, do not originate from either **tprAPc** or **APc.**

7.3 Thermal and photo-efficiency of degradation in aminoporphycenes

Emission spectra were recorded for **tprAPc** samples stored in the dark and for irradiated samples to ascertain the thermal and photo-efficiency of degradation in aminoporphycenes (Figure 7.8). Both irradiated and non-irradiated samples were obtained from the same mother liquor. Emission was recorded for each solution excited at different wavelengths. A substantial amount of F_2 and F_3 was observed in the irradiated sample after just five minutes of irradiation with 56 mW LED, and these bands steadily increased upon further irradiation. After 47 h of irradiation, F_2 had grown to about 40% of the intensity of F_1. For the non-irradiated sample, the rate of appearance of the bands was relatively slow, as F_2 and F_3 were barely observed even after eleven days. The faster rate of decomposition of aminoporphycene and subsequent formation of F_2 and F_3 bands upon irradiation (Figure 7.8) shows that the photoinduced degradation is much more efficient than the decomposition in the dark. Following 47 hours of irradiation, the sample was stored in the dark, and the emission was recorded after 2 and 7 days. The obtained spectra (Figure 7.8) show that the products of photodegradation are thermally stable, since no changes were observed for the absolute and relative emission intensities for samples stored in the dark for 2 and 7 days after irradiation.

7.4 Structural elucidation of products of degradation

Having confirmed that F_2 and F_3 emissions originate from photoproducts and not aminoporphycenes, HPLC and LC-MS experiments alongside quantum chemical calculations were performed to elucidate the structure of the degradation products. In the LC-MS experiments, ions of [M+H]+ 354 m/z and [M-H]- 352 m/z were found, suggesting a mass of 353. This mass of 353 is linked to the F_2-emitting species with a molecular formula $C_{20}H_{11}N_5O_2$. A difference of 28 exists between the 353 mass and 325, being the mass of aminoporphycene. This difference indicates that four hydrogen atoms are removed while adding two oxygen atoms. Since the ratio of removed hydrogen and oxygen atoms is 2:1, it suggests bridging by oxygen.

On the other hand, a signal of [M+H]+ 408 m/z and [M-H]- 406 m/z suggested a mass of 407, with a proposed formula $C_{20}H_{17}N_5O_5$, which was associated with the F_3-emitting species. Using quantum chemical calculations, attempts have been made to suggest possible structures of the degradation products involving bridging with oxygen (see Figure 7.9).
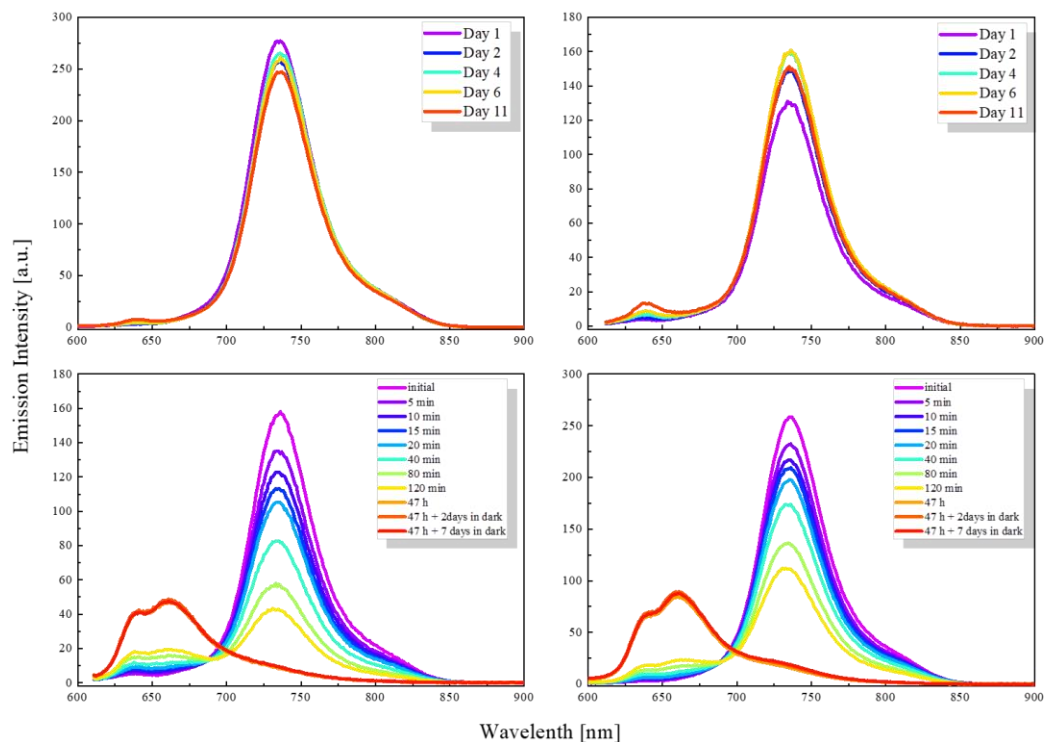
Figure 7.8 Changes in the emission spectra of **tprAPc** *in acetonitrile. Top: solution kept in the dark for 10 days after preparation. Bottom: irradiated sample. Excitation wavelength: left, 365 nm, right 600 nm.*

Since amino groups are known for their penetration and interaction with biological matter, it is unclear if the stability of aminoporphycenes is enhanced upon binding with biological cells. This, however, was not the focus of this study, and further study is recommended to investigate the stability of aminoporphycenes to biological applications. In the next chapter, we quantify the photostability of electron-donating aminoporphycenes in contrast to their electron-withdrawing counterparts – nitroporphycenes.
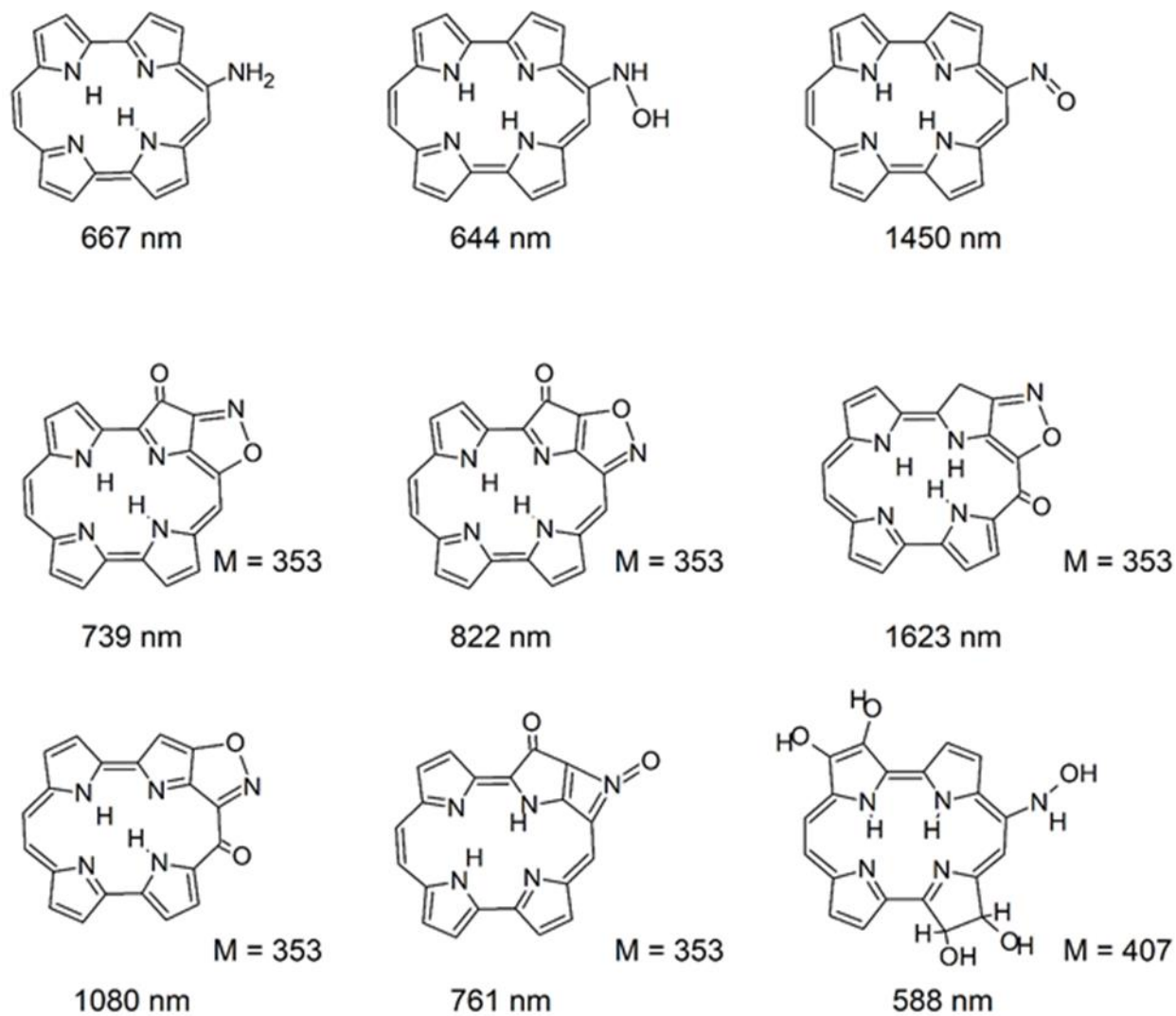
Figure 7.9 Wavelengths of $S_1 \leftarrow S_0$ absorption were calculated for different porphycenes. Middle and bottom rows: Possible structure corresponding to the formulas deduced from MS results: $C_{10}H_{11}N_5O_2$ (M = 353) and $C_{20}H_{17}N_5O_5$ (M = 407). Reprinted from ref.[238]

7.5 Summary

Our work on 9-substituted aminoporphycenes resulted in some major findings;

- The electron-donating property of the amino group makes aminoporphycenes unstable both in the solid state and in solution.

- The degradation process follows an oxygenation pathway with increased efficiency upon irradiation.

- Aminoporphycenes exhibit 'triple' emission, with F_1 being the actual emission from aminoporphycene; F_2 and F_3 are emissions from the degradation products of aminoporphycene.

- Aminoporphycenes are unique, rather due to their instability than their exhibition of dual fluorescence.

- The F_2 and F_3 intensities are dependent on the excitation wavelength, with wavelengths between 560 nm and 620 nm enhancing F_2 and F_3 intensities such that they become comparable to F_1.

- Degradation of aminoporphycenes is more efficient in polar solvents than in non-polar counterparts.

- The degradation pathway is suggested to be photomodification rather than photodestruction, since the products retain similar spectral properties of porphycene.

- In the case of biological applications, since the amino substituent better interacts with biological cells, we propose the synthesis of aminoporphycenes with protecting groups to facilitate their use in applications such as PDT.

Chapter 8

8.1 Photostability in 9-substituted porphycenes: Possible agents for photodynamic therapy?

Photochemical stability is an essential property of any fluorophore, which determines the dye's suitability in varying applications, especially when extended fluorescent ability is necessary.[211,244] The ability of a chromophore to withstand many cycles of excitation and relaxation back to the ground state without an irreversible loss of fluorescence is photostability. Depending on the intended use of the fluorophore, either high, moderate, or low photostability may be required.[211] In single-molecule imaging, for instance, highly photostable fluorophores are needed.[153] Similarly, in the photodynamic therapy of tumors, the high stability of the sensitizer is an essential property of the sensitizer. On the other hand, low stability of dyes is required in pollutant treatment and environmental protection from pollutants.

During an excitation event, the fluorophore in the excited state can emit fluorescence and return to the ground state, or the excited fluorophore can undergo intersystem crossing to the triplet state. In the triplet state, the fluorophore can either emit phosphorescence or participate in a series of chemical reactions, leading ultimately to an irreversible loss of fluorescence ability. The irreversible loss of fluorescence to a series of excitation-relaxation events is known as photobleaching. During the photobleaching of a fluorophore, the triplet state is a principal intermediate responsible for allowing electron-transfer or energy-transfer reactions with molecular oxygen, resulting in photobleaching. Therefore, quenching of the triplet state has been identified as an efficient way to enhance the stability of dyes. In addition, there has been vast development in other areas of fluorophore stabilization, such as antifading agents, removal of oxygen, and other protective agents that ensure the photostability of the fluorophore during long-term irradiation for PDT, cell imaging, and other applications.

Photostability is quantified as a function of the quantum yield of photobleaching or photodegradation, which is discussed in detail in section 1.7. When determining the yield of photobleaching, certain conditions need to be maintained, such as irradiation of the whole volume and calculating the quantum yield with data obtained before 10% decomposition is achieved. The aim of calculating the yield of photobleaching before the 10% degradation of the sample is to exclude the involvement of resulting photoproducts in the calculation.

Photostability in porphyrinoids is a subject of interest due to the applications of porphyrinoids in PDT. Query into the stability of porphyrins to UV/vis radiation proposes that the quantum yield of photobleaching in porphyrins is of the order of 10^{-7}, as contained in the literature.[212,216] Porphycenes, on the other hand, have received less attention in terms of quantifying their photostability. There is no report specifically on the photostability of porphycenes substituted with strong electron donating and withdrawing groups. In this chapter, we discuss the photodegradation quantum yield of 9-aminoporphycene (**APc**), 9-nitroporphycene (**NPc**), 9-amino-2,7,12,17-tetra-*t*-butylporphycene (**ttAPc**), and 9-nitro-2,7,12,17-tetra-*t*-butylporphycene (**ttNPc**). We illustrate the influence of strong electron-withdrawing and donating groups on the photostability of these compounds with reference to parent unsubstituted porphycene.

9-aminoporphycene **(APc)**

9-amino-2,7,12,17-tetra-*tert*-butylporphycene **(ttAPc)**

9-nitroporphycene **(NPc)**

9-nitro-2,7,12,17-tetra-*tert*-butylporphycene **(ttNPc)**
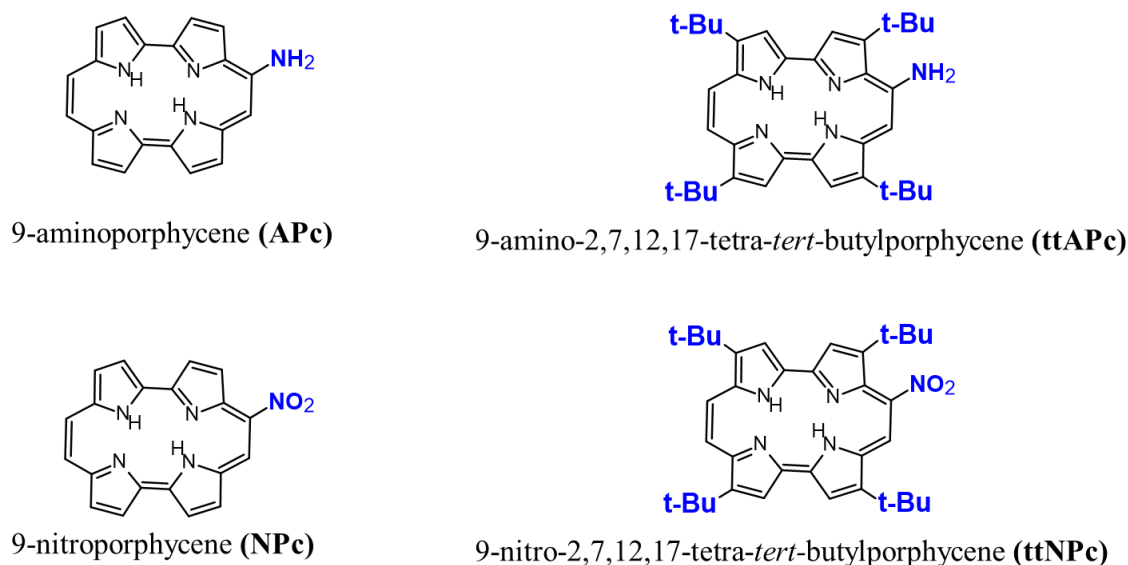
Figure 8.1 Compounds investigated in Chapter 8

8.2 Methodology

Reported compounds were synthesized by Dr. Agnieszka Gajewska and Dr. Arkadiusz Listkowski from Prof. Waluk's research group at the Institute of Physical Chemistry, Polish Academy of Sciences, Warsaw, Poland. The light source for irradiation is an LED from Thorlabs, centered at 565 nm with a power of 56 mW. The profile of the LED illuminating source is rather a broad one, which spans 450 nm to ~700 nm, as shown in Figure 8.2. Sample solutions were prepared by dissolving a known amount of the sample in acetonitrile, ensuring we obtain a concentration

between 10^{-6} and 10^{-5} M. When the concentration of the sample solutions was higher than 10^{-5}M, incomplete dissolution of the solute and possible aggregation were observed. After several trial experiments, a concentration of 10^{-5} was found to be optimal for the calculation of the quantum yield of photodegradation. Samples were placed in a 1 cm pathlength cell with a volume of 3.5 × 10^{-3} Liters. During the illumination experiment, the cell (containing the sample solution and a magnetic stirring bar) was placed on a magnetic stirrer and illuminated with a continuous light source. Changes in absorption were observed for the irradiated sample at specific time intervals. After a series of experiments to determine what time interval was suitable for which compound, the optimal interval was five minutes for the aminoporphycenes and 24 h for the nitroporphycenes and parent unsubstituted porphycene, which was used as a reference in this study.
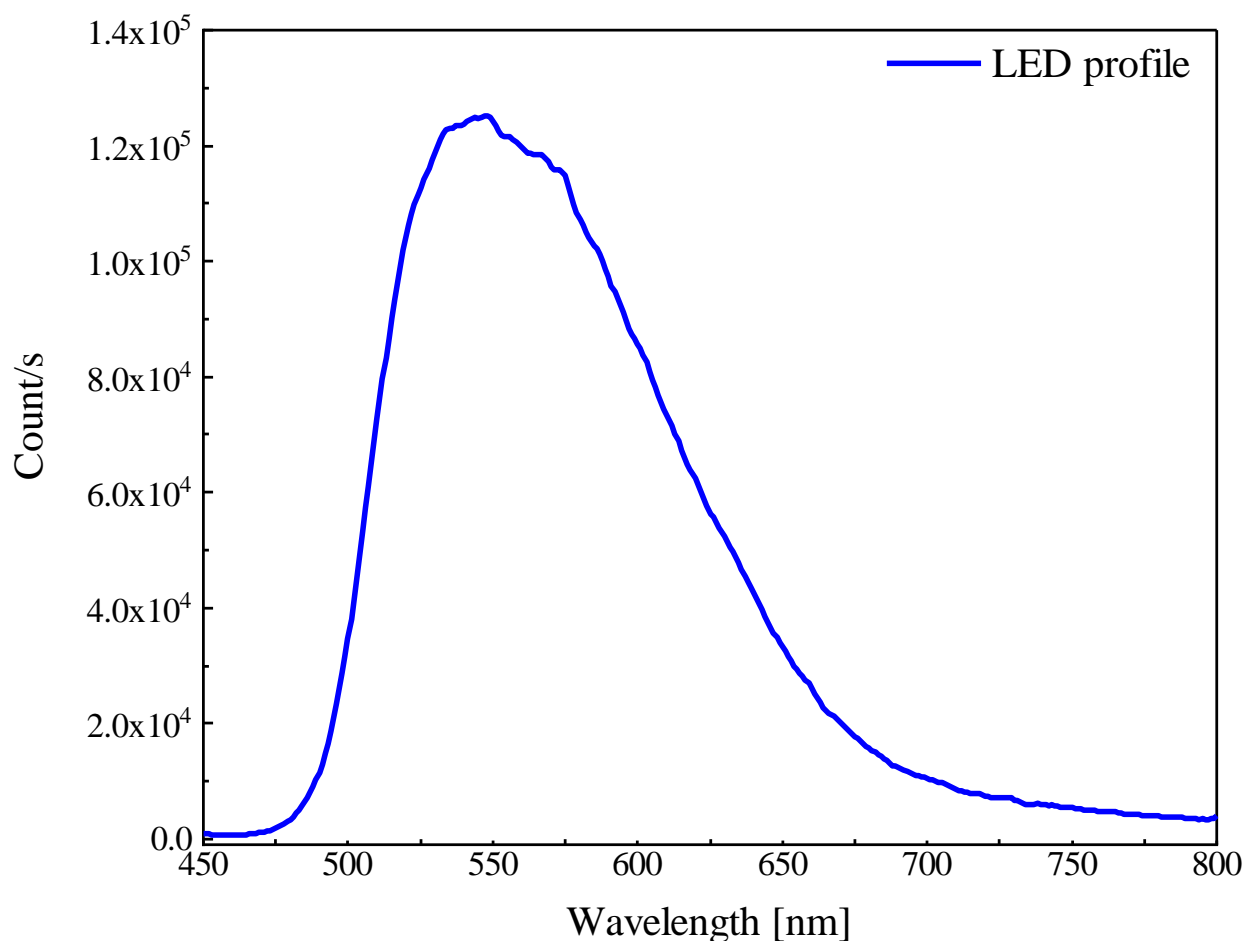
Figure 8.2 Profile of the LED, centered at 565 nm with a power of 56 mW.

The quantum yield of photobleaching was obtained using the equations (8.1 - (8.6) discussed in detail in section 4.2.6

$$\phi_b = \frac{N_b(t)}{Q_{total}(t)}$$
(8.1)

where $N_b(t)$ is the number of photobleached molecules over time t, $Q_{total}(t)$ is the total number of photons absorbed by the sample from the initial irradiation time (t = 0) to time t. The number of photons absorbed per unit time by the irradiated sample at time t is given as $Q_{abs}(t)$.

$$N_b(t) = \frac{(A_0 - A_t) \times N_{av} \times V}{1000 \times \varepsilon \times l}$$
(8.2)

$$Q_{total}(t) = \int_0^t Q_{abs}(t)dt$$
(8.3)

$$Q_{abs}(t) = \int_{\lambda_1}^{\lambda_2} I_0(\lambda) \times \left(1 - 10^{A(\lambda,t)}\right)d\lambda$$
(8.4)

where A_0 and A_t are the absorbances observed before irradiation (t = 0) and after irradiation over t, respectively. N_{AV} is the Avogadro number, V is the sample volume in Liters, ε is the molar absorptivity, and l is the optical path length. ϕ_b was determined from a plot of A_0/A_t against F(t)

$$\frac{A_0}{A_t} = 1 + bF(t)$$
(8.5)

$$F(t) = \frac{Q_{total}(t)}{A_t}$$
(8.6)

According to equation (8.5), a plot of A_0/A_t against F(t) should give a perfectly straight line assuming zero interference from photoproducts.

8.3 Results

The fit of A_0/A_t should give a straight line in the absence of photoproducts. In our case, the fit was linear for the initial points. As such, we present photodegradation quantum yield for the first few points of the fit, which represents the most accurate date possible. We also present the result of how the yield varies when different different wavelengths are monitored.

The changes in absorption spectra when each of the studied compounds was irradiated are shown in Figure 8.3 and Figure *8.4* **Error! Reference source not found.**, and the photobleaching quantum yield values obtained from fitting the plot of A_0/A_t against F(t) are presented in Table 8.1. A clear distinction exists in the photobleaching quantum values of the aminoporphycenes (**APc** and **ttAPc**) and nitroporphycenes (**NPc** and **ttNPc**). **APc** and **ttAPc** behave in a similar fashion, yielding higher quantum yields of photobleaching (10^{-4}), which is three orders of magnitude higher than the values for **NPc** and **ttNPc** (Table 8.1)

Table 8.1 Quantum yield of photobleaching for studied compounds. Results are resented for when the first 3, 4, 5, and 6 points after illumination are considered in the calculation.

	Concentration	λ monitored (nm)	3 Points	4 Points	5 Points	6 Points
ttAPc	1.8×10^{-5} M	367	6.7×10^{-5}	6.3×10^{-5}	6.0×10^{-5}	5.8×10^{-5}
		402	5.7×10^{-5}	5.6×10^{-5}	5.4×10^{-5}	5.3×10^{-5}
		560	1.8×10^{-4}	1.5×10^{-4}	1.3×10^{-4}	1.2×10^{-4}
		580	2.5×10^{-4}	2.1×10^{-4}	1.8×10^{-4}	1.6×10^{-4}
		673	1.1×10^{-4}	1.0×10^{-4}	0.9×10^{-4}	0.9×10^{-4}
APc	1.2×10^{-5} M	357	5.6×10^{-5}	5.2×10^{-5}	5.0×10^{-5}	4.8×10^{-5}
		387	6.0×10^{-5}	5.5×10^{-5}	5.1×10^{-5}	4.8×10^{-5}
		560	6.4×10^{-5}	5.8×10^{-5}	5.4×10^{-5}	5.1×10^{-5}
		586	4.5×10^{-5}	3.9×10^{-5}	3.6×10^{-5}	3.4×10^{-5}
		683	8.1×10^{-5}	7.4×10^{-5}	6.8×10^{-5}	6.3×10^{-5}
ttNPc	1.98×10^{-5} M	353	1.4×10^{-7}	1.6×10^{-7}	1.5×10^{-7}	1.5×10^{-7}
		395	1.6×10^{-7}	1.7×10^{-7}	1.7×10^{-7}	1.6×10^{-7}
		580	2.3×10^{-7}	2.4×10^{-7}	2.5×10^{-7}	2.2×10^{-7}
		622	2.5×10^{-7}	2.5×10^{-7}	2.5×10^{-7}	2.4×10^{-7}
NPc	6.6×10^{-6} M	388	6.9×10^{-8}	6.2×10^{-8}	5.6×10^{-8}	5.4×10^{-8}
		560	2.9×10^{-8}	4.3×10^{-8}	4.9×10^{-8}	4.5×10^{-8}
		580	6.5×10^{-8}	8.3×10^{-8}	9.1×10^{-8}	8.3×10^{-8}
		599	4.8×10^{-8}	6.6×10^{-8}	6.5×10^{-8}	5.7×10^{-8}
		625	5.7×10^{-8}	6.8×10^{-8}	7.2×10^{-8}	6.3×10^{-8}

High yields of photobleaching indicate instability in the compound. Therefore, aminoporphycenes are less stable than the nitro counterparts. This behavior corroborates what was discussed in Chapter 7, where new emission bands are observed for amino-substituted porphycenes due to their degradation in the dark and as a photoinduced process.
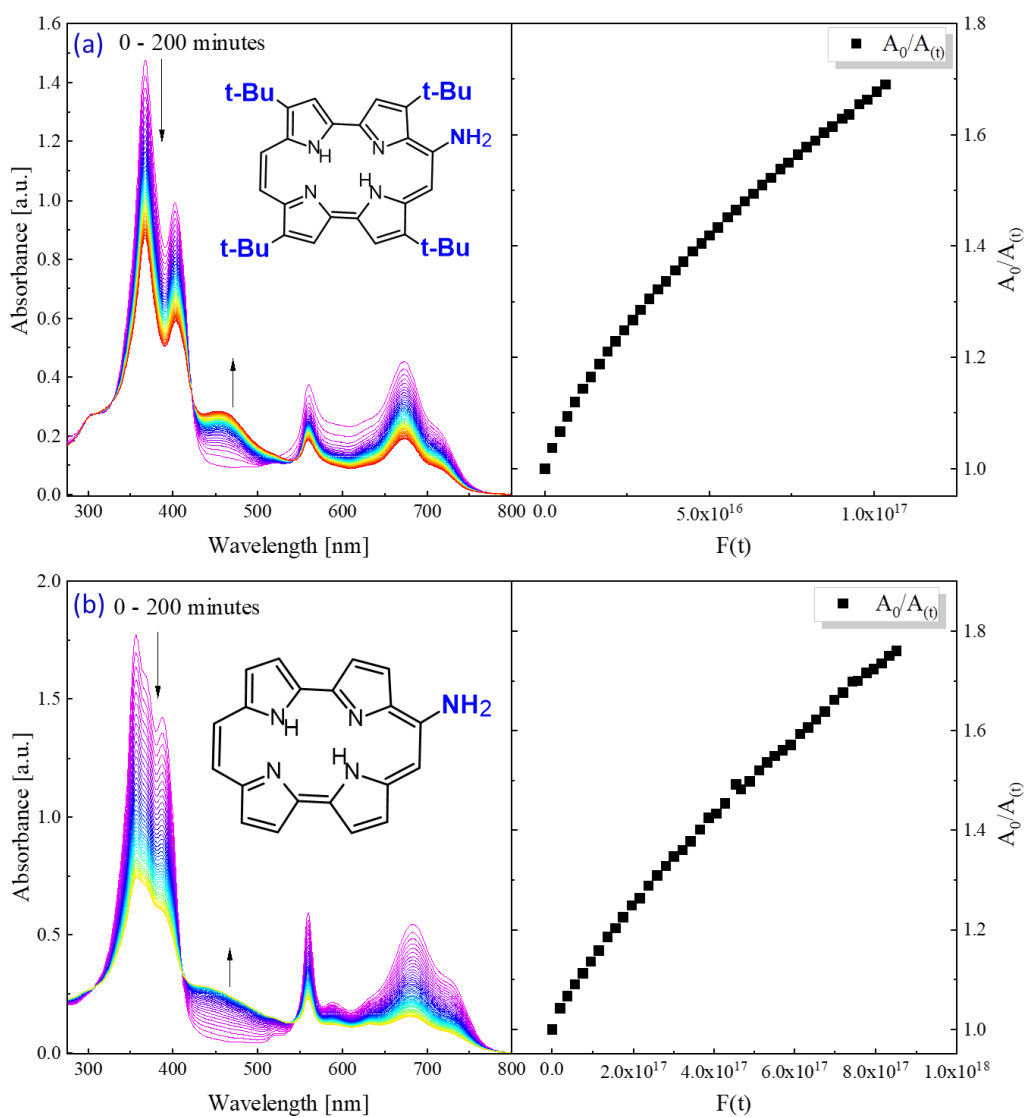
Figure 8.3 Changes in the absorption spectra of 9-amino-2,712,17-tetra-*tert*-butylporphycene (a) and 9-aminoporphycene (b), after irradiating at 5-minute intervals for 200 minutes. Light source: 56 mW LED centered at 565 nm. The arrows signify the direction of change.
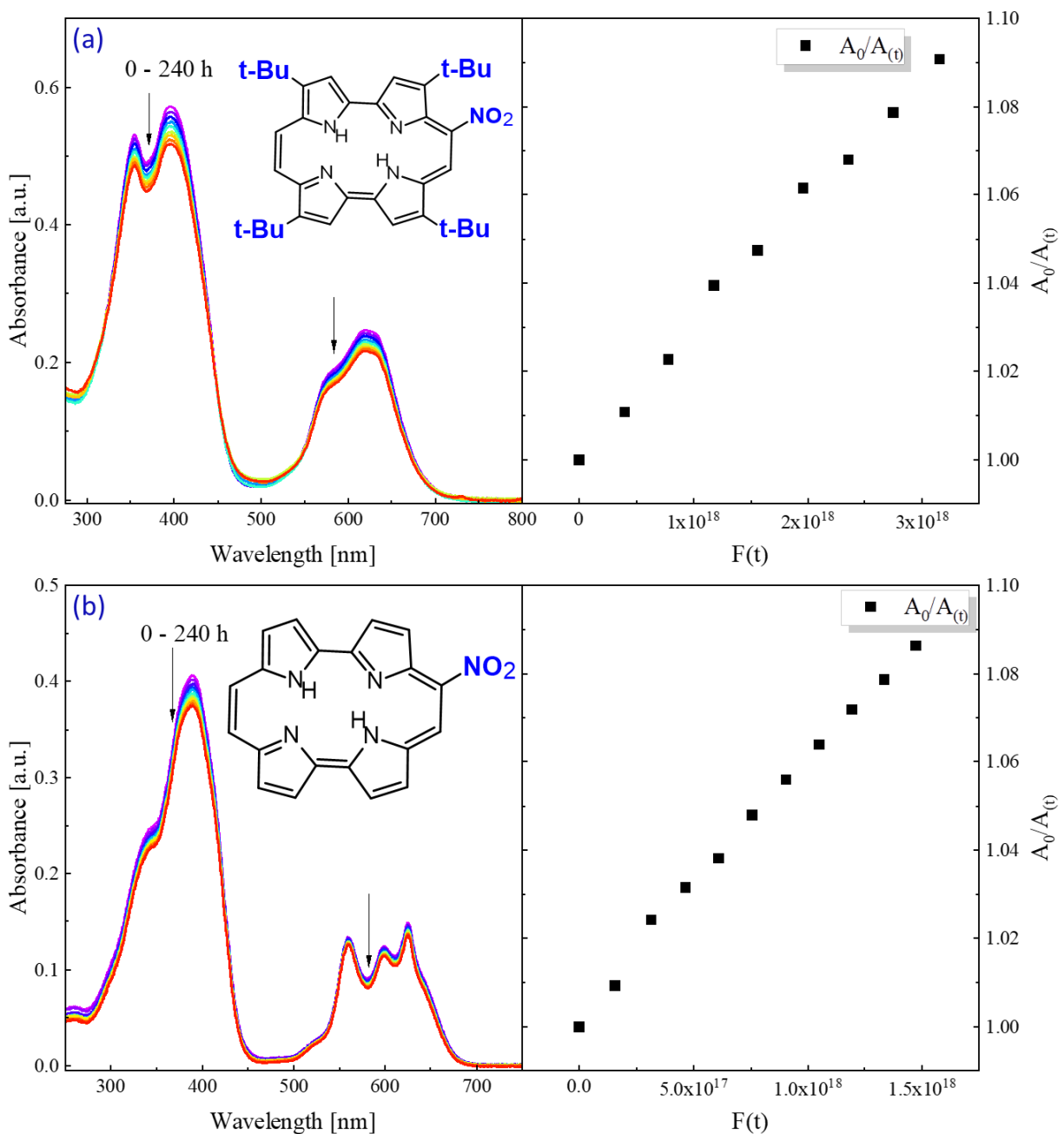
Figure 8.4 Changes in the absorption spectra of 9-nitro-2,712,17-tetra-*tert*-butylporphycene (a) and 9-nitroporphycene (b) after irradiating at 24 h intervals for 240 hours. Light source: 56 mW LED centered at 565 nm. The arrows signify the direction of change.

8.4 Summary

Amino-substituted porphycenes have been reported as possessing antimicrobial and antibacterial properties. This is due to the ability of the amino-substituent to interact with biological tissues. There is not much-reported literature on nitroporphycenes compared to their amino counterparts. In the course of this Ph.D. study, I have examined electron acceptor and electron donor substituents and the role they place in the photostability of nitroporphycenes and aminoporphycenes, respectively. In our studies, we establish that substitution with the amino group renders porphycene more susceptible to degradation, both as a reaction occurring in the dark and even more efficient as a light-motivated process. Nitroporphycenes are three orders of magnitude more stable than their amino counterparts. Studies into the triplet lifetimes and singlet oxygen generation, along with the photostability of nitroporphycenes, indicate they are excellent candidates for use as photosensitizers in PDT. Amino porphycenes, on the other hand, need to be incorporated with protective agents to enhance their stability and, therefore, take advantage of their suitability in biological applications.

Chapter 9

9.1 Spectroscopic and solvent studies of the pull, push, and push-pull derivative of 9,19-disubstituted porphycenes

The position and nature of substituents play essential roles in determining the resulting properties of our porphycene systems. In Chapter 5, we discussed the influence of single amino and nitro substitution on the spectral and photophysical properties of porphycenes. One would wonder to what degree the effects will increase, decrease, or vary when porphycenes are doubly substituted with amino and nitro groups. Here, results are presented for porphycenes, which, alongside the *β*-tetra-*tert*-butyl substitution, have two other substituents at positions nine (9) and nineteen (19), see Figure 9.1. The substitution pattern is thereby dubbed the *'pull'* – for the nitro (*electron-pulling*) derivative, *'push'* – for the amino (*as it pushes or donates electrons to the system*) derivative, and *'push-pull'* for the derivative comprising both the amino and nitro groups.

Another important factor when characterizing the properties of porphycenes is the media or environment of the solute [95,96]. Fluorescence was increased when the porphycene samples substituted with methyl and ethyl groups were placed in a more viscous environment.[95,96] Even rates of tautomerization have been found to be directly influenced by the nature of the environment. Going by this concept, initial fluorescence measurements of our compounds indicate these series of compounds to be extremely weak emitters. The weak emission is somewhat an expected outcome, vested with the knowledge from the single nitro and amino-tetra-*tert*-butyl derivative discussed in Chapter 5. We performed further studies to investigate the response of these compounds when studied in more viscous solvents.

9,19-di-amino-2,7,12,17-tetra-*tert*-butylporphycene (**ttdAPc**)

9,19-di-nitro-2,7,12,17-tetra-*tert*-butylporphycene (**ttdNPc**)

9-amino-19-nitro-2,7,12,17-tetra-*tert*-butylporphycene (**ttANPc**)
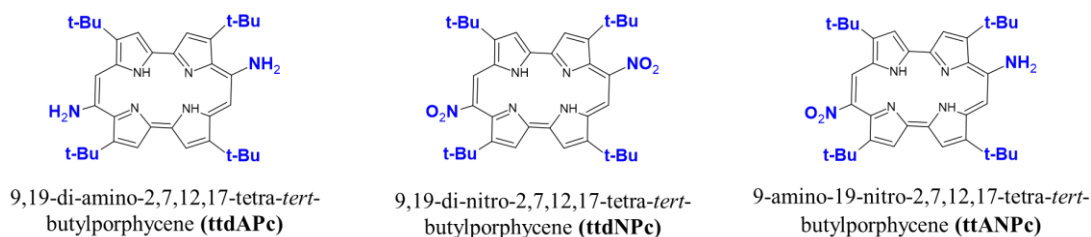
Figure 9.1 Compounds presented in Chapter Nine

9.2 Absorption and MCD studies

The absorption spectra (Figure 9.2) of 9,19-dinitro-2,7,12,17-tetra-*tert*-butylporphycene (**ttdNPc**) exhibit similar spectral features as typical porphycenes. They are characterized by the low-energy Q-bands and high-energy Soret bands. The lowest energy band is obtained in DMSO as it exerts the largest redshift. The dinitro derivative has similar spectral features to the single nitroporphycenes (**NPc**). In contrast, the diamino derivative (**ttdAPc**) differs significantly in terms of absorption patterns relative to the single substituted **APc** - aminoporphycene (Figure 9.3). While the Q-region of **APc** consists of at least five bands, that of **ttdAPc** is made of two bands. Moreover, the lowest energy absorption band in **APc** is located at 730 nm, while similar band in **ttdAPc** is situated at 690 nm. The push-pull effect of the amino and nitro group in 9-amino-19-nitro-2,7,12,17-tetra-*tert*-butylporphycene (**ttANPc**) results in two distinct absorption bands, almost of equal intensity in the Q-region and a broad Soret band (Figure 9.3)
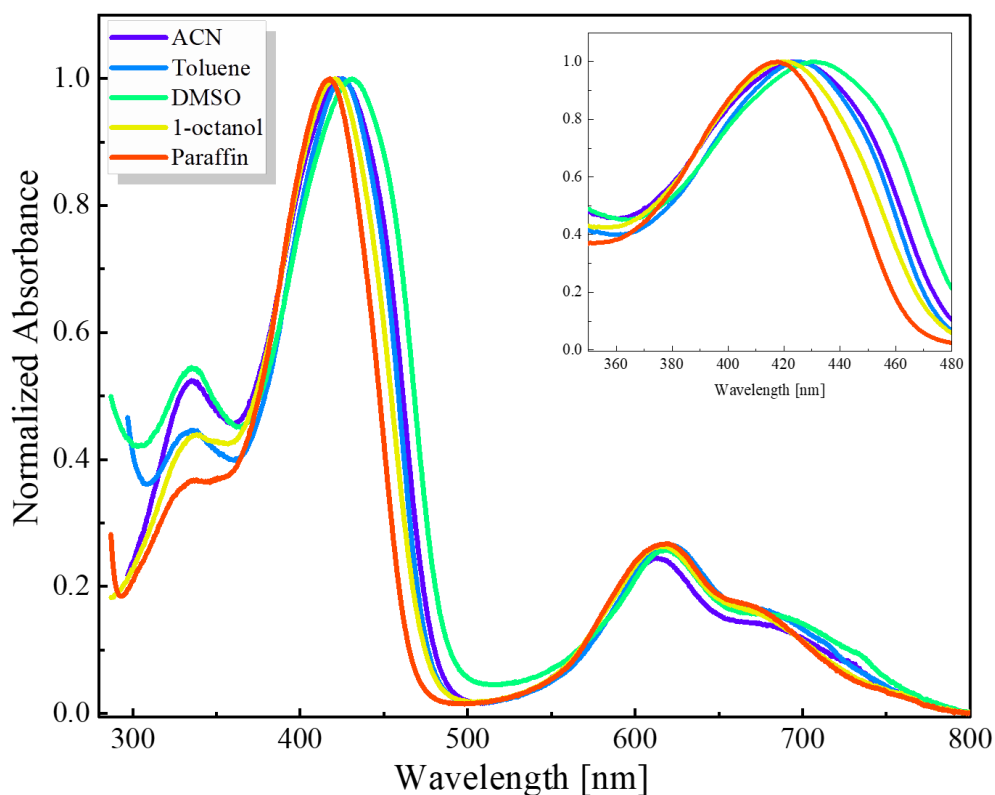
Figure 9.2 Room temperature absorption spectra of 9,19-dinitro-2,7,12,17-tetra-tert-butylporphycene obtained with varying solvents.

*Figure 9.3 Room temperature absorption spectra of 9,19-diamino-2,7,12,17-tetra-tert-butylporphycene (**left**) and 9-amino-19-nitro-2,7,12,17-tetra-tert-butylporphycene obtained with varying solvents.*

The MCD spectra, contrasted with the absorption of the investigated porphycenes, are shown in Figure 9.4. At least 2 electronic transitions are observed in the Q region. The Soret region maintains transitions similar to what is obtained for other nitroporphycenes contained in our recent report.[232]
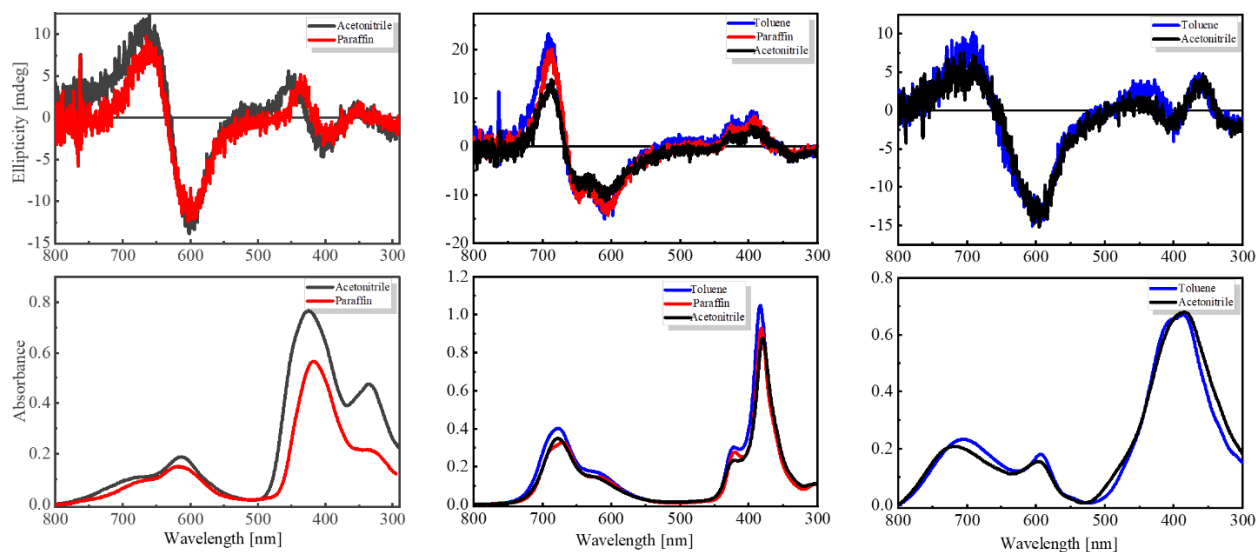
Figure 9.4 Room temperature MCD (top) and absorption spectra (bottom) of 9,19-dinitro-2,7,12,17-tetra-tert-butylporphycene (left), 9,19-diamino-2,7,12,17-tetra-tert-butylporphycene (middle), and 9-amino-19-nitro-2,7,12,17-tetra-tert-butylporphycene (right).

9.3 Fluorescence spectra

The emission data collected for the 9,19-dinitro-2,7,12,17-tetra-*tert*-butylporphycene (**ttdNPc**) indicate the derivative to be a very weak emitter (Figure 9.5), similar to 9-nitro-2,7,12,17-tetra-*tert*-butylporphycene (**ttNPc**). For such low efficiency emitters, there is a possibility to observe emission from impurities rather than the sample itself. Therefore, extreme care and examination with thin-layer chromatography (TLC) were performed to ensure the purity of the sample and that the obtained emission was actually that of the studied sample. The dinitro derivatives (**ttdNPc**) are very weak emitters with fluorescence patterns similar to that of the 9-nitroporphycene (**NPc**) (Table 9.1). The emission peaked at 684 nm for the dinitro derivative, and it is independent of the excitation wavelength. The emission spectra were unusually narrow for certain solvents; however, the fluorescence pattern in DMSO was broader. The emission spectra of **ttdAPc** and **ttANPc** are shown *Figure 9.6*.

Table 9.1 Quantum yield of fluorescence measured at room temperature for the 9,19-disubstituted tetra-*tert*-butyl derivatives

Compounds / Solvents	ttdNPc	ttdAPc	ttANPc
Acetonitrile	1.7×10^{-4}	1.4×10^{-4}	2.5×10^{-4}
Toluene	3.0×10^{-4}	1.5×10^{-4}	1.5×10^{-4}
DMSO	4.7×10^{-4}	1.7×10^{-3}	
1-Octanol	2.3×10^{-4}	3.8×10^{-3}	5.9×10^{-4}
Parrafin oil	3.5×10^{-4}	6.0×10^{-4}	4.1×10^{-4}

ttdNPc = 9,19-dinitro-2,7,12,17-tetra-*tert*-butylporphycene; **ttdAPc** = 9,19-diamino-2,7,12,17-tetra-*tert*-butylporphycene; **ttANPc** = 9-amino-19-nitro-2,7,12,17-tetra-*tert*-butylporphycene

Fluorescence QY values in the order of 10^{-3} and 10^{-4} were obtained for **ttdNPc**, **ttdAPc,** and **ttANPc**. These values are similar to those of mono-substituted amino and nitro *tert*-butyl derivatives discussed previously in section 5.4. Previous knowledge has it that higher fluorescence quantum yield was obtained for porphycenes when the samples were studied in a highly viscous solvent. Given the low QY of fluorescence of our studied samples, it was pertinent to investigate the possibility of fluorescence recovery with increasing solvent viscosity. The study revealed that although fluorescence was recovered with increasing solvent viscosity, the QY-viscosity relationship was not linear (Figure 9.7).
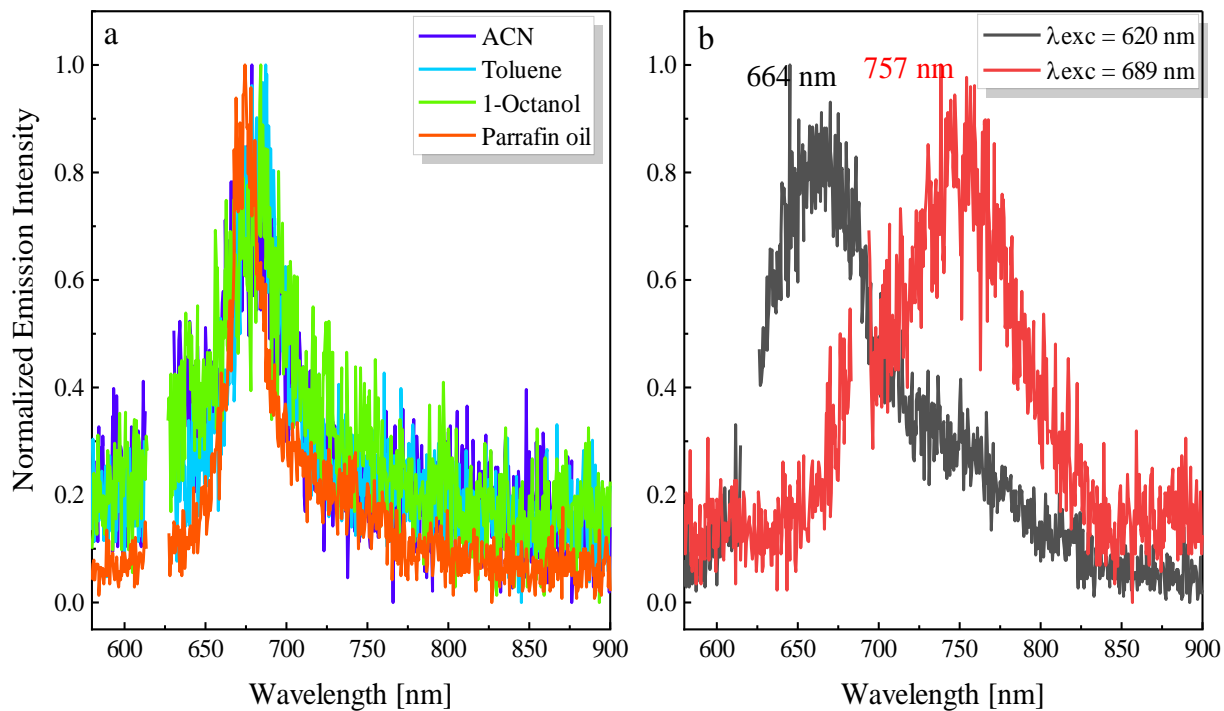
Figure 9.5. Room temperature fluorescence emission 9,19-dinitro-2,7,12,17-tetra-tert-butylporphycene measured in a: different solvents (λ of excitation = 620 nm) and b: DMS.
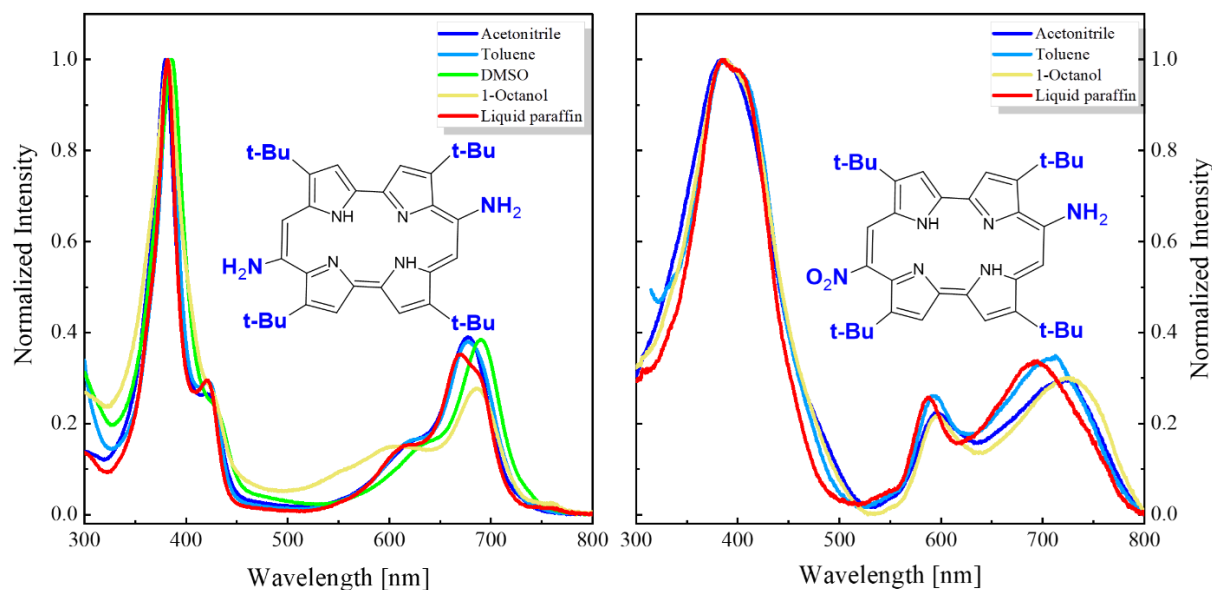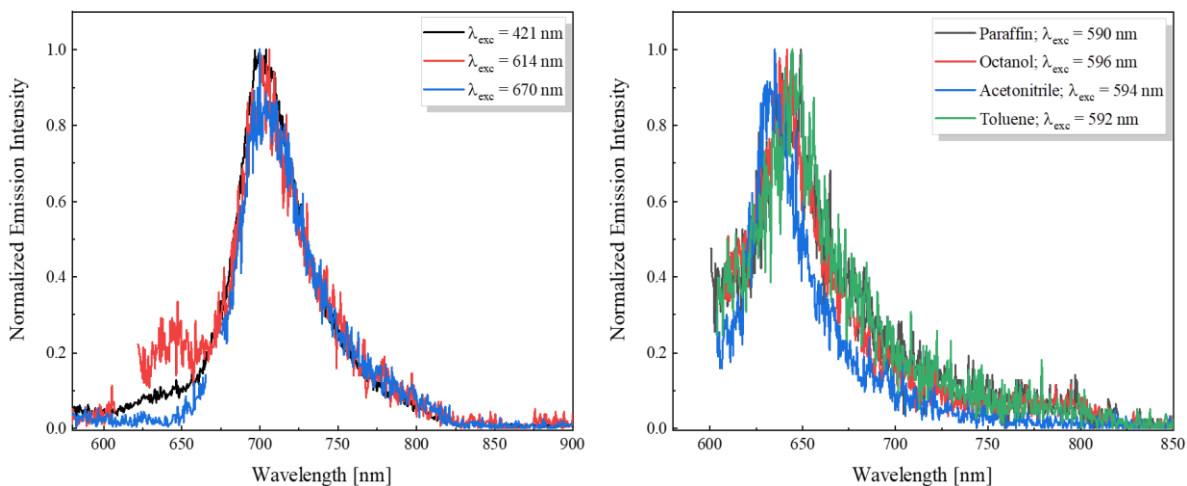

Figure 9.6 Room temperature emission spectra of 9,19-diamino-2,7,12,17-tetra-tert-butylporphycene in paraffin (left) and 9-amino-19-nitro-2,7,12,17-tetra-tert-butylporphycene in different solvents (right).
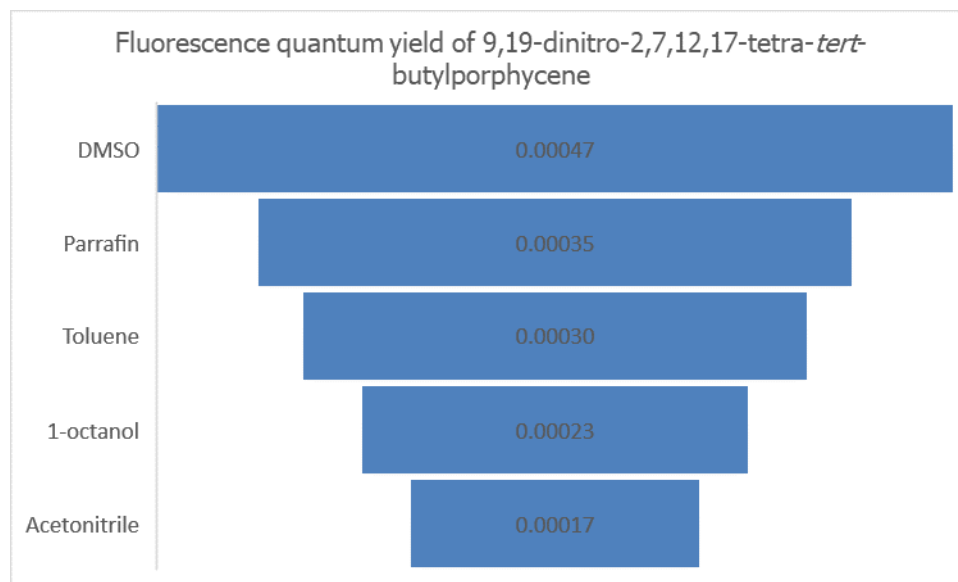
Figure 9.7 Chart of the relationship between solvent and yield of fluorescence in 9,19-dinitro-2,7,12,17-tetra-tert-butylporphycene

The fluorescence QY in **ttdNPc** peaked at DMSO, which has lower viscosity compared to paraffin and 1-octanol. The high yield in DMSO compared to other solvents of higher viscosity may have its link to hydrogen-bond formation ability in DMSO. Moreover, QY in 1-octanol presented a value lower than that of toluene. This raises the question of the influence of polarity and/or hydroxyl groups in the yield of fluorescence. The data suggests that viscosity is not the singular factor in the choice of solvent while studying fluorescence recovery in weak emitters. Other solvent properties, such as polarity and hydroxyl group (e.g., in 1-octanol), play an equally important role in the resulting yield.

The excited state lifetimes for the three compounds were very short-lived (Table 9.2), with lifetimes in the sub-nanosecond range, and given the resolution of our experimental set-up, we safely report lifetimes of < 50 ps for **ttANPc**. In **ttdNPc** and **ttdAPc**, viscosity dependence could still be observed even with the extremely short-lived excited state. The error in this measurement is rather large, but these values show a clear trend.

Table 9.2 Lifetime of fluorescence in ttdNPc, ttdAPc, and ttANPc

Compounds / Solvents	ttdNPc	ttdAPc	ttANPc
Acetonitrile	15 ps	< 30 ps	< 50 ps
Toluene	22 ps	< 30 ps	< 50 ps
DMSO		< 30 ps	< 50 ps
1-Octanol	35 ps	50 ps	< 50 ps
Parrafin oil	70 ps	64 ps	< 50 ps

ttdNPc = 9,19-dinitro-2,7,12,17-tetra-*tert*-butylporphycene; **ttdAPc** = 9,19-diamino-2,7,12,17-tetra-*tert*-butylporphycene; **ttANPc** = 9-amino-19-nitro-2,7,12,17-tetra-*tert*-butylporphycene

9.4 Summary

For the *tert*-butyl derivatives of *meso*-substituted porphycenes, fluorescence quantum yield is strongly diminished when contrasted with other alkyl derivatives, such as the tetra-*n*-propyl derivative.[227] Particularly low QY of fluorescence is observed for the three investigated compounds (**ttdNPc**, **ttdAPc**, and **ttANPc**), similar to what has been reported for *tert*-butyl porphycenes with a single *meso*-substitution of nitro and amino group (**ttNPc** and **ttAPc**). The low emission yield suggests an efficient non-radiative deactivation pathway to the ground state and/or efficient transfer of the singlet state to the triplet state. Low quantum yields of singlet oxygen formation obtained for **ttAPc** and **ttNPc** (Table 5.6) strongly suggest that the dominant nonradiative channel is the $S_0 \leftarrow S_1$ internal conversion. Therefore, push, pull, and push-pull compounds are suitable compounds for applications such as viscosity sensors. Further studies are recommended for samples of **ttdNPc**, **ttdAPc**, and **ttANPc** placed in rigid glassy or polymer environments.

Chapter 10

10.1 β and β' nitro porphycenes: position effects in *meso*-tetraphenyl derivatives of porphycene

Literature has it that the *meso* (9,10,19,20) position in porphycenes is highly sensitive to peripheral perturbations such as substitution. Several works conducted on *meso*-substituted porphycenes have confirmed the sensitivity of the *meso* position to the type and nature of the substituents.[36,102,116] Moreover, studies prove that substitution at the *meso* position can significantly distort the shape and size of the inner cavity of porphycenes, resulting in elongation or shortening of the cavity.[52] Tetraphenyl substitution at positions 9,10,19,20, for instance, results in a more rectangular shape in porphycene compared to the parent unsubstituted Pc.[52]

Following the first synthesis of 2,7,12,17-tetraphenylporphycene,[118] there are numerous studies on the synthesis,[245,246] photophysics and photodynamic properties[43,247,248] of this molecule. Sánchez-Garcia and co-workers reported on the synthesis of 9-nitro- 9,19-dinitro and 9,20-dinitro-2,7,12,17-tetraphenylporhycene.[116] *Meso*-aryl derivatives, on the other hand, have received less attention. Anju and co-workers, in 2008, first reported the synthesis, electronic absorption, and emission properties of 9,10,19,20-tetraarylporphycene and its metal complexes.[221] Waluk and co-workers recently reported the influence of tetra-*meso* aryl substitution and mixed *meso* substitution (aryl and alkyl) on the strength of the hydrogen bonds, N-N distances, and, therefore, the emissive properties of the macrocycle.[170] In their study, they observed large fluorescence quantum yields for the *meso*-dimethyl and diphenyl derivative, as well as the *meso*-tetraphenyl porphycene derivative. In the case of the latter, a yield that was more than three times higher was observed in non-polar *n*-hexane relative to the polar acetonitrile. This, once again, highlights solvent effects on the photophysical properties of porphycene systems.

9,10,19,20-tetraphenylporphycene **(tphPc)**   2-nitro-9,10,19,20-tetraphenylporphycene **(2tphNPc)**   3-nitro-9,10,19,20-tetraphenylporphycene **(3tphNPc)**
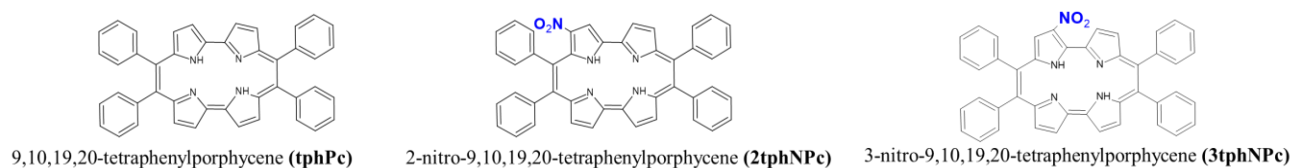
Figure 10.1 Structure of compounds studied in chapter 10

Given the role of *meso*-aryl groups on the overall spectroscopy and radiative properties of porphycenes and the position-dependence influence of substituents on the porphycene systems, it is crucial to examine the combined influence of *meso*-tetraphenyl substitution with an alternating position of the nitro substituent at *β* and *β′*. This chapter describes two *meso*-tetraphenylporphycenic systems with nitro groups placed at *β* and *β′* positions (Figure 10.1). Results are presented for 2-nitro-9,10,19,20-tetraphenylporphycene (**2tphNPc**) and 3-nitro-9,10,19,20-tetraphenylporphycene (**3tphNPc**), to illustrate how much difference the nitro substituent makes just by being placed at different positions on the porphycene macrocycle. At the later stage of this chapter, we compare and contrast the spectral and photophysical parameters for seven nitroporphycene derivatives.

10.2 Spectroscopy and photophysics

The absorption spectra (Figure 10.2) of **2tphNPc** and **3tphNPc** possess characteristic features of porphycene-like absorption. The lower-intensity, low-energy Q-bands and the higher-intensity, high-energy Soret bands are observed for both compounds. However, the low energy region in **2tphNPc** and **3tphNPc** consists of two bands in contrast to the typical 'three-fingers' pattern in porphycene and its 9,10,19,20-tetraphenyl derivative (**tphPc**).[221] The lowest energy absorption band in both compounds is obtained in non-polar toluene. Moreover, when comparing the absorption spectra of **2tphNPc** and **3tphNPc**, the latter exhibits a larger redshift. The time evolution of transient absorption spectra obtained for **3tphNPc** is represented in Figure 10.3, with the bleaching bands observed between 350 – 470 nm and 575 – 745 nm.

Both **2tphNPc** and **3tphNPc** exhibit single emission, which is characteristic of porphycenes (Figure 10.4). This emission is independent of excitation wavelength and consistent with what is obtained in literature for *meso*-tetraphenyl substituted porphycene.[221] Interestingly, the emission band for **2tphNPc** was broad and blue-shifted, up to 25 nm blue shift in toluene vs what is obtained for **3tphNPc** in a similar solvent (Figure 10.4). While **3tphNPc** emits a fluorescence QY comparable with that of 9-nitroporphycene (**NPc**) and 2-nitro-7,12,17-tri-*tert*-butylporphycene (**2NttPc**) - see Figure 10.5 and Table *10.1*, **2tphNPc**, on the other hand, is a very weak emitter with QY values in the order of 10^{-4}. The QY value for **2tphNPc** is similar to that of tetra-*tert*-butyl porphycene derivatives discussed in Chapter 5. Our recent study (discussed thoroughly in Chapter

6) on 2-nitro-7,12,17-tri-*tert*-butylporphycene (**2NttPc**), involving the placement of a nitro group at the β (position 2) along with tri-*tert*-butyl groups on positions 7,12, and 17 resulted in a near 20% yield of fluorescence in toluene and ~10% yield in acetonitrile.[232] The variation in the emission yield between **2tphNPc** and **3tphNPc** again points to the importance of substituent position (and equally its vicinity). Since **2tphNPc** has a phenyl group in the vicinity of the nitro substituent, we suggest that the lowered quantum yield of fluorescence (and other spectral and photophysical differences) of this compound relative to **3tphNPc** points to possible steric interaction between the phenyl and nitro group, resulting in marked differences between the photophysical and general properties of the two systems. Previous studies on 9,10,19,20-tetraphenylporphycene demonstrate the system exhibits a single emission band with the main band at 659 and a vibronic feature at 715 nm. In addition, a fluorescence quantum yield value of 0.23 is reported in argon-saturated solutions.[221]
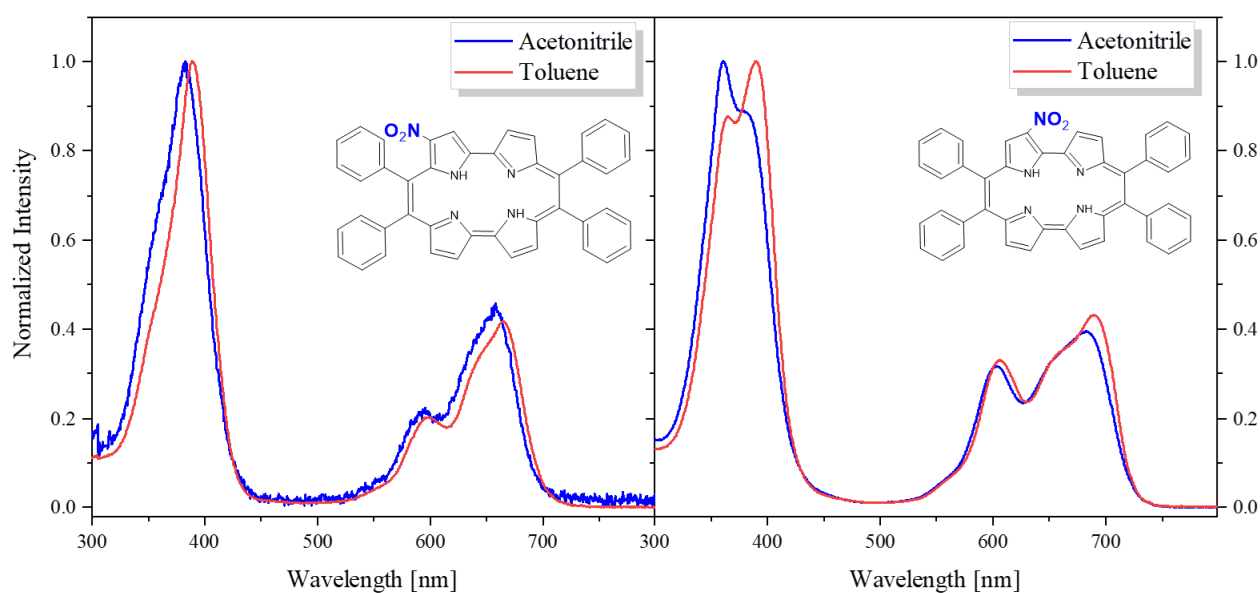
Figure 10.2 Room temperature absorption (bold line) and emission (dotted line) of 2-nitro-9,10,19,20-tetraphenylporphycene (a) and 3-nitro-9,10,19,20-tetraphenylporphycene (b). Solvent: acetonitrile (blue line) and toluene (red line).

The general trend of higher quantum yield of fluorescence in less polar solvents is preserved in **2tphNPc** and **3tphNPc**. With the apparent significance of substituent position on the photophysics of studied *meso*-tetraphenyl compounds, it is vital to assess how they compare to other nitroporphycenes derivatives. This now leads us to the comparison of spectral and photophysical properties of seven nitro derivatives (Figure 10.6) of porphycene.
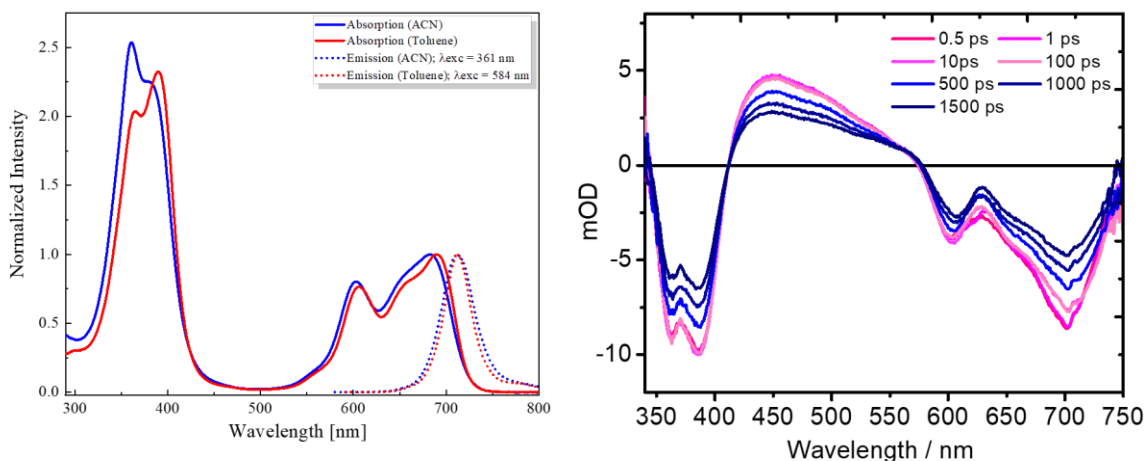
Figure 10.3 Absorption and emission spectra in acetonitrile and toluene (left); transient absorption spectra (right) of 3-nitro-9,10,19,20-tetraphenylporphycene.
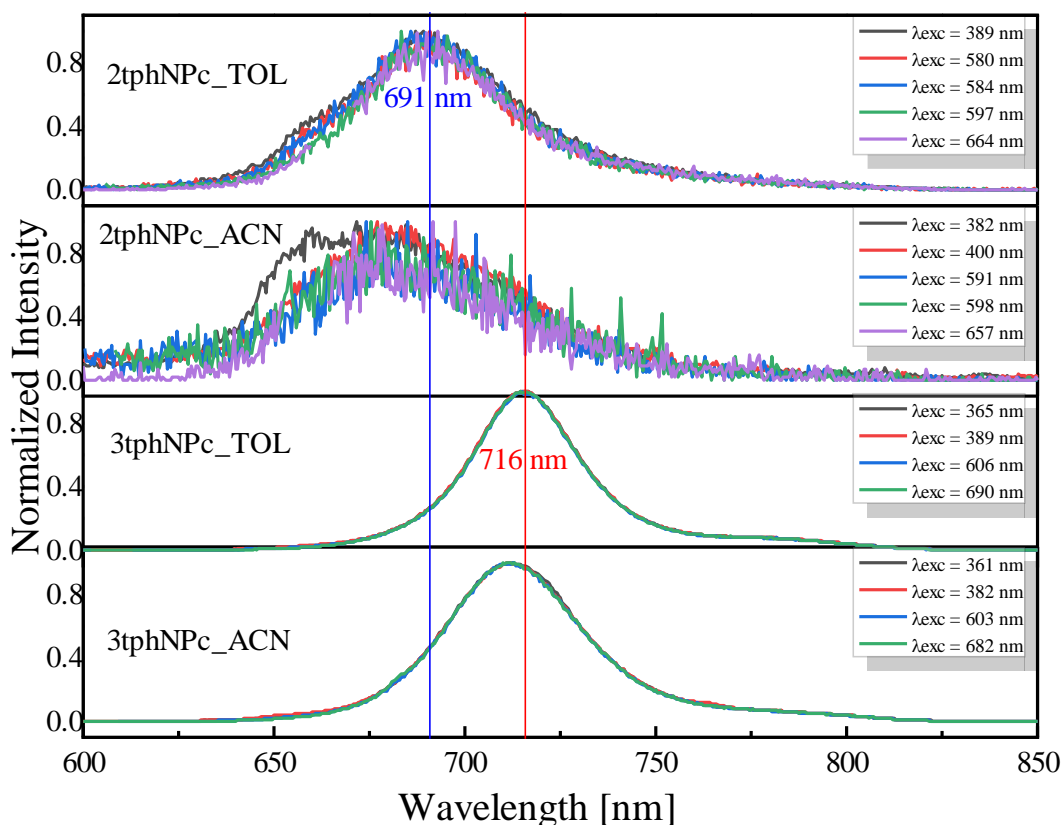
*Figure 10.4 Emission spectra of 2-nitro-9,10,19,20-tetraphenylporphycene (**2tphNPc**) and 3-nitro-9,10,19,20-tetraphenylporphycene (**3tphNPc**) in Acetonitrile (ACN) and toluene (TOL). The red and blue lines signify the lowest energy emission peak in **3tphNPc** and **2tphNPc,** respectively.*

Table 10.1 Spectroscopy and photophysical parameters of **2tphNPc** and **3tphNPc**

	Absorption peaks (nm)		Emission peaks (nm)		Fluorescence quantum yield (ϕ_f)		Decay lifetimes τ(ns)	
	Acetonitrile	Toluene	Acetonitrile	Toluene	Acetonitrile	Toluene	Acetonitrile	Toluene
2tphNPc	658	665	709	687	8.2×10^{-4}	9.3×10^{-4}	< 50 ps	< 50 ps
	598	598						
	381	389						
3tphNPc	682	690	713	712	3.4×10^{-2}	1.0×10^{-1}	2.1 ± 0.1	4.3 ± 0.1
	603	606						
	379	389						
	360	365						
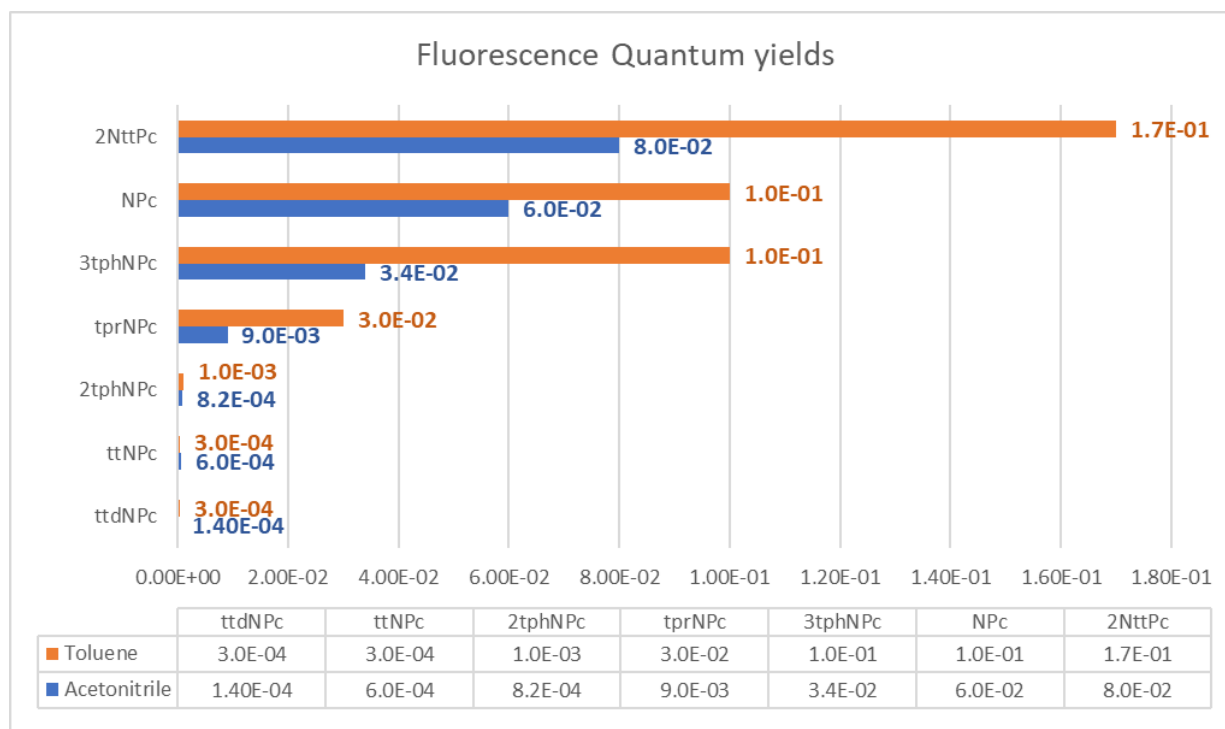
*Figure 10.5 Comparison between fluorescence quantum yields for all nitroporphycenes investigated in this research work. 9-nitroporphycene (**NPc**); 9-nitro-2,7,12,17-tetrapropylporphycene (**tprNPc**); 9-nitro-2,7,12,17-tetra-t-butylporphycene (**ttNPc**); 2-nitro-7,12,17-tri-t-butylporphycene (**2NttPc**); 2-nitro-9,10,19,20-tetraphenylporphycene (**2tphNPc**) and 3-nitro-9,10,19,20-tetraphenylporphycene (**3tphNPc**)*

10.3 Comparison of the nitroporphycenes

A comparison of the absorption data for all the nitro derivatives indicates that the largest red shift is observed for the 9,10,19,20-tetraphenyl derivative. This confirms the sensitivity of the *meso* position to substitution.
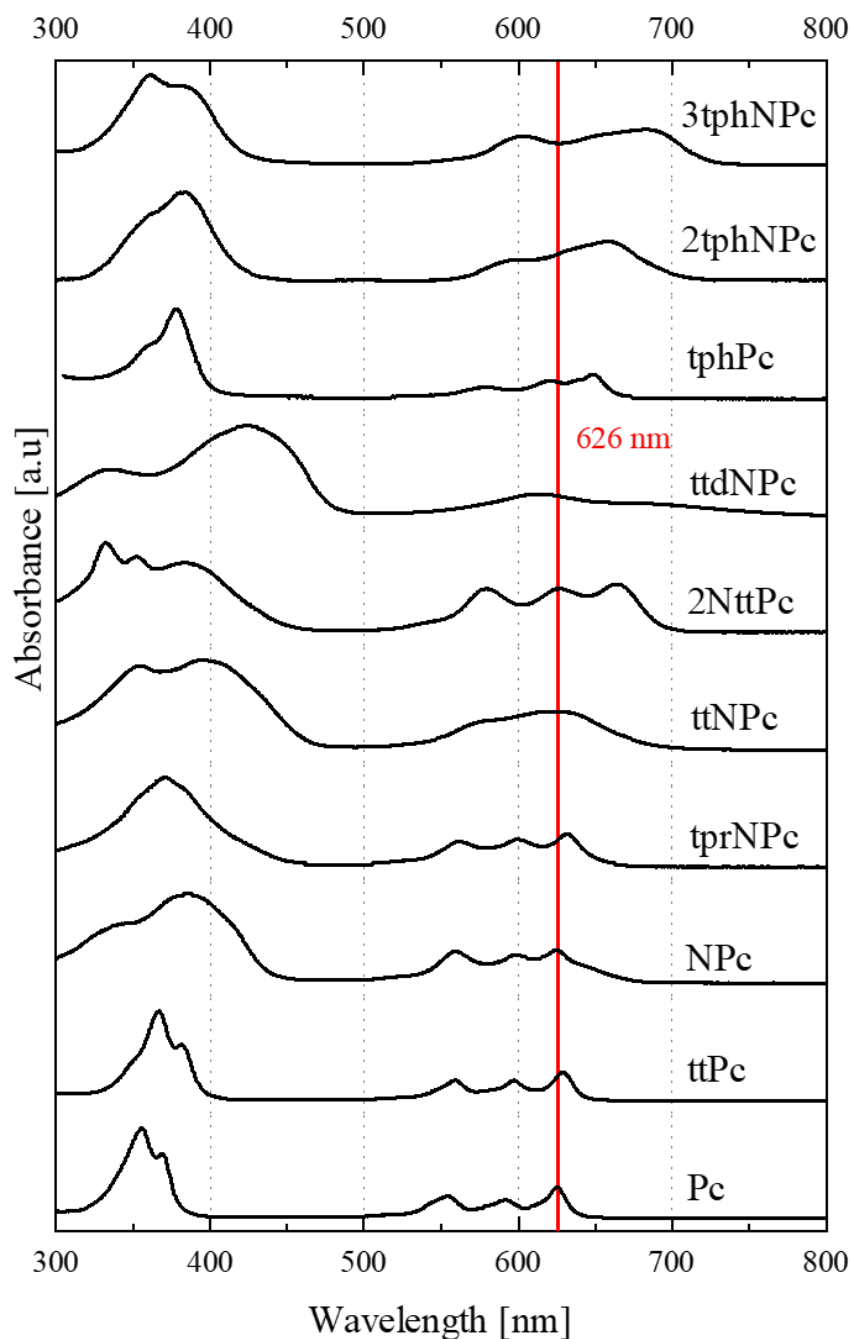
*Figure 10.6 Comparison of the room temperature absorption spectra for porphycene (**Pc**) and all studied nitroporphycenes. The red line signifies the location of the lowest energy absorption band with reference to porphycene (**Pc**).*

Figure 10.6 shows the changes in the absorption spectra for nitroporphycene (**NPc**), 9-nitro-2,7,12,17-tetrapropylporphycene (**tprNPc**), 9-nitro-2,7,12,17-tetra-*t*-butylporphycene (**ttNPc**), 2-nitro-7,12,17-tri-*t*-butylporphycene (**2NttPc**), 9,19-dinitro-2,7,12,17-tetra-*t*-butylporphycene (**ttdNPc**), 2-nitro-9,10,19,20-tetraphenylporphycene (**2tphNPc**) and 3-nitro-9,10,19,20-tetraphenylporphycene (**3tphNPc**). For the nitro-tetraphenyl derivatives, the position of the nitro group relative to the phenyl groups induces steric interaction between both groups. This interaction is evident as the photophysical and spectroscopic differences between **2tphNPc** and **3tphNPc**.

The values for QY of fluorescence observed for **2tphNPc** and **3tphNPc** can be compared with the data reported for *meso*-tetraphenylporphycene. The reported values for symmetric *meso*-tetraphenylporphycene (**tphPc**) fall between 0.2 and 0.3, depending on the solvent,[170,221,222] except in acetonitrile where ϕ_f of **tphPc** was found to be 0.08.[170] The reported value is two times less in the **3tphNPc** and ten times less in the **2tphNPc**. Experiments were performed to ascertain the yield of triplet state and singlet oxygen (SO) generation for the reported nitroporphycenes derivatives (Table 10.2). The resulting data show a 30:1 yield of SO in **3tphNPc** and **2tphNPc**. The low yield of fluorescence and SO in **2tphNPc** compared to **3tphNPc** is due to the interaction of the nitro group at position 2 with the phenyl group at 20. This interaction is obviously absent in the **3tphNPc** derivative, where the nitro group is placed further from the phenyl groups. A wholesome look at the SO for all the nitro derivatives of porphycene, **tprNPc** gave the highest yield of ~ 60%, and **NPc** and **2NttPc** gave a substantial yield of singlet oxygen. The lowest yield was observed for the tetra-*tert*-butyl derivatives, which, recall, also had the lowest yield of fluorescence (see section 5.3). This confirms that in the tetra-*tert*-butyl derivatives, non-radiative processes (involving $S_0 \leftarrow S_1$ internal conversion) are dominant. For **NPc, 2NttPc,** and **tprNPc**, given that they are moderate emitters, highly photostable (ϕ_{pb} for **NPc** in the order of 10^{-7}), and possess a high yield of the singlet oxygen formation, we can safely propose these compounds as possible candidates for 2nd generation sensitizing agents in PDT.

Table 10.2 Triplet lifetime and singlet oxygen generation for nitroporphycenes

	ϕ_Δ		τ_T (ns)
	Toluene	Acetonitrile	Toluene
3tphNPc	0.27	0.15	226
2tphNPc	0.01	0.007	[a]
tprNPc	0.61	[b]	192
NPc	0.49	0.49	164
2NtttPc	0.35	0.34	201
ttNPc	0.03	0.01	[a]

[a]signal was too weak to be observed
[b]insoluble in acetonitrile

10.4 Summary

- *Meso*-tetraphenyl porphycenes substituted at β and β' with nitro groups exhibit the largest red shift in absorption among the reported nitroporphycenes – highlighting the influence of *meso* substitution on the spectral properties of porphycenes.

- All nitroporphycenes derivatives exhibit a single emission band.

- There are two orders of magnitude differences in the fluorescence quantum yield of **2tphNPc** and **3tphNPc,** with the latter being a better emitter.

- Due to the proximity of both nitro and phenyl substituents, the low yield in fluorescence and singlet oxygen generation of **2tphNPc** results from steric interactions between the nitro and phenyl groups.

- The differences in the spectral, fluorescence quantum yield, singlet oxygen generation, and triplet lifetimes between **2tphNPc** and **3tphNPc** highlight the position-dependent effect of substitution patterns.

- **NPc**, **2NttPc**, and **tprNPc** are good emitters, possess excellent yields of singlet oxygen, are photostable, and are therefore proposed as candidates for 2nd-generation sensitizing agents in PDT.

Section III

Chapter 11

11.1 Putting it all together

11.1.1 Spectroscopy

- Amino and nitro porphycenes vary substantially in the intensity of UV/vis light absorbed, with red-shifted absorption bands appearing in the aminoporphycenes relative to the nitro counterpart.

- All aminoporphycenes exhibit similar red-shifted absorption patterns with at least five bands in the Q region, with the exception of 9,19-diamino-2,7,12,17-tetra-*tert*-butylporphycene (**ttdAPc**).

- All studied nitro derivatives absorb between 280 – 650 nm. However, with a four-fold introduction of phenyl groups at the *meso* position, about 50 nm shift to the red is observed. The red shift is larger in **3tphNPc** than in **2tphNPc**.

- The influence of alkyl substitution (*n*-propyl, *tert*-butyl) is not visible in the absorption spectra of both nitro and aminoporphycenes, as such specific effects are overshadowed by effects from the electron-donating (amino) and withdrawing (nitro) groups.

- Single emission is observed for nitro and aminoporphycenes. Emissions in both compounds are independent of excitation wavelength. Very weak emission from *trans-2* is seen in amino derivatives.

11.1.2 Photophysics

Table 11.1 Summary of photophysical parameters for the studied compounds

	Solvent	ϕ_{fl}	τ_{fl}(ns)	τ_T(ns)	ϕ_Δ	k_r $(10^7$ $s^{-1})$	k_r/n^2 $(10^7$ $s^{-1})$	$k_{nr}(10^8)$
APc	toluene	0.03	2.00 ± 0.05	118	0.21	1.50	0.67	4.85
	acetonitrile	0.01	1.40 ± 0.05	-	0.12	0.71	0.39	7.07
	n-hexane	-	2.60 ± 0.10	-	-	-	-	-
	methanol	-	1.00 ± 0.05	-	-	-	-	-
tprAPc	toluene	0.04	2.40 ± 0.05	165	0.26	1.67	0.75	4.00
	acetonitrile	0.02	1.90 ± 0.05	-	0.28	1.05	0.58	5.16
ttAPc	toluene	$3.6×10^{-3}$	0.15 ± 0.03	[a]	0.05	2.40	1.07	**66.40**
	acetonitrile	$6.0×10^{-4}$	-	-	0.02	-	-	-
	Paraffin oil	-	1.01 ± 0.05	-	-	-	-	-
NPc	toluene	0.10	3.40 ± 0.	164	0.49	2.94	1.31	2.65
	acetonitrile	0.06	2.70 ± 0.2	-	0.49	2.22	1.23	3.48
	n-hexane	-	4.40 ± 0.2	-	-	-	-	-
	acetonitrile:water 80:20 v/v	-	2.20 ± 0.1	-	-	-	-	-
tprNPc	toluene	0.03	1.10 ± 0.10	192	0.61	2.73	1.22	8.82
	acetonitrile	0.009	0.50 ± 0.00	-	[a]	1.80	0.99	**19.80**
ttNPc	toluene	$3.0×10^{-4}$	[a]	[a]	0.03	-	-	-
	acetonitrile	$6.0×10^{-4}$	[a]	-	0.01	-	-	-
	n-hexane	$4.0×10^{-4}$	-	-	-	-	-	-
	ethanol	$3.0×10^{-4}$	-	-	-	-	-	-
	DMSO	$5.0×10^{-4}$	-	-	-	-	-	-
2NttPc	toluene	0.17	-	201	0.35	-	-	-
	acetonitrile	0.08	4.7	-	0.34	1.70	0.94	1.96
	n-hexane	-	6.1	-	-	-	-	-
2tphNPc	toluene	$9.3×10^{-4}$	< 50 ps	[a]	0.01	-	-	-
	acetonitrile	$8.2×10^{-4}$	< 50 ps	-	0.007	-	-	-
3tphNPc	toluene	$1.0×10^{-1}$	4.3 ± 0.10	226	0.27	2.33	1.04	2.09
	acetonitrile	$3.4×10^{-2}$	2.1 ± 0.10	-	0.15	1.62	0.89	4.75

[a]decay too short (<50 ps) to be reliably determined.
- not determined

(Continued)

	Solvent	ϕ_{fl}	$\tau_{fl}(ns)$	$\tau_T(ns)$	ϕ_Δ	k_r	k_{IC}	k_{ISC}
ttdAPc	toluene	1.5×10^{-4}	< 30 ps	-	-	-	-	-
	acetonitrile	1.4×10^{-4}	< 30 ps	-	-	-	-	-
	DMSO	1.7×10^{-3}	< 30 ps	-	-	-	-	-
	1-octanol	3.8×10^{-3}	50 ps	-	-	-	-	-
	parrafin oil	6.0×10^{-4}	64 ps	-	-	-	-	-
ttdNPc	toluene	3.0×10^{-4}	22 ps	-	-	-	-	-
	acetonitrile	1.7×10^{-4}	12 ps	-	-	-	-	-
	DMSO	4.7×10^{-4}	-	-	-	-	-	-
	1-octanol	2.3×10^{-4}	35 ps	-	-	-	-	-
	parrafin oil	3.5×10^{-4}	70 ps	-	-	-	-	-
ttANPc	toluene	1.5×10^{-4}	< 50 ps	-	-	-	-	-
	acetonitrile	2.5×10^{-4}	< 50 ps	-	-	-	-	-
	DMSO		< 50 ps	-	-	-	-	-
	1-octanol	5.9×10^{-4}	< 50 ps	-	-	-	-	-
	parrafin oil	4.1×10^{-4}	< 50 ps	-	-	-	-	-

[a]decay too short (<50 ps) to be reliably determined.
- not determined

11.1.3 Tautomerization

According to calculations and experiments, two *trans* tautomers exist in the ground state of both amino and nitroporphycenes, with *trans-1* and *trans-2* being stabilized in aminoporphycenes and nitroporphycenes, respectively. In the excited state, the energy gap between the two *trans* forms becomes larger. In S_0 two *trans* tautomers are close in energy for *meso* substitution. The stabilized form in the ground state remains stabilized in the excited state. One-way tautomerization is observed, going from the destabilized specie to the more stable specie, resulting in emission for this specie.

11.1.4 Photodegradation

Photodegradation studies prove a glaring three-order-of-magnitude difference in the photostability quantum yield of amino and nitroporphycenes. While the nitroporphycenes are very stable (Quantum of photobleaching = 10^{-7}) under dark conditions and when exposed to light, aminoporphycenes are unstable (both as powders and in condensed phase) under dark conditions and when exposed to light. A quantum yield of photobleaching in the order 10^{-4} is obtained for aminoporphycenes studied (**APc**, **tprAPc**, and **ttAPc**). In our investigation, we have established

that aminoporphycenes emit single emission, and not double (as previously assumed) nor triple emission. The high energy emission bands observed for aminoporphycenes originate from the products of degradation of aminoporphycenes.

With the established photostability, singlet oxygen yields, triplet state lifetimes for nitroporphycenes (9-nitroporphycene (**NPc**), 9-nitro-2,7,12,17-tetra-*n*-propylporphycene (**tprNPc**), 2-nitro-7,12,17-tri-*tert*-butylporphycene (**2NttPc**), and 3-nitro-9,10,19,20-tetraphenylporphycene (**3tphNPc**)), we propose these compounds as candidates for sensitization in photodynamic therapy.

11.1.5 Position effects

With respect to the position effect of a specific substituent of the properties and reactivity of porphycene derivatives, our studies on *meso*-tetraphenylporphycenes, one with a nitro group at position 2 (**2tphNPc**) and the other at position 3 (**3tphNPc**) reveal interesting photochemistry. While the later emitted 10% fluorescence in toluene, ~30% yield of singlet oxygen generation and a long-lived triplet state (above 200 ns), the former emitted fluorescence in the order of 10^{-4}, with 1% yield of singlet oxygen generation. The signal for the triplet lifetime was too weak to be determined for **2tphNPc.** The differences in the photophysics of two molecules with a nitro group placed at different positions further confirms the importance of the localization of the substituent, as well as its immediate surroundings. We attribute the peculiar behavior of 2tphNPc to the steric interaction between the nitro group and the adjacent phenyl group.

11.2 Future outlook

- Investigation on the possible application of studied nitroporphycenes in PDT and photodynamic inactivation of bacteria (PDI).

- Determination of tautomerization rates for amino and nitro derivatives of porphycene.

- Investigation on the possibility of increasing stability in aminoporphycenes, either via protonation of the amino substituent of introduction of some stabilizing/protecting groups to the macrocycle.

- Since **ttdNPc**, **ttdAPc**, and **ttANPc** are very weak emitters, further studies are recommended for samples of **ttdNPc**, **ttdAPc**, and **ttANPc** placed in rigid glassy or polymer environments. There lies a possibility for these derivatives of porphycenes to be applicable in viscosity sensing.

References

1. Battersby, A. R., Fookes, C. J. R., Matcham, G. W. J. & McDonald, E. Biosynthesis of the pigments of life: formation of the macrocycle. *Nature* **285**, 17–21 (1980).

2. Battersby, A. R. Tetrapyrroles: The pigments of life. *Nat. Prod. Rep.* **17**, 507–526 (2000).

3. Bonnett, R. Nomenclature. in *The Porphyrins Structure and Synthesis, Part A* vol. I 1–643 (Academic Press, 1978).

4. Kim, D. H., Holten, D., Gouterman, M. & Buchler, J. W. Comparative photophysics of Platinum(II) and Platinum(IV) Porphyrins. *J. or Am. Chem. Soc.* **14**, 4015–4017 (1984).

5. Ostapko, J., Buczyńska, J., Pszona, M., Kowalska, P. & Waluk, J. Synthesis, spectroscopy, and photophysics of porphyrins attached to gold nanoparticles via one or two linkers. *J. Porphyr. Phthalocyanines* **18**, 686–697 (2014).

6. Kelm, A., Ostapko, J., Gajewska, A., Sánchez-Iglesias, A. & Waluk, J. Spectral and photophysical modifications of porphyrins attached to core-shell nanoparticles. Theory and experiment. *Methods Appl. Fluoresc.* **9**, 045003 (2021).

7. Sen, P., Soy, R., Mgidlana, S., Mack, J. & Nyokong, T. Light-driven antimicrobial therapy of palladium porphyrins and their chitosan immobilization derivatives and their photophysical-chemical properties. *Dye. Pigment.* **203**, 110313 (2022).

8. La, D. D. *et al.* Advances and prospects of porphyrin-based nanomaterials via self-assembly for photocatalytic applications in environmental treatment. *Coord. Chem. Rev.* **463**, 214543 (2022).

9. Renn, A., Wild, U. P. & Rebane, A. Multidimensional holography by persistent spectral hole burning. *J. Phys. Chem. A* **106**, 3045–3060 (2002).

10. Monti, D. *et al.* Porphyrin-based nanostructures for sensing applications. *J. Sensors* **2009**, (2009).

11. Bellnier, D. A., Ho, Y.-K., Pandey, R. K., Missert, J. R. & Dougherty, T. J. Distribution and Elimination of Photofrin II in Mice. *Photochem. Photobiol.* **50**, 221–228 (1989).

12. Kessel, D. In vitro photosensitization with a benzoporphyrin derivative. *Photochem. Photobiol.* **49**, 579–582 (1989).

13. Richter, A. M., Cerruti-Sola, S., Sternberg, E. D., Dolphin, D. & Levy, J. G. Biodistribution of tritiated benzoporphyrin derivative (3H-BPD-MA), a new potent photosensitizer, in normal and tumor-bearing mice. *J. Photochem. Photobiol. B, Biol.* **5**, 231–244 (1990).

14. Richter, A. M. *et al.* Photosensitising potency of structural analogues of benzoporphyrin derivative (BPD) in a mouse tumour model. *Br. J. Cancer* **63**, 87–93 (1991).

15. Szaciłowski, K., Macyk, W., Drzewiecka-Matuszek, A., Brindell, M. & Stochel, G. Bioinorganic photochemistry: Frontiers and mechanisms. *Chem. Rev.* **105**, (2005).

16. Silva, E. F. F. *et al.* Mechanisms of Singlet-Oxygen and Superoxide-Ion Generation by Porphyrins and Bacteriochlorins and their Implications in Photodynamic Therapy. *Chem. – A Eur. J.* **16**, 9273–9286 (2010).

17. Dąbrowski, J. M. *et al.* Engineering of relevant photodynamic processes through structural modifications of metallotetrapyrrolic photosensitizers. *Coord. Chem. Rev.* **325**, 67–101 (2016).

18. Dougherty, T. J. *et al.* Photodynamic therapy. *J. Natl. Cancer Inst.* **90**, 889–905 (1998).

19.   Malik, Z. & Lugaci, H. Destruction of erythroleukaemic cells by photoactivation of endogenous porphyrins. *Br. J. Cancer* **56**, 589–595 (1987).

20.   Berg, K. *et al.* Porphyrin-related photosensitizers for cancer imaging and therapeutic applications. *J. Microsc.* **218**, 133–147 (2005).

21.   Agostinis, P. *et al.* Photodynamic Therapy of Cancer: An Update. *CA Cancer J Clin* **61**, 250–281 (2011).

22.   Decker, C., Schubert, H., May, S. & Fahr, A. Pharmacokinetics of temoporfin-loaded liposome formulations: correlation of liposome and temoporfin blood concentration. *J. Control. Release* **166**, 277–285 (2013).

23.   Hu, F. Q. *et al.* Enhanced cellular uptake of chlorine e6 mediated by stearic acid–grafted chitosan oligosaccharide micelles. *J. Drug Target.* **17**, 384–391 (2009).

24.   Hye Myeong Lee *et al.* Ursodeoxycholic acid-conjugated chitosan for photodynamic treatment of HuCC-T1 human cholangiocarcinoma cells. *Int. J. Pharm.* **454**, 74–81 (2013).

25.   Mfouo-Tynga, I. S., Dias, L. D., Inada, N. M. & Kurachi, C. Features of third generation photosensitizers used in anticancer photodynamic therapy: Review. *Photodiagnosis Photodyn. Ther.* **34**, 102091 (2021).

26.   Barker, D. S., Henderson, R. W. & Storey, E. The in vivo localization of porphyrins. *Br. J. Exp. Pathol.* **51**, 628 (1970).

27.   Kou, J., Dou, D. & Yang, L. Porphyrin photosensitizers in photodynamic therapy and its applications. *Oncotarget* **8**, 81591–81603 (2017).

28.   Vogel, E., Kocher, M., Schmickler, H. & Lex, J. Porphycene - a Novel Porphyrin Isomer. *Angew. Chem. Int. Ed. Engl* **25**, 257–259 (1986).

29.   García-Díaz, M. *et al.* Temocene: The porphycene analogue of temoporfin (Foscan®). *Medchemcomm* **2**, 616–619 (2011).

30.   Sessler, J. L. *et al.* Corrphycene: A New Porphyrin Isomer. *Angew. Chemie Int. Ed. English* **33**, 2308–2312 (1994).

31.   Callot, H. J., Rohrer, A., Tschamber, T. & Metz, B. A Novel Porphyrin Isomer: Hemiporphycene. Formation and Single-Crystal X-ray Diffraction Structure Determination of Hemiporphycene Nickel Complex. *New J. Chem.* **19**, 155–159 (1995).

32.   Vogel, E. *et al.* Octaethylhemiporphycene: Synthesis, Molecular Structure, and Photophysics. *Angew. Chemie int Ed. Engl* **36**, 1651–1654 (1997).

33.   Ostapko, J. *et al.* Parent, Unsubstituted Hemiporphycene: Synthesis and Properties. *Chem. - A Eur. J.* **22**, 17311–17320 (2016).

34.   Vogel, E. *et al.* Palladium Complexes of the New Porphyrin Isomers (Z)- and (E)-Isoporphycene - PdII-Induced Cyclization of Tetrapyrrolealdehydes. *Angew. Chemie (International Ed. English)* **36**, 353–357 (1997).

35.   Vogel, E. *et al.* Isoporphycene: The fourth constitutional lsomer of porphyrin with an N4 core- occurrence of E/Z isomerism. *Angew. Chemie - Int. Ed.* **38**, 2919–2923 (1999).

36.   Waluk, J. Spectroscopy and Tautomerization Studies of Porphycenes. *Chem. Rev.* **117**, 2447–2480 (2017).

37. Stockert, J. *et al.* Porphycenes: Facts and Prospects in Photodynamic Therapy of Cancer. *Curr. Med. Chem.* **14**, 997–1026 (2007).

38. Richert, C. *et al.* Photodynamic Antitumor Agents:*β*-Methoxyethyl Groups Give Access to Functionalized Porphycenes and Enhance Cellular Uptake and Activity. *J. Med. Chem.* **37**, 2797–2807 (1994).

39. Gottfried, V., Davidi, R., Averbuj, C. & Kimel, S. In vivo damage to chorioallantoic membrane blood vessels by porphycene-induced photodynamic therapy. *J. Photochem. Photobiol. B Biol.* **30**, 115–121 (1995).

40. Dellian, M., Richert, C., Gamarra, F. & Goetz, A. E. Photodynamic eradication of amelanotic melanoma of the hamster with fast-acting photosensitizers. *Int. J. Cancer* **65**, 246–248 (1996).

41. Abels, C., Szeimies, R. M., Steinbach, P., Richert, C. & Goetz, A. E. Targeting of the tumor microcirculation by photodynamic therapy with a synthetic porphycene. *J. Photochem. Photobiol. B Biol.* **40**, 305–312 (1997).

42. Segalla, A., Fedeli, F., Reddi, E., Jori, G. & Cross, A. Effect of chemical structure and hydrophobicity on the pharmacokinetic properties of porphycenes in tumour-bearing mice. *Int. J. Cancer* **72**, 329–336 (1997).

43. Rubio, N. *et al.* A comparison between the photophysical and photosensitising properties of tetraphenyl porphycenes and porphyrins. *New J. Chem.* **29**, 378–384 (2005).

44. Ruiz-González, R. *et al.* Efficient induction of apoptosis in HeLa cells by a novel cationic porphycene photosensitizer. *Eur. J. Med. Chem.* **63**, 401–414 (2013).

45. Masiera, N. *et al.* Antimicrobial photodynamic therapy by means of porphycene photosensitizers. *J. Photochem. Photobiol. B Biol.* **174**, 84–89 (2017).

46. Lin, J. *et al.* Photosensitizer-loaded gold vesicles with strong plasmonic coupling effect for imaging-guided photothermal/photodynamic therapy. *ACS Nano* **7**, 5320–5329 (2013).

47. Haug, R. & Richert, C. A porphycene-DNA hybrid and its DNA-templated interactions with a porphyrin. *J. Porphyr. Phthalocyanines* **16**, 545–555 (2012).

48. Aramendia, P. F. *et al.* The Photophysical Properties of Porphycenes: Potential Photodynamic Therapy Agents. *Photochem. Photobiol.* **44**, 555–559 (1986).

49. Waluk, J. *et al.* Electronic States of Porphycenes. *J. Am. Chem. Soc.* **113**, 5511–5527 (1991).

50. Braslavsky, S. E. *et al.* Photophysical properties of porphycene derivatives (18π porphyrinoids). *J. Photochem. Photobiol. B Biol.* **40**, 191–198 (1997).

51. Gil, M., Jasny, J., Vogel, E. & Waluk, J. Ground and excited state tautomerization in 9-acetoxy-2,7,12,17-tetra-*n*-propylporphycene. *Chem. Phys. Lett.* **323**, 534–541 (2000).

52. Waluk, J. Structure, Spectroscopy, Photophysics, and Tautomerism of Free-Base Porphycenes and Other Porphyrin Isomers. in *Handbook of Porphyrin Science* (eds. Karl M. Kadish, Kevin M. Smith & Roger Guilard) vol. 7 359–435 (World Scientific Publishing Co. Pte. Ltd., 2010).

53. Mártire, D. O., Russell, S., Dietrich, H. J., Cobos, C. J. & Braslavsky, S. E. Photophysics of novel 22π porphyrinoids. *J. Porphyr. Phthalocyanines* **16**, 499–507 (2012).

54. Bernard, C., Gisselbrecht, J. P., Gross, M., Vogel, E. & Lausmann, M. Redox Properties of Porphycenes and Metalloporphycenes. A Comparison with Porphyrins. *Inorg. Chem.* **33**, 2393–2401 (1994).

55. Lopez, E. J. G. *et al.* Light-Activated Antibacterial Polymeric Surface Based on Porphycene. *Appl. Polym. Mater.* **5**, 943–956 (2023).

56. Aukauloo, M. a & Guilard, R. The Etioporphycerin - Synthesis and Characterization of a New Porphyrin Isomer. *New J. Chem.* **18**, 1205–1207 (1994).

57. Chmielewski, P. J., Latos-Grażyński, L., Rachlewicz, K. & Glowiak, T. Tetra-p-tolylporphyrin with an Inverted Pyrrole Ring: A Novel Isomer of Porphyrin. *Angew. Chemie Int. Ed. English* **33**, 779–781 (1994).

58. Furuta, H., Asano, T. & Ogawa, T. 'N-Confused Porphyrin': A New Isomer of Tetraphenylporphyrin. *J. Am. Chem. Soc.* **116**, 767–768 (1994).

59. Lash, T. D., Lammer, A. D. & Ferrence, G. M. Neo-confused porphyrins, a new class of porphyrin isomers. *Angew. Chemie - Int. Ed.* **50**, 9718–9721 (2011).

60. Costa, R. D., Malig, J., Brenner, W., Jux, N. & Guldi, D. M. Electron accepting porphycenes on graphene. *Adv. Mater.* **25**, 2600–2605 (2013).

61. Saeki, H., Misaki, M., Kuzuhara, D., Yamada, H. & Ueda, Y. Fabrication of phase-separated benzoporphycene/[6,6]-phenyl-C 61-butyric acid methyl ester films for use in organic photovoltaic cells. *Jpn. J. Appl. Phys.* **52**, 111601 (2013).

62. Saeki, H. *et al.* Thermal conversion behavior and morphology control of benzoporphycene from a novel soluble precursor. *Appl. Phys. Express* **6**, 3–6 (2013).

63. Saeki, H. *et al.* Effect of crystallinity in small molecular weight organic heterojunction solar cells. *J. Mater. Chem. C* **2**, 5357–5364 (2014).

64. Lo, W. C., Che, C. M., Cheng, K. F. & Mak, T. C. W. Catalytic and asymmetric cyclopropanation of styrenes catalysed by ruthenium porphyrin and porphycene complexes. *Chem. Commun.* **043**, 1205–1206 (1997).

65. Hayashi, T. *et al.* Cobaltporphycenes as catalysts. The oxidation of vinyl ethers via the formation and dissociation of cobalt-carbon bonds. *Organometallics* **20**, 3074–3078 (2001).

66. Berlicka, A. & König, B. Porphycene-mediated photooxidation of benzylamines by visible light. *Photochem. Photobiol. Sci.* **9**, 1359–1366 (2010).

67. Oohora, K., Kihira, Y., Mizohata, E., Inoue, T. & Hayashi, T. C(sp3)-H bond hydroxylation catalyzed by myoglobin reconstituted with manganese porphycene. *J. Am. Chem. Soc.* **135**, 17282–17285 (2013).

68. Ono, T., Shinjo, H., Koga, D. & Hisaeda, Y. Synthesis of a *meso*-Tetraalkylporphycene Bearing Reactive Sites: Toward Porphycene–Polydimethylsiloxane Hybrids with Enhanced Photophysical Properties. *Eur. J. Org. Chem.* **46**, 7578–7583 (2019).

69. Ogiso, A. *et al.* Optical recording medium and porphycene compound - Patent US-6627288-B1 - PubChem. (2000).

70. Barbe, J. *et al.* Electrocrystallization and X-ray structure of a new porphycene-based material, [Ni(OMPc)]$_{2.5}$(BF$_4$)$_2$·C$_{10}$H$_7$Cl. *J. Chem. Soc., Chem. Commun.* 2757–2758 (1994).

71.	Miller, D. C., Bollinger, J. C., Hoffman, B. M. & Ibers, J. A. Structural, Magnetic, and Charge-Transport Properties of a New One-Dimensional Molecular Conductor, Ni(tprpc)I1.67 (tprpc = 2,7,12,17-Tetrapropylporphycenato). *Inorg. Chem.* **33**, 3354–3357 (1994).

72.	Kumagai, T. *et al.* Controlling intramolecular hydrogen transfer in a porphycene molecule with single atoms or molecules located nearby. *Nat. Chem.* **6**, 41–46 (2014).

73.	Che, C. M. *et al.* A high-performance organic field-effect transistor based on platinum(II) porphyrin: Peripheral substituents on porphyrin ligand significantly affect film structure and charge mobility. *Chem. - An Asian J.* **3**, 1092–1103 (2008).

74.	Stępień, M., Donnio, B. & Sessler, J. L. Discotic liquid-crystalline materials based on porphycenes: A mesogenic metalloporphycene-tetracyanoquinodimethane (TCNQ) adduct. *Chem. - A Eur. J.* **13**, 6853–6863 (2007).

75.	Hayashi, T. *et al.* Blue myoglobin reconstituted with an iron porphycene shows extremely high oxygen affinity. *J. Am. Chem. Soc.* **124**, 11226–11227 (2002).

76.	Matsuo, T. *et al.* Ligand binding properties of myoglobin reconstituted with iron porphycene: Unusual O_2 binding selectivity against CO binding. *J. Am. Chem. Soc.* **126**, 16007–16017 (2004).

77.	Matsuo, T. *et al.* Preparation and O_2 binding study of myoglobin having a cobalt porphycene. *Inorg. Chem.* **44**, 9391–9396 (2005).

78.	Matsuo, T., Ikegami, T., Sato, H., Hisaeda, Y. & Hayashi, T. Ligand binding properties of two kinds of reconstituted myoglobins with iron porphycene having propionates: Effect of *β*-pyrrolic position of two propionate side chains in porphycene framework. *J. Inorg. Biochem.* **100**, 1265–1271 (2006).

79.	Hayashi, T. *et al.* Crystal structure and peroxidase activity of myoglobin reconstituted with iron porphycene. *Inorg. Chem.* **45**, 10530–10536 (2006).

80.	Matsuo, T., Murata, D., Hisaeda, Y., Hori, H. & Hayashi, T. Porphyrinoid chemistry in hemoprotein matrix: Detection and reactivities of iron(IV)-oxo species of porphycene incorporated into horseradish peroxidase. *J. Am. Chem. Soc.* **129**, 12906–12907 (2007).

81.	Matsuo, T., Ito, K., Nakashima, Y., Hisaeda, Y. & Hayashi, T. Effect of peripheral trifluoromethyl groups in artificial iron porphycene cofactor on ligand binding properties of myoglobin. *J. Inorg. Biochem.* **102**, 166–173 (2008).

82.	Platt, J. R. Classification of spectra of cata-condensed hydrocarbons. *J. Chem. Phys.* **17**, 484–495 (1949).

83.	Moffitt, W. The electronic spectra of cata-condensed hydrocarbons. *J. Chem. Phys.* **22**, 320–333 (1954).

84.	Gouterman, M. Spectra of porphyrins. *J. Mol. Spectrosc.* **6**, 138–163 (1961).

85.	Michl, J. Magnetic circular dichroism of aromatic molecules. . *Tetrahedron* **40**, 3845–3934 (1984).

86.	Cañete, M. *et al.* Necrotic cell death induced by photodynamic treatment of human lung adenocarcinoma A-549 cells with palladium(II)-tetraphenylporphycene. *Int. J. Oncol.* **24**, 1221–1228 (2004).

87.	Radziszewski, J. G., Waluk, J. & Michl, J. FT visible absorption spectroscopy of porphine in noble gas matrices. *J. Mol. Spectrosc.* **140**, 373–389 (1990).

88.   Starukhin, A., Vogel, E. & Waluk, J. Electronic spectra of porphycenes in rare gas and nitrogen matrices. *J. Phys. Chem. A* **102**, 9999–10006 (1998).

89.   Waluk, J. & Michl, J. The Perimeter Model and Magnetic Circular Dichroism of Porphyrin Analogues. *J. Org. Chem.* **56**, 2729–2735 (1991).

90.   Vogel, E. *et al.* Tetraoxaporphycene Dication. *Angew. Chemie Int. Ed. English* **27**, 406–409 (1988).

91.   Bachmann, R., Gerson, F., Gescheidt, G. & Vogel, E. Tetraoxaporphycene: ESR/ENDOR, UV/Visible/Near-IR, and MO-theoretical study of its five redox stages. *J. Am. Chem. Soc.* **115**, 10282–10285 (1993).

92.   Nußbaumer, T., Krieger, C. & Neidlein, R. 21,23-Dithia-3,13-diazaporphycenes2Novel Aromatic Porphycene AnaloguesIncorporating Thiazole. *European J. Org. Chem.* **2000**, 2449–2457 (2000).

93.   Gil, M., Organero, J. A., Waluk, J. & Douhal, A. Ultrafast dynamics of alkyl-substituted porphycenes in solution. *Chem. Phys. Lett.* **422**, 142–146 (2006).

94.   Fita, P., Radzewicz, C. & Waluk, J. Electronic and vibrational relaxation of porphycene in solution. *J. Phys. Chem. A* **112**, 10753–10757 (2008).

95.   Gil, M. *et al.* Unusual, solvent viscosity-controlled tautomerism and photophysics: *Meso*-alkylated porphycenes. *J. Am. Chem. Soc.* **132**, 13472–13485 (2010).

96.   Sobolewski, A. L., Gil, M., Dobkowski, J. & Waluk, J. On the origin of radiationless transitions in porphycenes. *J. Phys. Chem. A* **113**, 7714–7716 (2009).

97.   Nonell, S., Aramendia, P. F., Heihoff, K., Negri, R. M. & J, S. E. B. Laser-Induced Optoacoustics Combined with Near- Infrared Emission . An Alternative. *J. Phys. Chem.* **94**, 5879–5883 (1990).

98.   Justino, L. L. G., Golec, B., Gorski, A. & Waluk, J. Phosphorescence and Photophysical Parameters of Porphycene in Cryogenic Matrices. *Photochem 2022, Vol. 2, Pages 217-224* **2**, 217–224 (2022).

99.   Radziszewski, J. G., Waluk, J., Nepraš, M. & Michl, J. Fourier transform fluorescence and phosphorescence of porphine in rare gas matrices. *J. Phys. Chem.* **95**, 1963–1969 (1991).

100.   Bossi, A. *et al.* Porphycene protonation: A fast and reversible reaction enabling optical transduction for acid sensing. *ChemPhotoChem* **4**, 5264–5270 (2020).

101.   Lament, B., Karpiuk, J. & Waluk, J. Determination of triplet formation efficiency from kinetic profiles of the ground state recovery. *Photochem. Photobiol. Sci.* **2**, 267–272 (2003).

102.   Arad, O., Rubio, N., Sánchez-García, D., Borrell, J. I. & Nonell, S. Asymmetric porphycenes: synthesis and photophysical properties of 9-substituted 2,7,12,17-tetraphenylporphycenes. *J. Porphyr. Phthalocyanines* **13**, 376–381 (2009).

103.   Duran-Frigola, M., Tejedor-Estrada, R., Sánchez-García, D. & Nonell, S. Dual fluorescence in 9-amino-2,7,12,17-tetraphenylporphycene. *Phys. Chem. Chem. Phys.* **13**, 10326–10332 (2011).

104.   Fita, P. *et al.* Tautomerization in 2,7,12,17-tetraphenylporphycene and 9-amino-2,7,12,17-tetraphenylporphycene: Influence of asymmetry on the direction of the transition moment. *Chem. - A Eur. J.* **18**, 13160–13167 (2012).

105.   Planas, O., Tejedor-Estrada, R. & Nonell, S. Tautomerism and dual fluorescence in 9-substituted n-propyl- and methoxyethyl-porphycenes. *J. Porphyr. Phthalocyanines* **16**, 633–640 (2012).

106. Planas, O., Gallavardin, T. & Nonell, S. Unusual Properties of Asymmetric Porphycenes. in *Handbook of Porphyrin Science* (eds. Karl M. Kadish, Kevin M. Smith & Roger Guilard) vol. 41 299–349 (World Scientific Publishing Co. Pte. Ltd., 2016).

107. Czerski, I. *et al.* The long and winding road to new porphycenes. *J. Porphyr. Phthalocyanines* **16**, 589–602 (2012).

108. Vogel, E. *et al.* 2,7,12,17-Tetrapropylporphycene—Counterpart of Octaethylporphyrin in the Porphycene Series. *Angew. Chemie Int. Ed. English* **26**, 928–931 (1987).

109. Kuzuhara, D. *et al.* First synthesis of dodecasubstituted porphycenes. *Chem. - A Eur. J.* **17**, 3376–3383 (2011).

110. Berman, A. *et al.* Photophysics and Photoinduced-Electron-Transfer Reactions of Zinc and Free-Base Octaethylporphycenes. *J. Phys. Chem.* **96**, 3041–3047 (1992).

111. Vogel, E. *et al.* New Porphycene Ligands: Octaethyl- and Etioporphycene (OEPc and EtioPc)—Tetra- and Pentacoordinated Zinc Complexes of OEPc. *Angew. Chemie Int. Ed. English* **32**, 1600–1604 (1993).

112. Guilard, R., Aukauloo, M. A., Tardieux, C. & Vogel, E. Synthesis of a new alkylated porphycene. *Synthesis (Stuttg).* **2**, 1480–1482 (1995).

113. Vogel, E., Köcher, M., Lex, J. & Ermer, O. Steric Modulation of the Porphycene System by Alkyl Substituents: 9,10,19,20-Tetraalkylporphycenes. *Isr. J. Chem.* **29**, 257–266 (1989).

114. Birklund-Andersen, K., Vogel, E. & Waluk, J. Electronic transition moment directions and tautomerization of 9,10,19,20-tetra-*n*-propylporphycene. *Chem. Phys. Lett.* **271**, 341–348 (1997).

115. Ciąck Piotr *et al.* Tautomerism in Porphycenes : Analysis of Rate-Affecting Factors. *J. Phys. Chem. B* **119**, 2292–2301 (2015).

116. Anguera, G., Llinàs, M. C., Batllori, X. & Sánchez-García, D. Aryl nitroporphycenes and derivatives: First regioselective synthesis of dinitroporphycenes. *J. Porphyr. Phthalocyanines* **15**, 865–870 (2011).

117. Lan, Z., Nonell, S. & Barbatti, M. Theoretical characterization of absorption and emission spectra of an asymmetric porphycene. *J. Phys. Chem. A* **116**, 3366–3376 (2012).

118. Nonell, S. *et al.* Synthesis of 2,7,12,17-tetraphenylporphycene (TPPo). First aryl-substituted porphycene for the photodynamic therapy of tumors. *Tetrahedron Lett.* **36**, 3405–3408 (1995).

119. Sánchez-García, D., Borrell, J. I. & Nonell, S. One-pot synthesis of substituted 2,2'-bipyrroles. A straightforward route to aryl porphycenes. *Org. Lett.* **11**, 77–79 (2009).

120. Brenner, W., Malig, J., Oelsner, C., Guldi, D. M. & Jux, N. Synthesis and physico-chemical properties of porphycenes. *J. Porphyr. Phthalocyanines* **16**, 651–662 (2012).

121. Kuzuhara, D., Nakaoka, H., Okabe, T., Aratani, N. & Yamada, H. Synthesis, properties and crystal structures of 2,7,12,17-tetraarylporphycenes. *Heterocycles* **90**, 1214–1227 (2015).

122. D'Souza, F. *et al.* Electrochemical, UV/visible, and EPR characterization of metalloporphycenes containing first-row transition metals. *J. Phys. Chem.* **98**, 11885–11891 (1994).

123. D'Souza, F. *et al.* Effect of Peripheral Substitution and Extended Conjugation on the Redox Potentials of Nickel Porphycenes. *Inorg. Chem.* **35**, 5743–5746 (1996).

124. Kuzuhara, D., Yamada, H., Mori, S., Okujima, T. & Uno, H. Synthesis, structures and properties of benzoporphycenes and naphthoporphycenes. *J. Porphyr. Phthalocyanines* **15**, 930–942 (2011).

125. Okawara, T., Abe, M., Shimakoshi, H. & Hisaeda, Y. Hydroxy-Functionalized Porphycenes: Structure, Spectroscopy, and Electrochemistry. *Bull. Chem. Soc. Jpn.* **84**, 718–728 (2011).

126. Kadish, K. M. *et al.* Physicochemical Characterization of σ-Bonded Aryl Iron(III) Porphycenes. X-ray Structures of (EtioPc)Fe(3,5-$C_6F_2H_3$) and (EtioPc)In(C_6H_5), Where EtioPc Is the Dianion of 2,7,12,17-Tetraethyl-3,6,13,16-tetramethylporphycene. *Inorg. Chem.* **37**, 6168–6175 (1998).

127. Rana, A., Lee, S., Kim, D. & Panda, P. K. *β*-Octakis(methylthio)porphycenes: Synthesis, characterisation and third order nonlinear optical studies. *Chem. Commun.* **51**, 7705–7708 (2015).

128. Kadish, K. M. *et al.* Synthesis and Electrochemical Reactivity of σ-Bonded and N-Substituted Cobalt Porphycenes. *Inorg. Chem.* **37**, 2693–2700 (1998).

129. Oertling, W. A., Wu, W., Lopez-garriga, J. J., Kim, Y. & Chang, C. K. Optical absorptions and Raman scattering of metalloporphycenes reveal electronic and vibronic properties distinct from those of metalloporphyrins. *J. Am. Chem. Soc.* **113**, 127–134 (1991).

130. Cuesta, L. *et al.* Metalloporphycenes : Synthesis and Characterization of (Pentamethylcyclopentadienyl) ruthenium Sitting-Atop and π -Complexes. *J. Am. Chem. Soc.* **131**, 13538–13547 (2009).

131. Sarma, T. & Panda, P. K. Effect of *β-β′* Fusion on metal ion complexation of porphycene. *J. Chem. Sci.* **127**, 235–240 (2015).

132. Kadish, K. M. *et al.* Electrochemistry of New σ-Bonded Metal(III) Complexes with Tetrapyrrole Ligands. Reactions of (EtioPc)M(C_6H_5) and (EtioPc)FeCl Where M = Fe or In and EtioPc Is the Dianion of 2,7,12,17-Tetraethyl-3,6,13,16-tetramethylporphycene. *Inorg. Chem.* **33**, 4474–4479 (1994).

133. Malsch, K. & Hohlneicher, G. The force field of porphycene: A theoretical and experimental approach. *J. Phys. Chem. A* **101**, 8409–8416 (1997).

134. Dobkowski, J., Galievsky, V., Starukhin, A. & Waluk, J. Relaxation in excited states of porphycene in low-temperature argon and nitrogen matrices. *Chem. Phys. Lett.* **318**, 79–84 (2000).

135. Kyrychenko, A., Gawinkowski, S., Urbańska, N., Pietraszkiewicz, M. & Waluk, J. Matrix isolation spectroscopy and molecular dynamics simulations for 2,7,12,17-tetra-*tert*-butylporphycene in argon and xenon. *J. Chem. Phys.* **127**, 1–12 (2007).

136. Dobkowski, J., Galievsky, V., Gil, M. & Waluk, J. Time-resolved fluorescence studies of porphycene isolated in low-temperature gas matrices. *Chem. Phys. Lett.* **394**, 410–414 (2004).

137. Dobkowski, J., Lobko, Y., Gawinkowski, S. & Waluk, J. Energy relaxation paths in matrix-isolated excited molecules: Comparison of porphycene with dibenzoporphycenes. *Chem. Phys. Lett.* **416**, 128–132 (2005).

138. Gawinkowski, S. *et al.* Vibrations and hydrogen bonding in porphycene. *Phys. Chem. Chem. Phys.* **14**, 5489–5503 (2012).

139. Kyrychenko, A. & Waluk, J. Molecular dynamics simulations of matrix deposition. I. Site structure analysis for porphyrin in argon and xenon. *J. Chem. Phys.* **119**, 7318–7327 (2003).

140. Kyrychenko, A., Gorski, A. & Waluk, J. Molecular dynamics and density functional theory simulations of matrix deposition. II. Absolute site structure assignment for porphyrin in xenon. *J. Chem. Phys.* **121**, 12017–12025 (2004).

141. Kyrychenko, A. & Waluk, J. Molecular dynamics simulations of matrix deposition. III. Site structure analysis for porphycene in argon and xenon. *J. Chem. Phys.* **123**, 1–10 (2005).

142. Sepioł, J. *et al.* Proton tunnelling in porphycene seeded in a supersonic jet. *Chem. Phys. Lett.* **296**, 549–556 (1998).

143. Mengesha, E. T., Sepio, J., Borowicz, P. & Waluk, J. Vibrations of porphycene in the S0 and S1 electronic states: Single vibronic level dispersed fluorescence study in a supersonic jet. *J. Chem. Phys.* **138**, 1–14 (2013).

144. Mengesha, E. T., Zehnacker-Rentien, A., Sepioł, J., Kijak, M. & Waluk, J. Spectroscopic study of jet-cooled deuterated porphycenes: Unusual isotopic effects on proton tunneling. *J. Phys. Chem. B* **119**, 2193–2203 (2015).

145. Fita, P. *et al.* Spectroscopic and microscopic investigations of tautomerization in porphycenes: condensed phases, supersonic jets, and single molecule studies. *Phys. Chem. Chem. Phys* **19**, 4921 (2017).

146. Nosenko, Y., Jasny, J., Pietraszkiewicz, M. & Mordzinski, A. Laser spectroscopy of porphycene derivatives: A search for proton tunneling in 2,7,12,17-tetra-*tert*-butylporphycene. *Chem. Phys. Lett.* **399**, 331–336 (2004).

147. Vdovin, A. *et al.* Evidence for two forms, double hydrogen tunneling, and proximity of excited states in bridge-substituted porphycenes: Supersonic jet studies. *J. Am. Chem. Soc.* **128**, 2577–2586 (2006).

148. Vdovin, A., Waluk, J., Dick, B. & Slenczka, A. Mode-selective promotion and isotope effects of concerted double-hydrogen tunneling in porphycene embedded in superfluid helium nanodroplets. *ChemPhysChem* **10**, 761–765 (2009).

149. Listkowski, A. *et al.* Fluorinated Porphycenes: Synthesis, Spectroscopy, Photophysics, and Tautomerism. *Chempluschem* **85**, 2197–2206 (2020).

150. Kasprzycki, P. *et al.* Influence of local microenvironment on the double hydrogen transfer in porphycene. *Phys. Chem. Chem. Phys* **22**, 17117–17128 (2020).

151. Piwoński, H. *et al.* Imaging of tautomerism in a single molecule. *J. Am. Chem. Soc.* **127**, 5302–5303 (2005).

152. Piwoński, H. *et al.* Polarized spectroscopy studies of single molecules of porphycenes: Tautomerism and orientation. *J. Phys. Chem. C* **113**, 11514–11519 (2009).

153. Bednarz, A. *et al.* Substituent screening effect on single-molecule photostability: Comparison of three differently substituted porphycenes. *Methods Appl. Fluoresc.* **9**, 035004 (2021).

154. Ciąćka, P. C., Fita, P., Listkowski, A., Radzewicz, C. & Waluk, J. Evidence for Dominant Role of Tunneling in Condensed Phases andat High Temperatures: Double Hydrogen Transfer in Porphycenes. *J. Phys. Chem. Lett* **7**, 38 (2016).

155. Langer, U. *et al.* 15N NMR study of proton localization and proton transfer thermodynamics and kinetics in polycrystalline porphycene. *J. Phys. Org. Chem.* **13**, 23–34 (2000).

156. Wehrle, B., Limbach, H. -H, Köcher, M., Ermer, O. & Vogel, E. 15N-CPMAS-NMR Study of the Problem of NH Tautomerism in Crystalline Porphine and Porphycene. *Angew. Chemie Int. Ed. English* **26**, 934–936 (1987).

157. Frydman, B., Fernandez, C. O. & Vogel, E. Variable-Temperature Solid-State13C- and15N-CPMAS NMR Analyses of Alkyl-Substituted Porphycenes. *J. Org. Chem.* **63**, 9385–9391 (1998).

158. Shibl, M. F., Tachikawa, M. & Kühn, O. The geometric (H/D) isotope effect in porphycene: Grid-based Born-Oppenheimer vibrational wavefunctions vs. multi-component molecular orbital theory. *Phys. Chem. Chem. Phys.* **7**, 1368–1373 (2005).

159. Pietrzak, M., Shibl, M. F., Bröring, M., Kühn, O. & Limbach, H. H. 1H/2H NMR studies of geometric H/D isotope effects on the coupled hydrogen bonds in porphycene derivatives. *J. Am. Chem. Soc.* **129**, 296–304 (2007).

160. Fita, P., Garbacz, P., Nejbauer, M., Radzewicz, C. & Waluk, J. Ground and Excited State Double Hydrogen Transfer in Symmetric and Asymmetric Potentials: Comparison of 2,7,12,17-Tetra-*n*-propylporphycene with 9-Acetoxy-2,7,12,17-tetra-*n*-propylporphycene. *Chem. Eur. J* **17**, 3672–3678 (2011).

161. Gorski, A., Vogel, E., Sessler, J. L. & Waluk, J. Magnetic circular dichroism of octaethylcorrphycene and its doubly protonated and deprotonated forms. *J. Phys. Chem. A* **106**, 8139–8145 (2002).

162. Gorski, A., Vogel, E., Sessler, J. L. & Waluk, J. Magnetic circular dichroism of neutral and ionic forms of octaethylhemiporphycene. *Chem. Phys.* **282**, 37–49 (2002).

163. Schlabach, M., Scherer, G. & Limbach, H. H. Kinetic HH/HD/DH/DD Isotope Effects on Nondegenerate Stepwise Reversible Double Proton Transfer Reactions. NMR Study of the Tautomerism of *meso*-Tetraphenylchlorin. *J. Am. Chem. Soc.* **113**, 3550–3558 (1991).

164. Braun, J., Limbach, H. H., Williams, P. G., Morimoto, H. & Wemmer, D. E. Observation of kinetic tritium isotope effects by dynamic NMR. The tautomerism of porphyrin. *J. Am. Chem. Soc.* **118**, 7231–7232 (1996).

165. Braun, J. *et al.* Kinetic H/D/T isotope and solid state effects on the tautomerism of the conjugate porphyrin monoanion. *J. Am. Chem. Soc.* **118**, 11101–11110 (1996).

166. Schlabach, M. *et al.* NMR and NIR Studies of the Tautomerism of 5,10,15,20-Tetraphenylporphyrin including Kinetic HH/HD/DD Isotope and Solid State Effects. *Berichte der Bunsengesellschaft für Phys. Chemie* **96**, 821–833 (1992).

167. Braun, J. *et al.* NMR Study of the Tautomerism of Porphyrin Including the Kinetic HH/HD/DD Isotope Effects in the Liquid and the Solid State. *J. Am. Chem. Soc.* **116**, 6593–6604 (1994).

168. Frydman, L. *et al.* High-resolution solid-state carbon-13 NMR spectra of porphine and 5,10,15-20-tetraalkylporphyrins: implications for the nitrogen-hydrogen tautomerization process. *J. Am. Chem. Soc.* **110**, 336–342 (2002).

169. Waluk, J. Ground- and excited-state tautomerism in porphycenes. *Acc. Chem. Res.* **39**, 945–952 (2006).

170. Listkowski, A. *et al.* Controlling Emissive Properties by Intramolecular Hydrogen Bonds: Alkyl and Aryl *meso*-Substituted Porphycenes. *Chem. - A Eur. J.* **27**, 6324–6333 (2021).

171. Gil, M. & Waluk, J. Vibrational gating of double hydrogen tunneling in porphycene. *J. Am. Chem. Soc.* **129**, 1335–1341 (2007).

172. Fita, P., Urbanska, N., Radzewicz, C. & Waluk, J. Ground-and excited-state tautomerization rates in porphycenes. *Chem. - A Eur. J.* **15**, 4851–4856 (2009).

173. Kijak, M. *et al.* 2 + 2 Can Make Nearly a Thousand! Comparison of Di- and Tetra-*Meso*-Alkyl-Substituted Porphycenes. *J. Phys. Chem. A* **124**, 4594–4604 (2020).

174. Fita, P. *et al.* Double hydrogen transfer in low symmetry porphycenes. *Zeitschrift fur Phys. Chemie* **227**, 1009–1020 (2013).

175. Ciąćka, P. C. *et al.* Tautomerism in Porphycenes: Analysis of Rate-Affecting Factors. *J. Phys. Chem. B* **119**, 2292–2301 (2014).

176. Nogala, W. *et al.* Tailored gold nanostructure arrays as catalysts for oxygen reduction in alkaline media and a single molecule SERS platform. *Nanoscale* **7**, 10767–10774 (2015).

177. Gawinkowski, S. *et al.* Single molecule Raman spectra of porphycene isotopologues. *Nanoscale* **8**, 3337–3349 (2016).

178. Pszona, M., Gawinkowski, S., Jäger, R., Kamińska, I. & Waluk, J. Influence of bulky substituents on single-molecule SERS sensitivity. *J. Chem. Phys.* **156**, (2022).

179. Ladenthin, J. N. *et al.* Hot Carrier-Induced Tautomerization within a Single Porphycene Molecule on Cu(111). *ACS Nano* **9**, 7287–7295 (2015).

180. Guardiano, M., Biolo, R., Jori, G. & Schaffner, K. Tetra-*n*-propylporphycene as a tumour localizer: pharmacokinetic and phototherapeutic studies in mice. *Cancer Lett.* **44**, 1–6 (1989).

181. Leunig, M. *et al.* Tumour localisation kinetics of photofrin and three synthetic porphyrinoids in an amelanotic melanoma of the hamster. *Br. J. Cancer* **68**, 225–234 (1993).

182. Sung, H. *et al.* Global Cancer Statistics 2020: GLOBOCAN Estimates of Incidence and Mortality Worldwide for 36 Cancers in 185 Countries. *CA Cancer J Clin* **71**, 209–249 (2021).

183. Deo, S. V. S., Sharma, J., Kumar, S. & Oncol, A. S. GLOBOCAN 2020 Report on Global Cancer Burden: Challenges and Opportunities for Surgical Oncologists. *Ann. Surg. Oncol.* **29**, 6497–6500 (2022).

184. Ochsner, M. Photophysical and photobiological processes in the photodynamic therapy of tumours. *J. Photochem. Photobiol. B Biol.* **39**, 1–18 (1997).

185. Raab, O. Uber die Wirkung, fluorescirender Stoffe auf infusorien. *Z. Biol.* **39**, 524–546 (1900).

186. von Tappeiner, H. & Jodlbauer, A. Über die Wirkung der photodynamischen (fluorescierenden) Stoffe aufProtozoen und Enzyme. *Dtsch. Arch. Klin. Med.* **39**, 427–487 (1904).

187. Figge, F. H. J., Weiland, G. S. & Manganiello, L. O. J. Cancer Detection and Therapy. Affinity of Neoplastic, Embryonic, and Traumatized Tissues for Porphyrins and Metalloporphyrins. *Proc. Soc. Exp. Biol. Med.* **68**, 640–641 (1948).

188. Figge, F. H. J., Weiland, G. S. & Manganiello, L. O. J. Studies on cancer detection and therapy; the affinity of neoplastic, embryonic, and traumatized tissue for porphyrins, metalloporphyrins, and radioactive zinc hematoporphyrin. *Anat. Rec.* **101**, 657–657 (1948).

189. Rassmussen-Taxdal, D. S., Ward, G. E. & Figge, F. H. J. Fluorescence of human lymphatic and cancer tissues following high doses of intravenous hematoporphyrin. *Cancer* **8**, 78–81 (1955).

190. Lipson, R. L., Baldes, E. J. & Olsen, A. M. Hematoporphyrin derivative: a new aid for endoscopic detection of malignant disease. *J. Thorac. Cardiovasc. Surg.* **42**, 623–629 (1961).

191. Lipson, R. L., Baldes, E. J. & Olsen, A. M. The use of a derivative of hematoporphyrin in tumor detection. *J. Natl. Cancer Inst.* **26**, 1–11 (1961).

192. Gregorie Jr, H. B., Stevenson Jr, T. B., Robertson Jr, H. C. & Ward, J. L. Preliminary Observations in a Clinical Study of Hematoporphyrin-derivative Fluorescence in Malignant Neoplasms. *Am. Surg.* **30**, 656-663. (1964).

193. Gregorie, H. B. *et al.* Hematoporphyrin-Derivative Fluorescence in Malignant Neoplasms. *Ann. Surg.* **167**, 820–828 (1968).

194. Diamond, I. *et al.* Photodynamic Therapy of Malignant Tumors. *Lancet* **300**, 1175–1177 (1972).

195. Dougherty, T. J., Grindey, G. B., Fiel, R., Weishaupt, K. R. & Boyle, D. G. Photoradiation Therapy. II. Cure of Animal Tumors With Hematoporphyrin and Light. *JNCI J. Natl. Cancer Inst.* **55**, 115–121 (1975).

196. Weishaupt, K. R., Gomer, C. J. & Dougherty, T. J. Identification of Singlet Oxygen as the Cytotoxic Agent in Photo-inactivation of a Murine Tumor. *Cancer Res.* **36**, 2326–2329 (1976).

197. Gomer, C. J. & Dougherty, T. J. Determination of [3H]-and [14C]Hematoporphyrin Derivative Distribution in Malignant and Normal Tissue. *Cancer Res.* **39**, 146–151 (1979).

198. Dougherty, T. J. *The Circuitous Route by a Group of Novices to a New FDA Approved Cancer Therapy: How Did We Do This?. Outskirts Press,* (2015).

199. Cheng, J. *et al.* Effective Treatment of Human Lung Cancer by Targeting Tissue Factor with a Factor VII-Targeted Photodynamic Therapy. *Curr. Cancer Drug Targets* **11**, 1069–1081 (2011).

200. Yoshida, T. *et al.* Clinical Study of Photodynamic Therapy for Laryngeal Cancer. *Nippon Jibiinkoka Gakkai Kaiho* **98**, 795–804 (1995).

201. Wöhrle, D., Hirth, A., Bogdahn-Rai, T., Schnurpfeil, G. & Shopova, M. Photodynamic therapy of cancer: Second and third generations of photosensitizers. *Russ. Chem. Bull. 1998 475* **47**, 807–816 (1998).

202. Nonell, S., Borrell, J. I., Teixid, J. & Villanueva, A. Substituted Porphycene for the Photodynamic Therapy of Tumors. *Science (80-.).* **36**, 3405–3408 (1995).

203. Gonzalez Lopez, E. J., Santamarina, S. C., Alvarez, M. G., Heredia, D. A. & Durantini, E. N. Porphycenes as broad-spectrum antimicrobial photosensitizers. Potentiation with potassium iodide. *J. Photochem. Photobiol. A Chem.* **435**, 114288 (2023).

204. Krammer, B. & Verwanger, T. Photodynamic Therapy. in *Applied Photochemistry. When Light Meets Molecules* (eds. Giacomo Bergamini & Serena Silvi) vol. 92 377–396 (Springer, 2016).

205. Baptista, M. S. *et al.* Type I and Type II Photosensitized Oxidation Reactions: Guidelines and Mechanistic Pathways. *Photochem. Photobiol.* **93**, 912–919 (2017).

206. Rost, F. W. D. Photobleaching, photoactivation, and quenching. in *Quantitative Fluorescence Microscopy* 115–127 (Cambridge University Press, New York, 1991).

207. Gensch, T., Böhmer, M. & Aramendía, P. F. Single molecule blinking and photobleaching separated by wide-field fluorescence microscopy. *J. Phys. Chem. A* **109**, 6652–6658 (2005).

208. Griffini, G., Brambilla, L., Levi, M., Del Zoppo, M. & Turri, S. Photo-degradation of a perylene-based organic luminescent solar concentrator: Molecular aspects and device implications. *Sol. Energy Mater. Sol. Cells* **111**, 41–48 (2013).

209. Fritzsche, M. & Charras, G. Dissecting protein reaction dynamics in living cells by fluorescence recovery after photobleaching. *Nat. Protoc.* **10**, 660–680 (2015).

210. Bonnett, R. & Martínez, G. Photobleaching of sensitisers used in photodynamic therapy. *Tetrahedron* **57**, 9513–9547 (2001).

211. Demchenko, A. P. Photobleaching of organic fluorophores: Quantitative characterization, mechanisms, protection. *Methods and Applications in Fluorescence* vol. 8 at https://doi.org/10.1088/2050-6120/ab7365 (2020).

212. Ostapko, J. *et al.* Towards More Photostable, Brighter, and Less Phototoxic Chromophores: Synthesis and Properties of Porphyrins Functionalized with Cyclooctatetraene. *Chem. – A Eur. J.* **26**, 16666–16675 (2020).

213. Lill, Y. & Hecht, B. Single dye molecules in an oxygen-depleted environment as photostable organic triggered single-photon sources. *Appl. Phys. Lett.* **84**, 1665–1667 (2004).

214. Corredor, C. C., Belfield, K. D., Bondar, M. V., Przhonska, O. V. & Yao, S. One- and two-photon photochemical stability of linear and branched fluorene derivatives. *J. Photochem. Photobiol. A Chem.* **184**, 105–112 (2006).

215. Tinnefeld, P. & Cordes, T. 'Self-healing' dyes: Intramolecular stabilization of organic fluorophores. *Nat. Methods* **9**, 426–427 (2012).

216. Buczyńska, J. *et al.* Synthesis and Photostability of Cyclooctatetraene-Substituted Free Base Porphyrins. *Chemistry (Easton).* **3**, 104–115 (2021).

217. Alamiry, M. A. H., Harriman, A., Haefele, A. & Ziessel, R. Photochemical bleaching of an elaborate artificial light-harvesting antenna. *Chem Phys Chem* **16**, 1867-1872. (2015).

218. Bonnett, R. & Martinez, G. Photobleaching studies on azabenzoporphyrins and related systems: A comparison of the photobleaching of the zinc(II) complexes of the tetrabenzoporphyrin, 5-azadibenzo[b,g]porphyrin and phthalocyanine systems. *J. Porphyr. Phthalocyanines* **4**, 544–550 (2000).

219. Baba, T., Shimakoshi, H., Endo, A., Adachi, C. & Hisaeda, Y. Photophysical and photocatalytic properties of *β*-sulfonatoporphycenes. *Chem. Lett.* **37**, 264–265 (2008).

220. Taneda, M. *et al.* Synthesis and characterizations of *meso*-disubstituted asymmetric porphycenes. *Tetrahedron Lett.* **54**, 5727–5729 (2013).

221. Anju, K. S., Ramakrishnan, S., Thomas, A. P., Suresh, E. & Srinivasan, A. 9,10,19,20-Tetraarylporphycenes. *Org. Lett.* **10**, 5545–5548 (2008).

222. Ganapathi, E., Chatterjee, T. & Ravikanth, M. Facile Synthesis of 9,10,19,20-Tetraarylporphycenes. *European J. Org. Chem.* **2014**, 6701–6706 (2014).

223. Atkins P & de Paula J. *Atkins' Physical Chemistry*. (W. H. Freeman and Company, 2006).

224. Lakowicz, J. R. *Principles of Fluorescence Spectroscopy*. (Springer US, 2006).

225. Klán, P. & Wirz, J. *Photochemistry of Organic Compounds: From Concepts to Practice*. (John Wiley & Sons Ltd, Publication, 2009).

226. Valeur, B. & Berberan-Santos, M. N. *Molecular Fluorescence: Principles and Applications, Second Edition*. *Molecular Fluorescence: Principles and Applications, Second Edition* (Wiley-VCH, 2012).

227. https://www.cyberphysics.co.uk/topics/radioact/Radio/EMSpectrumcolor.jpg.

228. Del Valle, J. C. & Catalán, J. Kasha's rule: A reappraisal. *Phys. Chem. Chem. Phys.* **21**, 10061–10069 (2019).

229. Vogel E, Koch P, Rahbar A & Cross A. Patent nr WO1992012636. (1992).

230. Vogel E, Mueller M, Halpen O & Cross A. Patent nr WO96/31451. (1996).

231. Mbakara, I. *et al.* Spectroscopic investigation of photophysics and tautomerism of amino- and nitroporphycenes. *Phys. Chem. Chem. Phys.* **24**, 29655–29666 (2022).

232. Gajewska, A., Mbakara, I. & Waluk, I. 2-nitro-7,12,17-tri-*tert*-butylporphycene: Spectroscopy, photophysics, and tautomerism. *J. Porphyr. Phthalocyanines* **27**, 563–568 (2023).

233. Brouwer, A. M. Standards for photoluminescence quantum yield measurements in solution (IUPAC Technical Report). Pure and Applied Chemistry, 83(12), 2213–2228 . *Pure Appl. Chem.* **83**, 2213–2228 (2011).

234. Andersson, L. A. Magnetic Circular Dichroism, Theory. in *Encyclopedia of Spectroscopy and Spectrometry* 660–666 (Elsevier, 2017).

235. Duvanel, G., Banerji, N. & Vauthey, E. Excited-state dynamics of donor - Acceptor bridged systems containing boron - Dipyrromethene chromophore: Interplay between charge separation and reorientational motion. *J. Phys. Chem. A* **111**, (2007).

236. Lang, B. Photometrics of ultrafast and fast broadband electronic transient absorption spectroscopy: State of the art. *Rev. Sci. Instrum.* **89**, (2018).

237. Frisch, M. *et al.* Gaussian 16, Revision B.01. at (2016).

238. Mbakara, I., Gajewska, A., Nawara, K. & Waluk, J. Instability of 9-aminoporphycenes. *J. Porphyr. Phthalocyanines* A-H (2023).

239. Pati, N. N., Kumar, B. S. & Panda, P. K. *β*-Hexaalkylporphycenes: Positional effect of alkyl groups toward design and control of structural and photophysical properties in isomeric hexaethylporphycenes. *Org. Lett.* **19**, 134–137 (2017).

240. Pati, N. N., Kumar, B. S., Chandra, B. & Panda, P. K. Unsymmetrical Bipyrrole-Derived *β*-Tetraalkylporphycenes and C–H···Br–C Interaction Induced 2D Arrays of the 2:1 Supramolecular Sandwich Complex of Their cis-/trans-Dibromo Isomers. *European J. Org. Chem.* **2017**, 741–745 (2017).

241. Nagamaiah, J., Dutta, A., Sahoo, S. ., Sahoo, S. & Panda, P. . 3,6,13,16-Tetraalkylporphycenes: synthesis and exploration of the effect of alkyl groups on the structure, photophysical properties, and basicity. . *New J. Chem.* **46**, 14586–14596 (2022).

242. Nagamaiah, J. *et al.* 3,6,13,16-Tetrapropylporphycene: Rational synthesis, complexation, and halogenation. . *J. Org. Chem.* **87**, 2721-2729. (2022).

243. Vogel E, Mueller M, Halpen O & Cross A. 9-substituted porphycenes - United States Patent. (1997).

244. Gong, W. *et al.* Redefining the photo-stability of common fluorophores with triplet state quenchers: Mechanistic insights and recent updates. *Chem. Commun.* **55**, 8695–8704 (2019).

245. Gavalda, A. *et al.* A non-tetradecarboxylative synthesis of 2,7,12,17-tetraphenylporphycene. *J. Porphyr. Phthalocyanines* **5**, 846–852 (2001).

246. Berezin, D. B. *et al.* Synthesis and physico-chemical properties of 2,7,12,17-tetraphenylporphycene and its metal complexes. *Russ. J. Gen. Chem.* **85**, 1876–1884 (2015).

247. Arnbjerg, J. *et al.* Two-photon absorption in tetraphenylporphycenes: Are porphycenes better candidates than porphyrins for providing optimal optical properties for two-photon photodynamic therapy? *J. Am. Chem. Soc.* **129**, 5188–5199 (2007).

248. Rubio, N., Martínez-Junza, V., Estruga, J. & Borrell, J. I. Ground- and excited-state interactions of biomolecules for type-I photodynamic therapy. 99–106 (2009).